# MOLECULAR TARGETED THERAPY IN ONCOLOGY: LESSONS FROM PHARMACOGENETICS AND PHARMACOEPIGENETICS

EDITED BY: Saber Imani, Matteo Becatti and Md. Asaduzzaman Khan

PUBLISHED IN: Frontiers in Molecular Biosciences

frontiers Research Topics

# frontiers



ISSN 1664-8714
ISBN 978-2-88974-855-6
DOI 10.3389/978-2-88974-855-6

## About Frontiers

Frontiers is more than just an open-access publisher of scholarly articles: it is a pioneering approach to the world of academia, radically improving the way scholarly research is managed. The grand vision of Frontiers is a world where all people have an equal opportunity to seek, share and generate knowledge. Frontiers provides immediate and permanent online open access to all its publications, but this alone is not enough to realize our grand goals.

## Frontiers Journal Series

The Frontiers Journal Series is a multi-tier and interdisciplinary set of open-access, online journals, promising a paradigm shift from the current review, selection and dissemination processes in academic publishing. All Frontiers journals are driven by researchers for researchers; therefore, they constitute a service to the scholarly community. At the same time, the Frontiers Journal Series operates on a revolutionary invention, the tiered publishing system, initially addressing specific communities of scholars, and gradually climbing up to broader public understanding, thus serving the interests of the lay society, too.

## Dedication to Quality

Each Frontiers article is a landmark of the highest quality, thanks to genuinely collaborative interactions between authors and review editors, who include some of the world's best academicians. Research must be certified by peers before entering a stream of knowledge that may eventually reach the public - and shape society; therefore, Frontiers only applies the most rigorous and unbiased reviews.
Frontiers revolutionizes research publishing by freely delivering the most outstanding research, evaluated with no bias from both the academic and social point of view. By applying the most advanced information technologies, Frontiers is catapulting scholarly publishing into a new generation.

## What are Frontiers Research Topics?

Frontiers Research Topics are very popular trademarks of the Frontiers Journals Series: they are collections of at least ten articles, all centered on a particular subject. With their unique mix of varied contributions from Original Research to Review Articles, Frontiers Research Topics unify the most influential researchers, the latest key findings and historical advances in a hot research area! Find out more on how to host your own Frontiers Research Topic or contribute to one as an author by contacting the Frontiers Editorial Office: frontiersin.org/about/contact

# MOLECULAR TARGETED THERAPY IN ONCOLOGY: LESSONS FROM PHARMACOGENETICS AND PHARMACOEPIGENETICS

Topic Editors:
**Saber Imani,** China Regional Research Center, International Centre for Genetic Engineering and Biotechnology, China
**Matteo Becatti,** University of Firenze, Italy
**Md. Asaduzzaman Khan,** Southwest Medical University, China

**Citation:** Imani, S., Becatti, M., Khan, M. A., eds. (2022). Molecular Targeted Therapy in Oncology: Lessons From Pharmacogenetics and Pharmacoepigenetics. Lausanne: Frontiers Media SA. doi: 10.3389/978-2-88974-855-6

# Table of Contents

frontiers in Molecular Biosciences

EDITORIAL
published: 15 March 2022
doi: 10.3389/fmolb.2022.822188

# Editorial: Molecular Targeted Therapy in Oncology: Lessons From Pharmacogenetics and Pharmacoepigenetics

*Saber Imani*[1,2]*, *Matteo Becatti*[3]* and *Md. Asaduzzaman Khan*[4]*

[1]China Regional Research Center, International Centre for Genetic Engineering and Biotechnology Taizhou, Jiangsu, China, [2]Department of Oncology, Affiliated Hospital of Southwest Medical University Luzhou, Luzhou, China, [3]Department of Experimental and Clinical Biomedical Sciences "Mario Serio", University of Firenze, Firenze, Italy, [4]The Research Center for Preclinical Medicine, Southwest Medical University, Luzhou, China

**Keywords: cancer, molecular targeted therapy, pharmacogenetics, pharmacoepigenetics, signaling pathways, drug resistance**

## Editorial on the Research Topic

### Molecular Targeted Therapy in Oncology: Lessons from Pharmacogenetics and Pharmacoepigenetics

OPEN ACCESS

***Edited and reviewed by:***
*William C. Cho,*
*QEH, Hong Kong SAR, China*

***Correspondence:**
*Saber Imani*
*saberimani@swmu.edu.cn*
*Matteo Becatti*
*matteo.becatti@unifi.it*
*Md. Asaduzzaman Khan*
*asadkhan@swmu.edu.cn*

***Specialty section:***
*This article was submitted to Molecular Diagnostics and Therapeutics, a section of the journal Frontiers in Molecular Biosciences*

***Received:*** *25 November 2021*
***Accepted:*** *16 February 2022*
***Published:*** *15 March 2022*

***Citation:***
*Imani S, Becatti M and Khan MA (2022) Editorial: Molecular Targeted Therapy in Oncology: Lessons From Pharmacogenetics and Pharmacoepigenetics. Front. Mol. Biosci. 9:822188. doi: 10.3389/fmolb.2022.822188*

The Human Genome Project is moving away from basingclinical decisions on signs and symptoms of diseases to a new concept of medicine. Pharmacogenetics and pharmacoepigenetics are multidisciplinary research areas of "personalized genomic medicine", representing a new approach to healthcare aimed at customizing patients' medical treatment according to their individual genomic profile.

In the current Research Topic (RT), we provide an overview on the new trends, achievements, and challenges lying ahead in cancer. Original articles and reviews summarize the current knowledge on genomics and epigenetics modifications to study therapeutic approaches, biomarkers, and mechanisms involved in diseases and drug resistance.

In recent years, the multi-OMICS data have provided a platform linking the cancer-specific genomic/epigenomic alterations to interconnected transcriptome, proteome, and metabolome networks which underlie the molecular-targeted therapies in oncology (Jung et al., 2021). The development of high-throughput sequencing technologies and artificial intelligence have allowed a large data explosion and systematic study of the cancer genome. For the first time, data were available for complete genome sequences in a large number of cancer types. Open data have promoted the advance of scientific discovery. The era of genomics and big data has brought the need for collaboration and data sharing in order to make effective use of this new knowledge. Consequently, the storage and analysis of these data in an efficient manner pose a major challenge to researchers. In this RT, five studies that employed publicly accessible databases useful for cancer diagnosis and prognosis are presented (Deng et al.; Fan et al.; Feng et al.; Xiang et al.; Zhang et al.). This approach provides a new opportunity to optimize treatments by understanding the basis of biological mechanisms and utilizing genomic/epigenomic contributions to treatment response. In the context of tumor-specific therapeutical biomarkers in immunotherapy, programmed death-1 homolog (PD-1H) is a new regulator of T cell-mediated immune responses (Villarroel-Espindola et al., 2018). Chen et al. showed that PD-1H could be a prognostic indicator and a potential immunotherapeutic target in human esophageal squamous cell carcinoma (ESCC) patients (Chen et al.).

Tyrosine kinases receptors (TKRs) are transmembrane proteins acting as signal transducers that regulate essential cellular processes such as proliferation, differentiation, metabolism, and cell death. Alterations in the TKR pathway occur in a broad spectrum of cancers, underlying their key role in cancer progression and as therapeutic targets (Krause and Van Etten, 2005; SudheshDev et al., 2021). In this RT, Wu et al. investigated the neurotrophic tyrosine receptor kinase (NTRK) gene fusion status in triple negative breast cancer (TNBC) patients (Wu et al.). In the same line, Yang et al. investigated the function of ELK1 transcription factor in pancreatic cancer progression (Yan et al.), demonstrating the key role of ELK1 in cancer cell proliferation and invasion.

Notch and Wnt signaling are other critical pathways involved in cell fate decision, cell proliferation/differentiation, and cancer progression. In addition, two review papers summarized the current knowledge on the molecular mechanisms by which Notch3 and Wnt modulate cancer stemness and chemoresistance, metastasis, and angiogenesis. Xiu et al. suggested potential treatment strategies to block Notch3 signaling, such as non-coding RNAs, antibodies, and antibody-drug conjugates (Xiu et al.). Furthermore, the article by Xie et al. summarized the current knowledge and recent advances on the Wnt signaling pathway in head and neck squamous cell cancer (Xie et al.), suggesting that Wnt could be a new potential target for innovative therapeutic approaches.

Oxaliplatin is a popular therapeutic agent against cancer associated with neuropathic pain. The genetic and epigenetic mechanism of oxaliplatin on neuropathic pain has been discussed by (Branca et al.). Understanding the ability of oxaliplatin to alter the genetic and epigenetic profiles of neural cells might be helpful to find new treatments for neuropathy in cancer patients.

In conclusion, this RT provides a comprehensive collection on the role of epigenetics and epigenomics in cancer drug discovery and development, providing a detailed view of the field, from basic principles to applications in cancer disease therapeutics.

## AUTHOR CONTRIBUTIONS

All authors listed have made a substantial, direct, and intellectual contribution to the work and approved it for publication.

## REFERENCES

Jung, H. D., Sung, Y. J., and Kim, H. U. (2021). Omics and Computational Modeling Approaches for the Effective Treatment of Drug-Resistant Cancer Cells. *Front. Genet.* 12, 742902. doi:10.3389/fgene.2021.742902

Krause, D. S., and Van Etten, R. A. (2005). Tyrosine Kinases as Targets for Cancer Therapy. *N. Engl. J. Med.* 353 (2), 172–187. doi:10.1056/NEJMra044389

Sudhesh Dev, S., Zainal Abidin, S. A., Farghadani, R., Othman, I., and Naidu, R. (2021). Receptor Tyrosine Kinases and Their Signaling Pathways as Therapeutic Targets of Curcumin in Cancer. *Front. Pharmacol.* 12, 772510. doi:10.3389/fphar.2021.772510

Villarroel-Espindola, F., Yu, X., Datar, I., Mani, N., Sanmamed, M., Velcheti, V., et al. (2018). Spatially Resolved and Quantitative Analysis of VISTA/PD-1H as a Novel Immunotherapy Target in Human Non-small Cell Lung Cancer. *Clin. Cancer Res.* 24 (7), 1562–1573. doi:10.1158/1078-0432.CCR-17-2542

**Conflict of Interest:** The authors declare that the research was conducted in the absence of any commercial or financial relationships that could be construed as a potential conflict of interest.

frontiers in Molecular Biosciences

ORIGINAL RESEARCH
published: 07 December 2020
doi: 10.3389/fmolb.2020.599340

# m$^5$C RNA Methylation Primarily Affects the ErbB and PI3K–Akt Signaling Pathways in Gastrointestinal Cancer

*Shixin Xiang[1,2†], Yongshun Ma[1,2†], Jing Shen[1,2], Yueshui Zhao[1,2], Xu Wu[1,2], Mingxing Li[1,2], Xiao Yang[1], Parham Jabbarzadeh Kaboli[1,2], Fukuan Du[1,2], Huijiao Ji[1,2], Yuan Zheng[3], Xiang Li[1], Jing Li[4], Qinglian Wen[5]* and Zhangang Xiao[1,2]**

[1] Laboratory of Molecular Pharmacology, Department of Pharmacology, School of Pharmacy, Southwest Medical University, Luzhou, China, [2] South Sichuan Institute of Translational Medicine, Luzhou, China, [3] Neijiang Health and Health Vocational College, Neijiang, China, [4] Department of Oncology and Hematology, Hospital (T.C.M.) Affiliated to Southwest Medical University, Luzhou, China, [5] Department of Oncology, Affiliated Hospital of Southwest Medical University, Luzhou, China

OPEN ACCESS

**Edited by:**
Saber Imani,
Affiliated Hospital of Southwest Medical University, China

**Reviewed by:**
Maria Celeste Cantone,
Istituto Auxologico Italiano (IRCCS), Italy
Mazaher Maghsoudloo,
University of Tehran, Iran
Amit Kumar Pandey,
Amity University Gurgaon, India

***Correspondence:**
Zhangang Xiao
xzg555898@hotmail.com
Qinglian Wen
wql73115@163.com

† These authors have contributed equally to this work

**Specialty section:**
This article was submitted to Molecular Diagnostics and Therapeutics, a section of the journal Frontiers in Molecular Biosciences

**Received:** 27 August 2020
**Accepted:** 28 October 2020
**Published:** 07 December 2020

**Citation:**
Xiang S, Ma Y, Shen J, Zhao Y, Wu X, Li M, Yang X, Kaboli PJ, Du F, Ji H, Zheng Y, Li X, Li J, Wen Q and Xiao Z (2020) m$^5$C RNA Methylation Primarily Affects the ErbB and PI3K–Akt Signaling Pathways in Gastrointestinal Cancer. Front. Mol. Biosci. 7:599340. doi: 10.3389/fmolb.2020.599340

5-Methylcytosine (m$^5$C) is a kind of methylation modification that occurs in both DNA and RNA and is present in the highly abundant tRNA and rRNA. It has an important impact on various human diseases including cancer. The function of m$^5$C is modulated by regulatory proteins, including methyltransferases (writers) and special binding proteins (readers). This study aims at comprehensive study of the m$^5$C RNA methylation-related genes and the main pathways under m$^5$C RNA methylation in gastrointestinal (GI) cancer. Our result showed that the expression of m$^5$C writers and reader was mostly up-regulated in GI cancer. The *NSUN2* gene has the highest proportion of mutations found in GI cancer. Importantly, in liver cancer, higher expression of almost all m$^5$C regulators was significantly associated with lower patient survival rate. In addition, the expression level of m$^5$C-related genes is significantly different at various pathological stages. Finally, we have found through bioinformatics analysis that m$^5$C regulatory proteins are closely related to the ErbB/PI3K–Akt signaling pathway and *GSK3B* was an important target for m$^5$C regulators. Besides, the compound termed streptozotocin may be a key candidate drug targeting on GSK3B for molecular targeted therapy in GI cancer.

**Keywords: m$^5$C, RNA methylation, ErbB, PI3K–Akt, gastrointestinal cancer, survival**

## INTRODUCTION

Gastrointestinal (GI) cancer is one of the leading causes of death worldwide. It refers to cancers of the upper and lower digestive tracts and mainly includes colorectal adenocarcinoma (CRC), gastric cancer (GC), pancreatic cancer (PC), hepatocellular carcinoma (HCC), and esophageal cancer (EC) (Toomey et al., 2013). Nearly 4.1 million people are diagnosed with GI cancer each year. Epigenetic changes are common events in both initiation and progression of GI cancer (Vedeld et al., 2018). Currently, there are many ways to treat GI cancer. However, most of the treatment outcomes are still poor (Bilgin et al., 2017).

RNA methylation modifications mainly include $m^6A$, $m^5C$, $m^1A$, $m^7G$, and so on. Previous studies have shown that these modifications play important roles in the stability, processing, and genetic information transmission of mRNA (Liu and Jia, 2014; Oerum et al., 2017). Known mutations in RNA-modifying enzymes are closely related to human diseases, including cancers, cardiovascular diseases, metabolic diseases, and mitochondrial-related defects (Jonkhout et al., 2017). The degree of methylation of specific genes can be used as a diagnostic indicator of cancer (Li W. et al., 2017; Traube and Carell, 2017). 5-Methylcytosine ($m^5C$) includes DNA and RNA methylation modifications, in which the methyl group is transferred to a specific base by using *S*-adenosylmethionine (SAM) as a methyl donor under the catalysis of methyltransferase. $m^5C$ RNA modification has been found to be highly abundant in tRNA and rRNA (Motorin et al., 2010). Meanwhile, high throughput sequencing has been used to verify the widespread presence of $m^5C$ in non-coding RNA and coding RNA (Squires et al., 2012). It has been reported that $m^5C$ modification controls many functions: protein translational regulation, RNA processing, regulating stem cell function and stress response, and promoting tRNA stability and protein synthesis (Aslan et al., 1967; Blanco et al., 2016; Liu et al., 2017; Tuorto et al., 2012). However, the involvement of $m^5C$ modification in GI cancer has not been systematically reported yet.

5-Methylcytosine modification is regulated by methyltransferases (writers, including *NSUN1-7* and *TRDMT1* [*tRNA aspartic acid methyltransferase 1*]) and binding protein (reader, i.e., *ALYREF* [*Aly/REF export factor*]). *NSUN1-7* and *TRDMT1* are known writers for chemical RNA modifications (Jacob et al., 2017). *NSUN1* (NOP2 nucleolar protein/rRNA MTase) plays an important role in maintaining cell proliferation capacity and is possibly involved in the regeneration of nervous tissue (Kosi et al., 2015; Hong et al., 2016). *NSUN2* (*NOP2/Sun RNA methyltransferase 2*/mRNA and tRNA MTase) is a main RNA modification methyltransferase. Its mechanism of action includes controlling cell division, growth arrest, and promoting premature senescence (Xing et al., 2015; Cai et al., 2016; W. Wang, 2016; Yang X. et al., 2017). It has been reported that *NSUN2* mutations lead to intellectual disability in human diseases (Abbasi-Moheb et al., 2012). *NSUN3* (NOP2/Sun RNA methyltransferase 3/mt-tRNA MTase) and *NSUN4* (NOP2/Sun RNA methyltransferase 4/mt-rRNA MTase) have important impacts on the mitochondria (Metodiev et al., 2014; Schosserer et al., 2015; Nakano et al., 2016). *NSUN5* (NOP2/Sun RNA methyltransferase 5/rRNA MTase) is a conserved rRNA methyltransferase (Schosserer et al., 2015). *NSUN6* (NOP2/Sun RNA methyltransferase 6/tRNA MTase) modifies tRNAs in their biogenesis (Haag et al., 2015). *NSUN7* (*NOP2/Sun RNA methyltransferase family member 7*) gene product plays a role in sperm motility (Khosronezhad et al., 2015). *TRDMT1* (also known as *DNMT2*) was previously considered as a DNA MTase, but it is now primarily regarded as a tRNA MTase (Schaefer and Lyko, 2010; Squires et al., 2012; Jeltsch et al., 2017). Up to now, the $m^5C$ eraser is still unknown, and the only known binding protein (reader) of $m^5C$ is *ALYREF*. *ALYREF* as an $m^5C$ reader can promote mRNA export (Yang X. et al., 2017). In general, $m^5C$ methyltransferases are strongly associated with diseases.

Currently, there is little research progress in the biological function and mechanism of $m^5C$ in GI cancer. In this study, we analyzed the gene expression level, alteration frequency, and association with survival of $m^5C$ regulators in GI cancer. Meanwhile, we also studied their related pathways and key target, for which a druggable compound was found in the hope of providing new treatment for patients with GI cancer.

# MATERIALS AND METHODS

## Data Processing

The expression level and clinical data of $m^5C$ regulators in five types of GI cancers were extracted from the TCGA database[1] (Tomczak et al., 2015) (download date: 2019-05-05). There were 1,696 cancer samples and 148 normal samples. The standardized TCGA and GTEX transcriptome data are derived from the UCSC database[2]. In total, there were 1,451 cancer samples and 1,044 normal samples.

## Somatic Alteration Analysis

The cBioportal analysis of the GISTIC 2.0 database was used to analyze the alteration frequency and percentage of $m^5C$ regulatory factors in GI cancers and protein affected by $m^5C$ regulators (Cerami et al., 2012). OncoPrint can summarize distinct genomic alterations across samples in the $m^5C$ regulatory factors, including mutations, CNAs, and changes in gene expression or protein abundance (Gao et al., 2013).

## Protein Structure Alteration

The protein structure alteration was analyzed in cBioportal using the Mutations tab. The query was limited to respective $m^5C$ regulatory factors in different types of GI cancer. Lollipop of each protein structure change of GI cancer was linked to COSMIC (Tate et al., 2019). The detailed mutation annotation was originated from OncoKB, CIViC, and Hotspot (Tate et al., 2019).

## Pathway Analysis

Proteomic data were collected by Reverse Phase Protein Array (RPPA) based on TCGA data from cBioportal[3]. For the enriched proteins, significant change in expression was determined by the standard of $\log_2$ based ratio (μ mean altered/μ mean unaltered) ($\log > 0$ for over-expression and $\log < 0$ for under-expression) and queried event results in $P$ value $<0.05$. The $-\log_{10}$ $P$ value $>1.30$ proteins were selected for further downstream pathway analysis. Differential proteins are shown by the volcano plot using GraphPad Prism 7. The selected proteins from this criterion were used to predict pathways by two conditions: (a) the sum of altered protein in each pathway and (b) the statistical $P$ value score of significant pathway (Li D. et al., 2020). Finally, the screened

[1]http://cancergenome.nih.gov

[2]https://xenabrowser.net/

[3]http://www.cbioportal.org/

differential proteins were used to predict the pathway in the DAVID function annotation tool[4].

## Gene Ontology Analysis

The Gene Ontology (GO) enrichment analysis of the m$^5$C RNA methylation modification was analyzed *via* the DAVID function annotation tool (Dennis et al., 2003). GO contains biological processes, cell components, and molecular functions. In this analysis, count represents the number of genes contained in the GO term. Therefore, the count and *P* values are considered together to obtain important metabolic process.

## Protein–Protein Interaction Network Analysis

We analyzed the network of interactions between proteins by using the STRING and Cytoscape software. The STRING database is a meta resource, including both physical and functional interactions (Jensen et al., 2009). STRING can be reached at http://string-db.org/. The minimum required interaction score is set to medium confidence and select all active interaction sources. Cytoscape is a public software that can integrate models of biomolecular interaction networks (Shannon et al., 2003).

## Correlation and Co-expression Analysis

To better understand the co-expression between m$^5$C regulatory factors and the differentially expressed genes (DEGs) associated with key downstream pathways, we used the R statistical software by R package heatmap (Chan, 2018). Parameters of co-expression analysis were set as: 0.8–1.0 strongly correlated, 0.6–0.8 strong correlation, 0.4–0.6 moderate intensity correlation, 0.2–0.4 weak correlation, and 0.0–0.2 very weak correlation or no correlation. Correlation between *GSK3B* (*glycogen synthase kinase 3 beta*) and m$^5$C regulators was analyzed using the linear regression. The 95% confidence intervals were presented by dot lines. The data have been standardized.

## Network Pharmacology Analysis

Differentially expressed genes related to the *GSK3B* gene were obtained by R package limma. The samples were divided into two groups according to the median expression values of the *GSK3B* gene and $|\log_2$ fold-change (FC)$| > 1$, and the *P* value $<0.05$ was set as a threshold. According to the *P* value ranking, the first 150 DEGs that were significantly up-regulated and the first 150 DEGs that were significantly down-regulated were included for potential drug target analysis. The Connectivity Map (CMap) is a gene expression profile database based on interventional gene expression (Subramanian et al., 2017). It is mainly used to analyze the functional connections between small molecule compounds, genes, and diseases (Lamb et al., 2006). PharmMapper is a comprehensive target pharmacophore database that can search potential drug target identification (Wang et al., 2017). PharmMapper comes from TargetBank, DrugBank, BindingDB, and potential drug target databases, and nearly 53,000 receptor-based pharmacophore models are used for prediction (Liu et al., 2010; Wang et al., 2016).

[4]https://david.ncifcrf.gov

## Statistical Analysis

*T* test is used for comparison between two groups of data, and one-way ANOVA is applied to compare multiple groups. Survival analysis was performed using Kaplan–Meier curve with *P* value calculated using the log-rank test. The correlation of mRNA expression was analyzed by Pearson test. Chi-square test was used to test the association of m$^5$C regulator expression with clinicopathological parameters. $P < 0.05$ was considered statistically significant.

# RESULTS

## The Expression Level of m$^5$C Regulators in GI Cancer

The workflow of the study and nomenclature and mechanism of m$^5$C writer and reader was demonstrated in **Figures 1A,B**. To characterize the expression of m$^5$C writers and reader in GI cancer, we first used the TCGA data. Overall, the expression level of *NSUN3*, *NSUN4*, *NUSN6*, *NUSN7*, and *TRDMT1* was lower than that of other m$^5$C regulators (**Figure 2A**). When comparing the expression level between 1,696 cancer and 148 normal samples, heat map showed that the expression of m$^5$C writers and reader was generally higher in GI cancer than in normal samples (**Figure 2A**). The combination of the TCGA and GTEX databases was used to compare the expression level of m$^5$C writer and reader between tumor tissue and normal samples in GI cancer. The results indicated that writers and reader were mostly up-regulated in GI cancer (**Figure 2B**). Meanwhile, we did principal component analysis of gene expression in 1,695 samples of the five cancer types (**Supplementary Figure S1**). X and Y axes explained 39.5 and 16.4% of the total variance, respectively. The further apart the two samples, the greater the difference in genetic background between them would be. From the figure, the five cancers were almost distinctively separated.

## Mutation of m$^5$C Regulators

In order to identify mutations of m$^5$C regulators, cBioPortal for Cancer Genomic was used (Cerami et al., 2012; Gao et al., 2013). As shown in **Figures 3A,B**, mutation and amplification were frequently seen in m$^5$C regulators. *NSUN2*, *NSUN5*, and *ALYREF* showed relatively higher copy number amplification. In **Figure 3B**, we also found that there are many types of mutations in m$^5$C RNA methylation regulators, such as inframe mutation, missense mutation, amplification, and deep deletion. Among them, amplification has the largest proportion of types, and deep deletion also accounts for a large proportion. Overall, about 13% of the samples (246/1,924) had genetic changes, and the mutation rate of m$^5$C regulators was relatively higher in esophagus and stomach cancers than in other cancer types. Furthermore, 28% (52/186) of EC, 8% (14/186) of PC, 19% (91/478) of stomach cancer, 5% (33/640) of colorectal cancer, 13% (56/442) of liver cancer, and 12% (234/1,928) of GI cancer had genomic changes

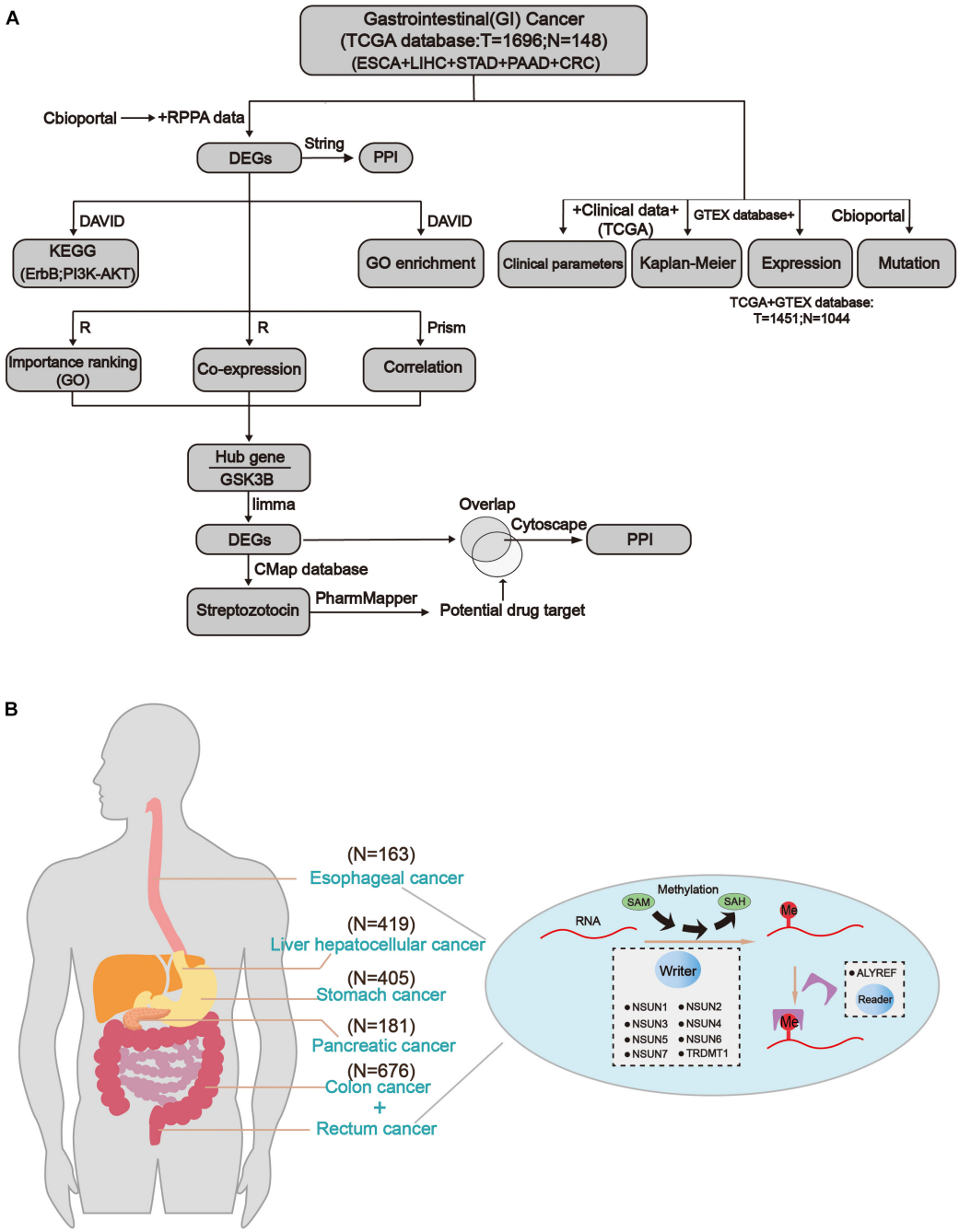


**FIGURE 1 |** Comprehensive molecular profiling of m$^5$C writers and reader in GI cancer. **(A)** The workflow of the study. **(B)** The regulation mechanism of m$^5$C in GI cancers (esophageal cancer, liver cancer, gastric cancer, colon cancer, and rectal cancer). m$^5$C formation is catalyzed by writer and SAM (*S*-adenosylmethionine). In addition, reader can recognize methylated mRNA and mediate its export from the nucleus. They work together on m$^5$C RNA methylation modification.

of m$^5$C regulators. Notably, the mutation frequencies of *NSUN2* in esophagus and stomach cancers, *NSUN3* in esophagus cancer, and *ALYREF* in liver cancer were particularly high. Changes in protein structure were shown in **Figure 3C**. Mutation in protein sequence was more often found in *NSUN1* and *NSUN2* than in other genes.

## Impact of m$^5$C Regulator Alterations on Patient Survival

Next, we used clinical information in the TCGA database to evaluate the influence of m$^5$C writers and reader expression on the survival rate in patients with GI cancer. Kaplan–Meier analysis showed that the differential expression of some

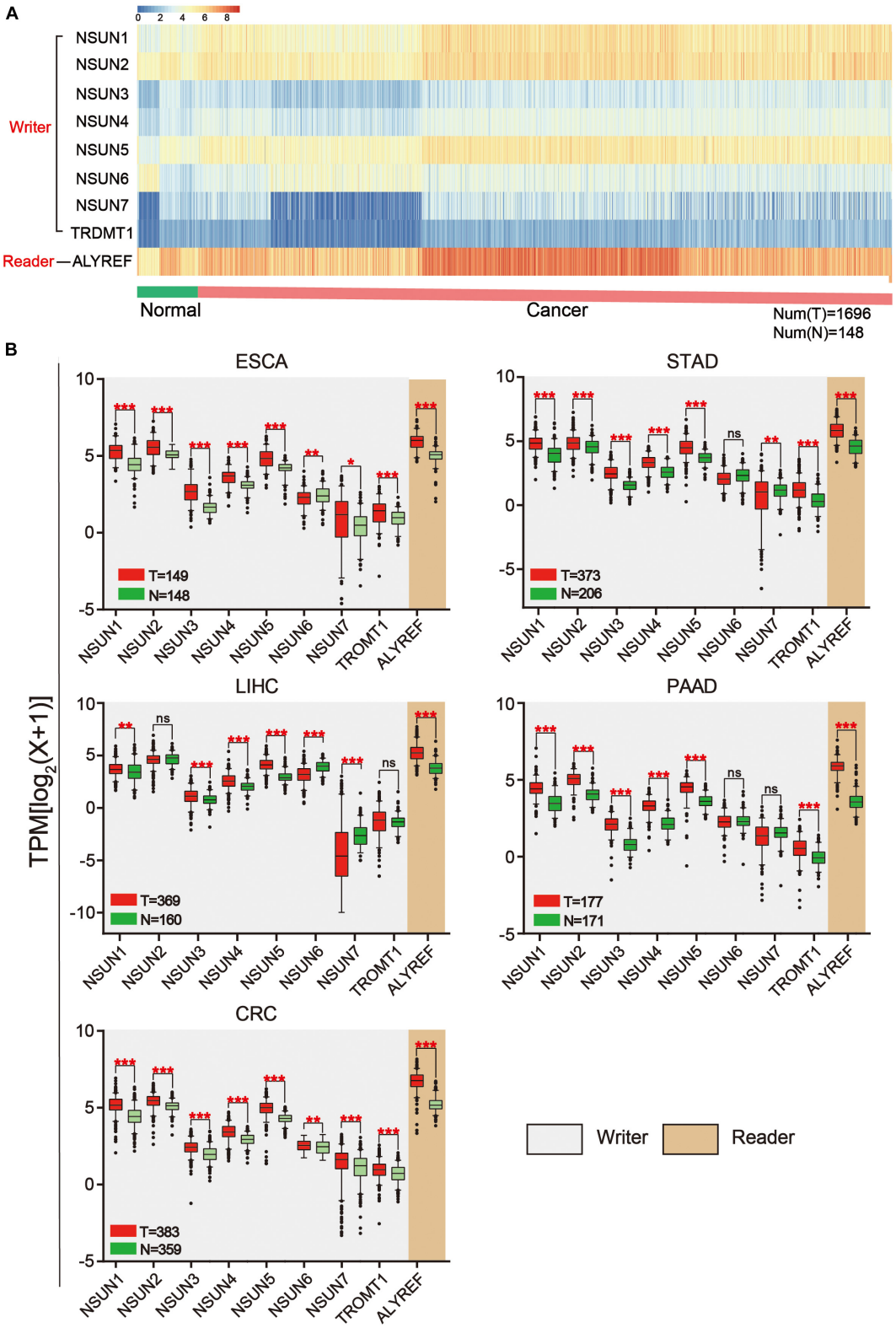


**FIGURE 2 |** Expression of m$^5$C writers and reader in GI cancer. **(A)** Based on RNA sequencing data from the TCGA database, a heat map of m$^5$C writer and reader expression was drawn. Data were collected from cancer patients (*n* = 1,568) and healthy patients (*n* = 139). Each sample was normalized and was represented by a square. Red and blue regions represented higher and lower expression levels, respectively. **(B)** RNA sequencing data were used to compare the expression level of each m$^5$C regulator between tumor and normal samples in different GI cancer types.

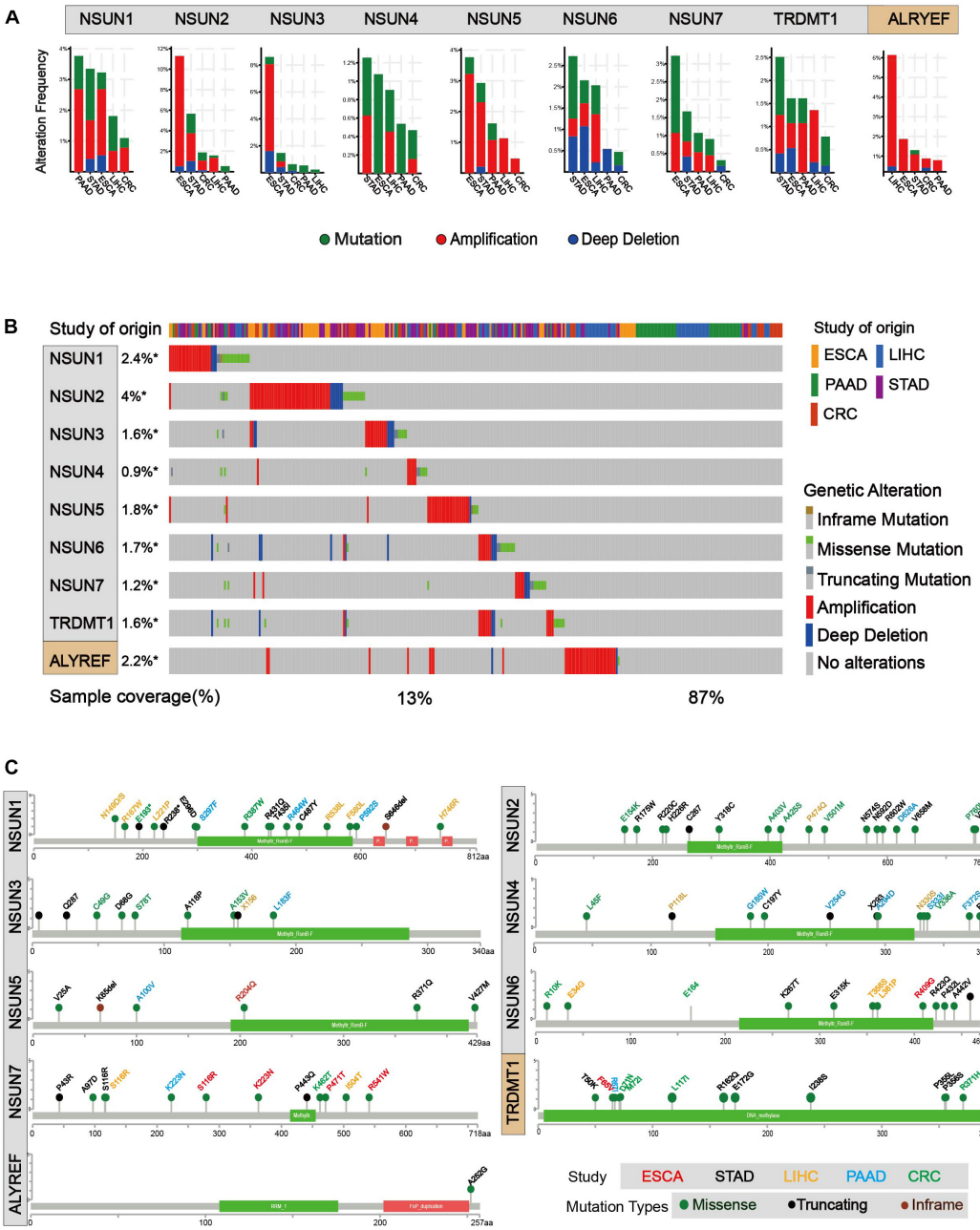


**FIGURE 3 |** Mutations of m$^5$C writer and reader in GI cancer. **(A)** Alteration frequency of m$^5$C regulatory factors in GI cancer, including mutations, amplification, and deletion, and multiple changes were analyzed from the TCGA database and studied in cBioPortal. About 28% (52/186) of esophageal cancer, 8% (14/186) of pancreatic cancer, 19% (91/478) of stomach cancer, 5% (33/640) of colorectal cancer, 13% (56/442) of liver cancer, and 12% (234/1,928) of GI cancer had genomic changes of m$^5$C regulators. **(B)** The alteration frequency of m$^5$C regulatory factors in gastrointestinal cancer from the TCGA database was analyzed in cBioPortal. The gene alteration frequencies of m$^5$C regulators in GI cancer was 2.4% in *NSUN1*, 4% in *NSUN2*, 1.8% in *NSUN5*, and 2.2% in *ALYREF*, etc. **(C)** Protein structure alteration (missense, truncating, and inframe mutation) was analyzed in GI cancers.

m$^5$C writers and reader was significantly related to overall survival (OS) (**Figure 4** and **Supplementary Table S1**). In this picture, we can find that except the *NSUN7* gene, the survival rates of other genes have significant differences in the different GI cancers. Among them, the *P* value of the *NSUN5* and *ALYREF* genes in colorectal cancer, liver cancer, and GC is less than 0.05, and the *NSUN6* gene also has significant differences in colorectal cancer, liver cancer, and PC. Remarkably, high expression of almost all m$^5$C regulators was significantly associated with shorter OS in HCC patients. These results suggest that m$^5$C regulators may play an important role in the survival of HCC patients.

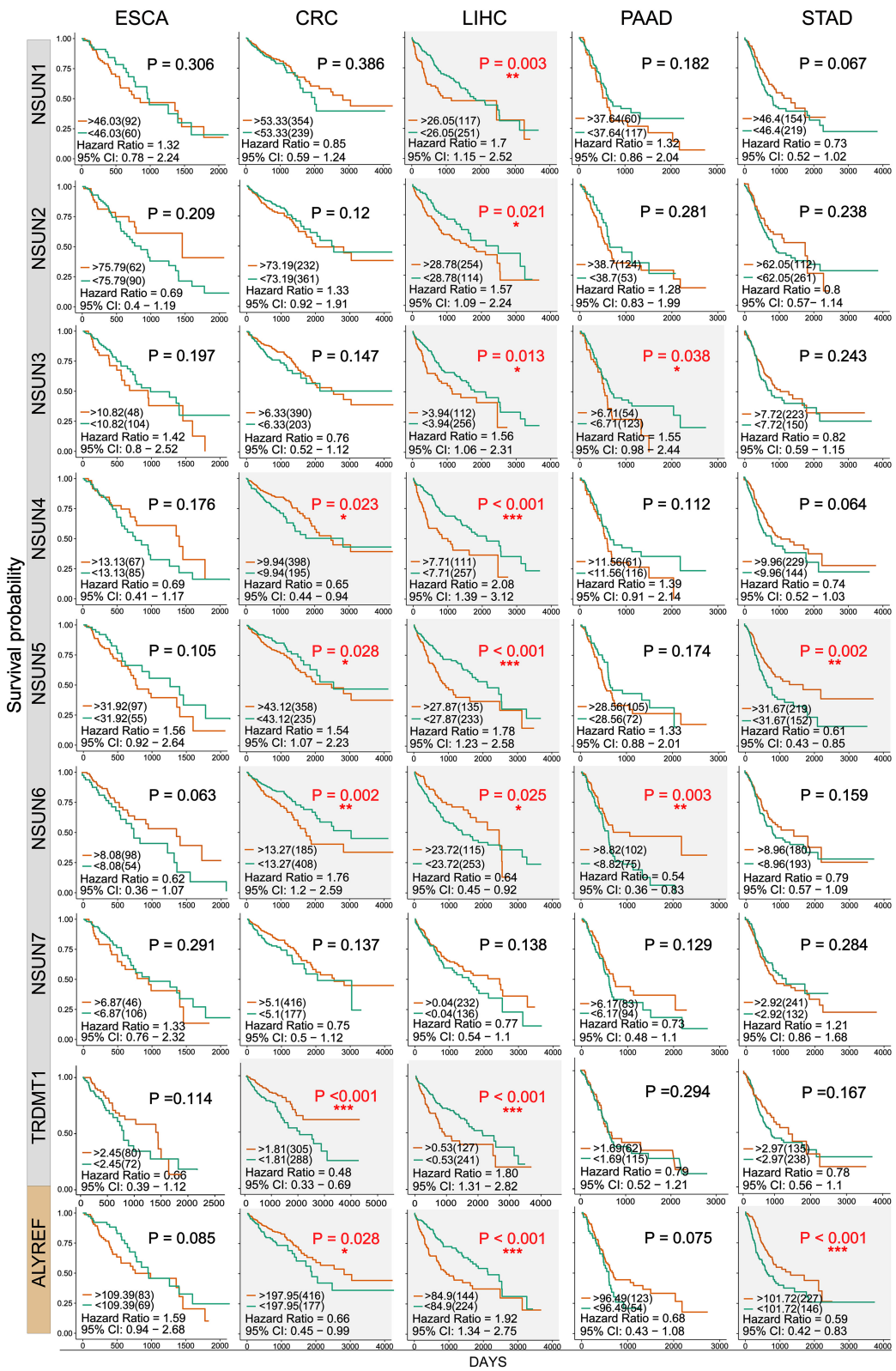


**FIGURE 4 |** Kaplan–Meier survival curves of m$^5$C regulatory factors in GI cancer. Kaplan–Meier survival curves were drawn based on the differential expression level of m$^5$C regulatory factors in GI cancer. The red and green curves showed survival curves of the high and low expression groups, respectively. *$P$ < 0.05, **$P$ < 0.01, and ***$P$ < 0.001 between the two groups.

## Association of m$^5$C Regulators With Clinicopathological Parameters

We investigated the association of m$^5$C regulator expression with gender (male and female), cancer status (tumor and normal), tumor grade (G1, G2, and G3), and pathological stage (stage I, stage II, stage III, and stage IV) as shown in **Table 1**. The results showed that the overall expression of m$^5$C writers was significantly associated with pathological stage and tumor differentiation grade and the expression of m$^5$C reader was significantly associated with gender, cancer status, and pathological stage. The association of respective m$^5$C regulator with these parameters is shown in **Figure 5**. The expression of *ALYREF* and *NSUN6* was significantly higher in female than in male patients. The level of *NSUN3* and *NSUN6* was increased in tumor samples, whereas the level of *ALYREF*, *NSUN5*, and *NSUN7* was decreased in tumor samples. For tumor grade, all m$^5$C regulators gradually increased from G1 to G3 except *NSUN6*, which showed an opposite trend of expression. Similar to the result for tumor grade, the expression of all m$^5$C regulators was elevated from pathological stage I to IV, except for *NSUN6* whose expression was lowered. We also performed the same analysis of the nine m$^5$C writers and readers in different types of GI cancer and liver cancer separately (**Supplementary Table S2**).

## Pathways Associated With m$^5$C Regulators

We further analyzed proteins that were altered upon m$^5$C regulator mutation (mutation, amplification, and deep deletion). Since data were not found in liver cancer, subsequent analysis was done in other four types of GI cancer. Proteins that showed significant changes ($P < 0.05$) were shown in the volcano map (**Figure 6A**). All the differential proteins were summarized in **Supplementary Table S3**. In order to know which pathway the differential proteins are enriched, we used DAVID for Kyoto Encyclopedia of Genes and Genomes (KEGG) proteins enrichment. According to the downstream gene count and *P* value, bubble plots were constructed in different types of GI cancer (**Figure 6B**). The *P* value and the number of genes are shown in this figure. More detailed data can be found in **Supplementary Tables S3** and **S4**. In addition, a heat map was constructed (**Figure 6C**) considering P values of different pathways. Among 34 pathways, we found some major pathways affected by m$^5$C regulators: ErbB, PI3K–Akt, HIF-1, and mTOR signaling pathways. Combining the bubble plots and heat map results, we conclude that the ErbB signaling pathway and PI3K–Akt signaling pathway are the most important downstream pathways of m$^5$C RNA methylation modification.

## Function and Interaction of Downstream Pathway Proteins

We analyzed the 54 differential proteins (**Supplementary Table S3**) that were enriched in the ErbB and PI3K–Akt signaling pathways by GO terms biological process enriched *via* DAVID. The result demonstrated that these proteins were mainly involved in the regulation of protein binding, cytosol, and signal transduction (**Figure 7A**). To further understand the interaction between these differential proteins and m$^5$C regulators, we mapped protein–protein interaction (PPI) networks. The results showed that *ALYREF* and *RPS6* were important connections between differential proteins and m$^5$C regulators (**Figure 7B**).

## *GSK3B* Is Closely Related to m$^5$C Regulators

In order to determine the importance of functional annotations between different proteins, we conducted analysis by using the R/Bioconductor package GOSemSim. According to the ranking results of importance, the results showed that among downstream pathway-associated proteins, *GSK3B* plays a crucial role in the three major categories of GO, including biological processes, cell components, and molecular functions. Other important proteins included AKT1S1, RAF1, ERBB2, SRC, MAPK3, MAP2K1, BRAF, AKT1, and MAPK1 (**Figure 8A**). Next, we used the expression level of these genes to map the correlation between

**TABLE 1 |** Association of m$^5$C mRNA expression with clinicopathological parameters of GI cancer patients.

| | | Writer | | | | Reader | | | |
|---|---|---|---|---|---|---|---|---|---|
| | | **High** | **Low** | **$\chi^2$** | ***P*** | **High** | **Low** | **$\chi^2$** | ***P*** |
| Gender | Male | 999 | 50 | 0.1591 | 0.6900 | 487 | 562 | 13.86 | **0.0002***** |
| | Female | 616 | 28 | | | 359 | 285 | | |
| Cancer status | Tumor | 842 | 48 | 3.321 | 0.0684 | 397 | 493 | 26.22 | **<0.0001***** |
| | Normal | 573 | 20 | | | 345 | 248 | | |
| Grade | G1 | 103 | 6 | | | 47 | 62 | | |
| | G2 | 438 | 14 | 22.57 | 0.4798 | 226 | 226 | 2.651 | 0.4147 |
| | G3 | 497 | 19 | | | 256 | 260 | | |
| Pathological stage | Stage I | 334 | 33 | 8.508 | **0.0366*** | 101 | 266 | 20.8 | **0.0001***** |
| | Stage II | 580 | 63 | | | 233 | 410 | | |
| | Stage III | 435 | 26 | | | 175 | 286 | | |
| | Stage IV | 133 | 7 | | | 67 | 73 | | |

**P < 0.05, **P < 0.01, and ***P < 0.001.*

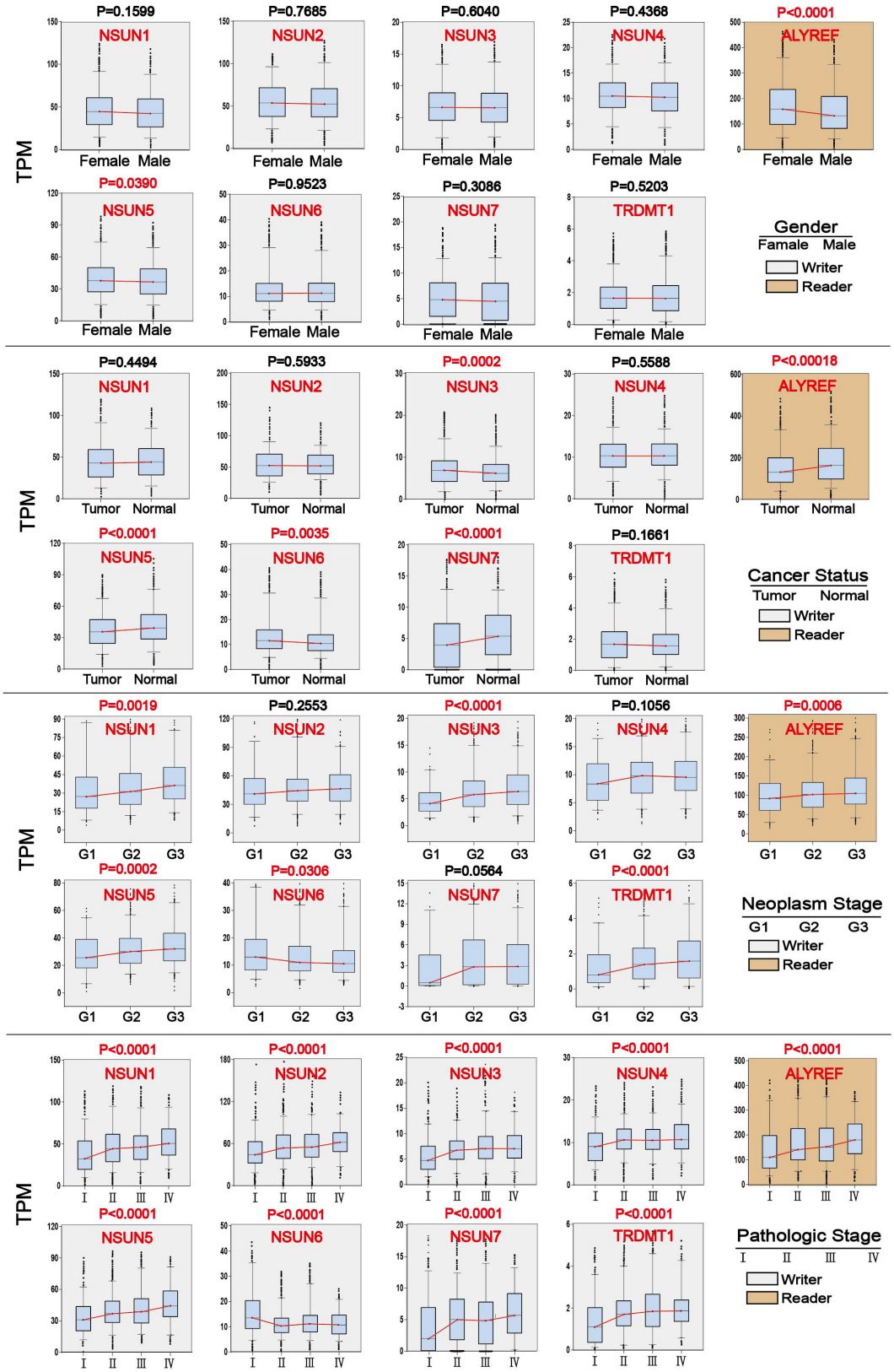


**FIGURE 5 |** Association of m$^5$C regulator expression with clinicopathological parameters in GI cancer. Clinical parameter analysis includes stage of tumor differentiation (G1, G2, and G3), pathological stage, and cancer status, and gender was analyzed by one-way ANOVA.

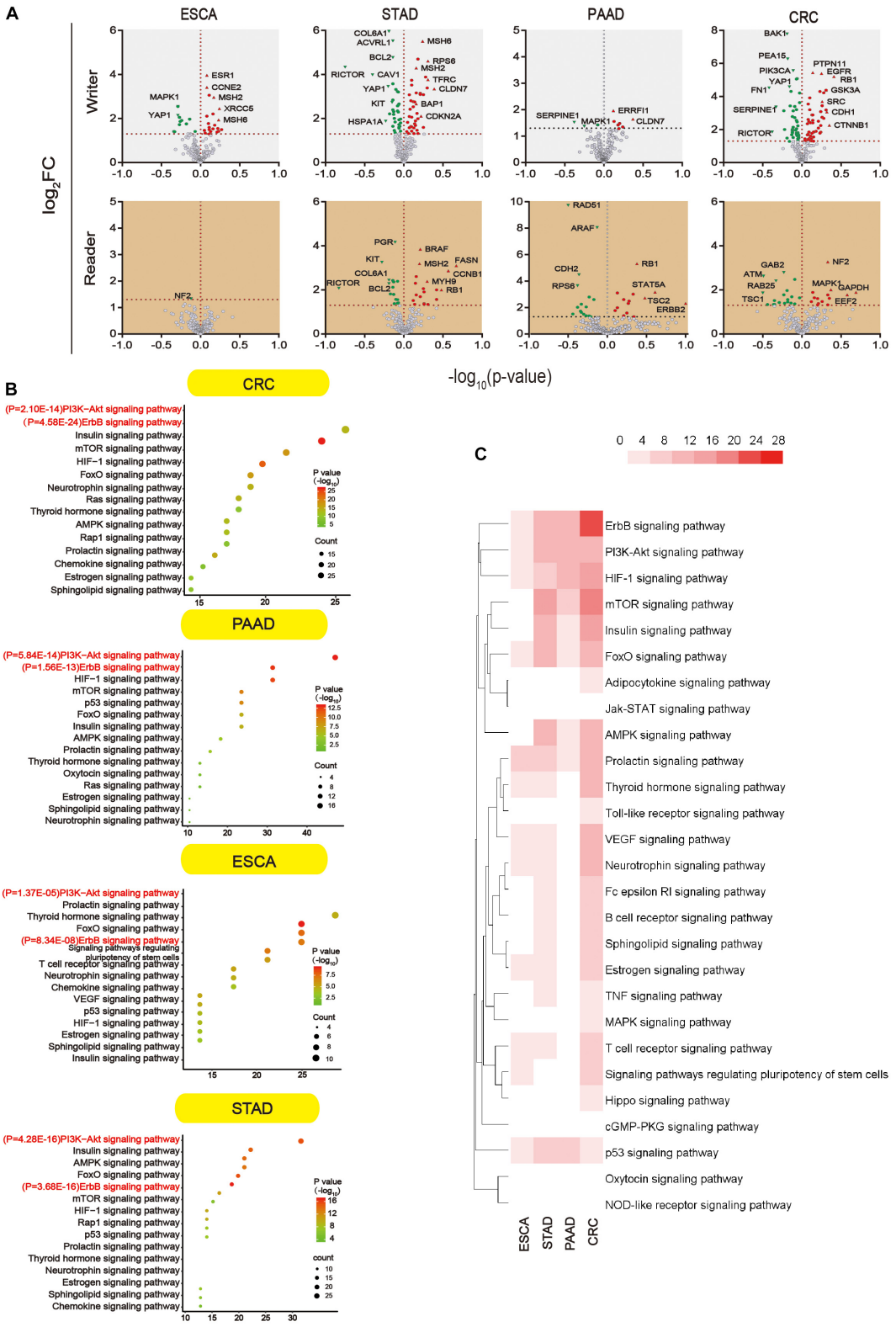


**FIGURE 6 |** Main signaling pathways affected by m$^5$C. **(A)** Volcano plot showing the proteins significantly affected by m$^5$C regulators mutation in GI cancer. -log$_{10}$ (*P* value) > 1.30 was considered a significant change. **(B)** Bubble plots showing the downstream pathways of m$^5$C based on gene count and *P* value. Prediction of the downstream pathways related to m$^5$C gene alterations was analyzed by KEGG pathway analysis *via* DAVID. **(C)** Heat map showing the important downstream pathways of m$^5$C in GI cancers based on *P* value.

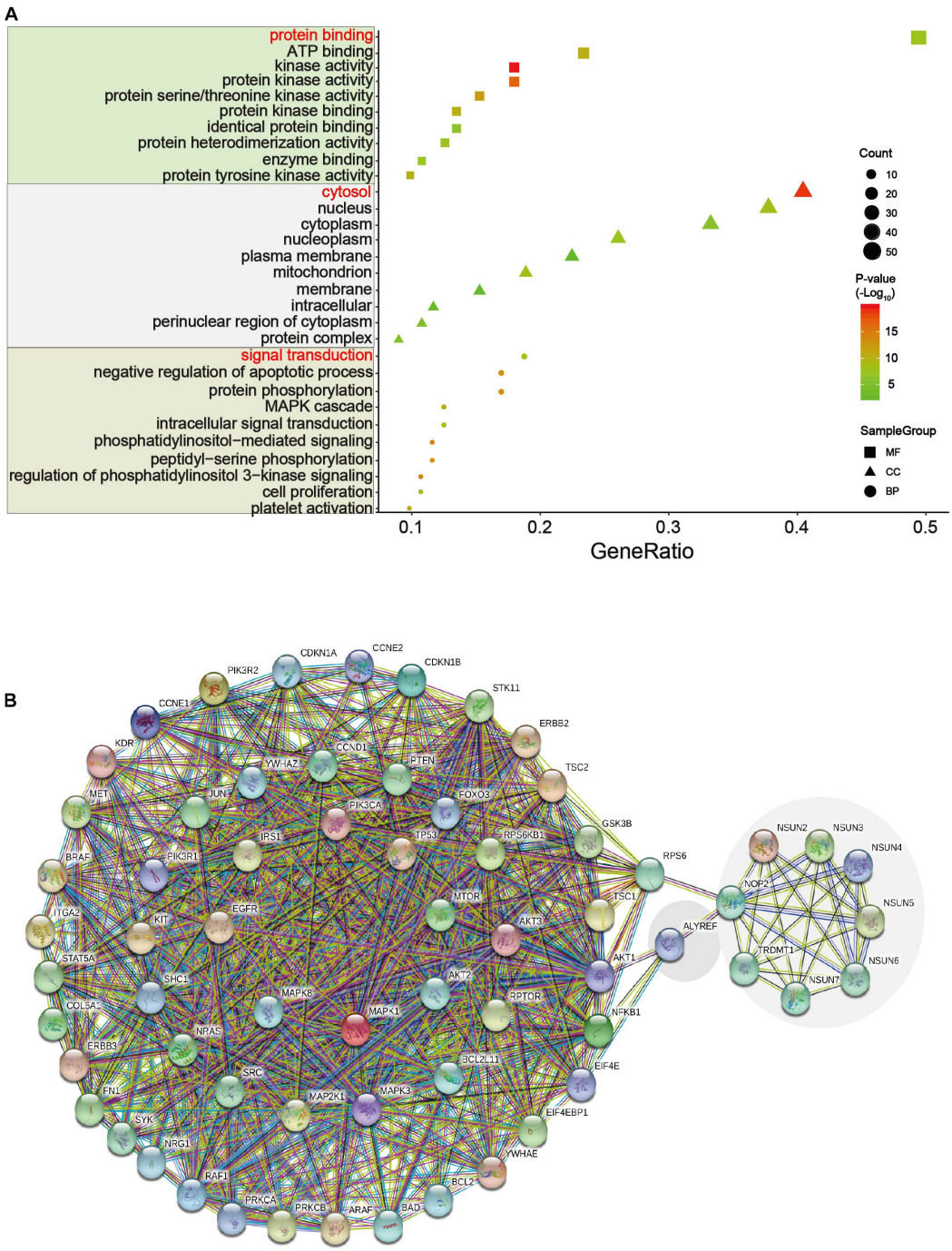


**FIGURE 7 |** GO and network analysis of proteins in two important pathways. **(A)** Gene Ontology (GO) enrichment analysis of the m$^5$C RNA methylation modification was analyzed *via* DAVID. GO contains biological processes, cell components, and molecular functions. In this picture, count represents the number of genes contained in the GO term. The count and *P* values were considered together to obtain important metabolic process. Three important metabolic processes are affected by m$^5$C RNA methylation, including protein binding, cytosol, and signal transduction. **(B)** Multicenter protein–protein interaction (PPI) network between m$^5$C regulatory proteins and differential proteins in the ErbB and PI3K–Akt pathways in the STRING database.

them. The results showed that *GSK3B* was positively correlated with most genes (**Figure 8B**). Then, we analyzed the correlation of GSK3B with m$^5$C regulators (**Figure 8C**). The result showed that *GSK3B* was significantly and positively correlated with all m$^5$C regulators except for *NSUN6* for which it showed negative correlation, indicating that *GSK3B* protein may be closely related to m$^5$C writer and reader. In the human disease methylation database (DiseaseMeth version 2.0), we found that *GSK3B* is not

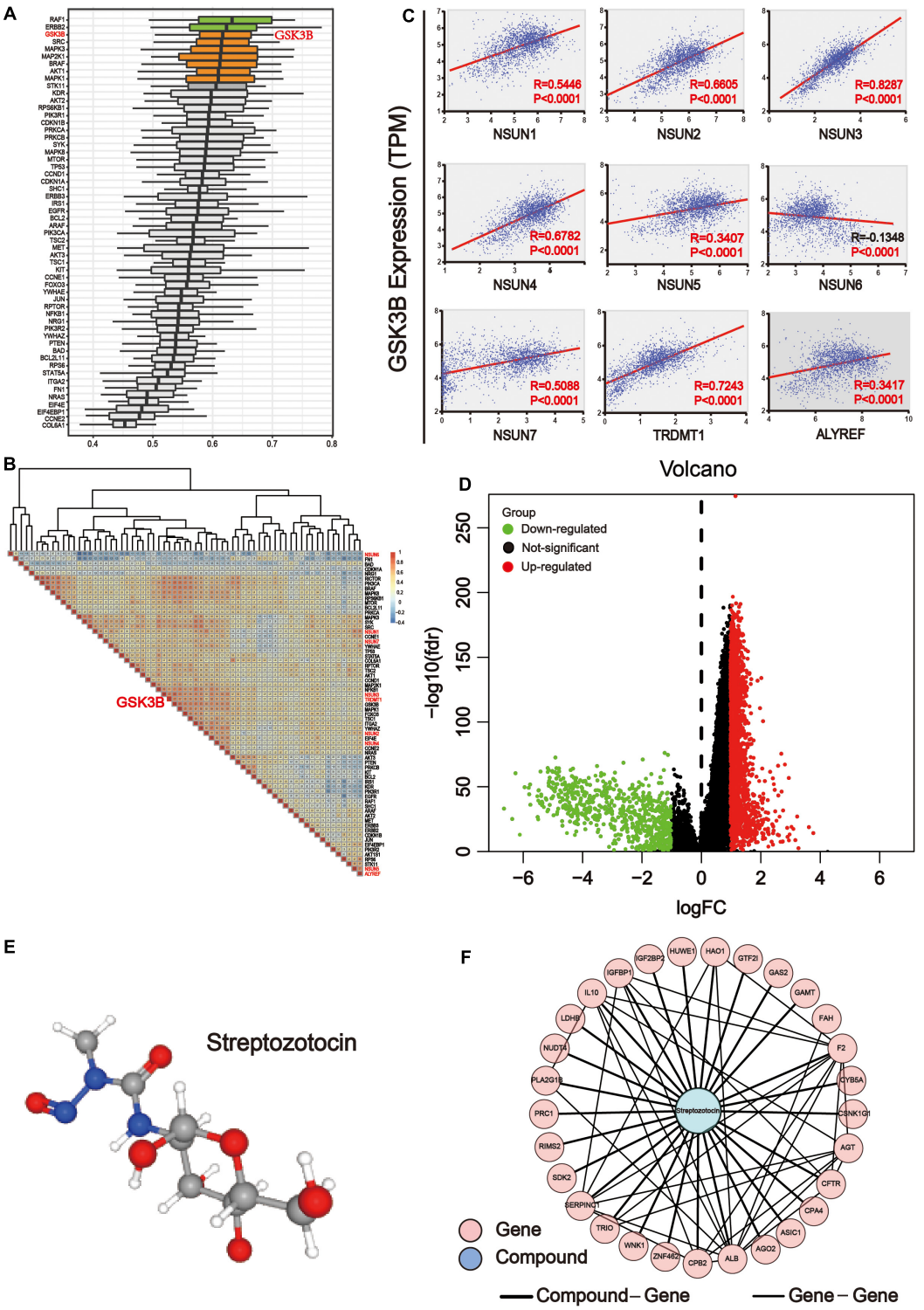


**FIGURE 8 |** GSK3B is closely related to m$^5$C regulators. **(A)** The importance of key proteins of the downstream pathway in the three major categories of Gene Ontology (GO), including biological processes, cell components, and molecular functions. The *X* axis is the score obtained by comprehensively considering the weight of the three categories of GO. The higher the score, the more important the protein is involved in the GO project. **(B)** Co-expression analysis of m$^5$C differential proteins of the ErbB and PI3K–Akt pathways. The co-expression scores of related genes were displayed. The color intensity reflects the reliability of co-expression; meanwhile, red and blue indicate high correlation and low correlation, respectively. **(C)** Correlation analysis between writers and reader protein of m$^5$C with *GSK3B*. There were significant differences between GSK3B and all genes. **(D)** The samples were grouped according to the median expression of GSK3B gene, and differential expression analysis was performed. **(E)** 3D structure of streptozotocin. **(F)** PPI network analysis between the common genes between streptozotocin.

influenced by DNA methylation in GI cancer (**Supplementary Figure S2**). In conclusion, we believe that m$^5$C writer and reader mainly affect genes in the ErbB/PI3K–Akt signaling pathway, and that *GSK3B* may be an important downstream target of m$^5$C regulators.

## Network Pharmacology Analysis of the *GSK3B* Gene in GI Cancer

The transcriptome data of GI cancer were integrated, and tumor samples were divided into the high and low expression groups according to the median level of the *GSK3B* gene expression. In total, 2,071 significantly up-regulated and 695 significantly down-regulated genes were identified (**Figure 8D**). In order to find the probable drug targeting the *GSK3B* gene *via* the CMap database, we screened the first 150 genes in the up-regulated and down-regulated genes, respectively. Streptozotocin was the highest score in the prediction. Next, the PubChem database was applied to obtain the 3D structure of streptozotocin (**Figure 8E**). Next, 280 target genes were gained through the PharmMapper database. Then, we chose the common genes between 274 drug targets and 2,766 differential genes of the *GSK3B* gene, and finally, 29 genes were used for PPI network with this compound on streptozotocin, including *HUWE1*, *AGT*, *HAO1*, *CPB2*, *WNK1*, *CPA4*, *ZNF462*, *RIMS2*, *GAS2*, *CFTR*, *PLA2G1B*, *F2*, *SERPINC1*, *TRIO*, *FAH*, *CSNK1G1*, *AGO2*, *PRC1*, *ASIC1*, *CYB5A*, *GTF2I*, *IL10*, *IGFBP1*, *SDK2*, *GAMT*, *LDHB*, *ALB*, *NUDT4*, and *IGF2BP2* (**Figure 8F**).

# DISCUSSION

5-Methylcytosine modifications of RNA are ubiquitous in nature and play important roles in many biological processes, such as protein translational regulation, RNA processing, and stress response (Hussain et al., 2013; Yuan et al., 2014; Liu et al., 2017); RNA stability (Tuorto et al., 2012; Zhang et al., 2012); RNA transport (Yang X. et al., 2017); and mRNA translation (Tang et al., 2015; Xing et al., 2015; Sun et al., 2019). Currently, the modification mechanism of m$^5$C in cancer is being explored. Nonetheless, the exact catalytic mechanism of m$^5$C methylation remained unclear (Li Q. et al., 2017; Liu et al., 2017; Trixl and Lusser, 2019). Herein, we conducted a comprehensive analysis of known m$^5$C writers (*NSUN1-7* and *TRDMT1*) and reader (*ALYREF*) in GI cancer. Overall, the expression level of m$^5$C regulators was distinctly different across all samples (**Figure 2A**). Notably, the expression of *NSUN1*, *NSUN3*, *NSUN4*, *NSUN5*, and *ALYREF* was all significantly elevated in GI cancer (**Figure 2B**). Meanwhile, the genomic and protein structure alterations of m$^5$C regulators were also determined (**Figure 3**). Overall, the mutation rate of m$^5$C regulators in GI cancer was not high, and it was relatively higher in esophagus and stomach cancers than in other cancers (**Figures 3A,B**). The mutation rate for *NSUN2* was the highest. In accordance with our finding, copy number gain of *NSUN2* has been reported in breast, oral, and colorectal cancers (Frye et al., 2010; Okamoto et al., 2012), which leads to the increased expression of it in cancers. Alteration in protein structure was seen in all m$^5$C regulators (**Figure 3C**). There were more protein alteration sites in *NSUN1* and *NSUN2* than in other regulators, whereas there was only one alteration site in *ALYREF*. Although study on the role of m$^5$C regulatory proteins in cancer was very limited, *NSUN2* was relatively well-studied among m$^5$C regulators. There were a few reports on the elevated expression of *NSUN2* in a range of cancer, including oral (Okamoto et al., 2012), head and neck (Lu et al., 2018), colorectal (Okamoto et al., 2012), breast (Frye et al., 2010; Yi et al., 2017), ovarian (Yang J. C.et al., 2017), and GI cancers (Okamoto et al., 2012), which was consistent with our bioinformatics analysis. *TDMT1*/*DNMT2*, a member of DNA methyltransferases, was shown to be down-regulated in liver (Saito et al., 2001), stomach, and colorectal cancers (Kanai et al., 2001). In contrast, it was significantly over-expressed in stomach and liver cancers from our study and decreased in PC (**Figure 2B**).

Next, we used clinical information to evaluate the association of m$^5$C regulator expression with patient survival and clinicopathological parameters. Notably, high expression of almost all m$^5$C regulators was significantly associated with shorter OS in HCC patients except *NSUN7*, indicating that dysregulation of m$^5$C regulators may strongly influence liver cancer patient survival (**Figure 4** and **Supplementary Table S1**). High expression of *NSUN2* has been reported to predict poor survival in head and neck cancer (Lu et al., 2018). It was only found to be associated with shorter survival in liver cancer from our study. For clinicopathological parameters, consistent with previous result (**Figure 2B**), the level of *NSUN3* and *NSUN6* was increased in tumor samples versus normal samples (**Figure 5**). For tumor grade, the expression of m$^5$C regulators increased from G1 to G3 except *NSUN6*, which showed an opposite trend of expression. The result for pathological grade was similar to that for tumor grade. The expression of all m$^5$C regulators was elevated from pathological stage I to IV, except for *NSUN6* whose expression was decreased (**Figure 5**). Similar to our result, *NSUN2* has been found to be significantly correlated with clinical stage and pathological differentiation in breast cancer (Yi et al., 2017).

In an attempt to find out the major targets or pathways modulated by m$^5$C regulators, we first determined proteins that were significantly altered upon m$^5$C regulator gene alteration. The results demonstrated that alteration in m$^5$C regulators led to the decreased expression of oncogenic YAP1 and RICTOR and increased expression of DNA mismatch repair proteins MSH2 and MSH6 (**Figure 6A**). We then further determined which signaling pathways these differential proteins mainly belong to. By taking the gene count and P value into account, we found that PI3K–Akt and ErbB were the most important pathways affected by m$^5$C regulators among other pathways including the mTOR and HIF-1 pathways (**Figures 6B,C**). The differential proteins in the PI3K–Akt and ErbB pathways play important roles in regulating protein binding, cytosol, and signal transduction from GO analysis (**Figure 7A**). The PI3K–Akt and ErbB pathways are important cancer-related pathways. Studies have shown that the ErbB signaling pathway is regulated by miR-200a/141 in the epithelial–mesenchymal transition (EMT)-related microRNA-200 family in renal cell carcinoma (RCC) (Yoshino et al., 2013). At the same time, accumulating evidence has elucidated that the PI3K–Akt signaling pathway is highly activated (Guo et al., 2015; Hao et al., 2019) and is a validated

therapeutic target in RCC (Lin et al., 2014). Key miRNAs and target genes have been reported to be mainly related to the PI3K–Akt signaling pathway in GI cancers (Lai et al., 2019). A bioinformatics analysis showed that the DEGs of EC compared with normal tissues are mainly enriched in the PI3K–Akt signaling pathway (Li M. et al., 2020; Yu-Jing et al., 2020). Moreover, GLI1 co-expressed and DEGs between tumor samples and normal tissues were both largely enriched in the PI3K–Akt pathway in STAD (Yu et al., 2018; Li et al., 2019). In PAAD, 4-miRNA as independent prognostic factor was found to be related to the PI3K–Akt signaling pathway (Wang et al., 2019). Growing evidence revealed that the ErbB and PI3K–Akt signaling pathways play vital roles in colorectal cancer by regulating microRNA, lncRNA, mRNA, etc. (Szmida et al., 2015; Song et al., 2018; Wei et al., 2019; Zhong et al., 2019; Wan et al., 2020). These findings indicate that GI cancer is closely related to the ErbB and PI3K–Akt signaling pathways. By visualizing the PPI network of $m^5C$ regulators and their potential downstream targets in the PI3K–Akt and ErbB pathways, we found that $m^5C$ regulators formed a group and were closely connected with the differential protein group by NOP2, ALYREF, and RPS6 (**Figure 7B**).

Further analysis revealed that *GSK3B* was an important potential target for $m^5C$ regulators (**Figure 8**). It showed strong association with $m^5C$ regulators (**Figure 8B**) and differential proteins and was also important in GO biological processes (**Figure 8A**). Importantly, *GSK3B* was significantly and positively associated with nearly all $m^5C$ regulators, whereas it was negatively correlated with NSUN6, indicating that it probably is a downstream target of $m^5C$ regulators (**Figure 8C**). In order to further explore the targeted drugs of the *GSK3B* gene in GI cancer, we divided the tumor samples into two groups based on the median GSK3B expression level for differential expression analysis (**Figure 8D**). The first 150 genes were selected from the significantly up-regulated and down-regulated differential genes, respectively, for potential drug target analysis. The results showed that streptozotocin (P-selectin inhibitor) was used for further analysis with the highest score of 96.16 (**Figure 8E**). Next, the targeted gene of the compound on streptozotocin was identified *via* the PharmMapper database, then we found 29 common genes of the gene target and GSK3B differential genes, and PPI network was used to display the relationship of 29 genes and the streptozotocin (**Figure 8F**). *GSK3B* has been shown to be frequently up-regulated in many types of cancer (Darrington et al., 2012; T. Zhang et al., 2019), and inhibition of it was considered efficient in suppressing tumor growth (Edderkaoui et al., 2018; Wu et al., 2019). Moreover, there have been many studies on GSK3B inhibitors, including Metavert molecule in PAAD (Edderkaoui et al., 2018), BT-000775 molecule in BRCA (Ogunleye et al., 2019), BIO molecule in TNBCs (triple-negative breast cancers) (Vijay et al., 2019), AR-A014418 and SB-216763 molecules in STSs (soft tissue sarcomas) (Abe et al., 2020), etc.

In summary, our study demonstrated for the first time the comprehensive analysis of $m^5C$ modulators in GI cancer. The dysregulation of $m^5C$ regulators in GI cancer was shown, its association with patient survival and clinicopathological parameters were analyzed, and the main downstream pathway and major target were determined. Besides, the compound termed streptozotocin may be a key candidate drug for targeted therapy in GI cancer. This is a pioneer study of the relationship between $m^5C$ dysregulation and cancer, but our results lack experimental verification, which warrants further validation of the involvement of $m^5C$ regulators and their downstream targets in GI cancer.

## DATA AVAILABILITY STATEMENT

The original contributions presented in the study are included in the article/**Supplementary Material**, further inquiries can be directed to the corresponding author/s.

## AUTHOR CONTRIBUTIONS

SX, YM, and QW analyzed the data and wrote the manuscript. JS, ZX, and QW provided funding. YSZ, XW, and ML designed the study. PK and YZ prepared and adjusted the figures. XY, XL, and JL reviewed and revised the manuscript. All authors contributed to the article and approved the submitted version.

## FUNDING

This work was supported by the National Natural Science Foundation of China (Grant nos. 81602166 and 81672444) and Sichuan Science and Technology Plan Project (2018JY0079).

## SUPPLEMENTARY MATERIAL

The Supplementary Material for this article can be found online at: https://www.frontiersin.org/articles/10.3389/fmolb.2020.599340/full#supplementary-material

**Supplementary Figure 1 |** PCA analysis of GI cancer. Principal component analysis of liver cancer, colorectal cancer, gastric cancer, pancreatic cancer, and esophageal cancer according to genes expression level. *N* = 1,695 data points. *X* and *Y* axes show principal component 1 and principal component 2 that explain 39.5 and 16.4% of the total variance, respectively. Prediction ellipses are such that with probability 0.95, a new observation from the same group will fall inside the ellipse. The further apart the two samples are, the greater the difference in genetic background between them will be.

**Supplementary Figure 2 |** DNA methylation analysis of differential genes in GI cancer. DNA methylation analysis of key downstream pathways in GI cancer. The darker the blue, the lower the DNA methylation, and the darker the red, the higher the DNA methylation.

**Supplementary Table 1 |** Survival curve data of $m^5C$ writer and reader in GI cancer.

**Supplementary Table 2 |** The data of Chi-square analysis on cancer status (tumor and normal), pathological stage (stage I, stage II, stage III, and stage IV), gender (male and female), and tumor differentiation (G1, G2, and G3) in different types of GI cancer and liver cancer separately.

**Supplementary Table 3 |** Differential proteins in important pathways.

**Supplementary Table 4 |** The data of different pathways in GI cancer.

## REFERENCES


Abbasi-Moheb, L., Mertel, S., Gonsior, M., Nouri-Vahid, L., Kahrizi, K., Cirak, S., et al. (2012). Mutations in NSUN2 cause autosomal-recessive intellectual disability. *Am. J. Hum. Genet.* 90, 847–855. doi: 10.1016/j.ajhg.2012.03.021

Abe, K., Yamamoto, N., Domoto, T., Bolidong, D., Hayashi, K., Takeuchi, A., et al. (2020). Glycogen synthase kinase 3beta as a potential therapeutic target in synovial sarcoma and fibrosarcoma. *Cancer Sci.* 111, 429–440. doi: 10.1111/cas.14271

Aslan, A., Vrabiescu, A., and Busila, V. (1967). [Studies of peripheral circulation with the postural oscillometric method in a group of aged persons treated with potentiated Gerovital H]. *Fiziol. Norm. Patol.* 13, 561–566.

Bilgin, B., Sendur, M. A., Bulent Akinci, M., Sener Dede, D., and Yalcin, B. (2017). Targeting the PD-1 pathway: a new hope for gastrointestinal cancers. *Curr. Med. Res. Opin.* 33, 749–759. doi: 10.1080/03007995.2017.1279132

Blanco, S., Bandiera, R., Popis, M., Hussain, S., Lombard, P., Aleksic, J., et al. (2016). Stem cell function and stress response are controlled by protein synthesis. *Nature* 534, 335–340. doi: 10.1038/nature18282

Cai, X., Hu, Y., Tang, H., Hu, H., Pang, L., Xing, J., et al. (2016). RNA methyltransferase NSUN2 promotes stress-induced HUVEC senescence. *Oncotarget* 7, 19099–19110. doi: 10.18632/oncotarget.8087

Cerami, E., Gao, J., Dogrusoz, U., Gross, B. E., Sumer, S. O., Aksoy, B. A., et al. (2012). The cBio cancer genomics portal: an open platform for exploring multidimensional cancer genomics data. *Cancer Discov.* 2, 401–404. doi: 10.1158/2159-8290.CD-12-0095

Chan, B. K. C. (2018). Data analysis using r programming. *Adv. Exp. Med. Biol.* 1082, 47–122. doi: 10.1007/978-3-319-93791-5_2

Darrington, R. S., Campa, V. M., Walker, M. M., Bengoa-Vergniory, N., Gorrono-Etxebarria, I., Uysal-Onganer, P., et al. (2012). Distinct expression and activity of GSK-3alpha and GSK-3beta in prostate cancer. *Int. J. Cancer* 131, E872–E883. doi: 10.1002/ijc.27620

Dennis, G. Jr., Sherman, B. T., Hosack, D. A., Yang, J., Gao, W., Lane, H. C., et al. (2003). DAVID: database for annotation, visualization, and integrated discovery. *Genome Biol.* 4:3.

Edderkaoui, M., Chheda, C., Soufi, B., Zayou, F., Hu, R. W., Ramanujan, V. K., et al. (2018). An Inhibitor of GSK3B and HDACs kills pancreatic cancer cells and slows pancreatic tumor growth and metastasis in mice. *Gastroenterology* 155, 1985.e5–1998.e5. doi: 10.1053/j.gastro.2018.08.028

Frye, M., Dragoni, I., Chin, S. F., Spiteri, I., Kurowski, A., Provenzano, E., et al. (2010). Genomic gain of 5p15 leads to over-expression of Misu (NSUN2) in breast cancer. *Cancer Lett.* 289, 71–80. doi: 10.1016/j.canlet.2009.08.004

Gao, J., Aksoy, B. A., Dogrusoz, U., Dresdner, G., Gross, B., Sumer, S. O., et al. (2013). Integrative analysis of complex cancer genomics and clinical profiles using the cBioPortal. *Sci. Signal.* 6:l1. doi: 10.1126/scisignal.2004088

Guo, H., German, P., Bai, S., Barnes, S., Guo, W., Qi, X., et al. (2015). The PI3K/AKT pathway and renal cell carcinoma. *J. Genet. Genomics* 42, 343–353. doi: 10.1016/j.jgg.2015.03.003

Haag, S., Warda, A. S., Kretschmer, J., Gunnigmann, M. A., Hobartner, C., and Bohnsack, M. T. (2015). NSUN6 is a human RNA methyltransferase that catalyzes formation of m5C72 in specific tRNAs. *RNA* 21, 1532–1543. doi: 10.1261/rna.051524.115

Hao, P., Kang, B., Li, Y., Hao, W., and Ma, F. (2019). UBE2T promotes proliferation and regulates PI3K/Akt signaling in renal cell carcinoma. *Mol. Med. Rep.* 20, 1212–1220. doi: 10.3892/mmr.2019.10322

Hong, J., Lee, J. H., and Chung, I. K. (2016). Telomerase activates transcription of cyclin D1 gene through an interaction with NOL1. *J. Cell. Sci.* 129, 1566–1579. doi: 10.1242/jcs.181040

Hussain, S., Sajini, A. A., Blanco, S., Dietmann, S., Lombard, P., Sugimoto, Y., et al. (2013). NSun2-mediated cytosine-5 methylation of vault noncoding RNA determines its processing into regulatory small RNAs. *Cell. Rep.* 4, 255–261. doi: 10.1016/j.celrep.2013.06.029

Jacob, R., Zander, S., and Gutschner, T. (2017). The dark side of the epitranscriptome: chemical modifications in long non-coding RNAs. *Int. J. Mol. Sci.* 18:2387. doi: 10.3390/ijms18112387

Jeltsch, A., Ehrenhofer-Murray, A., Jurkowski, T. P., Lyko, F., Reuter, G., Ankri, S., et al. (2017). Mechanism and biological role of Dnmt2 in nucleic acid methylation. *RNA Biol.* 14, 1108–1123. doi: 10.1080/15476286.2016.1191737

Jensen, L. J., Kuhn, M., Stark, M., Chaffron, S., Creevey, C., Muller, J., et al. (2009). STRING 8–a global view on proteins and their functional interactions in 630 organisms. *Nucleic Acids Res.* 37, D412–D416. doi: 10.1093/nar/gkn760

Jonkhout, N., Tran, J., Smith, M. A., Schonrock, N., Mattick, J. S., and Novoa, E. M. (2017). The RNA modification landscape in human disease. *RNA* 23, 1754–1769. doi: 10.1261/rna.063503.117

Kanai, Y., Ushijima, S., Kondo, Y., Nakanishi, Y., and Hirohashi, S. (2001). DNA methyltransferase expression and DNA methylation of CPG islands and peri-centromeric satellite regions in human colorectal and stomach cancers. *Int. J. Cancer* 91, 205–212. doi: 10.1002/1097-0215(200002)9999:9999<::aid-ijc1040>3.0.co;2-2

Khosronezhad, N., Hosseinzadeh Colagar, A., and Mortazavi, S. M. (2015). The Nsun7 (A11337)-deletion mutation, causes reduction of its protein rate and associated with sperm motility defect in infertile men. *J. Assist. Reprod. Genet.* 32, 807–815. doi: 10.1007/s10815-015-0443-0

Kosi, N., Alic, I., Kolacevic, M., Vrsaljko, N., Jovanov Milosevic, N., Sobol, M., et al. (2015). Nop2 is expressed during proliferation of neural stem cells and in adult mouse and human brain. *Brain Res.* 1597, 65–76. doi: 10.1016/j.brainres.2014.11.040

Lai, C. H., Liang, X. Z., Liang, X. Y., Ma, S. J., Li, J. G., Shi, M. F., et al. (2019). Study on miRNAs in pan-cancer of the digestive tract based on the illumina HiSeq system data sequencing. *Biomed. Res. Int.* 2019:8016120. doi: 10.1155/2019/8016120

Lamb, J., Crawford, E. D., Peck, D., Modell, J. W., Blat, I. C., Wrobel, M. J., et al. (2006). The Connectivity Map: using gene-expression signatures to connect small molecules, genes, and disease. *Science* 313, 1929–1935. doi: 10.1126/science.1132939

Li, D., Xiang, S., Shen, J., Xiao, M., Zhao, Y., Wu, X., et al. (2020). Comprehensive understanding of B7 family in gastric cancer: expression profile, association with clinicopathological parameters and downstream targets. *Int. J. Biol. Sci.* 16, 568–582. doi: 10.7150/ijbs.39769

Li, L., Zhu, Z., Zhao, Y., Zhang, Q., Wu, X., Miao, B., et al. (2019). FN1, SPARC, and SERPINE1 are highly expressed and significantly related to a poor prognosis of gastric adenocarcinoma revealed by microarray and bioinformatics. *Sci. Rep.* 9:7827. doi: 10.1038/s41598-019-43924-x

Li, M., Wang, K., Pang, Y., Zhang, H., Peng, H., Shi, Q., et al. (2020). Secreted phosphoprotein 1 (SPP1) and fibronectin 1 (FN1) are associated with progression and prognosis of esophageal cancer as identified by integrated expression profiles analysis. *Med. Sci. Monit.* 26:e920355. doi: 10.12659/MSM.920355

Li, Q., Li, X., Tang, H., Jiang, B., Dou, Y., Gorospe, M., et al. (2017). NSUN2-mediated m5C methylation and METTL3/METTL14-mediated m6A methylation cooperatively enhance p21 translation. *J. Cell Biochem.* 118, 2587–2598. doi: 10.1002/jcb.25957

Li, W., Zhang, X., Lu, X., You, L., Song, Y., Luo, Z., et al. (2017). 5-Hydroxymethylcytosine signatures in circulating cell-free DNA as diagnostic biomarkers for human cancers. *Cell. Res.* 27, 1243–1257. doi: 10.1038/cr.2017.121

Lin, A., Piao, H. L., Zhuang, L., Sarbassov dos, D., Ma, L., and Gan, B. (2014). FoxO transcription factors promote AKT Ser473 phosphorylation and renal tumor growth in response to pharmacologic inhibition of the PI3K-AKT pathway. *Cancer Res.* 74, 1682–1693. doi: 10.1158/0008-5472.CAN-13-1729

Liu, J., and Jia, G. (2014). Methylation modifications in eukaryotic messenger RNA. *J. Genet. Genomics* 41, 21–33. doi: 10.1016/j.jgg.2013.10.002

Liu, R. J., Long, T., Li, J., Li, H., and Wang, E. D. (2017). Structural basis for substrate binding and catalytic mechanism of a human RNA:m5C methyltransferase NSun6. *Nucleic Acids Res.* 45, 6684–6697. doi: 10.1093/nar/gkx473

Liu, X., Ouyang, S., Yu, B., Liu, Y., Huang, K., Gong, J., et al. (2010). PharmMapper server: a web server for potential drug target identification using pharmacophore mapping approach. *Nucleic Acids Res.* 38, W609–W614. doi: 10.1093/nar/gkq300

Lu, L., Zhu, G., Zeng, H., Xu, Q., and Holzmann, K. (2018). High tRNA transferase NSUN2 gene expression is associated with poor prognosis in head and neck squamous carcinoma. *Cancer Invest.* 36, 246–253. doi: 10.1080/07357907.2018.1466896

Metodiev, M. D., Spahr, H., Loguercio Polosa, P., Meharg, C., Becker, C., Altmueller, J., et al. (2014). NSUN4 is a dual function mitochondrial protein required for both methylation of 12S rRNA and coordination of mitoribosomal assembly. *PLoS Genet.* 10:e1004110. doi: 10.1371/journal.pgen.1004110

Motorin, Y., Lyko, F., and Helm, M. (2010). 5-methylcytosine in RNA: detection, enzymatic formation and biological functions. *Nucleic Acids Res.* 38, 1415–1430. doi: 10.1093/nar/gkp1117

Nakano, S., Suzuki, T., Kawarada, L., Iwata, H., Asano, K., and Suzuki, T. (2016). NSUN3 methylase initiates 5-formylcytidine biogenesis in human mitochondrial tRNA(Met). *Nat. Chem. Biol.* 12, 546–551. doi: 10.1038/nchembio.2099

Oerum, S., Degut, C., Barraud, P., and Tisne, C. (2017). m1A post-transcriptional modification in tRNAs. *Biomolecules* 7:20. doi: 10.3390/biom7010020

Ogunleye, A. J., Olanrewaju, A. J., Arowosegbe, M., and Omotuyi, O. I. (2019). Molecular docking based screening analysis of GSK3B. *Bioinformation* 15, 201–208. doi: 10.6026/97320630015201

Okamoto, M., Hirata, S., Sato, S., Koga, S., Fujii, M., Qi, G., et al. (2012). Frequent increased gene copy number and high protein expression of tRNA (cytosine-5-)-methyltransferase (NSUN2) in human cancers. *DNA Cell Biol.* 31, 660–671. doi: 10.1089/dna.2011.1446

Saito, Y., Kanai, Y., Sakamoto, M., Saito, H., Ishii, H., and Hirohashi, S. (2001). Expression of mRNA for DNA methyltransferases and methyl-CpG-binding proteins and DNA methylation status on CpG islands and pericentromeric satellite regions during human hepatocarcinogenesis. *Hepatology* 33, 561–568. doi: 10.1053/jhep.2001.22507

Schaefer, M., and Lyko, F. (2010). Solving the Dnmt2 enigma. *Chromosoma* 119, 35–40. doi: 10.1007/s00412-009-0240-6

Schosserer, M., Minois, N., Angerer, T. B., Amring, M., Dellago, H., Harreither, E., et al. (2015). Methylation of ribosomal RNA by NSUN5 is a conserved mechanism modulating organismal lifespan. *Nat. Commun.* 6:6158. doi: 10.1038/ncomms7158

Shannon, P., Markiel, A., Ozier, O., Baliga, N. S., Wang, J. T., Ramage, D., et al. (2003). Cytoscape: a software environment for integrated models of biomolecular interaction networks. *Genome Res.* 13, 2498–2504. doi: 10.1101/gr.1239303

Song, Y., Zhao, Y., Ding, X., and Wang, X. (2018). microRNA-532 suppresses the PI3K/Akt signaling pathway to inhibit colorectal cancer progression by directly targeting IGF-1R. *Am. J. Cancer Res.* 8, 435–449.

Squires, J. E., Patel, H. R., Nousch, M., Sibbritt, T., Humphreys, D. T., Parker, B. J., et al. (2012). Widespread occurrence of 5-methylcytosine in human coding and non-coding RNA. *Nucleic Acids Res.* 40, 5023–5033. doi: 10.1093/nar/gks144

Subramanian, A., Narayan, R., Corsello, S. M., Peck, D. D., Natoli, T. E., Lu, X., et al. (2017). A next generation connectivity map: L1000 platform and the first 1,000,000 profiles. *Cell* 171, 1437.e17–1452.e17. doi: 10.1016/j.cell.2017.10.049

Sun, Z., Xue, S., Xu, H., Hu, X., Chen, S., Yang, Z., et al. (2019). Effects of NSUN2 deficiency on the mRNA 5-methylcytosine modification and gene expression profile in HEK293 cells. *Epigenomics* 11, 439–453. doi: 10.2217/epi-2018-0169

Szmida, E., Karpinski, P., Leszczynski, P., Sedziak, T., Kielan, W., Ostasiewicz, P., et al. (2015). Aberrant methylation of ERBB pathway genes in sporadic colorectal cancer. *J. Appl. Genet.* 56, 185–192. doi: 10.1007/s13353-014-0253-6

Tang, H., Fan, X., Xing, J., Liu, Z., Jiang, B., Dou, Y., et al. (2015). NSun2 delays replicative senescence by repressing p27 (KIP1) translation and elevating CDK1 translation. *Aging* 7, 1143–1158. doi: 10.18632/aging.100860

Tate, J. G., Bamford, S., Jubb, H. C., Sondka, Z., Beare, D. M., Bindal, N., et al. (2019). COSMIC: the catalogue of somatic mutations in cancer. *Nucleic Acids Res.* 47, D941–D947. doi: 10.1093/nar/gky1015

Tomczak, K., Czerwinska, P., and Wiznerowicz, M. (2015). The cancer genome atlas (TCGA): an immeasurable source of knowledge. *Contemp. Oncol.* 19, A68–A77. doi: 10.5114/wo.2014.47136

Toomey, P. G., Vohra, N. A., Ghansah, T., Sarnaik, A. A., and Pilon-Thomas, S. A. (2013). Immunotherapy for gastrointestinal malignancies. *Cancer Control* 20, 32–42. doi: 10.1177/107327481302000106

Traube, F. R., and Carell, T. (2017). The chemistries and consequences of DNA and RNA methylation and demethylation. *RNA Biol.* 14, 1099–1107. doi: 10.1080/15476286.2017.1318241

Trixl, L., and Lusser, A. (2019). The dynamic RNA modification 5-methylcytosine and its emerging role as an epitranscriptomic mark. *Wiley Interdiscip. Rev. RNA* 10, e1510. doi: 10.1002/wrna.1510

Tuorto, F., Liebers, R., Musch, T., Schaefer, M., Hofmann, S., Kellner, S., et al. (2012). RNA cytosine methylation by Dnmt2 and NSun2 promotes tRNA stability and protein synthesis. *Nat. Struct. Mol. Biol.* 19, 900–905. doi: 10.1038/nsmb.2357

Vedeld, H. M., Goel, A., and Lind, G. E. (2018). Epigenetic biomarkers in gastrointestinal cancers: the current state and clinical perspectives. *Semin. Cancer Biol.* 51, 36–49. doi: 10.1016/j.semcancer.2017.12.004

Vijay, G. V., Zhao, N., Den Hollander, P., Toneff, M. J., Joseph, R., Pietila, M., et al. (2019). GSK3beta regulates epithelial-mesenchymal transition and cancer stem cell properties in triple-negative breast cancer. *Breast Cancer Res.* 21:37. doi: 10.1186/s13058-019-1125-0

Wan, M. L., Wang, Y., Zeng, Z., Deng, B., Zhu, B. S., Cao, T., et al. (2020). Colorectal cancer (CRC) as a multifactorial disease and its causal correlations with multiple signaling pathways. *Biosci. Rep.* 40:BSR20200265. doi: 10.1042/BSR20200265

Wang, W. (2016). mRNA methylation by NSUN2 in cell proliferation. *Wiley Interdiscip. Rev. RNA* 7, 838–842. doi: 10.1002/wrna.1380

Wang, X., Pan, C., Gong, J., Liu, X., and Li, H. (2016). Enhancing the enrichment of pharmacophore-based target prediction for the polypharmacological profiles of drugs. *J. Chem. Inf. Model.* 56, 1175–1183. doi: 10.1021/acs.jcim.5b00690

Wang, X., Shen, Y., Wang, S., Li, S., Zhang, W., Liu, X., et al. (2017). PharmMapper 2017 update: a web server for potential drug target identification with a comprehensive target pharmacophore database. *Nucleic Acids Res.* 45, W356–W360. doi: 10.1093/nar/gkx374

Wang, Z. X., Deng, T. X., and Ma, Z. (2019). Identification of a 4-miRNA signature as a potential prognostic biomarker for pancreatic adenocarcinoma. *J. Cell. Biochem.* 120, 16416–16426. doi: 10.1002/jcb.28601

Wei, R., Xiao, Y., Song, Y., Yuan, H., Luo, J., and Xu, W. (2019). FAT4 regulates the EMT and autophagy in colorectal cancer cells in part via the PI3K-AKT signaling axis. *J. Exp. Clin. Cancer Res.* 38:112. doi: 10.1186/s13046-019-1043-0

Wu, H., Lu, X. X., Wang, J. R., Yang, T. Y., Li, X. M., He, X. S., et al. (2019). TRAF6 inhibits colorectal cancer metastasis through regulating selective autophagic CTNNB1/beta-catenin degradation and is targeted for GSK3B/GSK3beta-mediated phosphorylation and degradation. *Autophagy* 15, 1506–1522. doi: 10.1080/15548627.2019.1586250

Xing, J., Yi, J., Cai, X., Tang, H., Liu, Z., Zhang, X., et al. (2015). NSun2 promotes cell growth via elevating cyclin-dependent kinase 1 translation. *Mol. Cell. Biol.* 35, 4043–4052. doi: 10.1128/MCB.00742-15

Yang, J. C., Risch, E., Zhang, M., Huang, C., Huang, H., and Lu, L. (2017). Association of tRNA methyltransferase NSUN2/IGF-II molecular signature with ovarian cancer survival. *Future Oncol.* 13, 1981–1990. doi: 10.2217/fon-2017-0084

Yang, X., Yang, Y., Sun, B. F., Chen, Y. S., Xu, J. W., Lai, W. Y., et al. (2017). 5-methylcytosine promotes mRNA export - NSUN2 as the methyltransferase and ALYREF as an m(5)C reader. *Cell Res.* 27, 606–625. doi: 10.1038/cr.2017.55

Yi, J., Gao, R., Chen, Y., Yang, Z., Han, P., Zhang, H., et al. (2017). Overexpression of NSUN2 by DNA hypomethylation is associated with metastatic progression in human breast cancer. *Oncotarget* 8, 20751–20765. doi: 10.18632/oncotarget.10612

Yoshino, H., Enokida, H., Itesako, T., Tatarano, S., Kinoshita, T., Fuse, M., et al. (2013). Epithelial-mesenchymal transition-related microRNA-200s regulate molecular targets and pathways in renal cell carcinoma. *J. Hum. Genet.* 58, 508–516. doi: 10.1038/jhg.2013.31

Yu, T., Jia, W., An, Q., Cao, X., and Xiao, G. (2018). Bioinformatic analysis of GLI1 and related signaling pathways in chemosensitivity of gastric cancer. *Med. Sci. Monit.* 24, 1847–1855. doi: 10.12659/msm.906176

Yuan, S., Tang, H., Xing, J., Fan, X., Cai, X., Li, Q., et al. (2014). Methylation by NSun2 represses the levels and function of microRNA 125b. *Mol. Cell. Biol.* 34, 3630–3641. doi: 10.1128/MCB.00243-14

Yu-Jing, T., Wen-Jing, T., and Biao, T. (2020). Integrated analysis of hub genes and pathways in esophageal carcinoma based on NCBI's gene expression omnibus (GEO) database: a bioinformatics analysis. *Med. Sci. Monit.* 26:e923934. doi: 10.12659/MSM.923934

Zhang, T., Ma, Y., Fang, J., Liu, C., and Chen, L. (2019). A deregulated PI3K-AKT signaling pathway in patients with colorectal cancer. *J. Gastrointest. Cancer* 50, 35–41. doi: 10.1007/s12029-017-0024-9

Zhang, X., Liu, Z., Yi, J., Tang, H., Xing, J., Yu, M., et al. (2012). The tRNA methyltransferase NSun2 stabilizes p16INK(4) mRNA by methylating the 3'-untranslated region of p16. *Nat. Commun.* 3:712. doi: 10.1038/ncomms1692

Zhong, M. E., Chen, Y., Zhang, G., Xu, L., Ge, W., and Wu, B. (2019). LncRNA H19 regulates PI3K-Akt signal pathway by functioning as a ceRNA and predicts poor prognosis in colorectal cancer: integrative analysis of dysregulated ncRNA-associated ceRNA network. *Cancer Cell. Int.* 19:148. doi: 10.1186/s12935-019-0866-2

**Conflict of Interest:** The authors declare that the research was conducted in the absence of any commercial or financial relationships that could be construed as a potential conflict of interest.

frontiers in Molecular Biosciences

REVIEW
published: 05 January 2021
doi: 10.3389/fmolb.2020.590912

# Roles of the Wnt Signaling Pathway in Head and Neck Squamous Cell Carcinoma

*Jing Xie*[1,2†], *Li Huang*[1,3†], *You-Guang Lu*[1,2*] *and Da-Li Zheng*[1*]

[1] *Fujian Key Laboratory of Oral Diseases, School and Hospital of Stomatology, Fujian Medical University, Fuzhou, China,*
[2] *Department of Preventive Dentistry, School and Hospital of Stomatology, Fujian Medical University, Fuzhou, China,*
[3] *Department of Dentistry, The First Affiliated Hospital of Fujian Medical University, Fuzhou, China*

Head and neck squamous cell carcinoma (HNSCC) is the most common type of head and neck tumor. It is a high incidence malignant tumor associated with a low survival rate and limited treatment options. Accumulating conclusions indicate that the Wnt signaling pathway plays a vital role in the pathobiological process of HNSCC. The canonical Wnt/β-catenin signaling pathway affects a variety of cellular progression, enabling tumor cells to maintain and further promote the immature stem-like phenotype, proliferate, prolong survival, and gain invasiveness. Genomic studies of head and neck tumors have shown that although β-catenin is not frequently mutated in HNSCC, its activity is not inhibited by mutations in upstream gene encoding β-catenin, NOTCH1, FAT1, and AJUBA. Genetic defects affect the components of the Wnt pathway in oral squamous cell carcinoma (OSCC) and the epigenetic mechanisms that regulate inhibitors of the Wnt pathway. This paper aims to summarize the groundbreaking discoveries and recent advances involving the Wnt signaling pathway and highlight the relevance of this pathway in head and neck squamous cell cancer, which will help provide new insights into improving the treatment of human HNSCC by interfering with the transcriptional signaling of Wnt.

**Keywords: Wnt signaling pathway, head and neck squamous cell carcinoma, canonical, non-canonical, epigenetic**

OPEN ACCESS

***Edited by:***
*Matteo Becatti,*
*University of Florence, Italy*

***Reviewed by:***
*Naoki Katase,*
*Nagasaki University, Japan*
*Michael Bordonaro,*
*Geisinger Commonwealth School of Medicine, United States*
*Martha Robles-Flores,*
*National Autonomous University of Mexico, Mexico*

***Correspondence:**
*You-Guang Lu*
*filyg63@fjmu.edu.cn*
*Da-Li Zheng*
*dalizheng@fjmu.edu.cn*

[†] *These authors have contributed equally to this work*

***Specialty section:***
*This article was submitted to Molecular Diagnostics and Therapeutics, a section of the journal Frontiers in Molecular Biosciences*

***Received:*** *03 August 2020*
***Accepted:*** *21 October 2020*
***Published:*** *05 January 2021*

***Citation:***
*Xie J, Huang L, Lu Y-G and Zheng D-L (2021) Roles of the Wnt Signaling Pathway in Head and Neck Squamous Cell Carcinoma. Front. Mol. Biosci. 7:590912. doi: 10.3389/fmolb.2020.590912*

## INTRODUCTION

Head and neck squamous cell carcinoma (HNSCC) is the sixth most common malignant tumor in the world (Alamoud and Kukuruzinska, 2018). HNSCC causes over 330,000 deaths worldwide, and more than 650,000 HNSCC cases are reported each year (Xi and Grandis, 2003). In the United States, the overall incidence of HNSCC is 11 per 100,000 people, and HNSCC is more common among black populations than white populations. It originates from the mucosa of various organs that have a squamous epithelial lining. These organs include the mouth, nasopharynx, and throat. Oral squamous cell carcinoma (OSCC) is the main type of HNSCC, which is characterized by poor prognosis and low survival rate. Local recurrence of the primary site and cervical lymph node metastasis are the main reasons for the failure of treatment in patients with OSCC. Therefore, elucidating the molecular mechanisms that regulate the occurrence and development of OSCC will help to understand the etiology of these diseases, allow the design of more effective strategies for the treatment of OSCC, and possibly improve treatment.

In 1982, Nusse found an oncogenic gene in mouse models of mammary cancer, named int1, and which has homology to the wingless gene of drosophila reported later by Sharma, and the two were collectively called Wnt (Nusse et al., 1991). The Wnt signaling pathways play important roles in embryonic development, tissue regeneration, cell proliferation, and cell differentiation and is abnormally activated in many types of cancers, such as colon cancer (Zheng and Yu, 2018; Flores-Hernández et al., 2020), liver cancer (Li et al., 2019), lung cancer (Ji et al., 2019), breast cancer (Ma et al., 2016), and childhood T-cell acute lymphoblastic leukemia (Ng et al., 2014). Previous studies have shown that dysfunction of the Wnt signaling pathway can promote the development of oral cancer (González-Moles et al., 2014) and that abnormalities in this pathway affect the prognosis of patients with HNSCC. More and more research highlights the importance of the Wnt signaling pathway for the prognosis of HNSCC patients and suggests the possibility of actively developing new gene therapy methods that target this pathway in HNSCC. Thus, this review summarizes recent research findings regarding the Wnt signaling pathway in HNSCC to improve our understanding of the mechanisms underlying the roles of this important signaling pathway in cancer cell activity.

## WNT SIGNALING PATHWAY

With the advancement of research, people are learning more and more about the Wnt signaling pathway. So far, 19 members of the Wnt family have been found in the human genome, including Wnt1, Wnt2, Wnt2b, Wnt3, Wnt3a, Wnt4, Wnt5a, Wnt5b, Wnt6, Wnt7a, Wnt7b, Wnt8a, Wnt8b, Wnt10a, Wnt10b, Wnt11, Wnt14, Wnt15, and Wnt16. These secreted glycoproteins usually contain 350–400 amino acids. In order to trigger the cellular response and activate intracellular signal transduction, the extracellular Wnt ligands combine with the 10 Frizzled (Fzd 1-10) receptors and several coreceptors, such as Lrp-5/6, Ryk, or Ror2 (Logan and Nusse, 2004; Kestler and Kühl, 2008). Intracellular signal transduction cascades diversify into three main branches, the canonical Wnt/β-catenin signaling pathway, and the non-canonical Wnt signaling pathway, which mainly comprises the Wnt/$Ca^{2+}$ and Wnt/PCP pathways (González-Moles et al., 2014).

## CANONICAL WNT SIGNALING PATHWAY

The hallmark of the canonical Wnt signaling pathway is the accumulation and transport of β-catenin proteins associated with adhesion junctions into the nucleus (Dawson et al., 2013). In an experimental analysis of the axial development of *Xenopus laevis* and the segmental polarity and wing development of Drosophila, researchers first clarified the role of this canonical pathway in embryonic development (Ng et al., 2019). glycogen synthase kinase 3 (GSK3)β is a central participant in the canonical Wnt pathway. The activity of the Wnt/β-catenin signaling pathway depends on the amount and cellular location of β-catenin (Lustig and Behrens, 2003). Wnt ligands interact with the Fzd receptors. When the Fzd receptors are unoccupied, cytoplasmic β-catenin is degraded by its destruction complex, which includes Axin, APC protein, GSK3, casein kinase 1α (CK1α), and β-catenin (Tejeda-Muñoz and Robles-Flores, 2015). Once the complex is formed, β-catenin begins to phosphorylate sequentially. The first phosphorylation is at Ser45 by CK1α, and subsequently at Thr41, Ser37, and Ser33 by GSK3β. Phosphorylated β-catenin is released from the complex allowing for its ubiquitination at the N-terminal end of the protein and subsequent degradation by E3. Axin and APC can also be phosphorylated by GSK3β and CK1α, resulting in the enhancement of β-catenin phosphorylation (Hagen and Vidal-Puig, 2002). This continuous degradation prevents the accumulation and translocation of β-catenin to the nucleus (MacDonald et al., 2009). When the Wnt/β-catenin signaling is activated, Wnt ligand binds to Fzd receptors and its co-receptor, low-density lipoprotein receptor-related protein 5/6 (Lrp5/6) (Gordon and Nusse, 2006). This complex leads to the recruitment of the scaffold protein (Disheveled, Dvl) to the receptors which are then phosphorylated. Subsequently, Axin, GSK3β, and CK1 migrate from the cytoplasm to the plasma membrane, which contributes to the inactivation of the destruction complex, resulting in β-catenin stabilization through dephosphorylation. Stable β-catenin translocates into the nucleus and interacts with T-cell factor (TCF) transcription factors to induce the expression of Wnt target genes such as c-Myc, cyclin D1, Axin-2, Lgr5, ITF-2, PPAR-δ, and matrix metalloproteinase 1 and 7 (MMP-1, MMP-7) (Wu and Pan, 2010; Velázquez et al., 2017). A variety of Wnt/β-catenin target genes have been identified, including cell proliferation regulation genes, development control genes, and genes related to tumor progression. Wnt1 class ligands (Wnt2, Wnt3, Wnt3a, and Wnt8a) play main roles through the canonical Wnt/β-catenin signaling pathway.

## NON-CANONICAL WNT SIGNALING PATHWAY

Non-canonical Wnt signaling is mediated through Fzds but Lrp5/6 is not involved and consists of two main branches (Valenta et al., 2012): the PCP pathway and the Wnt/$Ca^{2+}$ pathway. Non-canonical Wnt signaling is initiated by Wnt5a type ligands (Wnt4, Wnt5a, Wnt5b, Wnt6, Wnt7a, and Wnt11). These Wnt ligands bind to Fzd receptors. In addition, receptor tyrosine kinase-like orphan receptor 2 (Ror2), and receptor tyrosine kinase (Ryk) have been suggested as non-canonical signaling co-receptors, which are required for downstream activation. These signal transductions jointly activate the calcium-dependent signaling cascade by activating Dvl (Rao and Kühl, 2010). In the Wnt/$Ca^{2+}$ pathway, Wnt ligands bind to receptor complex, leading to the activation of phospholipase C (PLC). This results in inositol 1,4,5-triphosphate-3 (IP3) production and subsequent $Ca^{2+}$ release (Anastas and Moon, 2013). Calcium release and intracellular accumulation activate several calcium-sensitive proteins, including protein kinase C (PKC) and calcium/calmodulin-dependent kinase II (CaMKII)

(González-Moles et al., 2014). Calcineurin activates nuclear factor of activated T cells (NFAT) and subsequent NFAT-mediated gene expression (Saneyoshi et al., 2002). Some evidence had been found that parts of the non-canonical Wnt signaling proteins influence the canonical Wnt/β-catenin pathway (van Tienen et al., 2009; Fan et al., 2017). However, the specific mechanism is not yet clear, and more research is needed.

PCP was first demonstrated in insects because their cuticular surface has a rich morphology (Adler, 2012). The Wnt/PCP pathway mediates the event of collective migration, but abnormal activation leads to tumor migration ability. In the Wnt/PCP pathway, the binding of Wnt to Fzd and a co-receptor causes recruitment of Dvl to Fzd and its association with disheveled-associated activator of morphogenesis 1 (DAMM1). DAMM1 activates small G protein Rho, through guanine exchange factor and then activates Rho-associated protein kinase to reorganize the cytoskeleton and change cell polarity and migration (Peng et al., 2011). It is characteristic of the plane polarity signal that Rho-associated kinases can mediate cytoskeleton rearrangement. Alternatively, the PCP pathway can also be mediated by the triggering of RAC to initiate the c-Jun amino terminal kinase (JNK) signaling cascade (Javed et al., 2019). The activation of Dvl-mediated Wnt signal induces the activation of heterotrimeric G protein and promotes the transport of intracellular $Ca^{2+}$ to the extracellular environment (De, 2011). This transport activates JNK and Nemo-like kinase (NLK) which can phosphorylate TCF transcription factors and antagonize the canonical Wnt signaling pathway (Humphries and Mlodzik, 2018). Taken together, these observations indicate that the Wnt/$Ca^{2+}$ pathway is a key regulator of canonical signaling pathways and planar cell polarity pathways. On the other hand, non-canonical signaling pathways phosphorylate TCF through NLK, thereby mediating the activation of canonical Wnt signaling (**Figure 1**).

## ABERRANT WNT SIGNALING PATHWAY IN HNSCC

With the discovery that a number of Wnt genes are associated with the development of various human cancers, aberrant activation of Wnt signaling pathway became evident. To date, different roles of Wnt in HNSCC have been confirmed. Leethanakul et al. used microarray technology to reveal the role of Wnt in HNSCC for the first time. They found that homologs of both Fzd and Dvl were increased compared with normal tissue samples. This suggests that Wnt mediates invasiveness in the development of HNSCC (Leethanakul et al., 2000). Currently, several other studies have shown that abnormal activation of the Wnt signaling pathway facilitates tumor transformation in head and neck tissues (Iwai et al., 2005). For example, Wnt1-induced signaling pathway protein 1 (WISP-1) is involved in the progression of OSCC, and high expression of WISP-1 is significantly associated with treatment failure (Zhang C. et al., 2019). Wnt7b, an agonist of the canonical Wnt pathway, shows significantly increased expression in samples from patients with OSCC compared with matched samples of adjacent non-tumorous tissues (Shiah et al., 2016), and the Wnt/β-catenin signaling pathway prevents shedding-mediated apoptosis (anoikis) in SCC1 cells and promotes the growth of HNSCC-xenograft tumors *in vivo* (Farooqi et al., 2017). The Wnt/β-catenin signaling pathway may regulate the epithelial–mesenchymal transition in laryngeal squamous cell carcinoma, thereby regulating tumor development (Psyrri et al., 2014). In OSCC, the non-canonical Wnt/$Ca^{2+}$/PKC pathway is activated by Wnt5a, which promotes migration and invasion (Prgomet et al., 2015). Wnt5b has been found to be significantly increased in the highly metastatic cell line of OSCC cells. Wnt5b gene silencing can significantly inhibit the formation of filopodia-like protrusive structures and migration, whereas stimulation with Wnt5b can significantly increase the formation of filopodia-like protrusions in SAS-LM8 cells (Takeshita et al., 2014). The roles of more Wnt ligands in HNSCC are listed in **Table 1**. Thus, both canonical Wnt pathways and non-canonical Wnt pathways play great roles in HNSCC. Although Wnt1 type or Wnt5a type ligands activate canonical or non-canonical Wnt pathways, respectively, there is more research that suggests that the results of different Wnt ligands depend on specific combinations of Wnt receptors and coreceptors (Wang et al., 2013; Sakisaka et al., 2015). Besides the canonical Fzd and Lrp receptor, Ror and Ryk are also important alternative receptors for Wnt transduction.

Head and neck squamous cell carcinoma can be divided into human papillomavirus (HPV)-positive and HPV-negative tumors, each of which has its unique clinical, pathological, and epidemiological significance (Cancer Genome Atlas Network, 2015). Increasing evidence shows that Wnt/β- catenin signaling has an impact on the pathobiology of HPV- and HPV + HNSCC. HPV viral oncoprotein E6/E7 has been used to alter the prognosis of HPV-HNSCC patients (Liu et al., 2017). In oropharyngeal squamous cell carcinoma, β-catenin is driven to nuclear translation through E6 oncoprotein by activating epidermal growth factor receptors (EGFR). Some researchers have used small interfering RNAs to suppress E6 expression and erlotinib to downregulate EGFR activity and thereby eliminate the nuclear localization of β-catenin and the phosphorylation of EGFR while reducing the invasion characteristics of HPV + HNSCC cell lines *in vitro* (Nwanze et al., 2015). According to reports, E6/E7 may also suppress E3 ubiquitin ligase protein to induce nuclear translocation of β-catenin. The regulatory effect of E6/E7 on HPV + HNSCC requires further study. Recently, it was found that some microRNAs have potential roles in the attenuation of HPV+/HPV- HNSCC, although the effects are weak (Nwanze et al., 2015). More research is needed to deepen the understanding of the Wnt/β-catenin signaling pathway in HPV + HNSCC (Kobayashi et al., 2018). Due to limited tumor specimens and relevant clinical data, research on HPV + HNSCC lags behind than on HPV-HNSCC (Cancer Genome Atlas Network, 2015; Beck and Golemis, 2016).

## GENETIC AND EPIGENETIC CHANGES OF WNT SIGNALING IN HNSCC

Components of the Wnt signaling pathway, such as Wnt ligand proteins, Wnt antagonists, membrane receptors, and

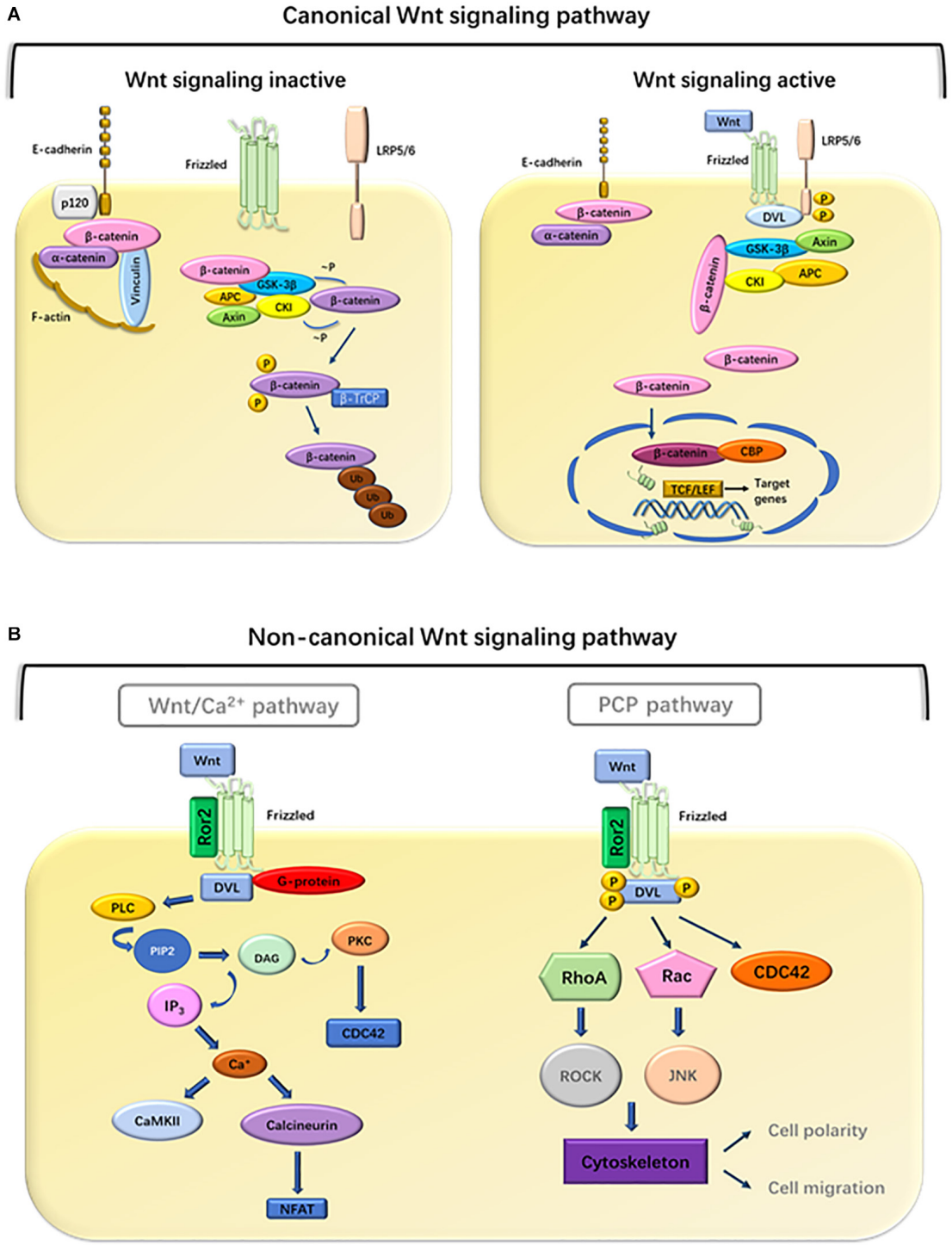


**FIGURE 1 |** Overview of the Wnt pathway. **(A)** Canonical pathway. Binding of Wnt to frizzled receptors activates disheveled (DVL), which disrupts the stability of the destruction complex, composed of Axin, APC, GSK3-β, CK1, and β-catenin. Subsequently, phosphorylation and degradation of β-catenin are inhibited, which allows the association of β-catenin with TCF transcription factors. In the absence of Wnt ligands, the complexes promote phosphorylation of β-catenin. Phosphorylated β-catenin becomes multiubiquitinated (Ub) and subsequently degraded in proteasomes (Foulquier et al., 2018). **(B)** Non-canonical pathway. In the Wnt/$Ca^{2+}$ pathway, Wnt ligands bind to a complex consisting of Fzd, DVL, and G-proteins, leading to the activation of PLC, which cleaves phosphatidylinositol 4,5 biphosphate (PIP2) into diacylglycerol (DAG) and IP3. DAG activates PKC whereas IP3 promotes the release of intracellular $Ca^{2+}$, which in turn activates CamKII and calcineurin (Russell and Monga, 2018). Calcineurin activates NFAT to regulate cell migration and cell proliferation. In the PCP pathway, Wnt ligands bind to a complex consisting of Fzd, Ror2, and DVL, which mediates the activation of RhoA and ROCK, or activation of Rac and JNK signaling, to regulate cell polarity and migration.

**TABLE 1 |** The roles of different Wnt ligands in HNSCC.

| Wnt ligands | Type of Wnt signaling | HNSCC Cell lines | Type of HNSCC | Function | References |
|---|---|---|---|---|---|
| Wnt1 | Canonical | SCC1483, SNU1076 | Oral squamous cell carcinoma | Promote invasion, inhibit apoptosis | Rhee et al., 2002; Zhang C. et al., 2019 |
| Wnt3 | Canonical | – | Oral leukoplakia | Cause dysplasia | Ishida et al., 2007 |
| Wnt3a | Canonical | – | Laryngeal squamous cell carcinoma | Worse histological grade, advanced clinical stage, and higher cervical lymph node metastatic potential | Zhang D. et al., 2019 |
| Wnt4 | Non-canonical | WRO, CAL62, FB2, and BCPAP | Thyroid carcinoma | Reduce migration | Filippone et al., 2014 |
| Wnt5a | Non-canonical | SCC9 | Oral squamous cell carcinoma | Enhance migration and invasion | Prgomet et al., 2017 |
| Wnt5a | Non-canonical | HTH-74, C-643 | Thyroid carcinoma | Decrease proliferation, migration, invasiveness, and clonogenicity | Kremenevskaja et al., 2005 |
| Wnt5a | Non-canonical | CNE-2, 5-8F | Nasopharyngeal carcinoma | Lead to tumorigenesis and metastasis | Zhu et al., 2014; Qin et al., 2015 |
| Wnt5a | Non-canonical | – | Laryngeal squamous cell carcinoma | High tumor stage and lymph node metastasis | Prgomet et al., 2017 |
| Wnt5b | Non-canonical | SAS-LM8 | Oral squamous cell carcinoma | Enhance migration and invasion | Zhang et al., 2017 |
| Wnt7a | Canonical | HSC3, CAL27 | Oral squamous cell carcinoma | Promote migration | Sakamoto et al., 2017 |
| Wnt7b | Canonical | DOK, FaDu | Oral squamous cell carcinoma | Promote proliferation and invasion | Xie et al., 2020 |
| Wnt10b | Canonical | SNU1076 | Head and neck squamous cell carcinoma | Promote growth and survival, inhibit apoptosis | Shiah et al., 2014 |
| Wnt11 | Non-canonical | – | Oral squamous cell carcinoma | Suppress tumor | Andrade Filho et al., 2011 |

intracellular conduction medium, are often disrupted by genetic or epigenetic inheritance in human tumors (Polakis, 2012). It is reported that the activation of the Wnt1 and Wnt pathways occurs due to epigenetic changes in secreted frizzled-related protein (SFRP), Wnt inhibitory factor (WIF), and the Wnt signaling pathway inhibitor Dickkopf 3 (DKK3). Previous data demonstrated that DKK-3 protein is mainly expressed in HNSCC (Katase et al., 2013), and its expression is associated to the high metastasis rate and poor prognosis of OSCC (Katase et al., 2012). Therefore, epigenetic changes of DKK3 may be closely related to the occurrence and development of HNSCC (Katase et al., 2020). Epigenetic alterations of SFRP, WIF-1, and DKK-3 genes can active Wnt pathways, resulting in delocalization of catenin in HNSCC (Pannone et al., 2010). It was recently reported that overexpression of β-catenin is significantly associated with increased transcriptional activity in HNSCC (Kartha et al., 2018). The destructive complex strictly controls the level of β-catenin in the cytoplasm. Previous studies have suggested that mutations in APC, Axin, and β-catenin are widespread in colon cancer (Hernández-Maqueda et al., 2013; Yu et al., 2018), esophageal cancer, and gastric cancer. The Axin1 mutation was first identified in hepatocellular carcinoma (Satoh et al., 2000). In a small, diverse group of colon cancer cases, activation of point mutations in β-catenin removed the regulated N-terminal Ser/Thr residue. Similar β-catenin mutations have also been reported in melanoma and other tumors (Morin et al., 1997; Rubinfeld et al., 1997). Mutations in these genes stabilize β-catenin, allowing it to accumulate in the nucleus, and subsequently activate the Wnt signaling pathway. However, mutants of APC, Axin, or β-catenin still ultimately depend on exogenous Wnts (Lammi et al., 2004). According to HNSCC studies, there are few gene mutations relevant to Wnt pathways in HNSCC, which indicates that abnormal β-catenin accumulation in oral cancer is not associated with mutations in these genes. Although Wnt/β-catenin mutations are not common in HNSCC, other signal pathways, such as FAT1 and AJUBA, can crosstalk with Wnt/β-catenin, resulting in changes in the activity of Wnt signaling pathway (Cancer Genome Atlas Network, 2015; Beck and Golemis, 2016). Mutations in these signaling cascades are almost entirely related to HPV-negative tumors and to the absence of epithelial differentiation programs. Another possible mechanism for the degradation and inactivation of β-catenin involves EGFR signaling (Lee et al., 2010). In OSCC, EGFR stabilizes β-catenin and enhances nuclear accumulation of β-catenin through phosphorylation, possibly via two molecular mechanisms: (1) binding directly and then β-catenin is phosphorylated and (2) phosphorylation through GSK-3β to regulate the activity of the destruction complex (Billin et al., 2000; Hu and Li, 2010).

DNA methylation and histone modification also play important parts in the occurrence of HNSCC. Epigenetic regulation may contribute to the silencing of Wnt related genes. Because there is no changes of methylation levels in the CpG island of APC, Axin, and β-catenin genes in OSCC (Shiah et al., 2016), downregulation of Wnt signaling in OSCC and HNSCC is usually due to methylation of different Wnt pathway inhibitors, such as SFRP-2, WIF-1, DKK-1 (Katase et al., 2010), Dachshund family transcription factor 1 (DACH1), and RUNT-related transcription factor 3 (RUNX3). Microarray-based genome-wide epigenetic analyses of human cancer have shown that inhibitors of Wnt signaling pathway are common sites for promoter methylation silencing. However, these Wnt pathway inhibitors may have different levels of methylation in OSCC and HNSCC cells, and may be significantly related to tumor recurrence or disease-free survival. For example, in OSCC cell, the WIF-1 and SFRP2 genes are frequently

methylated, whereas the DACH1 and Dkk1 genes are less frequently methylated (Farooqi et al., 2017). In the same way, the WIF-1 gene is often methylated in primary oropharyngeal cancer tissue and associated with poorer survival (Paluszczak et al., 2015). In addition, methylation of the E-cadherin promoter is the main reason for the loss of membrane β-catenin expression, which leads to the release of β-catenin from the E-cadherin/β-catenin complex into the cytoplasm (Wong et al., 2018). By performing chromatin immunoprecipitation promoter array and gene expression analyses in hepatocellular carcinoma, Cheng et al. (2011) found that enhancer of zeste homolog 2 (EZH2) occupancy of the promoter decreased the expression of several Wnt antagonists including Axin2, NKD1, PPP2R2B, DKK1, and SFRP5. EZH2 is the core components of polycomb repressor complex 2 (PRC2) and has methyltransferase activity. It can catalyze histone 3 lysine 27 trimethylation (H3K27me) and eliminate PRC2-mediated gene suppression. Thus, overexpression of EZH2 promotes the neoplastic transformation of epithelial cells. These findings show that inhibiting the activity of Wnt antagonists through DNA methylation and histone modification enables to the constitutive activation of Wnt/β-catenin signaling. Moreover, testing body fluids to detect DNA methylation is feasible and minimally invasive. Therefore, the Wnt antagonist gene such as SFRP-2, WIF-1, and DKK-1 secreted in plasma can be used as a biomarker for diagnosis and prognosis (Shiah et al., 2016).

## WNT SIGNALING PATHWAY IN CANCER STEM CELLS OF HNSCC

Stem cells (SCs) have the ability of self-renewal and differentiation. The maintenance and repair of tissue homeostasis depends on the activity of tissue-specific SCs. Cancer SCs (CSCs) are a subset of cells that are resistant to chemotherapy and radiotherapy and often promote relapse by stopping or evading clinical treatment (Mannelli and Gallo, 2012). Like other cancer tissues, HNSCC tissue contains small cell subsets with stem-like characteristics (CSCs), which can bring about tumors with hierarchical structure.

According to reports, aberrant Wnt signaling has a promoting effect on different forms of cancer (such as colon cancer, liver cancer, and lung cancer), and plays a key role in guarding CSCs (Vermeulen et al., 2010). Le et al. co-cultured HNSCC tumor spheres and cancer-related fibroblast (CAF) cell line in 3D environment to simulate the interaction *in vivo* and found that Wnt3a activated Wnt signals in cancer cells and CAF. The activation of Wnt increases the characteristics of CSC, such as sphere formation and invasiveness (Lamb et al., 2013; Le et al., 2019). Non-canonical Wnt signals in CSCs are activated by Wnt5a, Wnt11, or other non-canonical Wnt ligands. It is known that non-canonical Wnt signals promote the survival and drug resistance of CSCs through activation of PI3K-AKT signal and YAP/TAZ-mediated transcription. But there are few studies on the role of non-canonical Wnt signaling pathway in the CSC of HNSCC, most of the findings focus on the Wnt/β-catenin signaling pathway. Recent advances suggest that Wnt/β-catenin signaling is involved in the differentiation and development of CSCs in HNSCC. One proposed mechanism is that Wnt/β-catenin may play a specific role in asymmetric cell division, which allows Dvl, Fzd, Axin, and APC to divide asymmetrically in the cytoplasm, producing a progenitor cell and a cell destined to differentiate (Lien and Fuchs, 2014). The analysis of CSC proliferation stimulated by canonical Wnt signal pathway inhibitors has become the latest experimental method to study the role of this signal pathway in CSC self-renewal. In nasopharyngeal carcinoma, CSC isolated from HNE1 cell line treated with Wnt-C59, an inhibitor of Wnt, can reduce the proliferation of CSC (Cheng et al., 2015). In addition, several other studies have shown that numerous canonical Wnt signal pathway inhibitors, including SFRP4, all-trans retinoic acid (Atra), and active natural compounds and honokiol, can reduce the expression of β-catenin and ultimately inhibit the proliferation of CSC in HNSCC (Lim et al., 2012; Yao et al., 2017). The Wnt/β-catenin signaling pathway also plays an important role in regulating differentiation of SC during early embryonic development (Vlad et al., 2008) and cancer including HNSCC. It is reported that CSC isolated from M3a2 and M4e (HNSCC cell lines) are highly activated. The CSCs injected into nude mice differentiate into tumor cells, resulting in five times larger tumor growth than non-CSC after 8 weeks (Lee et al., 2014).

A study showed that the expression of CD44 + was essential for maintaining tumor heterogeneity in HNSCC (Prince et al., 2007). The CSCs with high CD44+ were shown to be characterized by high aldehyde dehydrogenase activity (ALDH) and by expression of c-Met and SOX2. According to reports, CD44+/ALDH (high) cells have stronger oncogenicity and self-renewal ability than CD44 + ALDH (low) cells. ALDH is thought to cause treatment resistance and tumor prevalence by regulating the expression of phosphoinositide 3-kinase (PI3K) and SOX2 signaling pathway (Bertrand et al., 2014). The mesenchymal–epithelial transition factor c-Met has been reported to interact with the Wnt/β-catenin pathway in HNSCC (Arnold et al., 2017). The roles of c-Met and Wnt/β-catenin have been widely studied in colon cancer cells, in which their activities determine the fate of cells in CSC. However, the activation of c-Met inhibitor in the presence of β-catenin has been found to result in the elimination of CSCs in HNSCCs (Arnold et al., 2017). It has been reported that FZD8, a modulator of the Wnt/β-catenin pathway, increases the expression of CSCs in HNSCCs by activating the (extracellular regulated MAP kinase) ERK/c-fos signaling axis (Bordonaro et al., 2016; Chen and Wang, 2019).

Due to the presence of drug-resistance CSCs, disease recurrence is the main marker of HNSCC. A large body of evidence suggests that Wnt confers chemotherapeutic resistance by upregulating CSC activity in HNSCC. The use of the Fzd/Wnt antagonist SFRP4 was found to increase the drug sensitivity of HNSCC by 25%. SFRP4 was shown to compete directly with Wnt, significantly enhancing cisplatin-induced apoptosis and reducing the activity of tumor cells (Warrier et al., 2014). Furthermore, the use of antagonists had no effect on non-tumorigenic mouse embryonic fibroblasts, suggesting that Wnt

signaling plays an important role in the development and differentiation of CSCs related to HNSCC. However, the potential mechanism underlying the upregulation of chemical resistance in CSCs remains unclear, as does the mechanism by which Wnt mediates the activation of CSCs. Studies have identified five types of ABC transporters, ABCC1 to ABCC5, as main mediators in the canonical hyperactivation of the Wnt pathway in spheroid cells of HNSCC. The ability of spheroid cells to exhibit CSC-induced chemotherapy resistance was eliminated after knocking out the genes for β-catenin synthesis. However, this knock out resulted in the loss of SC tags necessary for self-renewal (Song et al., 2010; Yao et al., 2013). Although research on Wnt signal modulators has made great progress, few drugs have been imported for clinical use. Since CSCs have the same characteristics (self-renewal, differentiation) as normal SCs, they present an obstacle to the development of suitable pharmaceutical formulations for HNSCC.

## WNT SIGNALING AS A THERAPEUTIC TARGET FOR HNSCC

Wnt signaling plays an important role in tumorigenesis and acts as a regulator of CSCs renewal in the process of cell homeostasis; thus, it is an attractive therapeutic target. To date, several approaches have been developed, and a few have moved on to clinical trials. One of them is to block the activity of Wnt with specific inhibitor. PORCN, also known as porcupine, is an enzyme which can limit the activation of Wnt signals in serine residues and promote the palmitoylation of Wnt. Using small inhibitors of PORCN, such as IWP, C59, and LGK974 caused rapid decreases in the expression of Wnt signaling (Proffitt et al., 2013). *In vitro*, C59 inhibited the activity of PORCN, and then inhibited the Wnt palmitoylation, Wnt interaction with carrier protein Wntless/WLS, Wnt secretion, and Wnt activation of β-catenin reporter protein. The chick chorioallantoic membrane (CAM) experiment proved that LGK974 can inhibit the growth and metastasis of HNSCC (Rudy et al., 2016). Studies have also shown that PORCN directly prevents the excessive production of Wnt, thus inhibiting the interaction between Wnt and Fzd protein. At present, the inhibition of PORCN on Wnt is being verified *in vivo* and *in vitro*. Additionally, inhibitors of tankyrase stabilize axin and antagonize Wnt signaling including XAV939, IWR, G007-LK, and G244-LM, though they have not yet entered clinical trials (Huang et al., 2009; Lau et al., 2013; Kulak et al., 2015). Moreover, ICG-001, a small molecule that inhibits the transcription of CREB binding proteins, downregulates β-catenin/T cell factor signaling by specifically binding to cyclic AMP response element-binding protein (Emami et al., 2004; Bordonaro and Lazarova, 2015). ICG-001 is currently in phase I clinical trials in patients with HNSCC. Furthermore, OMP-18R5 is a human monoclonal antibody against the Fzd receptor and is currently in phase I clinical trials. Wnt ligands and their compound receptors are also being evaluated in clinical trials (Kawakita et al., 2014). Examples include Omp-54F28, a chimera of human IgG1 and Fzd8, which is related to the growth of pancreatic cancer cells. Currently, most clinical trials use small RNAs as biomarkers for cancer detection, diagnosis, and prognostic evolution (Hayes et al., 2014). To date, no clinical trial has used miRNAs to predict prognosis and the clinical effect in HNSCC patients. A more comprehensive understanding of the involvement of the Wnt pathway in HNSCC is necessary to develop effective therapeutics for oral cancer.

## CONCLUSION

As outlined above, aberrant activation of the Wnt signaling pathway may impact on HNSCC. In addition to gene mutations in the Wnt component, abnormal changes downstream of EGFR are involved in regulating the Wnt/β-catenin pathway, which can reshape the histone/chromatin structure of the target gene. Because the epigenetic alterations of Wnt antagonists are the cause of Wnt signal activation, it may become a potential biomarker for predicting OSCC recurrence in plasma. Appropriate methods are required to deal with CSC generated by aberrant Wnt signaling. Wnt signaling is one of the regulators of CSC generation involving HNSCC. Because of the complexity of non-canonical signal pathway, most of the research on Wnt in HNSCC is focused on canonical WNT signal pathway, but there are few related studies on non-canonical signal pathway. More attention needs to be paid to non-canonical signaling pathways in the future. The evaluation of various aspects of signal transduction can expand our understanding of both this key pathway and the crosstalk between signaling pathways in cells. Such advancement will enable the development of a broad range of therapeutic interventions to eradicate and respond to HNSCC recurrence.

## AUTHOR CONTRIBUTIONS

JX and LH contributed equally in conceiving the review focus, conducting the literature review, summarizing the manuscript, writing the first draft, and finalizing the manuscript. D-LZ and Y-GL designed and directed the review. JX, LH, D-LZ, Y-GL revised and made corrections to the manuscript. All authors have read and agreed to the final version of the manuscript.

## FUNDING

This work was supported by the National Natural Sciences Foundation of China (Grant No. 81872186), Innovation Foundation of Department of Science and Technology of Fujian (Grant No. 2017Y9096), and Scientific research funding of School and Hospital of Stomatology, Fujian Medical University (Grant Nos. 2018KQYJ01 and 2015-KQYY-LJ-2).

## ACKNOWLEDGMENTS

We thank Dr. April Darling (University of Pennsylvania School of Medicine) for the language editing for this manuscript.

## REFERENCES


Adler, P. N. (2012). The frizzled/stan pathway and planar cell polarity in the *Drosophila* wing. *Curr. Top. Dev. Biol.* 101, 1–31. doi: 10.1016/B978-0-12-394592-1.00001-6

Alamoud, K. A., and Kukuruzinska, M. A. (2018). Emerging insights into Wnt/β-catenin signaling in head and neck cancer. *J. Dent. Res.* 97, 665–673. doi: 10.1177/0022034518771923

Anastas, J. N., and Moon, R. T. (2013). WNT signalling pathways as therapeutic targets in cancer. *Nat. Rev. Cancer* 13, 11–26. doi: 10.1038/nrc3419

Andrade Filho, P. A., Letra, A., Cramer, A., Prasad, J. L., Garlet, G. P., Vieira, A. R., et al. (2011). Insights from studies with oral cleft genes suggest associations between WNT-pathway genes and risk of oral cancer. *J. Dent. Res.* 90, 740–746. doi: 10.1177/0022034511401622

Arnold, L., Enders, J., and Thomas, S. M. (2017). Activated HGF-c-met axis in head and neck cancer. *Cancers* 9:169. doi: 10.3390/cancers9120169

Beck, T. N., and Golemis, E. A. (2016). Genomic insights into head and neck cancer. *Cancers Head Neck* 1:1. doi: 10.1186/s41199-016-0003-z

Bertrand, G., Maalouf, M., Boivin, A., Battiston-Montagne, P., Beuve, M., Levy, A., et al. (2014). Targeting head and neck cancer stem cells to overcome resistance to photon and carbon ion radiation. *Stem Cell Rev .Rep.* 10, 114–126. doi: 10.1007/s12015-013-9467-y

Billin, A. N., Thirlwell, H., and Ayer, D. E. (2000). Beta-catenin-histone deacetylase interactions regulate the transition of LEF1 from a transcriptional repressor to an activator. *Mol. Cell Biol.* 20, 6882–6890. doi: 10.1128/mcb.20.18.6882-6890.2000

Bordonaro, M., and Lazarova, D. L. (2015). CREB-binding protein, p300, butyrate, and Wnt signaling in colorectal cancer. *World J. Gastroenterol.* 21, 8238–8248. doi: 10.3748/wjg.v21.i27.8238

Bordonaro, M., Shirasawa, S., and Lazarova, D. L. (2016). In hyperthermia increased ERK and WNT signaling suppress colorectal cancer cell growth. *Cancers* 8:49. doi: 10.3390/cancers8050049

Cancer Genome Atlas Network (2015). Comprehensive genomic characterization of head and neck squamous cell carcinomas. *Nature* 517, 576–582. doi: 10.1038/nature14129

Chen, D., and Wang, C. Y. (2019). Targeting cancer stem cells in squamous cell carcinoma. *Precis. Clin. Med.* 2, 152–165. doi: 10.1093/pcmedi/pbz016

Cheng, A. S., Lau, S. S., Chen, Y., Kondo, Y., Li, M. S., Feng, H., et al. (2011). EZH2-mediated concordant repression of Wnt antagonists promotes β-catenin-dependent hepatocarcinogenesis. *Cancer Res.* 71, 4028–4039. doi: 10.1158/0008-5472.CAN-10-3342

Cheng, Y., Phoon, Y. P., Jin, X., Chong, S. Y., Ip, J. C., Wong, B. W., et al. (2015). Wnt-C59 arrests stemness and suppresses growth of nasopharyngeal carcinoma in mice by inhibiting the Wnt pathway in the tumor microenvironment. *Oncotarget* 6, 14428–14439. doi: 10.18632/oncotarget.3982

Dawson, K., Aflaki, M., and Nattel, S. (2013). Role of the Wnt-Frizzled system in cardiac pathophysiology: a rapidly developing, poorly understood area with enormous potential. *J. Physiol.* 591, 1409–1432. doi: 10.1113/jphysiol.2012.235382

De, A. (2011). Wnt/Ca2+ signaling pathway: a brief overview. *Acta Biochim. Biophys. Sin.* 43, 745–756. doi: 10.1093/abbs/gmr079

Emami, K. H., Nguyen, C., Ma, H., Kim, D. H., Jeong, K. W., Eguchi, M., et al. (2004). A small molecule inhibitor of beta-catenin/CREB-binding protein transcription [corrected]. *Proc. Natl. Acad. Sci. U.S.A.* 101, 12682–12687. doi: 10.1073/pnas.0404875101

Fan, J., Wei, Q., Liao, J., Zou, Y., Song, D., Xiong, D., et al. (2017). Noncanonical Wnt signaling plays an important role in modulating canonical Wnt-regulated stemness, proliferation and terminal differentiation of hepatic progenitors. *Oncotarget* 8, 27105–27119. doi: 10.18632/oncotarget.15637

Farooqi, A. A., Shu, C. W., Huang, H. W., Wang, H. R., Chang, Y. T., Fayyaz, S., et al. (2017). TRAIL, Wnt, sonic hedgehog, TGFβ, and miRNA signalings are potential targets for oral cancer therapy. *Int. J. Mol. Sci.* 18:1523. doi: 10.3390/ijms18071523

Filippone, M. G., Di Palma, T., Lucci, V., and Zannini, M. (2014). Pax8 modulates the expression of Wnt4 that is necessary for the maintenance of the epithelial phenotype of thyroid cells. *BMC Mol. Biol.* 15:21. doi: 10.1186/1471-2199-15-21

Flores-Hernández, E., Velázquez, D. M., Castañeda-Patlán, M. C., Fuentes-García, G., Fonseca-Camarillo, G., Yamamoto-Furusho, J. K., et al. (2020). Canonical and non-canonical Wnt signaling are simultaneously activated by Wnts in colon cancer cells. *Cell. Signal* 72:109636. doi: 10.1016/j.cellsig.2020.109636

Foulquier, S., Daskalopoulos, E. P., Lluri, G., Hermans, K. C. M., Deb, A., and Blankesteijn, W. M. (2018). WNT signaling in cardiac and vascular disease. *Pharmacol. Rev.* 70, 68–141. doi: 10.1124/pr.117.013896

González-Moles, M. A., Ruiz-Ávila, I., Gil-Montoya, J. A., Plaza-Campillo, J., and Scully, C. (2014). β-catenin in oral cancer: an update on current knowledge. *Oral Oncol.* 50, 818–824. doi: 10.1016/j.oraloncology.2014.06.005

Gordon, M. D., and Nusse, R. (2006). Wnt signaling: multiple pathways, multiple receptors, and multiple transcription factors. *J. Biol. Chem.* 281, 22429–22433. doi: 10.1074/jbc.R600015200

Hagen, T., and Vidal-Puig, A. (2002). Characterisation of the phosphorylation of beta-catenin at the GSK-3 priming site Ser45. *Biochem. Biophys. Res. Commun.* 294, 324–328. doi: 10.1016/S0006-291X(02)00485-0

Hayes, J., Peruzzi, P. P., and Lawler, S. (2014). MicroRNAs in cancer: biomarkers, functions and therapy. *Trends Mol. Med.* 20, 460–469. doi: 10.1016/j.molmed.2014.06.005

Hernández-Maqueda, J. G., Luna-Ulloa, L. B., Santoyo-Ramos, P., Castañeda-Patlán, M. C., and Robles-Flores, M. (2013). Protein kinase C delta negatively modulates canonical Wnt pathway and cell proliferation in colon tumor cell lines. *PLoS One* 8:e58540. doi: 10.1371/journal.pone.0058540

Hu, T., and Li, C. (2010). Convergence between Wnt-β-catenin and EGFR signaling in cancer. *Mol. Cancer* 9:236. doi: 10.1186/1476-4598-9-236

Huang, S. M., Mishina, Y. M., Liu, S., Cheung, A., Stegmeier, F., Michaud, G. A., et al. (2009). Tankyrase inhibition stabilizes axin and antagonizes Wnt signalling. *Nature* 461, 614–620. doi: 10.1038/nature08356

Humphries, A. C., and Mlodzik, M. (2018). From instruction to output: Wnt/PCP signaling in development and cancer. *Curr. Opin. Cell Biol.* 51, 110–116. doi: 10.1016/j.ceb.2017.12.005

Ishida, K., Ito, S., Wada, N., Deguchi, H., Hata, T., Hosoda, M., et al. (2007). Nuclear localization of beta-catenin involved in precancerous change in oral leukoplakia. *Mol. Cancer* 6:62. doi: 10.1186/1476-4598-6-62

Iwai, S., Katagiri, W., Kong, C., Amekawa, S., Nakazawa, M., and Yura, Y. (2005). Mutations of the APC, beta-catenin, and axin 1 genes and cytoplasmic accumulation of beta-catenin in oral squamous cell carcinoma. *J. Cancer Res. Clin. Oncol.* 131, 773–782. doi: 10.1007/s00432-005-0027-y

Javed, Z., Muhammad Farooq, H., Ullah, M., Zaheer Iqbal, M., Raza, Q., Sadia, H., et al. (2019). Wnt signaling: a potential therapeutic target in head and neck squamous cell carcinoma. *Asian Pac. J. Cancer Prev.* 20, 995–1003. doi: 10.31557/APJCP.2019.20.4.995

Ji, P., Zhou, Y., Yang, Y., Wu, J., Zhou, H., Quan, W., et al. (2019). Myeloid cell-derived LL-37 promotes lung cancer growth by activating Wnt/β-catenin signaling. *Theranostics* 9, 2209–2223. doi: 10.7150/thno.30726

Kartha, V. K., Alamoud, K. A., Sadykov, K., Nguyen, B. C., Laroche, F., Feng, H., et al. (2018). Functional and genomic analyses reveal therapeutic potential of targeting β-catenin/CBP activity in head and neck cancer. *Genome Med.* 10:54. doi: 10.1186/s13073-018-0569-7

Katase, N., Gunduz, M., Beder, L. B., Gunduz, E., Al Sheikh Ali, M., Tamamura, R., et al. (2010). Frequent allelic loss of Dkk-1 locus (10q11.2) is related with low distant metastasis and better prognosis in head and neck squamous cell carcinomas. *Cancer Invest.* 28, 103–110. doi: 10.3109/07357900903095680

Katase, N., Lefeuvre, M., Gunduz, M., Gunduz, E., Beder, L. B., Grenman, R., et al. (2012). Absence of Dickkopf (Dkk)-3 protein expression is correlated with longer disease-free survival and lower incidence of metastasis in head and neck squamous cell carcinoma. *Oncol. Lett.* 3, 273–280. doi: 10.3892/ol.2011.473

Katase, N., Lefeuvre, M., Tsujigiwa, H., Fujii, M., Ito, S., Tamamura, R., et al. (2013). Knockdown of Dkk-3 decreases cancer cell migration and invasion independently of the Wnt pathways in oral squamous cell carcinoma-derived cells. *Oncol. Rep.* 29, 1349–1355. doi: 10.3892/or.2013.2251

Katase, N., Nagano, K., and Fujita, S. (2020). DKK3 expression and function in head and neck squamous cell carcinoma and other cancers. *J. Oral Biosci.* 62, 9–15. doi: 10.1016/j.job.2020.01.008

Kawakita, A., Yanamoto, S., Yamada, S., Naruse, T., Takahashi, H., Kawasaki, G., et al. (2014). MicroRNA-21 promotes oral cancer invasion via the Wnt/β-catenin pathway by targeting DKK2. *Pathol. Oncol. Res.* 20, 253–261. doi: 10.1007/s12253-013-9689-y

Kestler, H. A., and Kühl, M. (2008). From individual Wnt pathways towards a Wnt signalling network. *Philos. Trans. R. Soc. Lond. B Biol. Sci.* 363, 1333–1347. doi: 10.1098/rstb.2007.2251

Kobayashi, K., Hisamatsu, K., Suzui, N., Hara, A., Tomita, H., and Miyazaki, T. (2018). A review of HPV-related head and neck cancer. *J. Clin. Med.* 7:241. doi: 10.3390/jcm7090241

Kremenevskaja, N., von Wasielewski, R., Rao, A. S., Schöfl, C., Andersson, T., and Brabant, G. (2005). Wnt-5a has tumor suppressor activity in thyroid carcinoma. *Oncogene* 24, 2144–2154. doi: 10.1038/sj.onc.1208370

Kulak, O., Chen, H., Holohan, B., Wu, X., He, H., Borek, D., et al. (2015). Disruption of Wnt/β-Catenin signaling and telomeric shortening are inextricable consequences of tankyrase inhibition in human cells. *Mol. Cell. Biol.* 35, 2425–2435. doi: 10.1128/MCB.00392-315

Lamb, R., Ablett, M. P., Spence, K., Landberg, G., Sims, A. H., and Clarke, R. B. (2013). Wnt pathway activity in breast cancer sub-types and stem-like cells. *PLoS One* 8:e67811. doi: 10.1371/journal.pone.0067811

Lammi, L., Arte, S., Somer, M., Jarvinen, H., Lahermo, P., Thesleff, I., et al. (2004). Mutations in AXIN2 cause familial tooth agenesis and predispose to colorectal cancer. *Am. J. Hum. Genet.* 74, 1043–1050. doi: 10.1086/386293

Lau, T., Chan, E., Callow, M., Waaler, J., Boggs, J., Blake, R. A., et al. (2013). A novel tankyrase small-molecule inhibitor suppresses APC mutation-driven colorectal tumor growth. *Cancer Res.* 73, 3132–3144. doi: 10.1158/0008-5472.CAN-12-4562

Le, P. N., Keysar, S. B., Miller, B., Eagles, J. R., Chimed, T. S., Reisinger, J., et al. (2019). Wnt signaling dynamics in head and neck squamous cell cancer tumor-stroma interactions. *Mol. Carcinog.* 58, 398–410. doi: 10.1002/mc.22937

Lee, C. H., Hung, H. W., Hung, P. H., and Shieh, Y. S. (2010). Epidermal growth factor receptor regulates beta-catenin location, stability, and transcriptional activity in oral cancer. *Mol. Cancer* 9:64. doi: 10.1186/1476-4598-9-64

Lee, S. H., Koo, B. S., Kim, J. M., Huang, S., Rho, Y. S., Bae, W. J., et al. (2014). Wnt/β-catenin signalling maintains self-renewal and tumourigenicity of head and neck squamous cell carcinoma stem-like cells by activating Oct4. *J. Pathol.* 4, 99–107. doi: 10.1002/path.4383

Leethanakul, C., Patel, V., Gillespie, J., Pallente, M., Ensley, J. F., Koontongkaew, S., et al. (2000). Distinct pattern of expression of differentiation and growth-related genes in squamous cell carcinomas of the head and neck revealed by the use of laser capture microdissection and cDNA arrays. *Oncogene* 19, 3220–3224. doi: 10.1038/sj.onc.1203703

Li, N., Li, D., Du, Y., Su, C., Yang, C., Lin, C., et al. (2019). Overexpressed PLAGL2 transcriptionally activates Wnt6 and promotes cancer development in colorectal cancer. *Oncol. Rep.* 41, 875–884. doi: 10.3892/or.2018.6914

Lien, W. H., and Fuchs, E. (2014). Wnt some lose some: transcriptional governance of stem cells by Wnt/β-catenin signaling. *Genes Dev.* 28, 1517–1532. doi: 10.1101/gad.244772.114

Lim, Y. C., Kang, H. J., Kim, Y. S., and Choi, E. C. (2012). All-trans-retinoic acid inhibits growth of head and neck cancer stem cells by suppression of Wnt/β-catenin pathway. *Eur. J. Cancer* 48, 3310–3318. doi: 10.1016/j.ejca.2012.04.013

Liu, H., Li, J., Zhou, Y., Hu, Q., Zeng, Y., and Mohammadreza, M. M. (2017). Human papillomavirus as a favorable prognostic factor in a subset of head and neck squamous cell carcinomas: a meta-analysis. *J. Med. Virol.* 89, 710–725. doi: 10.1002/jmv.24670

Logan, C. Y., and Nusse, R. (2004). The Wnt signaling pathway in development and disease. *Annu. Rev. Cell Dev. Biol.* 20, 781–810. doi: 10.1146/annurev.cellbio.20.010403.113126

Lustig, B., and Behrens, J. (2003). The Wnt signaling pathway and its role in tumor development. *J. Cancer Res. Clin. Oncol.* 129, 199–221. doi: 10.1007/s00432-003-0431-0

Ma, X., Yan, W., Dai, Z., Gao, X., Ma, Y., Xu, Q., et al. (2016). Baicalein suppresses metastasis of breast cancer cells by inhibiting EMT via downregulation of SATB1 and Wnt/β-catenin pathway. *Drug Des. Devel. Ther.* 10, 1419–1441. doi: 10.2147/DDDT.S102541

MacDonald, B. T., Tamai, K., and He, X. (2009). Wnt/beta-catenin signaling: components, mechanisms, and diseases. *Dev. Cell* 17, 9–26. doi: 10.1016/j.devcel.2009.06.016

Mannelli, G., and Gallo, O. (2012). Cancer stem cells hypothesis and stem cells in head and neck cancers. *Cancer Treat Rev.* 38, 515–539. doi: 10.1016/j.ctrv.2011.11.007

Morin, P. J., Sparks, A. B., Korinek, V., Barker, N., Clevers, H., Vogelstein, B., et al. (1997). Activation of beta-catenin-Tcf signaling in colon cancer by mutations in beta-catenin or APC. *Science* 275, 1787–1790. doi: 10.1126/science.275.5307.1787

Ng, L. F., Kaur, P., Bunnag, N., Suresh, J., Sung, I. C. H., Tan, Q. H., et al. (2019). WNT Signaling in Disease. *Cells* 8:826. doi: 10.3390/cells8080826

Ng, O. H., Erbilgin, Y., Firtina, S., Celkan, T., Karakas, Z., Aydogan, G., et al. (2014). Deregulated WNT signaling in childhood T-cell acute lymphoblastic leukemia. *Blood Cancer J.* 4:e192. doi: 10.1038/bcj.2014.12

Nusse, R., Brown, A., Papkoff, J., Scambler, P., Shackleford, G., McMahon, A., et al. (1991). A new nomenclature for int-1 and related genes: the Wnt gene family. *Cell* 64:231. doi: 10.1016/0092-8674(91)90633-a

Nwanze, J., Cohen, C., Schmitt, A. C., and Siddiqui, M. T. (2015). β-Catenin expression in oropharyngeal squamous cell carcinomas: comparison and correlation with p16 and human papillomavirus in situ hybridization. *Acta Cytol.* 59, 479–484. doi: 10.1159/000443602

Paluszczak, J., Sarbak, J., Kostrzewska-Poczekaj, M., Kiwerska, K., Jarmuż-Szymczak, M., Grenman, R., et al. (2015). The negative regulators of Wnt pathway-DACH1, DKK1, and WIF1 are methylated in oral and oropharyngeal cancer and WIF1 methylation predicts shorter survival. *Tumour Biol.* 36, 2855–2861. doi: 10.1007/s13277-014-2913-x

Pannone, G., Bufo, P., Santoro, A., Franco, R., Aquino, G., Longo, F., et al. (2010). WNT pathway in oral cancer: epigenetic inactivation of WNT-inhibitors. *Oncol. Rep.* 24, 1035–1041. doi: 10.3892/or.2010.1035

Peng, L., Li, Y., Shusterman, K., Kuehl, M., and Gibson, C. W. (2011). Wnt-RhoA signaling is involved in dental enamel development. *Eur. J. Oral Sci.* 119(Suppl. 1), 41–49. doi: 10.1111/j.1600-0722.2011.00880.x

Polakis, P. (2012). Wnt signaling in cancer. *Cold Spring Harb. Perspect. Biol.* 4:a008052. doi: 10.1101/cshperspect.a008052

Prgomet, Z., Andersson, T., and Lindberg, P. (2017). Higher expression of WNT5A protein in oral squamous cell carcinoma compared with dysplasia and oral mucosa with a normal appearance. *Eur. J. Oral Sci.* 125, 237–246. doi: 10.1111/eos.12352

Prgomet, Z., Axelsson, L., Lindberg, P., and Andersson, T. (2015). Migration and invasion of oral squamous carcinoma cells is promoted by WNT5A, a regulator of cancer progression. *J. Oral Pathol. Med.* 44, 776–784. doi: 10.1111/jop.12292

Prince, M. E., Sivanandan, R., Kaczorowski, A., Wolf, G. T., Kaplan, M. J., Dalerba, P., et al. (2007). Identification of a subpopulation of cells with cancer stem cell properties in head and neck squamous cell carcinoma. *Proc. Natl. Acad. Sci. U.S.A.* 104, 973–978. doi: 10.1073/pnas.0610117104

Proffitt, K. D., Madan, B., Ke, Z., Pendharkar, V., Ding, L., Lee, M. A., et al. (2013). Pharmacological inhibition of the Wnt acyltransferase PORCN prevents growth of WNT-driven mammary cancer. *Cancer Res.* 73, 502–507. doi: 10.1158/0008-5472.CAN-12-2258

Psyrri, A., Kotoula, V., Fountzilas, E., Alexopoulou, Z., Bobos, M., Televantou, D., et al. (2014). Prognostic significance of the Wnt pathway in squamous cell laryngeal cancer. *Oral Oncol.* 50, 298–305. doi: 10.1016/j.oraloncology.2014.01.005

Qin, L., Yin, Y. T., Zheng, F. J., Peng, L. X., Yang, C. F., Bao, Y. N., et al. (2015). WNT5A promotes stemness characteristics in nasopharyngeal carcinoma cells leading to metastasis and tumorigenesis. *Oncotarget* 6, 10239–10252. doi: 10.18632/oncotarget.3518

Rao, T. P., and Kühl, M. (2010). An updated overview on Wnt signaling pathways: a prelude for more. *Circ. Res.* 106, 1798–1806. doi: 10.1161/CIRCRESAHA.110.219840

Rhee, C. S., Sen, M., Lu, D., Wu, C., Leoni, L., Rubin, J., et al. (2002). Wnt and frizzled receptors as potential targets for immunotherapy in head and neck squamous cell carcinomas. *Oncogene* 21, 6598–6605. doi: 10.1038/sj.onc.1205920

Rubinfeld, B., Robbins, P., El-Gamil, M., Albert, I., Porfiri, E., and Polakis, P. (1997). Stabilization of beta-catenin by genetic defects in melanoma cell lines. *Science* 275, 1790–1792. doi: 10.1126/science.275.5307.1790

Rudy, S. F., Brenner, J. C., Harris, J. L., Liu, J., Che, J., Scott, M. V., et al. (2016). In vivo Wnt pathway inhibition of human squamous cell carcinoma growth and metastasis in the chick chorioallantoic model. *J. Otolaryngol. Head Neck Surg.* 45:26. doi: 10.1186/s40463-016-0140-8

Russell, J. O., and Monga, S. P. (2018). Wnt/β-Catenin signaling in liver development, homeostasis, and pathobiology. *Annu. Rev. Pathol.* 13, 351–378. doi: 10.1146/annurev-pathol-020117-044010

Sakamoto, T., Kawano, S., Matsubara, R., Goto, Y., Jinno, T., Maruse, Y., et al. (2017). Critical roles of Wnt5a-Ror2 signaling in aggressiveness of tongue squamous cell carcinoma and production of matrix metalloproteinase-2 via ΔNp63β-mediated epithelial-mesenchymal transition. *Oral Oncol.* 69, 15–25. doi: 10.1016/j.oraloncology.2017.03.019

Sakisaka, Y., Tsuchiya, M., Nakamura, T., Tamura, M., Shimauchi, H., and Nemoto, E. (2015). Wnt5a attenuates Wnt3a-induced alkaline phosphatase expression in dental follicle cells. *Exp. Cell Res.* 336, 85–93. doi: 10.1016/j.yexcr.2015.06.013

Saneyoshi, T., Kume, S., Amasaki, Y., and Mikoshiba, K. (2002). The Wnt/calcium pathway activates NF-AT and promotes ventral cell fate in Xenopus embryos. *Nature* 417, 295–299. doi: 10.1038/417295a

Satoh, S., Daigo, Y., Furukawa, Y., Kato, T., Miwa, N., Nishiwaki, T., et al. (2000). AXIN1 mutations in hepatocellular carcinomas, and growth suppression in cancer cells by virus-mediated transfer of AXIN1. *Nat. Genet.* 24, 245–250. doi: 10.1038/73448

Shiah, S. G., Hsiao, J. R., Chang, W. M., Chen, Y. W., Jin, Y. T., Wong, T. Y., et al. (2014). Downregulated miR329 and miR410 promote the proliferation and invasion of oral squamous cell carcinoma by targeting Wnt-7b. *Cancer Res.* 74, 7560–7572. doi: 10.1158/0008-5472.CAN-14-0978

Shiah, S. G., Shieh, Y. S., and Chang, J. Y. (2016). The role of Wnt signaling in squamous cell carcinoma. *J. Dent. Res.* 95, 129–134. doi: 10.1177/0022034515613507

Song, J., Chang, I., Chen, Z., Kang, M., and Wang, C. Y. (2010). Characterization of side populations in HNSCC: highly invasive, chemoresistant and abnormal Wnt signaling. *PLoS One* 5:e11456. doi: 10.1371/journal.pone.0011456

Takeshita, A., Iwai, S., Morita, Y., Niki-Yonekawa, A., Hamada, M., and Yura, Y. (2014). Wnt5b promotes the cell motility essential for metastasis of oral squamous cell carcinoma through active Cdc42 and RhoA. *Int. J. Oncol.* 44, 59–68. doi: 10.3892/ijo.2013.2172

Tejeda-Muñoz, N., and Robles-Flores, M. (2015). Glycogen synthase kinase 3 in Wnt signaling pathway and cancer. *IUBMB Life* 67, 914–922. doi: 10.1002/iub.1454

Valenta, T., Hausmann, G., and Basler, K. (2012). The many faces and functions of β-catenin. *EMBO J.* 31, 2714–2736. doi: 10.1038/emboj.2012.150

van Tienen, F. H., Laeremans, H., van der Kallen, C. J., and Smeets, H. J. (2009). Wnt5b stimulates adipogenesis by activating PPARgamma, and inhibiting the beta-catenin dependent Wnt signaling pathway together with Wnt5a. *Biochem. Biophys. Res. Commun.* 387, 207–211. doi: 10.1016/j.bbrc.2009.07.004

Velázquez, D. M., Castañeda-Patlán, M. C., and Robles-Flores, M. (2017). Dishevelled stability is positively regulated by PKCζ-mediated phosphorylation induced by Wnt agonists. *Cell. Signal* 35, 107–117. doi: 10.1016/j.cellsig.2017.03.023

Vermeulen, L., De Sousa, E., Melo, F., van der Heijden, M., Cameron, K., de Jong, J. H., et al. (2010). Wnt activity defines colon cancer stem cells and is regulated by the microenvironment. *Nat. Cell Biol.* 12, 468–476. doi: 10.1038/ncb2048

Vlad, A., Röhrs, S., Klein-Hitpass, L., and Müller, O. (2008). The first five years of the Wnt targetome. *Cell. Signal* 20, 795–802. doi: 10.1016/j.cellsig.2007.10.031

Wang, C., Zhao, Y., Su, Y., Li, R., Lin, Y., Zhou, X., et al. (2013). C-Jun N-terminal kinase (JNK) mediates Wnt5a-induced cell motility dependent or independent of RhoA pathway in human dental papilla cells. *PLoS One* 8:e69440. doi: 10.1371/journal.pone.0069440

Warrier, S., Bhuvanalakshmi, G., Arfuso, F., Rajan, G., Millward, M., and Dharmarajan, A. (2014). Cancer stem-like cells from head and neck cancers are chemosensitized by the Wnt antagonist, sFRP4, by inducing apoptosis, decreasing stemness, drug resistance and epithelial to mesenchymal transition. *Cancer Gene Ther.* 21, 381–388. doi: 10.1038/cgt.2014.42

Wong, S. H. M., Fang, C. M., Chuah, L. H., Leong, C. O., and Ngai, S. C. (2018). E-cadherin: its dysregulation in carcinogenesis and clinical implications. *Crit. Rev. Oncol. Hematol.* 121, 11–22. doi: 10.1016/j.critrevonc.2017.11.010

Wu, D., and Pan, W. (2010). GSK3: a multifaceted kinase in Wnt signaling. *Trends Biochem. Sci.* 35, 161–168. doi: 10.1016/j.tibs.2009.10.002

Xi, S., and Grandis, J. R. (2003). Gene therapy for the treatment of oral squamous cell carcinoma. *J. Dent. Res.* 82, 11–16. doi: 10.1177/154405910308200104

Xie, H., Ma, Y., Li, J., Chen, H., Xie, Y., Chen, M., et al. (2020). WNT7A promotes EGF-induced migration of oral squamous cell carcinoma cells by activating β-catenin/mmp9-mediated signaling. *Front. Pharmacol.* 11:98. doi: 10.3389/fphar.2020.00098

Yao, C. J., Lai, G. M., Yeh, C. T., Lai, M. T., Shih, P. H., Chao, W. J., et al. (2013). Honokiol eliminates human oral cancer stem-like cells accompanied with suppression of Wnt/ β -catenin signaling and apoptosis induction. *Evid Based Complement Alternat. Med.* 2013:146136. doi: 10.1155/2013/146136

Yao, C. J., Lai, G. M., Yeh, C. T., Lai, M. T., Shih, P. H., Chao, W. J., et al. (2017). Corrigendum to "Honokiol eliminates human oral cancer stem-like cells accompanied with suppression of Wnt/β-catenin signaling and apoptosis induction". *Evid Based Complement Alternat. Med.* 2017:9387837. doi: 10.1155/2017/9387837

Yu, C., Wang, Y., Li, G., She, L., Zhang, D., Chen, X., et al. (2018). LncRNA PVT1 promotes malignant progression in squamous cell carcinoma of the head and neck. *J. Cancer.* 9, 3593–3602. doi: 10.7150/jca.26465

Zhang, C., Hao, Y., Sun, Y., and Liu, P. (2019). Quercetin suppresses the tumorigenesis of oral squamous cell carcinoma by regulating microRNA-22/WNT1/β-catenin axis. *J. Pharmacol. Sci.* 140, 128–136. doi: 10.1016/j.jphs.2019.03.005

Zhang, D., Li, G., Chen, X., Jing, Q., Liu, C., Lu, S., et al. (2019). Wnt3a protein overexpression predicts worse overall survival in laryngeal squamous cell carcinoma. *J. Cancer* 10, 4633–4638. doi: 10.7150/jca.35009

Zhang, W., Yan, Y., Gu, M., Wang, X., Zhu, H., Zhang, S., et al. (2017). High expression levels of Wnt5a and Ror2 in laryngeal squamous cell carcinoma are associated with poor prognosis. *Oncol. Lett.* 14, 2232–2238. doi: 10.3892/ol.2017.6386

Zheng, X. L., and Yu, H. G. (2018). Wnt6 contributes tumorigenesis and development of colon cancer via its effects on cell proliferation, apoptosis, cell-cycle and migration. *Oncol. Lett.* 6, 1163–1172. doi: 10.3892/ol.2018.8729

Zhu, H. H., Zhu, X. Y., Zhou, M. H., Cheng, G. Y., and Lou, W. H. (2014). Effect of WNT5A on epithelial-mesenchymal transition and its correlation with tumor invasion and metastasis in nasopharyngeal carcinoma. *Asian Pac. J. Trop. Med.* 7, 488–491. doi: 10.1016/S1995-7645(14)60080-8

**Conflict of Interest:** The authors declare that the research was conducted in the absence of any commercial or financial relationships that could be construed as a potential conflict of interest.

frontiers in Molecular Biosciences

ORIGINAL RESEARCH
published: 11 January 2021
doi: 10.3389/fmolb.2020.611626

# Identification of a Five-Autophagy-Related-lncRNA Signature as a Novel Prognostic Biomarker for Hepatocellular Carcinoma

*Xiaoyu Deng[1], Qinghua Bi[1]*, Shihan Chen[2], Xianhua Chen[3], Shuhui Li[4], Zhaoyang Zhong[5], Wei Guo[6], Xiaohui Li[1]*, Youcai Deng[1]* and Yao Yang[1]**

[1] Institute of Materia Medica, College of Pharmacy, Army Medical University (Third Military Medical University), Chongqing, China, [2] Department of Hepatobiliary Surgery, The First Affiliated Hospital of Army Medical University (Third Military Medical University), Chongqing, China, [3] Diagosis and Treatment Center for Servicemen, The First Affiliated Hospital of Army Medical University (Third Military Medical University), Chongqing, China, [4] Department of Clinical Biochemistry, Faculty of Pharmacy and Laboratory Medicine, Army Medical University (Third Military Medical University), Chongqing, China, [5] Cancer Center, Daping Hospital and Research Institute of Surgery, Army Medical University (Third Military Medical University), Chongqing, China, [6] Department of Pharmacy, Southwest Hospital, Third Military Medical University, Chongqing, China

Although great progresses have been made in the diagnosis and treatment of hepatocellular carcinoma (HCC), its prognostic marker remains controversial. In this current study, weighted correlation network analysis and Cox regression analysis showed significant prognostic value of five autophagy-related long non-coding RNAs (AR-lncRNAs) (including TMCC1-AS1, PLBD1-AS1, MKLN1-AS, LINC01063, and CYTOR) for HCC patients from data in The Cancer Genome Atlas. By using them, we constructed a five-AR-lncRNA prognostic signature, which accurately distinguished the high- and low-risk groups of HCC patients. All of the five AR lncRNAs were highly expressed in the high-risk group of HCC patients. This five-AR-lncRNA prognostic signature showed good area under the curve (AUC) value (AUC = 0.751) for the overall survival (OS) prediction in either all HCC patients or HCC patients stratified according to several clinical traits. A prognostic nomogram with this five-AR-lncRNA signature predicted the 3- and 5-year OS outcomes of HCC patients intuitively and accurately (concordance index = 0.745). By parallel comparison, this five-AR-lncRNA signature has better prognosis accuracy than the other three recently published signatures. Furthermore, we discovered the prediction ability of the signature on therapeutic outcomes of HCC patients, including chemotherapy and immunotherapeutic responses. Gene set enrichment analysis and gene mutation analysis revealed that dysregulated cell cycle pathway, purine metabolism, and TP53 mutation may play an important role in determining the OS outcomes of HCC patients in the high-risk group. Collectively, our study suggests a new five-AR-lncRNA prognostic signature for HCC patients.

**Keywords: hepatocellular carcinoma, prognostic signature, long non-coding RNA, autophagy, stratification analysis, autophagy-related long non-coding RNA**

OPEN ACCESS

***Edited by:***
*Saber Imani,*
*Affiliated Hospital of Southwest Medical University, China*

***Reviewed by:***
*Mazaher Maghsoudloo,*
*University of Tehran, Iran*
*Marzieh Dehghan,*
*University of Zanjan, Iran*

***Correspondence:**
*Yao Yang*
*yang674040463@163.com*
*Youcai Deng*
*youcai.deng@tmmu.edu.cn*
*Xiaohui Li*
*lpsh008@aliyun.com*
*Qinghua Bi*
*biqinghuahua@sina.com*

***Specialty section:***
*This article was submitted to Molecular Diagnostics and Therapeutics, a section of the journal Frontiers in Molecular Biosciences*

***Received:*** *29 September 2020*
***Accepted:*** *02 December 2020*
***Published:*** *11 January 2021*

***Citation:***
*Deng X, Bi Q, Chen S, Chen X, Li S, Zhong Z, Guo W, Li X, Deng Y and Yang Y (2021) Identification of a Five-Autophagy-Related-lncRNA Signature as a Novel Prognostic Biomarker for Hepatocellular Carcinoma. Front. Mol. Biosci. 7:611626. doi: 10.3389/fmolb.2020.611626*

# INTRODUCTION

Hepatocellular carcinoma (HCC) is a kind of malignant neoplasm that is the sixth most commonly diagnosed cancer and the fourth leading cause of cancer-related death worldwide (Singal et al., 2020). Although great developments have been made in the treatment of HCC (Feng et al., 2020), its prognosis remains poor. Tumor extent, severity of liver dysfunction, and general health status of patients were confirmed as key predictors for HCC prognosis; however, the heterogeneity of HCC patients affected the accuracy and applicable scope of the current existing prediction methods (Liu et al., 2016). Therefore, new biomarkers with improved prediction efficiency are urgently necessary for the prognosis of HCC.

Autophagy describes a conserved cellular process that degrades the damaged and mutated cytoplasmic materials by lysosomes so as to maintain the cellular homeostasis under physiological or pathological conditions (Jiang and Mizushima, 2014). Previous studies have revealed that autophagy played various roles in different stages of HCC development (Gerada and Ryan, 2020). Several autophagy-related genes (ARGs), such as LC3 and ULK1, have become emerging biomarkers to predict the prognosis of HCC (Wu et al., 2018; Meng et al., 2020). However, messenger RNA could display unsatisfied prediction because of its low tissue specificity (Deveson et al., 2017) and instability *in vivo* and *in vitro* (Tombacz et al., 2021). Hence, it is still critical to develop novel autophagy-related biomarkers for the prognosis of HCC.

Long non-coding RNA (lncRNA) is a kind of powerful biological functional non-coding RNA, which is longer than 200 nucleotides (Derrien et al., 2012). Sixty-eight percent of human cell transcripts are classified as lncRNAs (Han and Chang, 2015), which play irreplaceable roles in many biological processes (Chen et al., 2017). A large number of lncRNAs were previously found dysregulated in HCC (Cui et al., 2017). Recently, Sun et al. have comprehensively summarized the relationship between autophagy-related lncRNAs (AR-lncRNAs) and HCC. They reported that several AR-lncRNAs participated in the progression of HCC by regulating the expression of autophagy-related proteins, such as ATG3, ATG7, USP22, SIRT1, and PTEN (Sun, 2018). Given that some lncRNAs have been proven much more specific than other biomarker in cancer (Soares et al., 2019), it remains unknown whether a prognostic model composed of multiple AR-lncRNAs could act more efficiently than the current known prognostic signatures for HCC.

As shown in **Figure 1**, in the present study, after applying weighted correlation network analysis (WGCNA) and several kinds of Cox regression analysis on the database of HCC patients in The Cancer Genome Atlas (TCGA), five AR lncRNAs (TMCC1-AS1, PLBD1-AS1, MKLN1-AS, LINC01063, and CYTOR) were identified to construct a prognostic signature for the overall survival (OS) outcomes of HCC patients. The sensitivity and specificity of the five-AR-lncRNA signature surpassed three recently published prognostic signatures for HCC (Wang et al., 2017; Huo et al., 2020; Yang et al., 2020). Furthermore, significant differences were found in the therapeutic outcomes, including immunotherapy and chemotherapy responses, between the high- and low-risk groups. The distinction in prognosis between the high- and low-risk groups may partially due to the differences in the expression levels of ARGs correlated with these five AR lncRNAs.

# METHODS

## Data Sources

The raw count RNA-seq data were downloaded from the TCGA–liver hepatocellular carcinoma (LIHC) dataset in the UCSC Xena (https://xenabrowser.net/datapages/) (Tomczak et al., 2015). The datasets contained a total of 424 samples (including 374 tumor samples and 50 non-tumor liver tissues), along with the corresponding clinical data [including 370 patients with OS information corresponding follow-up data and 319 patients with disease-free survival (DFS) corresponding follow-up data]. Patients with complete clinical prognostic data were included in the subsequent prognostic analysis.

Average raw read count >1 was applied to determine candidate genes that were reasonably expressed. Then, the raw count data were normalized by transcripts-per-million method and underwent a log2 transformation. LncRNAs were reannotated by gene symbol based on the gene annotation file "gencode.v35.long_noncoding_RNAs," which was downloaded from the GENCODE website (https://www.gencodegenes.org/human/) (Liu et al., 2019b). ARGs were obtained from the HADb (Human Autophagy Database, http://www.autophagy.lu/). A total of 222 ARGs with expression value were obtained.

## WGCNA

WGCNA package (Langfelder and Horvath, 2008) (version 1.60) in R was used to find highly correlated lncRNAs to combine lncRNA modules and to search the relationship between each module and each clinical trait of the 370 HCC tumor sample with OS information in TCGA database (Mo et al., 2019). Here, the power of $\beta = 3$ (scale free $R^2 = 0.85$) was selected as the soft threshold to ensure a scale-free network (**Supplementary Figure 1**). The dynamic tree cutting method was used to cluster the lncRNAs in layers, using 50 as a minimum size cutoff, and the cut height = 0.3 was applied to merge highly similar modules. Different lncRNA modules were labeled with different colors, and the gray module contained lncRNAs that cannot be merged. Pearson correlation analysis was applied to evaluate the correlation between lncRNAs in each module and each clinical feature. Autophagy pathway values of each HCC case were estimated by the gene set variation analysis (Liu et al., 2020), and the most relevant module related to autophagy was selected for further analysis.

## Establishment and Verification of AR-lncRNA Signature

First, the univariate Cox regression analysis was used to evaluate the relationship between the expression of the blue module lncRNAs and the OS of patients with HCC (Yang et al., 2018). LncRNAs with $p < 0.05$ was identified to have the prognostic value for HCC OS outcomes. Second, the lncRNAs with $p < 0.001$ in univariate Cox regulation analysis were further analyzed *via*

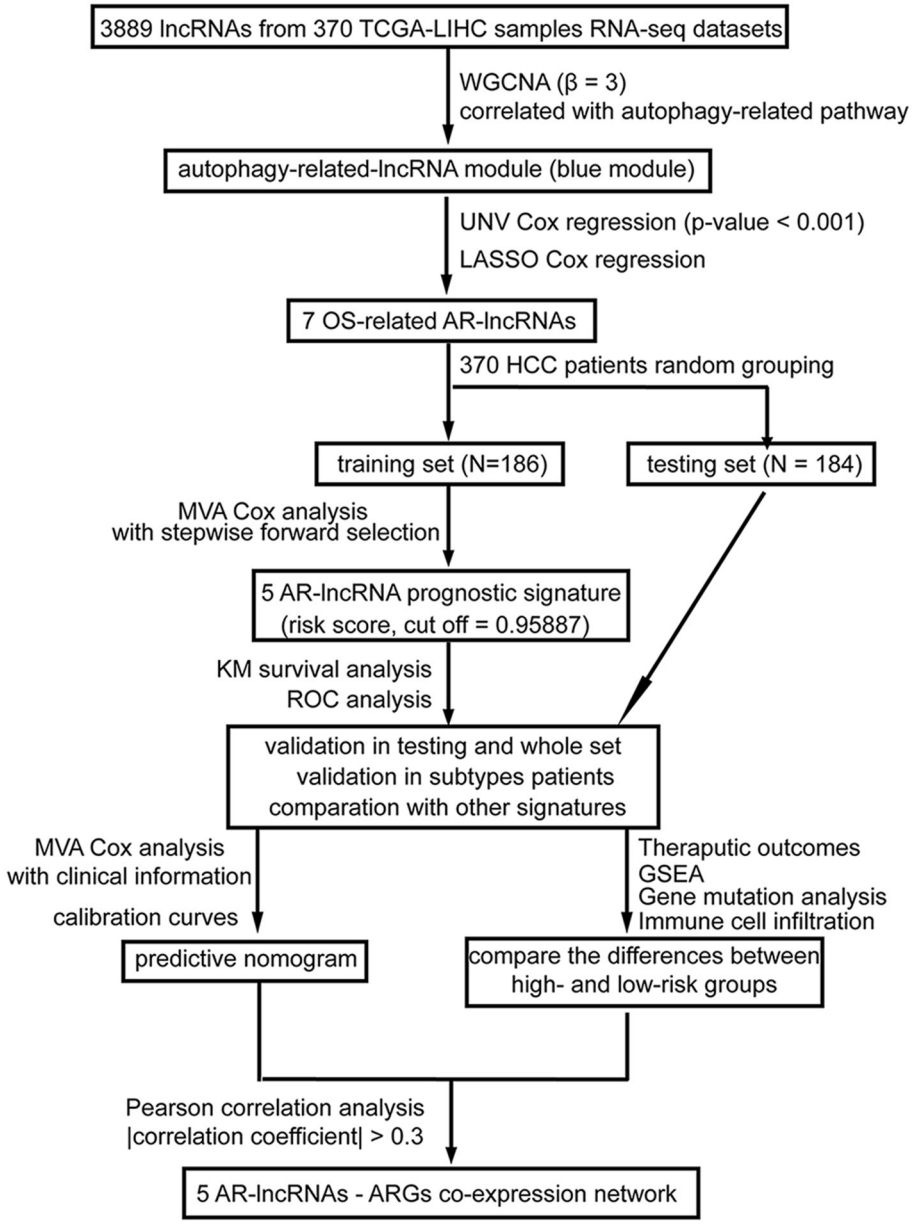


**FIGURE 1 |** A workflow of the processing. The flowchart indicates the establishment, validation, and potential mechanism exploration of the autophagy-related lncRNA (AR-lncRNA) signature. WGCNA, weighted correlation network analysis; UNV Cox regression, univariate Cox regression; LASSO Cox analysis, least absolute shrinkage and selection operator Cox regression analysis; OS, overall survival; AR-lncRNA, autophagy-related lncRNA; MVA Cox regression, multivariate Cox regression; KM survival analysis, Kaplan–Meier survival analysis; ROC analysis, receiver operating characteristic curve analysis; GSEA, gene set enrichment analysis.

the least absolute shrinkage and selection operator (LASSO) Cox regression analysis to select the most useful prognostic lncRNAs, called OS-related AR-lncRNAs, by using the glmnet package in R (Engebretsen and Bohlin, 2019). The "10-fold cross-validation" approach was used to facilitate parameter selection (Mao et al., 2019). Third, HCC patients were randomly divided into training set (186 cases) and testing set (184 cases). The data of the training set were used to generate the prognostic signature through forward conditional stepwise regression with multivariable Cox analysis using the OS-related AR-lncRNAs (Yang et al., 2018). A prognostic multi-lncRNA signature was conducted in which the risk score was calculated as follows: $risk\ score = \sum_{i=1}^{n} Coef_i \times x_i$ ($Coef_i$ was the estimated regression coefficient derived from multivariate Cox regression analysis using the R/survival package (Huang et al., 2020), and $x_i$ was the expression value of each selected AR-lncRNA). The median risk score in the training set was used as the cutoff point that divided HCC patients into a high-risk group and a low-risk group. Then, the formula was

used to calculate the risk score of each HCC patient in the testing and whole set, followed by grouping them into high- and low-risk groups. Log-rank testing method was used to compare the differences of OS outcomes between the high- and low-risk groups *via* Kaplan–Meier survival analysis (Yang et al., 2018). The receiver operating characteristic (ROC) curve analysis in the "survivalROC" package (Heagerty and Zheng, 2005; Huang et al., 2017, 2020) was applied to examine the accuracy of the identified AR-lncRNA signature. Area under the curve (AUC) of 3-year OS outcomes based on the time-dependent ROC curves was used to compare the prediction accuracy of our newly identified AR-lncRNA signature with other three recently published signatures. The concordance index (C-index) was calculated to compare the prediction accuracy of prognostic signatures (Wang et al., 2017; Huo et al., 2020; Yang et al., 2020) by "survcomp" package (Schroder et al., 2011).

## Stratification Analysis

The whole set of patients was stratified by different infection type [HBV ($n = 104$) or HCV ($N = 56$)], alcoholic hepatitis ($n = 117$), age [≥60 years ($N = 201$) or <60 years ($n = 169$)], TNM stages [stage I and II ($n = 256$) or stage III and IV ($n = 90$)], α-fetoprotein (AFP) level [high: >300 ($n = 65$) or low: ≤300 ($n = 212$)]. The formula of risk score acquired in the training set was used to calculate the risk score of each HCC patient in each stratification cohort, followed by grouping them into high- and low-risk groups. Log-rank testing method was used to compare the differences of OS outcomes between the high- and low-risk groups via Kaplan–Meier survival analysis.

## Construction and Assessment of a Prognostic Nomogram

Multivariable Cox analysis was used to testify the prognostic independence of the AR-lncRNA signature where $p < 0.05$ was regarded as statistically significant. A forest plot was used to display the results of the multivariable Cox analysis. The R package rms (Chen S. et al., 2020) was used to construct the nomogram to assess the 3- and 5-year survival possibility for HCC patients. C-index was calculated to identify the discrimination of the nomogram (Huang et al., 2019). Calibration curve of the nomogram was generated to evaluate the consistency between its predicted values and the actual observed values by "nomogramEx" package (Du et al., 2020).

## Immunotherapy and Drug Responsiveness

The Tumor Immune Dysfunction and Exclusion (TIDE) tool (http://tide.dfci.harvard.edu/) was used to compute TIDE score for each tumor sample, which serves as a surrogate to predict the immunotherapy responsiveness (Jiang et al., 2018). The R package pRRophetic (Geeleher et al., 2014) (version 0.5) was applied for drug sensitivity prediction by using ridge regression to estimate the half-maximal inhibitory concentration ($IC_{50}$) for each sample. Then, the prediction accuracy of drug sensitivity was evaluated by 10-fold cross-validation based on the Genomics of Drug Sensitivity in Cancer (https://www.cancerrxgene.org/) (Lui et al., 2020).

## Somatic Variants Analysis

Gene somatic mutation data with a total of 364 HCC samples based on the whole-exome sequencing platform of the TCGA-LIHC datasets were downloaded by TCGAbiolinks (Colaprico et al., 2016). Somatic variants analysis was performed by the R package maftools (Mayakonda et al., 2018) based on the TCGA-LIHC Mutect2 pipeline, which visualized the mutational signatures of the HCC cancer genome. Samples with frameshift insertions, missense mutations, multiple hits, nonsense mutations, splice-site mutations, frame shift deletions, in-frame insertions, or in-frame deletions were considered as positive for a mutation.

## Gene Set Enrichment Analysis

Genome-wide expression profiles of the HCC patients were subjected to gene set enrichment analysis (GSEA) (http://www.broad.mit.edu/gsea/) to analyze genes that were differentially expressed between the patients of the high- and low-risk groups (Yang et al., 2018). Gene sets used in this work were c2.cp.kegg.v7.0.symbols.gmt, which contained mainly Kyoto Encyclopedia of Genes and Genomes pathway and downloaded from the Molecular Signatures Database (MSigDB, http://software.broadinstitute.org/gsea/msigdb/index.jsp). Difference for which the NOM $p < 0.05$ was considered statistically significant.

## Immune Cell Infiltration

The immune cell infiltration status was acquired based on quanTIseq, a method to quantify the fractions of 10 immune cell types from bulk RNA-sequencing data (Finotello et al., 2019), by using the single-sample gene set enrichment approach (Zuo et al., 2020) to the transcriptomes of HCC.

## Correlation Between the Expression Levels of Selected lncRNAs and ARGs

All of the expression data of ARGs of HCC patients were normalized by log2 transformation. Pearson correlation analysis was applied to calculate the correlation between the signature-involved lncRNAs and ARGs. An ARG with a |correlation coefficient| >0.3 and $p < 0.05$ was considered to be the putative target of a lncRNA. The lncRNAs-ARG coexpression network was presented by Cytoscape (version 3.6.2). Correlation scatter plots of each paired lncRNA and ARG were shown for the whole set of HCC patients.

## Statistical Analysis

All dataset analyses were performed using R software (version 3.5.1). The association between each clinical trait and each module was determined using the $\chi^2$ test, Wilcoxon rank sum test, or unpaired *t*-test according the data type of each clinical trait. Univariate and multivariate Cox regression was used to assess prognostic significance. Kaplan–Meier and log-rank tests were used to perform survival analysis. The Student *t*-test was used to compare two independent groups. Mean ± standard deviation with statistical significance was set at $p < 0.05$.

# RESULTS

## Identification of AR-lncRNA Modules for HCC by WGCNA

We used WGCNA to analyze the lncRNAs detected in HCC samples. The dynamic tree cutting method was used to cluster the lncRNAs in layers, and then highly similar modules were merged (**Figure 2A**). Coexpression network by WGCNA analysis revealed that the 3,889 lncRNAs in HCC sample were grouped into nine modules (**Supplementary Table 2**). The highest association between lncRNA modules and clinical traits was found between the blue module and autophagy ($r^2 = 0.46$, $p < 0.05$). The blue module was negatively correlated to the sex of HCC patients ($r^2 = -0.12$, $p < 0.05$) and positively correlated to the stage of HCC patients ($r^2 = 0.16$, $p < 0.05$), respectively (**Figure 2B**). The correlation coefficient between memberships in blue module and memberships in the autophagy pathway of eigengenes in the blue module was 0.68 ($p < 0.001$) (**Figure 2C**), indicating indeed a relationship between the blue module and autophagy activity. Therefore, we defined the blue module as AR-lncRNA module. There were 1,023 lncRNAs in the AR-lncRNA module, among which 44.8% was antisense lncRNAs, and 38.1% was long intergenic non-coding RNAs (**Figure 2D**).

## Establishment and Verification of AR-lncRNA Prognostic Signature for HCC

As previously reported, autophagy pathway is associated with the prognosis of HCC patients (Zhu et al., 2020b);

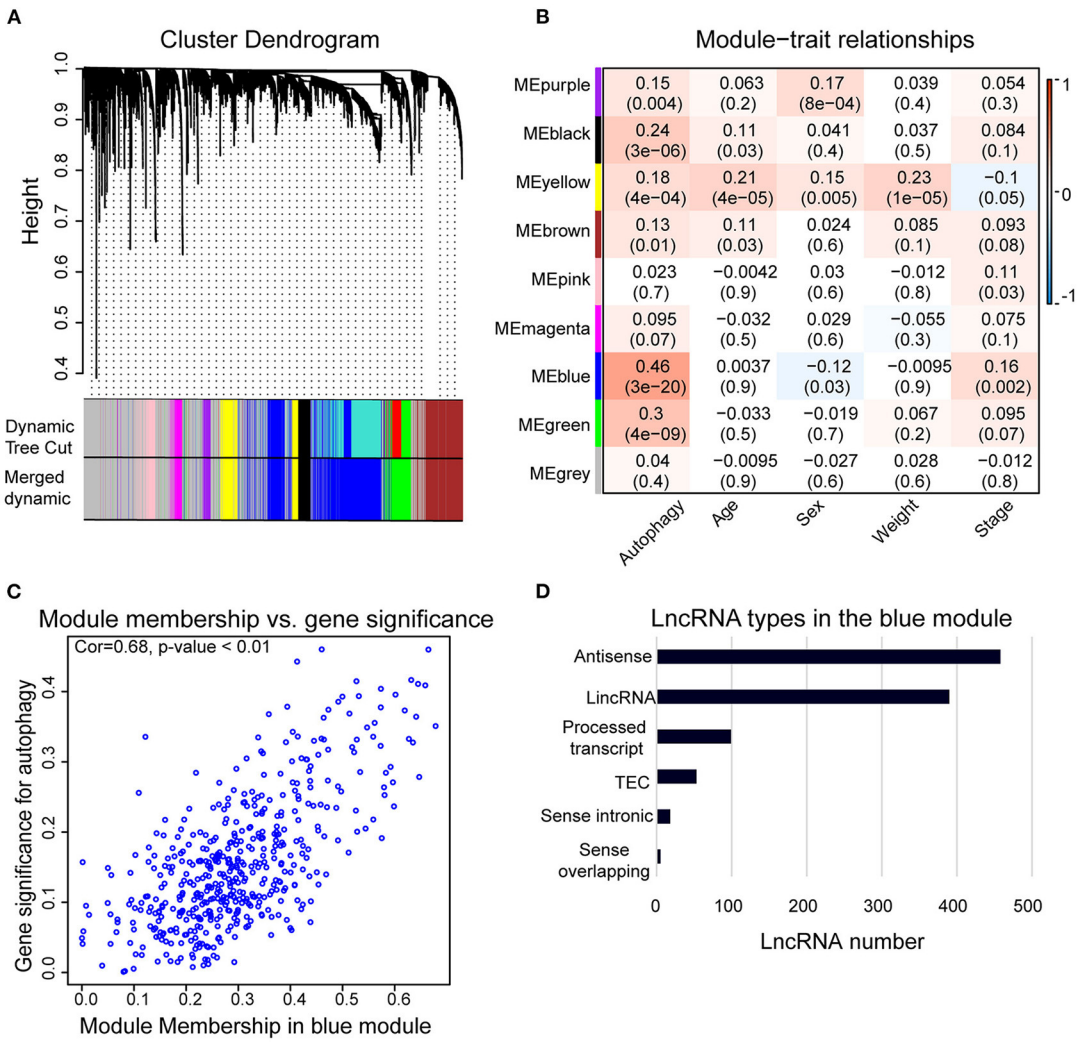


**FIGURE 2 |** Weighted correlation network analysis (WGCNA) of lncRNAs in hepatocellular carcinoma (HCC) samples. **(A)** Gene clustering tree (dendrogram) obtained by hierarchical clustering of adjacency-based dissimilarity. **(B)** Module–trait relationships. Each row corresponds to a module of eigengenes, and each column corresponds to a clinical feature, respectively. Each cell contains the corresponding value of correlation in the first line and *p*-value in the second line, respectively. The cell color presents the correlation according to the color legend. **(C)** Correlation between membership in the blue module and membership in the autophagy pathway of the eigengenes in blue module by Pearson correlation analysis. Cor, correlation coefficient. **(D)** Bar chart shows the types of lncRNAs in the blue module.

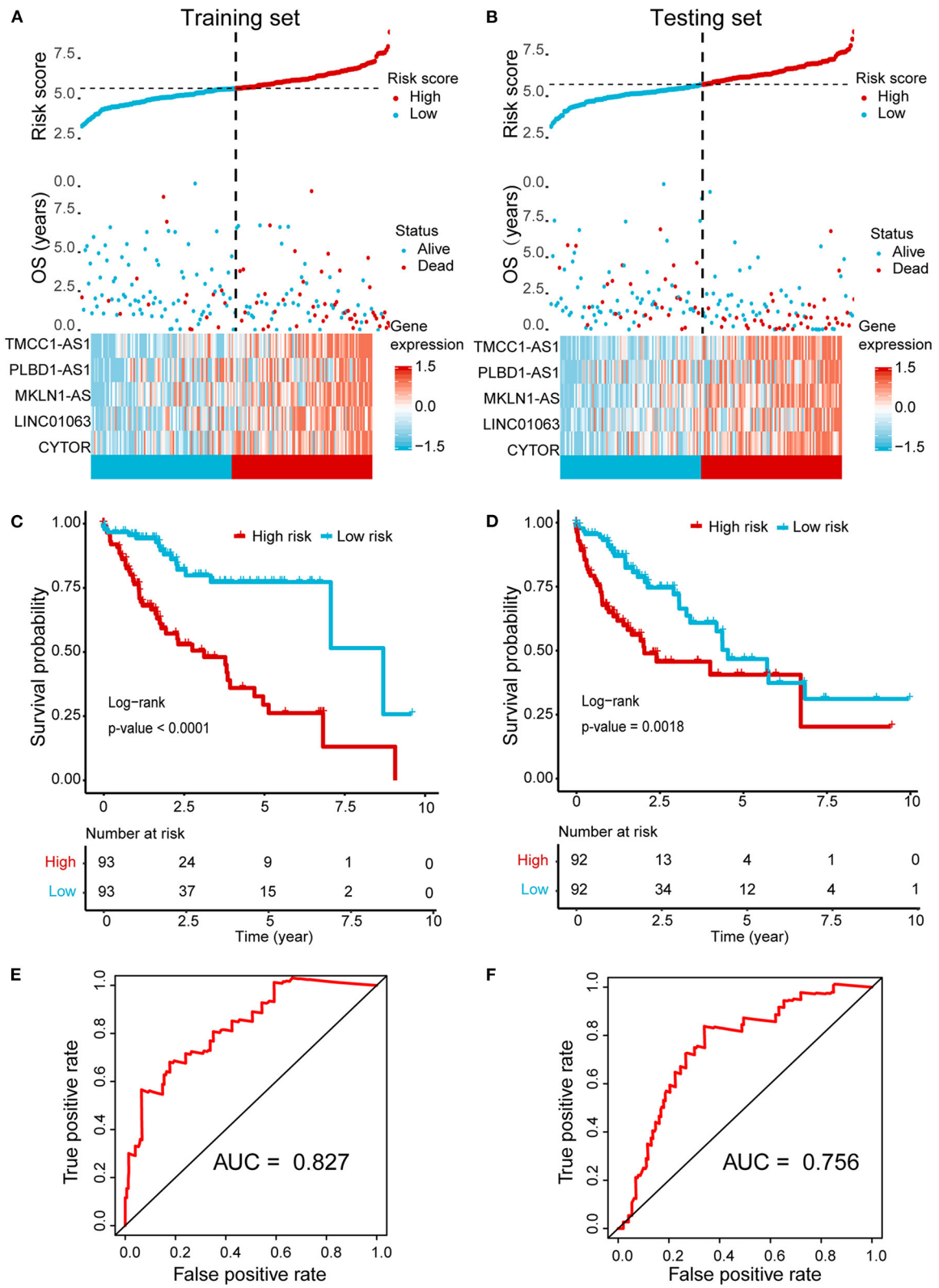


**FIGURE 3 |** Establishment and validation of a five-AR-lncRNA prognostic signature for HCC survival prediction. Patients with a high or a low expression of the selected five AR lncRNAs have significantly different survival probability. **(A,B)** The distribution of risk score, survival state, and expression heatmap of the selected five AR lncRNAs in the training set **(A)** and testing set **(B)**, respectively. **(C,D)** Kaplan–Meier survival curve for the high- and low-risk groups divided by the cutoff value in the training set **(C)** and testing set **(D)**, respectively. *p*-values were obtained via log-rank test. **(E,F)** The receiver operating characteristic curve (ROC) for the prognosis prediction of the signature at 3 years of overall survival (OS) in the training set **(E)** and testing set **(F)**, respectively.

univariate Cox regression analysis was used to explore the relationship between AR-lncRNAs and HCC prognosis. The data revealed that 354 among the total of 1,023 AR-lncRNAs (34.6%) performed the capacity of prognosis for HCC OS outcomes ($p < 0.05$) (**Supplementary Table 1**), indicating a critical role of AR-lncRNAs in HCC prognosis. Then, the LASSO Cox regression analysis identified seven OS-related AR-lncRNAs from the above identified 354 lncRNAs with univariate Cox regression, $p < 0.001$ (**Supplementary Figure 2**). Conformably, high expression of these seven OS-related AR-lncRNAs predicted a poor prognosis of HCC patients.

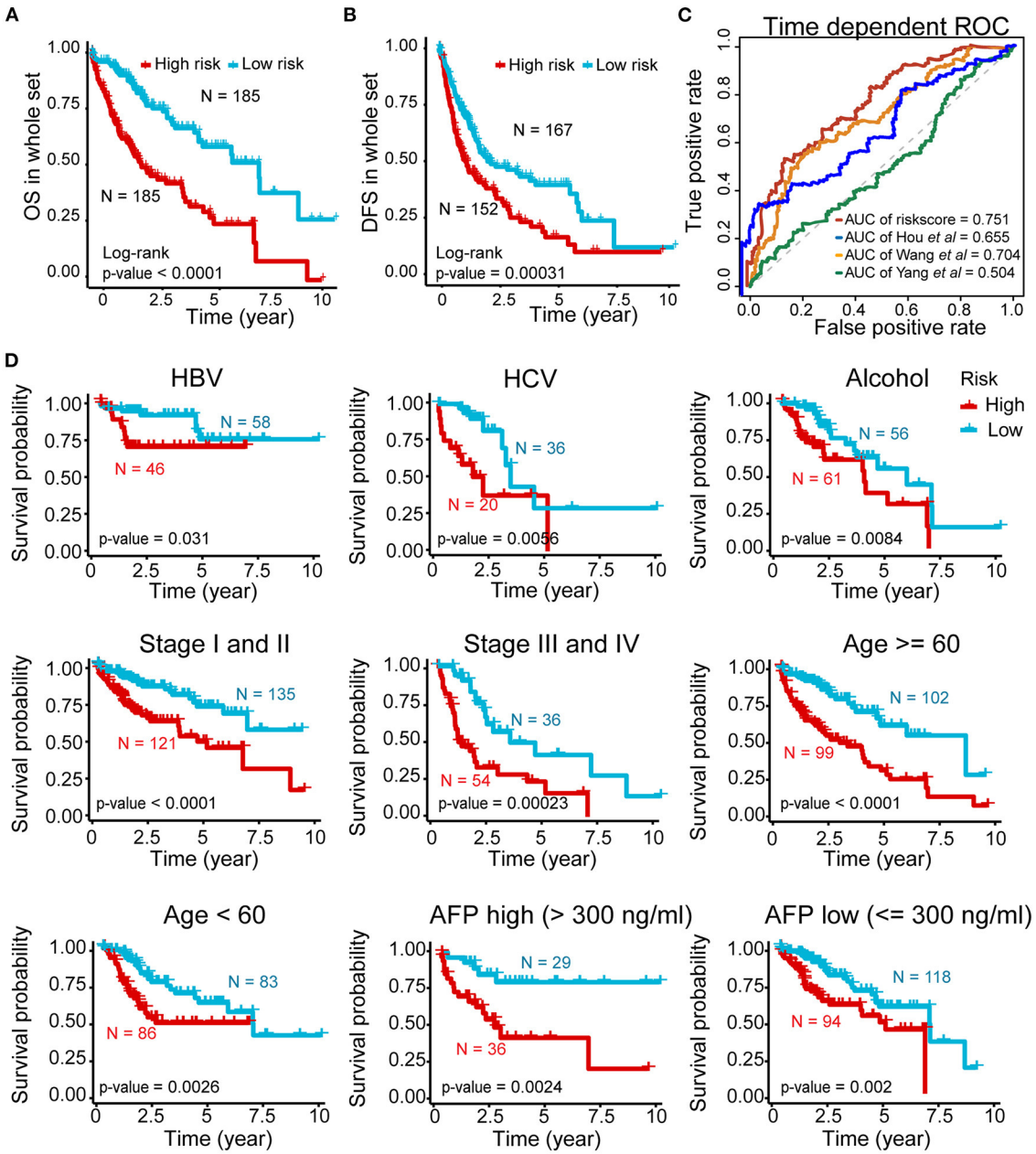


**FIGURE 4 |** Prognostic power of the five-AR-lncRNA prognostic signature in stratification analysis. **(A)** Kaplan–Meier survival curve for the high- and low-risk groups divided by the cutoff value in the whole set. **(B)** Disease-free survival (DFS) for the high- and low-risk patients. **(C)** The ROC analysis of OS outcomes for the five-AR-lncRNA signature (TMCC1-AS1, PLBD1-AS1, MKLN1-AS, LINC01063, CYTOR) by us; five-autophagy-related gene (ARG) signature (HDAC1, RHEB, ATIC, SPNS1, and SQSTM1) by Huo et al. (2020); four-lncRNA signature (ENSG00000234608, ENSG00000242086, ENSG00000273032, ENSG00000228463) by Yang et al. (2020) and four-lncRNA signature (RP11-322E11.5, RP11-150O12.3, AC093609.1, CTC-297N7.9) by Wang et al. (2017) **(D)** Kaplan–Meier curves of patients stratified by different clinicopathological traits. Hepatitis B virus, HBV; hepatitis C virus, HCV. *p*-values were obtained via log-rank test.

Next, we randomly divided the HCC patients in TCGA data into training set (186 cases) and testing set (184 cases). The above identified seven OS-related AR-lncRNAs were used for the prognostic module building by the forward conditional stepwise regression with multivariable Cox analysis in the training set. An AR-lncRNA signature, composed of five feature lncRNAs (TMCC1-AS1, PLBD1-AS1, MKLN1-AS, LINC01063, and CYTOR), was constructed for HCC prognosis. The risk score of each sample in the training set was calculated according to the expression of the five AR lncRNAs by using the following formula: risk score = CYTOR expression × 0.17456 + LINC01063 expression × 0.30093 + MKLN1-AS expression × 0.27462 + PLBS1-AS1 expression × 0.17218 + TMMC1-AS1 expression × 0.28974, in which the coefficients were derived from forward conditional stepwise regression with multivariable Cox analysis. Then, the risk scores were ranked from low to high. According to the cutoff point using the median risk score (cutoff = 0.958887), patients in training set were

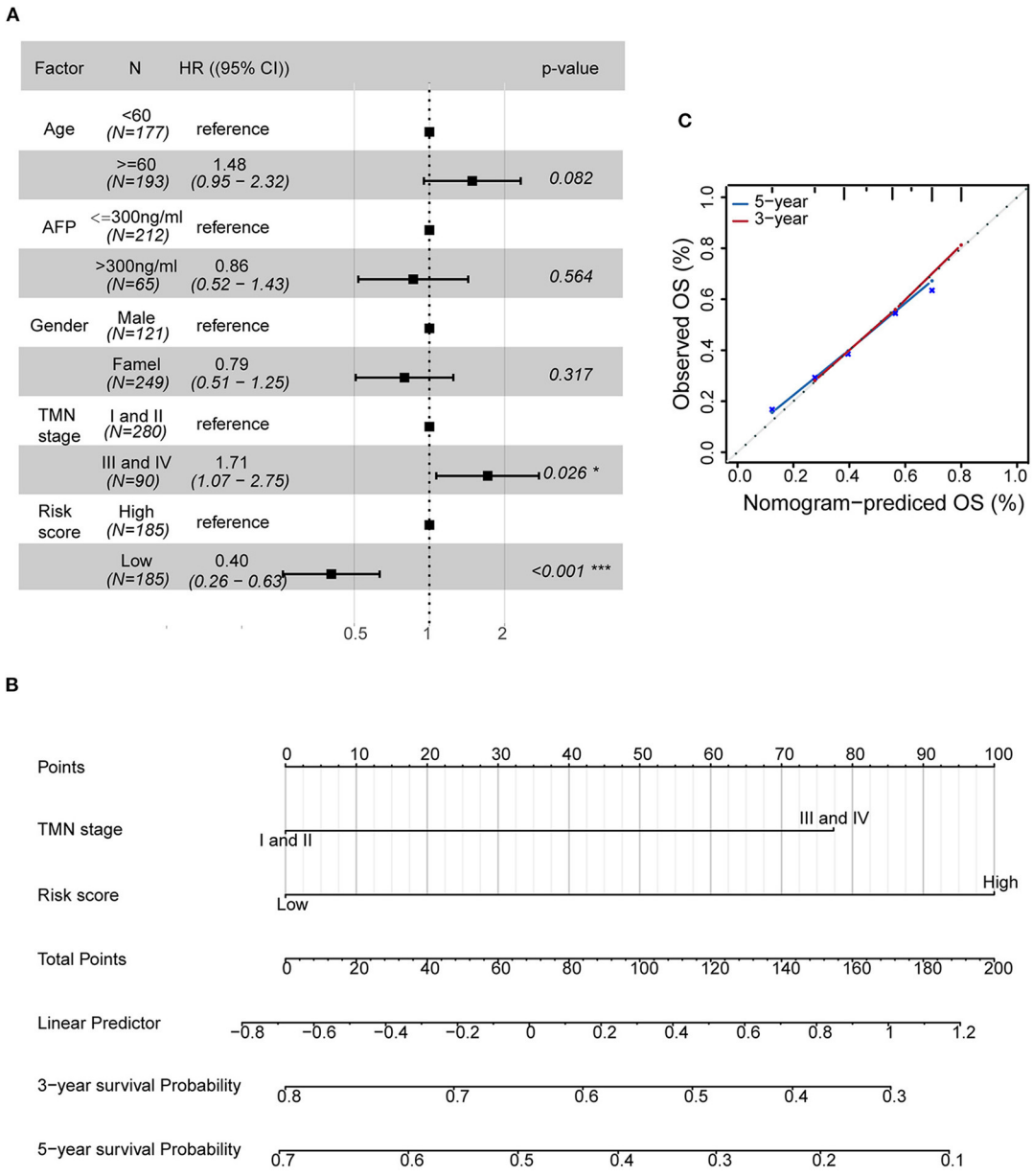


**FIGURE 5 |** Establishment of a nomogram containing independent factors of OS prediction. **(A)** The forest plot based on clinical characteristics and the five-AR-lncRNA signature by multivariate Cox regression analysis. CI, confidence interval; HR, hazard ratio. **(B)** A prognostic nomogram predicting 3- and 5-year OS outcomes of HCC based on TNM stage and the risk score of the five-AR-lncRNA signature. **(C)** Calibration curves for the nomogram of 3- (red) and 5-year (blue) OS prediction for the whole set of HCC patients.

divided into a high-risk group (93 cases, risk score ≥0.958887) and a low-risk group (93 cases, risk score <0.958887). The high-risk group showed higher expression of these five AR lncRNAs and had a poor living status and significantly shorter OS (log-rank test, $p < 0.0001$), compared with the low-risk group (**Figures 3A,C**). The median survival time for high- and low-risk patients was 2.5 and 7 years, respectively. The same formula was applied to the testing set and revealed a similar finding as that in the training set (**Figures 3B,D**). Of note, the AUC values of ROC curve of 3-year OS were 0.827 and 0.756 in the training set and testing set, respectively, indicating good sensitivity and specificity of this five-AR-lncRNA signature in predicting the survival rate of HCC patients (**Figures 3E,F**).

Further validation showed ideal distinction of 3-year OS outcomes between the high- and low-risk groups of the whole set ($p < 0.0001$) (**Figure 4A**). The prognostic power of our signature was also confirmed by good prediction effectiveness on the DFS of all HCC patients ($p < 0.001$) (**Figure 4B**).

Three previously published HCC-related signatures derived from TCGA successfully and significantly predict the OS outcomes, including five-ARG signature (HDAC1, RHEB, ATIC, SPNS1, and SQSTM1) by Huo et al. (2020) four-lncRNA signature (ENSG00000234608, ENSG00000242086, ENSG00000273032, ENSG00000228463) by Yang et al. (2020) and four-lncRNA signature (RP11-322E11.5, RP11-150O12.3, AC093609.1, CTC-297N7.9) by Wang et al. (2017). To compare the sensitivity and specificity of our five-AR-lncRNA signature for the prognosis prediction with these three existing signatures, we performed the time-dependent ROC analysis (Liao et al., 2020). The AUCs of 3-year OS for Hou's signature, Yang's signature, and Wang' signature was 0.655, 0.504, and 0.704, respectively, all of which were lower than that of our five-AR-lncRNA signature (AUC = 0.751) (**Figure 4C**). This indicated an obvious improvement in the estimation of survival rate of HCC patients achieved by this five-AR-lncRNA signature, which can also be seen from the restricted mean survival curve [C-index: 0.71 vs. 0.66 ($p < 0.05$), 0.51 ($p < 0.001$), and vs. 0.67 ($p < 0.05$)] (**Supplementary Figure 3**).

## Stratification Analysis Based on the AR-lncRNA Prognostic Signature

In order to explore the applicability of the five-AR-lncRNA signature, we next performed the stratification analysis. Patients from the whole set were stratified by different infection type (HBV, HCV, alcoholic hepatitis), age (≥60 or <60 years), TNM stages (stage I and II or stage III and IV), and AFP level (>300 or ≤300). Each subgroup was then divided into a high- and low-risk groups based on the median risk score derived from the training set. Kaplan–Meier curves showed that, for all subgroups, the high-risk group had a significant poorer survival rate than that in the low-risk group ($p < 0.05$) (**Figure 4D**). This indicated that the five-AR-lncRNA signature could accurately predicate the prognosis of HCC patients regardless of different clinical traits.

## Establishment of a Nomogram for HCC Prognosis Based on Independent Prognostic Factors

To examine the importance of the five-AR-lncRNA signature when considering other conventional clinical characteristics, we carried out the multivariate Cox regression analysis. The results revealed that after adjusting for other factors, the risk score of the five-AR-lncRNA signature served as an independent factor for the prognosis of HCC ($p < 0.001$) (**Figure 5A**). Among the other clinical characteristics, only TNM stage can act as an independent prognostic factor ($p < 0.05$) (**Figure 5A**).

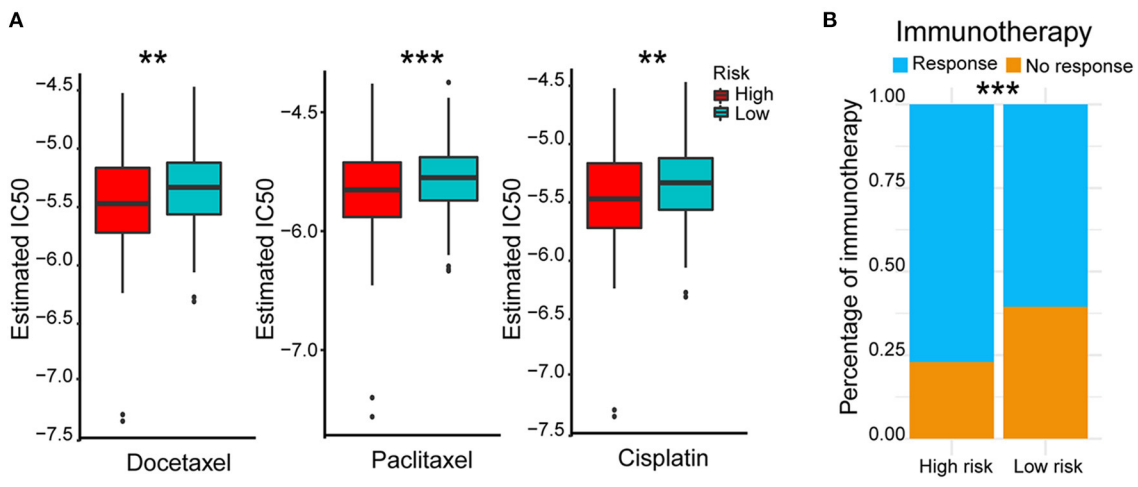


**FIGURE 6 |** Therapeutic outcomes of the high- and low-risk groups based on the five-AR-lncRNA signature. **(A)** Sensitivity to different chemotherapeutic drugs, docetaxel (left), paclitaxel (middle) and cisplatin (right), in the high- and low-risk groups. *p*-values were obtained via Wilcoxon rank sum test. **(B)** Response to immunotherapy in the high- and low-risk groups. *p*-values were obtained via Fisher exact test. $^{**}p < 0.01$ and $^{***}p < 0.001$, respectively.

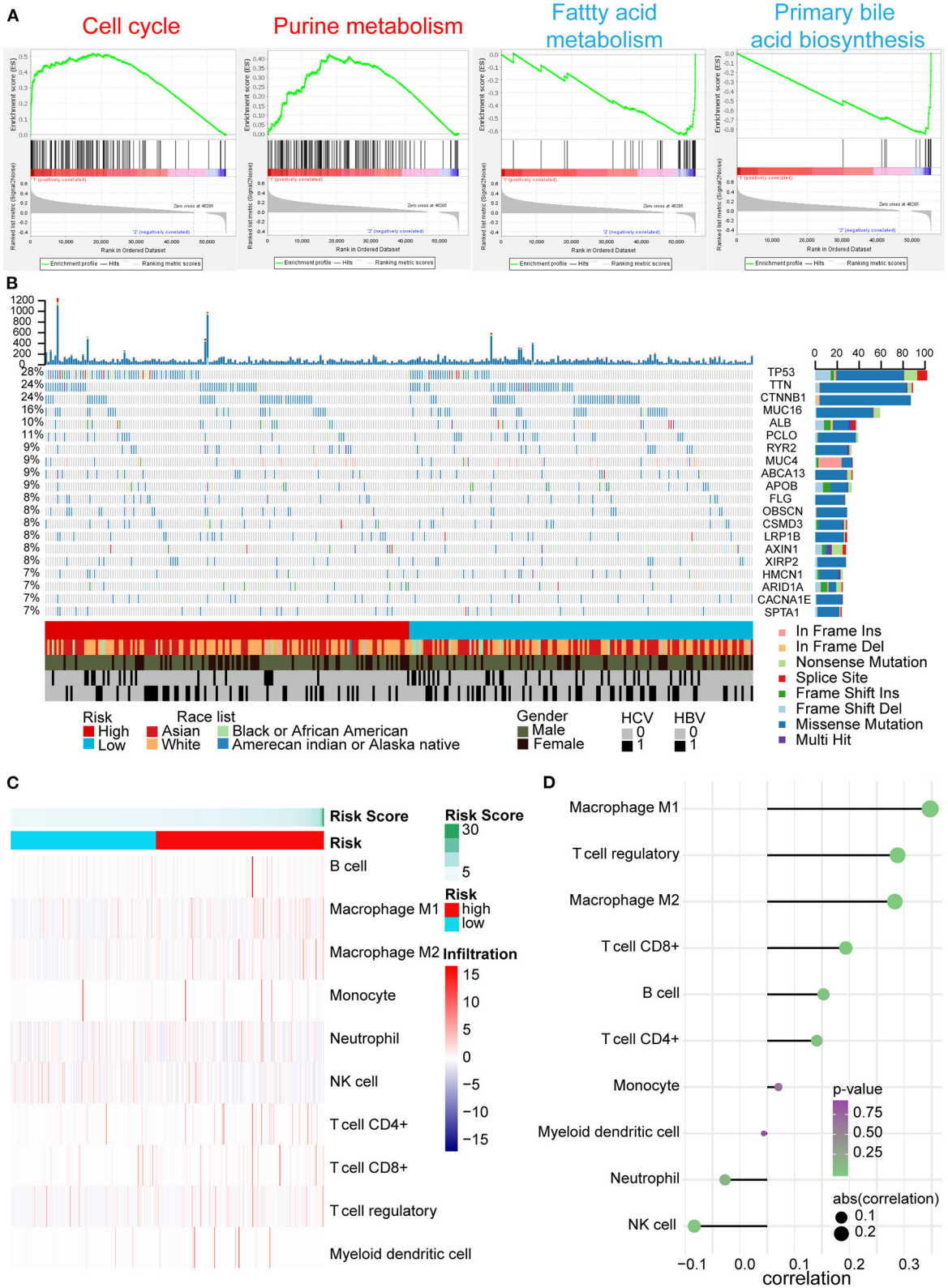


**FIGURE 7 |** GSEA, gene mutation analysis, and immune infiltration of the high- and low-risk groups based on the five-AR-lncRNA signature. **(A)** GSEA of the differentially expressed genes between the high-risk group (marked in red) vs. low-risk group (marked in blue). For each group, only two most significantly enriched functional gene sets are shown. **(B)** The genomic landscape and mutational signatures of 307 HCC patients (84.34% of 364 samples). Individual tumor mutation rates

*(Continued)*

**FIGURE 7 |** are shown in the top panel, whereas the risk, race, gender, and HCV and HBV infection status of HCC patients are detailed in turn in the bottom panel. The middle panel shows genes with statistically significant levels of mutation (MutSig suite, FDR <0.1). The name and type composition of each mutant gene are shown on the right, and mutation types are indicated in the legend at the bottom, respectively. **(C)** Association between risk score and immune cell population in low- and high- risk groups. **(D)** The bubble map shows the correlation between risk score and immune cell subset infiltration. *X* and *Y* axes represent the correlation coefficient and the type of infiltrated immune cell subset, respectively. The color of each bubble shows the *p*-value of correlation, whereas the size shows the absolute value of correlation coefficient.

The prognostic nomogram can assist individualized survival prediction and guide treatment strategies (Wang et al., 2019). Therefore, we used the above selected independent prognostic factors, including TNM stage and the risk score of the five-AR-lncRNA signature, to construct a prognostic nomogram for the 3- and 5-year OS prediction of each individual HCC patient (**Figure 5B**). The calibration curves showed an agreement between the predicted survival and actual survival (**Figure 5C**), and the C-index of nomogram reached 0.745 (95% confidence interval, 0.686–0.805), highlighting an ideal predictive value of our nomogram. So far, we facilitated the utilization of the five-AR-lncRNA signature for HCC.

## Therapeutic-Outcomes Analysis for the High- and Low-Risk Groups

In view of the survival differences between the high- and low-risk groups, we speculated that their responses to different treatments were different. Thus, we further analyzed different therapeutic outcomes of HCC patients, including chemotherapeutic responsiveness and immunotherapy sensitivity. HCC patients in the low-risk group showed stronger drug sensitivity to chemotherapy according to their lower 50% inhibiting concentration ($IC_{50}$) of docetaxel, paclitaxel, and cisplatin ($p < 0.01$) (**Figure 6A**) and better responses to immunotherapy ($p < 0.001$) (**Figure 6B**). These results indicated that the five-AR-lncRNA signature also had a certain degree of separability on the therapeutic response of HCC patients.

## GSEA, Somatic Variants Analysis, and Immune Infiltration for the High- and Low-Risk Groups

According to the above results, we further explored the potential explanations for this five-AR-lncRNA signature, which can distinguish the differences of survival and therapeutic outcome from HCC patients. GSEA results revealed that the high-risk group showed gene enrichment in cell cycle and purine metabolism pathways ($p < 0.05$) (**Supplementary Table 3**). The role of the former was well-established in cancer proliferation, invasion, and metastasis (Otto and Sicinski, 2017), whereas the latter was confirmed one of the markers for liver cancer as it promoted the progression of liver cancer (Chong et al., 2020). In contrast, the low-risk group showed gene enrichment in primary bile acid biosynthesis and fatty acid metabolism pathways ($p < 0.05$) (**Supplementary Table 4**), both of which were usually down-regulated in HCC patients (Wang et al., 2016) (**Figure 7A**).

Somatic variants analysis showed the top 20 mutated genes of HCC samples, including TP53, CTNNB1, ALB, AXIN1, and ARID1A (**Figure 7B**), which was concordant with the previously reported results (Cancer Genome Atlas Research Network. Electronic address and Cancer Genome Atlas Research, 2017). We found a significantly higher frequency of TP53 mutation in the high-risk group than that in the low-risk group (**Figure 7B**).

In tumor microenvironment, what constitutes immune cell subsets affects the antitumor effects of immunotherapy (Bao et al., 2019). With the increase in risk score, the ratio of M1, M2 macrophages, and regulatory T (Treg) cells increased markedly ($p < 0.05$); especially the ratio of M1 cells infiltration showed positive correlation with risk score (correlation coefficient = 0.3), whereas the ratio of natural killer (NK) cells decreased significantly accompanied by the increase of risk score ($p < 0.05$) (**Figures 7C,D**).

## Construction of the Five AR lncRNAs and ARGs Coexpression Network

Moreover, by constructing the lncRNAs-ARG coexpression network, we found an arsenal of ARGs correlated with the five AR lncRNAs ($p < 0.05$, |correlation coefficient| >0.3) (**Supplementary Table 5**) and the largest number of ARGs coexpressed with MKLN1-AS1 (**Figure 8A**). For instance, BECN1, a central protein triggering the autophagy protein cascade (Han et al., 2018), coexpressed with more than two selected AR-lncRNAs and displayed the highest correlation coefficient with MKLN1-AS1 (correlation coefficient = 0.678). The other reported ARGs, including FKBP1A, TP53BP1, and SH3GLB1 (Ge et al., 2014; Wild et al., 2016; Sharma et al., 2018), also showed significant expression correlation with some of these AR-lncRNAs (correlation coefficient >0.6, $p < 0.001$) (**Figure 8B**). The above evidence elucidated that these five AR lncRNAs in our signature may affect the prognosis of HCC patients *via* regulating ARGs expression.

# DISCUSSION

Prognostic models for HCC based on lncRNAs have been reported continuously (Wang et al., 2017; Yang et al., 2020). However, because of the heterogeneity of each cohort and different analysis methods of each study, the predictive effectiveness of their results is not universally applicable (Liu et al., 2016). In this current study, we for the first time achieved a five-AR-lncRNA signature of HCC prognosis. This five-AR-lncRNA signature can be applied to all TCGA-HCC patients even classified by a variety of sorting schemes (including different etiology, TNM stage, age, and AFP level). It showed ideal distinctions of OS outcomes between the high- and low-risk groups with good AUC values. In addition, the accuracy of our five-AR-lncRNA signature also surpassed that of three recently

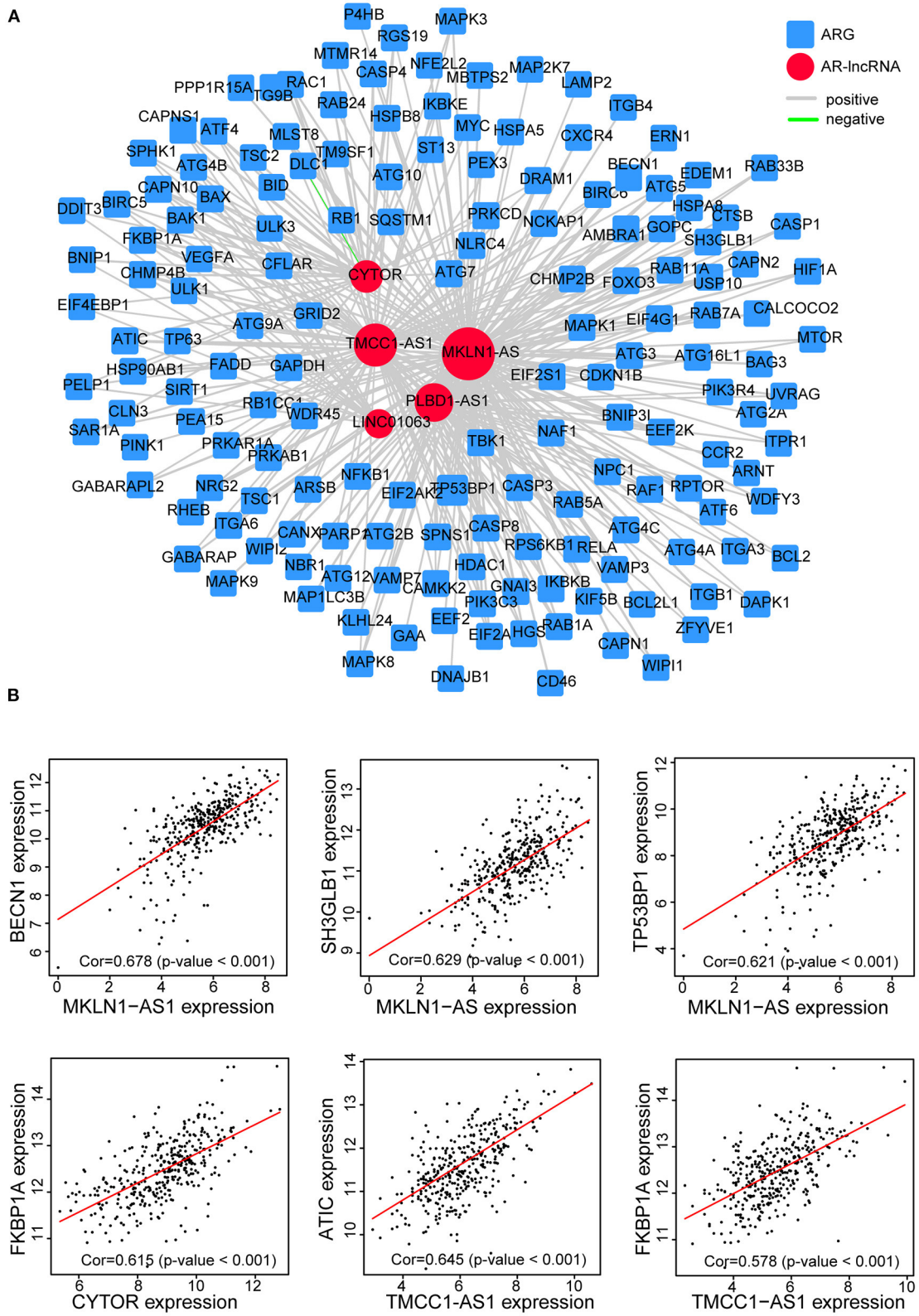


**FIGURE 8 |** Establishment of the five-AR-lncRNA-ARG coexpression network in HCC. **(A)** LncRNAs-ARG coexpression network was established among five signature-involved lncRNAs and ARGs. Each red round node stands for one AR-lncRNA, whereas each blue square node stands for one ARG. Within this coexpression network, gray line represents positive association pair, whereas green line represents negative association pair. The size of each round node is proportional to the number of ARG genes it correlated with. The thickness of a line represents the correlation coefficient. **(B)** Representative correlation scatter plots of ARGs and the five AR lncRNAs by Pearson correlation analysis.

reported prediction signature of HCC based on ARGs or OS-related lncRNAs (Wang et al., 2017; Huo et al., 2020; Yang et al., 2020). The nomogram model, consisting of the TNM stages and the risk score derived from the five-AR-lncRNA signature, can visually predict the 3- and 5-year OS outcomes for individual HCC patient. Of note, the five-AR-lncRNA signature was also able to identify significant differences in chemotherapeutic and immunotherapy responses for HCC patients.

Our five AR lncRNAs include TMCC1-AS1, PLBD1-AS1, MKLN1-AS, LINC01063, and CYTOR, all of which were highly expressed in the high-risk group with poor OS. Consistent with our findings, previous studies have shown that HCC patients with higher expression of TMCC1-AS1 showed shorter OS when compared with the low-expression ones (Zhao et al., 2018; Deng et al., 2020). CYTOR has been reported as an adverse factor of pan cancers *via* promoting proliferation, migration, invasion, metastasis, and drug resistance of tumor cells (Wang et al., 2018; Zhang and Li, 2018; Liu et al., 2019a; Zou et al., 2019; Chen W. et al., 2020; Zhu et al., 2020a). MKLN1-AS has also been reported to be a risk factor of liver cancer (Xiao et al., 2019), although it is also reported as a protective lncRNA of HCC in HBV-positive patients, which might due to the analysis being restricted to HBV-HCC (Zhao et al., 2020). Despite this, our signature could also effectively distinguish the different OS outcomes of high- and low-risk groups of HBV-HCC patients. In addition, we also contributed two new risk lncRNAs, LINC01063 and PLBD1-AS1, for HCC. Our data showed that the expression levels of PLBD1-AS1 and LINC01063 were correlated with tumor suppressor p53-binding protein 1 (TP53BP1) (correlation coefficient = 0.44), and charged multivesicular body protein 4B (CHMP4B) (correlation coefficient = 0.36), respectively. TP53BP1 recruitment can mediate the activation of autophagy by tumor self-DNA damage response (Sharma et al., 2018). CHMP4B recruitment is important at a late step of mitophagosome formation (Zhen et al., 2020). Further studies are warranted to confirm the definite role and mechanism of LINC01063 and PLBD1-AS1 in the development of HCC regarding an autophagy mechanism.

Preliminary mechanism explorations by GSEA and somatic variants analysis revealed that dysregulated cell cycle, purine metabolism, and TP53 mutation may play important roles resulting in poor OS outcomes of HCC patients in the high-risk group. Consistent with these findings, CYTOR has been reported to promote cyclin D1 expression, which regulated G1-to-S phase progression and formed active complexes that promoted cell cycle progression (Alao, 2007), resulting in inhibition of cell apoptosis (Galamb et al., 2020). TMCC1-AS1 correlated with AICAR transformylase (ATIC) (correlation coefficient = 0.61), an autophagy-related protease that catalyzed the last two steps in the purine biosynthesis pathway (Huo et al., 2020). The mutation of TP53, which was proven the most common mutation in patients with liver cancer, showed higher frequency in the high-risk group. Previous study has reported that TP53 inhibited autophagy by inhibiting AMPK but activating mTOR signaling pathway (Zhao et al., 2020). As such, it is interesting to further explore the casual role between TP53 mutation and dysregulated autophagy during HCC development.

Prediction of therapeutic response is helpful for the precision medicine in cancer treatment, especially for the selection of the first line of treatments that determines the prognosis of cancer patient. Our data showed that the five-AR-lncRNA signature was also able to identify significant differences between chemotherapeutic and immunotherapy responses. The low-risk group was more sensitive to cisplatin, docetaxel, and paclitaxel, which were frequently used chemotherapeutic drugs for HCC (Jin et al., 2018; Sung et al., 2020; Tekchandani et al., 2020). This might because of the different autophagy activities between the high- and low-risk groups. Previous studies have demonstrated that high levels of autophagy activity led to reduced sensitivity of hepatocellular carcinoma cells to chemotherapeutic drugs (Xiong et al., 2017). Moreover, the infiltration and function of immune cells in the tumor microenvironment could be weakened by the activation of autophagy-related signaling pathways in tumor microenvironment, which may also affect the efficiency of immunotherapy; for example, tumor cell autophagy weakens the killing function of NK cells (Huang et al., 2018; Yao et al., 2018). M2 cells and Treg cells, serving as immunosuppressive cells, played negatively prognostic role in HCC (Fridman et al., 2017). Consistently, in this current study, with the increase of risk score, NK cell infiltration decreased significantly, whereas the ratio of M2 macrophages and Treg cells significantly increased. Although the ratio of M1 macrophages, a positive factor for the prognosis of HCC (Fridman et al., 2017), increased with the increase of risk score, its role might be overwhelmed by above negative ones. In a word, the relationship among tumor autophagy and immune infiltration implied that regulating the infiltration of innate and acquired immune cells by controlling the level of autophagy may be a novel strategy to improve antitumor immunotherapy of HCC.

Collectively, our five-AR-lncRNA signature can predict not only the OS outcomes, but also the therapeutic response of HCC patients. Prognostic nomogram, using clinical TNM stages and the risk score of the five-AR-lncRNA, provides a firsthand prognostic tool for HCC patients. Therefore, further validations in other independent cohorts and mechanism studies will provide solid evidence to apply this five-AR-lncRNA signature as a clinical index of HCC precise treatment and prognosis.

## DATA AVAILABILITY STATEMENT

The datasets presented in this study can be found in online repositories. The names of the repository/repositories and accession number(s) can be found in the article/**Supplementary Material**.

## AUTHOR CONTRIBUTIONS

XD designed and performed the experiments, analyzed the data, and wrote the manuscript. QB, SC, XC, SL, ZZ, and WG performed the analysis. XL designed the research, supervised the study, and wrote the paper. YD and YY devised the concept, designed the research, and wrote the paper. All authors contributed to the article and approved the submitted version.

## FUNDING

This study was supported by grants from the National Natural Science Foundation of China (Nos. 81874313 and 81922068 to YD; No. 81520108029 to XL; No. 81703522 to WG).

## SUPPLEMENTARY MATERIAL

The Supplementary Material for this article can be found online at: https://www.frontiersin.org/articles/10.3389/fmolb.2020.611626/full#supplementary-material

**Supplementary Figure 1 |** Determination of parameter β of the adjacency function in the WGCNA algorithm.

**Supplementary Figure 2 |** Screening for AR-lncRNAs which related to OS outcomes of HCC. **(A)** Least absolute shrinkage and selection operator (LASSO) regression coefficient profiles of AR-lncRNAs in the blue module. Seven AR-lncRNAs were selected out. **(B–H)** Kaplan-Meier survival curve for patients with a high- or low-expression of the seven AR-lncRNAs which were closely associated with overall survival (OS) of HCC patients ($p$-value < 0.01).

**Supplementary Figure 3 |** Comparison of the five-AR-lncRNA signature with three published prognostic signatures for HCC. Restricted mean survival (RMS) curves and concordance index (C-index) for the five-AR-lncRNA signature and other published signatures including five-ARG signature by Huo et al. (2020) **(A)**, 4-lncRNA signature by Yang et al. (2020) **(B)** and 4-lncRNA by Wang et al. (2017) **(C)**, respectively.

**Supplementary Table 1 |** Univariate Cox regression analysis of the AR-lncRNAs significantly related to HCC OS outcomes.

**Supplementary Table 2 |** Gene list of different modules of lncRNAs based on WGCNA in HCC.

**Supplementary Table 3 |** Detailed enrichment results of GSEA for high-risk group based on the AR-lncRNAs prognostic signature.

**Supplementary Table 4 |** Detailed enrichment results of GSEA for low-risk group based on the AR-lncRNAs prognostic signature.

**Supplementary Table 5 |** The co-expression network established from five AR-lncRNAs and ARGs in HCC.

## REFERENCES

Alao, J. P. (2007). The regulation of cyclin D1 degradation: roles in cancer development and the potential for therapeutic invention. *Mol. Cancer* 6:24. doi: 10.1186/1476-4598-6-24

Bao, X., Shi, R., Zhang, K., Xin, S., Li, X., Zhao, Y., et al. (2019). Immune landscape of invasive ductal carcinoma tumor microenvironment identifies a prognostic and immunotherapeutically relevant gene signature. *Front. Oncol.* 9:903. doi: 10.3389/fonc.2019.00903

Cancer Genome Atlas Research Network. Electronic address, w.b.e., and Cancer Genome Atlas Research, N. (2017). Comprehensive and integrative genomic characterization of hepatocellular carcinoma. *Cell* 169, 1327–1341.

Chen, S., Ma, W., Cao, F., Shen, L., Qi, H., Xie, L., et al. (2020). Hepatocellular carcinoma within the milan criteria: a novel inflammation-based nomogram system to assess the outcomes of ablation. *Front. Oncol.* 10:1764. doi: 10.3389/fonc.2020.01764

Chen, W., Du, M., Hu, X., Ma, H., Zhang, E., Wang, T., et al. (2020). Long noncoding RNA cytoskeleton regulator RNA promotes cell invasion and metastasis by titrating miR-613 to regulate ANXA2 in nasopharyngeal carcinoma. *Cancer Med.* 9, 1209–1219. doi: 10.1002/cam4.2778

Chen, Y. G., Satpathy, A. T., and Chang, H. Y. (2017). Gene regulation in the immune system by long noncoding RNAs. *Nat. Immunol.* 18, 962–972. doi: 10.1038/ni.3771

Chong, Y. C., Toh, T. B., Chan, Z., Lin, Q. X. X., Thng, D. K. H., Hooi, L., et al. (2020). Targeted inhibition of purine metabolism is effective in suppressing hepatocellular carcinoma progression. *Hepatol. Commun.* 4, 1362–1381. doi: 10.1002/hep4.1559

Colaprico, A., Silva, T. C., Olsen, C., Garofano, L., Cava, C., Garolini, D., et al. (2016). TCGAbiolinks: an R/Bioconductor package for integrative analysis of TCGA data. *Nucleic Acids Res.* 44:e71. doi: 10.1093/nar/gkv1507

Cui, H. X., Zhang, Y. X., Zhang, Q. J., Chen, W. M., Zhao, H. B., and Liang, J. (2017). A comprehensive genome-wide analysis of long noncoding RNA expression profile in hepatocellular carcinoma. *Cancer Med.* 6, 2932–2941. doi: 10.1002/cam4.1180

Deng, B., Yang, M., Wang, M., and Liu, Z. (2020). Development and validation of 9-long Non-coding RNA signature to predicting survival in hepatocellular carcinoma. *Medicine (Baltimore)* 99:e20422. doi: 10.1097/MD.0000000000020422

Derrien, T., Johnson, R., Bussotti, G., Tanzer, A., Djebali, S., Tilgner, H., et al. (2012). The GENCODE v7 catalog of human long noncoding RNAs: analysis of their gene structure, evolution, and expression. *Genome Res.* 22, 1775–1789. doi: 10.1101/gr.132159.111

Deveson, I. W., Hardwick, S. A., Mercer, T. R., and Mattick, J. S. (2017). The dimensions, dynamics, and relevance of the mammalian noncoding transcriptome. *Trends Genet.* 33, 464–478. doi: 10.1016/j.tig.2017.04.004

Du, Y., Shao, S., Lv, M., Zhu, Y., Yan, L., and Qiao, T. (2020). Radiotherapy versus surgery-which is better for patients with T1-2N0M0 glottic laryngeal squamous cell carcinoma? Individualized survival prediction based on web-based nomograms. *Front. Oncol.* 10:1669. doi: 10.3389/fonc.2020.01669

Engebretsen, S., and Bohlin, J. (2019). Statistical predictions with glmnet. *Clin. Epigenet.* 11:123. doi: 10.1186/s13148-019-0730-1

Feng, M., Pan, Y., Kong, R., and Shu, S. (2020). Therapy of primary liver cancer. *Innovation (N Y)* 1:100032. doi: 10.1016/j.xinn.2020.100032

Finotello, F., Mayer, C., Plattner, C., Laschober, G., Rieder, D., Hackl, H., et al. (2019). Molecular and pharmacological modulators of the tumor immune contexture revealed by deconvolution of RNA-seq data. *Genome Med.* 11:34. doi: 10.1186/s13073-019-0638-6

Fridman, W. H., Zitvogel, L., Sautes-Fridman, C., and Kroemer, G. (2017). The immune contexture in cancer prognosis and treatment. *Nat. Rev. Clin. Oncol.* 14, 717–734. doi: 10.1038/nrclinonc.2017.101

Galamb, O., Kalmar, A., Sebestyen, A., Danko, T., Kriston, C., Furi, I., et al. (2020). Promoter hypomethylation and increased expression of the long non-coding RNA LINC00152 support colorectal carcinogenesis. *Pathol. Oncol. Res.* 26, 2209–2223. doi: 10.1007/s12253-020-00800-8

Ge, D., Han, L., Huang, S. Y., Peng, N., Wang, P. C., Jiang, Z., et al. (2014). Identification of a novel MTOR activator and discovery of a competing endogenous RNA regulating autophagy in vascular endothelial cells. *Autophagy* 10, 957–971. doi: 10.4161/auto.28363

Geeleher, P., Cox, N., and Huang, R. S. (2014). pRRophetic: an R package for prediction of clinical chemotherapeutic response from tumor gene expression levels. *PLoS ONE* 9:e107468. doi: 10.1371/journal.pone.0107468

Gerada, C., and Ryan, K. M. (2020). Autophagy, the innate immune response and cancer. *Mol. Oncol.* 14, 1913–1929. doi: 10.1002/1878-0261.12774

Han, P., and Chang, C. P. (2015). Long non-coding RNA and chromatin remodeling. *RNA Biol.* 12, 1094–1098. doi: 10.1080/15476286.2015.1063770

Han, T. Y., Guo, M., Gan, M. X., Yu, B. T., Tian, X. L., and Wang, J. B. (2018). TRIM59 regulates autophagy through modulating both the transcription and the ubiquitination of BECN1. *Autophagy* 14, 2035–2048. doi: 10.1080/15548627.2018.1491493

Heagerty, P. J., and Zheng, Y. (2005). Survival model predictive accuracy and ROC curves. *Biometrics* 61, 92–105. doi: 10.1111/j.0006-341X.2005.030814.x

Huang, C., Liu, Z., Xiao, L., Xia, Y., Huang, J., Luo, H., et al. (2019). Clinical significance of serum CA125, CA19-9, CA72-4, and fibrinogen-to-lymphocyte ratio in gastric cancer with peritoneal dissemination. *Front. Oncol.* 9:1159. doi: 10.3389/fonc.2019.01159

Huang, F., Wang, B. R., and Wang, Y. G. (2018). Role of autophagy in tumorigenesis, metastasis, targeted therapy and drug resistance of hepatocellular carcinoma. *World J. Gastroenterol.* 24, 4643–4651. doi: 10.3748/wjg.v24.i41.4643

Huang, R., Chen, Z., Li, W., Fan, C., and Liu, J. (2020). Immune systemassociated genes increase malignant progression and can be used to predict clinical outcome in patients with hepatocellular carcinoma. *Int. J. Oncol.* 56, 1199–1211. doi: 10.3892/ijo.2020.4998

Huang, R., Liao, X., and Li, Q. (2017). Identification and validation of potential prognostic gene biomarkers for predicting survival in patients with acute myeloid leukemia. *Onco. Targets. Ther.* 10, 5243–5254. doi: 10.2147/OTT.S147717

Huo, X., Qi, J., Huang, K., Bu, S., Yao, W., Chen, Y., et al. (2020). Identification of an autophagy-related gene signature that can improve prognosis of hepatocellular carcinoma patients. *BMC Cancer* 20:771. doi: 10.1186/s12885-020-07277-3

Jiang, P., Gu, S., Pan, D., Fu, J., Sahu, A., Hu, X., et al. (2018). Signatures of T cell dysfunction and exclusion predict cancer immunotherapy response. *Nat. Med.* 24, 1550–1558. doi: 10.1038/s41591-018-0136-1

Jiang, P., and Mizushima, N. (2014). Autophagy and human diseases. *Cell Res.* 24, 69–79. doi: 10.1038/cr.2013.161

Jin, C., Bai, L., Lin, L., Wang, S., and Yin, X. (2018). Paclitaxel-loaded nanoparticles decorated with bivalent fragment HAb18 F(ab')2 and cell penetrating peptide for improved therapeutic effect on hepatocellular carcinoma. *Artif. Cells Nanomed. Biotechnol.* 46, 1076–1084. doi: 10.1080/21691401.2017.1360325

Langfelder, P., and Horvath, S. (2008). WGCNA: an R package for weighted correlation network analysis. *BMC Bioinform.* 9:559. doi: 10.1186/1471-2105-9-559

Liao, L. E., Hu, D. D., and Zheng, Y. (2020). A four-methylated lncRNAs-based prognostic signature for hepatocellular carcinoma. *Genes (Basel)* 11:908. doi: 10.3390/genes11080908

Liu, P. H., Hsu, C. Y., Hsia, C. Y., Lee, Y. H., Su, C. W., Huang, Y. H., et al. (2016). Prognosis of hepatocellular carcinoma: assessment of eleven staging systems. *J. Hepatol.* 64, 601–608. doi: 10.1016/j.jhep.2015.10.029

Liu, Q., Cheng, R., Kong, X., Wang, Z., Fang, Y., and Wang, J. (2020). Molecular and Clinical Characterization of PD-1 in Breast Cancer Using Large-Scale Transcriptome Data. *Front. Immunol.* 11:558757. doi: 10.3389/fimmu.2020.558757

Liu, Y., Li, M., Yu, H., and Piao, H. (2019a). lncRNA CYTOR promotes tamoxifen resistance in breast cancer cells via sponging miR-125a-5p. *Int. J. Mol. Med.* 45, 497–509. doi: 10.3892/ijmm.2019.4428

Liu, Y., Liu, B., Jin, G., Zhang, J., Wang, X., Feng, Y., et al. (2019b). An integrated three-long non-coding RNA signature predicts prognosis in colorectal cancer patients. *Front. Oncol.* 9:1269. doi: 10.3389/fonc.2019.01269

Lui, G. Y. L., Shaw, R., Schaub, F. X., Stork, I. N., Gurley, K. E., Bridgwater, C., et al. (2020). BET, SRC, and BCL2 family inhibitors are synergistic drug combinations with PARP inhibitors in ovarian cancer. *Ebiomedicine* 60:102988.

Mao, Y., Dong, L. X., Zheng, Y., Dong, J., and Li, X. (2019). Prediction of recurrence in cervical cancer using a nine-lncRNA signature. *Front. Genet.* 10:284. doi: 10.3389/fgene.2019.00284

Mayakonda, A., Lin, D. C., Assenov, Y., Plass, C., and Koeffler, H. P. (2018). Maftools: efficient and comprehensive analysis of somatic variants in cancer. *Genome Res.* 28, 1747–1756. doi: 10.1101/gr.239244.118

Meng, Y. C., Lou, X. L., Yang, L. Y., Li, D., and Hou, Y. Q. (2020). Role of the autophagy-related marker LC3 expression in hepatocellular carcinoma: a meta-analysis. *J. Cancer Res. Clin. Oncol.* 146, 1103–1113. doi: 10.1007/s00432-020-03174-1

Mo, X. G., Liu, W., Yang, Y., Imani, S., Lu, S., Dan, G., et al. (2019). NCF2, MYO1F, S1PR4, and FCN1 as potential noninvasive diagnostic biomarkers in patients with obstructive coronary artery: a weighted gene co-expression network analysis. *J. Cell. Biochem.* 120, 18219–18235. doi: 10.1002/jcb.29128

Otto, T., and Sicinski, P. (2017). Cell cycle proteins as promising targets in cancer therapy. *Nat. Rev. Cancer* 17, 93–115. doi: 10.1038/nrc.2016.138

Schroder, M. S., Culhane, A. C., Quackenbush, J., and Haibe-Kains, B. (2011). survcomp: an R/Bioconductor package for performance assessment and comparison of survival models. *Bioinformatics* 27, 3206–3208. doi: 10.1093/bioinformatics/btr511

Sharma, A., Alswillah, T., Singh, K., Chatterjee, P., Willard, B., Venere, M., et al. (2018). USP14 regulates DNA damage repair by targeting RNF168-dependent ubiquitination. *Autophagy* 14, 1976–1990. doi: 10.1080/15548627.2018.1496877

Singal, A. G., Lampertico, P., and Nahon, P. (2020). Epidemiology and surveillance for hepatocellular carcinoma: new trends. *J. Hepatol.* 72, 250–261. doi: 10.1016/j.jhep.2019.08.025

Soares, J. C., Soares, A. C., Rodrigues, V. C., Melendez, M. E., Santos, A. C., Faria, E. F., et al. (2019). Detection of the prostate cancer biomarker PCA3 with electrochemical and impedance-based biosensors. *ACS Appl. Mater. Interfaces* 11, 46645–46650. doi: 10.1021/acsami.9b19180

Sun, T. (2018). Long noncoding RNAs act as regulators of autophagy in cancer. *Pharmacol. Res.* 129, 151–155. doi: 10.1016/j.phrs.2017.11.009

Sung, P. S., Choi, M. H., Yang, H., Lee, S. K., Chun, H. J., Jang, J. W., et al. (2020). Diffusion-Weighted Magnetic Resonance Imaging in Hepatocellular Carcinoma as a Predictor of a Response to Cisplatin-Based Hepatic Arterial Infusion Chemotherapy. *Front. Oncol.* 10:600233. doi: 10.3389/fonc.2020.600233

Tekchandani, P., Kurmi, B. D., Paliwal, R., and Paliwal, S. R. (2020). Galactosylated TPGS micelles for docetaxel targeting to hepatic carcinoma: development, characterization, and biodistribution study. *AAPS PharmSciTech.* 21:174. doi: 10.1208/s12249-020-01690-4

Tombacz, I., Weissman, D., and Pardi, N. (2021). Vaccination with messenger RNA: a promising alternative to DNA vaccination. *Methods Mol. Biol.* 2197, 13–31. doi: 10.1007/978-1-0716-0872-2_2

Tomczak, K., Czerwinska, P., and Wiznerowicz, M. (2015). The Cancer Genome Atlas (TCGA): an immeasurable source of knowledge. *Contemp Oncol. (Pozn).* 19, A68–77. doi: 10.5114/wo.2014.47136

Wang, M., Han, J., Xing, H., Zhang, H., Li, Z., Liang, L., et al. (2016). Dysregulated fatty acid metabolism in hepatocellular carcinoma. *Hepatic Oncol.* 3, 241–251. doi: 10.2217/hep-2016-0012

Wang, X., Yu, H., Sun, W., Kong, J., Zhang, L., Tang, J., et al. (2018). The long non-coding RNA CYTOR drives colorectal cancer progression by interacting with NCL and Sam68. *Mol. Cancer* 17:110. doi: 10.1186/s12943-018-0860-7

Wang, Z., Gao, L., Guo, X., Feng, C., Lian, W., Deng, K., et al. (2019). Development and validation of a nomogram with an autophagy-related gene signature for predicting survival in patients with glioblastoma. *Aging* 11, 12246–12269. doi: 10.18632/aging.102566

Wang, Z., Wu, Q., Feng, S., Zhao, Y., and Tao, C. (2017). Identification of four prognostic LncRNAs for survival prediction of patients with hepatocellular carcinoma. *PeerJ* 5:e3575. doi: 10.7717/peerj.3575

Wild, F., Khan, M. M., Straka, T., and Rudolf, R. (2016). Progress of endocytic CHRN to autophagic degradation is regulated by RAB5-GTPase and T145 phosphorylation of SH3GLB1 at mouse neuromuscular junctions *in vivo*. *Autophagy* 12, 2300–2310. doi: 10.1080/15548627.2016.1234564

Wu, D. H., Wang, T. T., Ruan, D. Y., Li, X., Chen, Z. H., Wen, J. Y., et al. (2018). Combination of ULK1 and LC3B improve prognosis assessment of hepatocellular carcinoma. *Biomed. Pharmacother.* 97, 195–202. doi: 10.1016/j.biopha.2017.10.025

Xiao, J. R., Wang, K., Liu, Y., Li, Z. W., Zhou, Y. J., Wang, H. Z., et al. (2019). Exploring of a prognostic long non-coding RNA signature of hepatocellular carcinoma by using public database. *Zhonghua Liu Xing Bing Xue Za Zhi* 40, 805–809. doi: 10.3760/cma.j.issn.0254-6450.2019.07.014

Xiong, H., Ni, Z., He, J., Jiang, S., Li, X., He, J., et al. (2017). LncRNA HULC triggers autophagy via stabilizing Sirt1 and attenuates the chemosensitivity of HCC cells. *Oncogene* 36, 3528–3540. doi: 10.1038/onc.2016.521

Yang, Y., Lu, Q., Shao, X., Mo, B., Nie, X., Liu, W., et al. (2018). Development of a three-gene prognostic signature for hepatitis B virus associated hepatocellular carcinoma based on integrated transcriptomic analysis. *J. Cancer* 9, 1989–2002. doi: 10.7150/jca.23762

Yang, Z., Yang, Y., Zhou, G., Luo, Y., Yang, W., Zhou, Y., et al. (2020). The prediction of survival in hepatocellular carcinoma based on a four long non-coding RNAs expression signature. *J. Cancer* 11, 4132–4144. doi: 10.7150/jca.40621

Yao, C., Ni, Z., Gong, C., Zhu, X., Wang, L., Xu, Z., et al. (2018). Rocaglamide enhances NK cell-mediated killing of non-small cell lung cancer cells by inhibiting autophagy. *Autophagy* 14, 1831–1844. doi: 10.1080/15548627.2018.1489946

Zhang, J., and Li, W. (2018). Long noncoding RNA CYTOR sponges miR-195 to modulate proliferation, migration, invasion and radiosensitivity in nonsmall cell lung cancer cells. *Biosci. Rep*. 38:BSR20181599. doi: 10.1042/BSR20181599

Zhao, Q. J., Zhang, J., Xu, L., and Liu, F. F. (2018). Identification of a five-long non-coding RNA signature to improve the prognosis prediction for patients with hepatocellular carcinoma. *World J. Gastroenterol*. 24, 3426–3439. doi: 10.3748/wjg.v24.i30.3426

Zhao, X., Bai, Z., Li, C., Sheng, C., and Li, H. (2020). Identification of a novel eight-lncRNA prognostic signature for HBV-HCC and analysis of their functions based on coexpression and ceRNA networks. *Biomed Res. Int*. 2020:8765461. doi: 10.1155/2020/8765461

Zhen, Y., Spangenberg, H., Munson, M. J., Brech, A., Schink, K. O., Tan, K. W., et al. (2020). ESCRT-mediated phagophore sealing during mitophagy. *Autophagy* 16, 826–841. doi: 10.1080/15548627.2019.1639301

Zhu, H., Shan, Y., Ge, K., Lu, J., Kong, W., and Jia, C. (2020a). LncRNA CYTOR promotes pancreatic cancer cell proliferation and migration by sponging miR-205-5p. *Pancreatology* 20, 1139–1148. doi: 10.1016/j.pan.2020.05.004

Zhu, Y., Wang, R., Chen, W., Chen, Q., and Zhou, J. (2020b). Construction of a prognosis-predicting model based on autophagy-related genes for hepatocellular carcinoma (HCC) patients. *Aging (Albany. NY)* 12, 14582–14592. doi: 10.18632/aging.103507

Zou, S. F., Yang, X. Y., Li, J. B., Ding, H., Bao, Y. Y., and Xu, J. (2019). UPF1 alleviates the progression of glioma via targeting lncRNA CYTOR. *Eur. Rev. Med. Pharmacol. Sci*. 23, 10005–10012.

Zuo, S., Wei, M., Wang, S., Dong, J., and Wei, J. (2020). Pan-cancer analysis of immune cell infiltration identifies a prognostic immune-cell characteristic score (ICCS) in lung adenocarcinoma. *Front. Immunol*. 11:1218. doi: 10.3389/fimmu.2020.01218

**Conflict of Interest:** The authors declare that the research was conducted in the absence of any commercial or financial relationships that could be construed as a potential conflict of interest.

frontiers in Molecular Biosciences

ORIGINAL RESEARCH
published: 26 January 2021
doi: 10.3389/fmolb.2020.616190

# CLIP4 Shows Putative Tumor Suppressor Characteristics in Breast Cancer: An Integrated Analysis

*Yu Fan[1]*, Lijia He[1], Yu Wang[2], Shaozhi Fu[1], Yunwei Han[1], Juan Fan[1] and Qinglian Wen[1]*

*[1]Department of Oncology, The Affiliated Hospital of Southwest Medical University, Nuclear Medicine and Molecular Imaging Key Laboratory of Sichuan Province, Academician (Expert) Workstation of Sichuan Province, Luzhou, China, [2]Health Management Department, The Affiliated Hospital of Southwest Medical University, Luzhou, China*

**Background**: CAP-Gly domain containing linker protein family member 4 (CLIP4) plays an important role in cancers. However, its expression, prognostic value, and biological effect in breast cancer remain unclear.

**Methods**: Data on patients diagnosed with breast cancer were retrieved from the TCGA-BRCA and other public omics databases. The expression profile of CLIP4 was analyzed using Oncomine, bc-GenExMiner, and TCGA. The prognostic value of CLIP4 was determined by Kaplan-Meier Plotter and Human Protein Atlas. Identification of genes co-expressed with CLIP4 and potential mechanism analyses were performed using UALCAN, STRING, Metascape, and GSEA. The epigenetic characteristics of CLIP4 were determined by DiseaseMeth and MEXPRESS.

**Results**: CLIP4 was downregulated and its expression was negatively correlated with estrogen receptor (ER), progesterone receptor (PR), human epidermal growth factor receptor type 2 (HER2) status, Nottingham prognostic index (NPI), and Scarff-Bloom-Richardson (SBR) grade in breast cancer, whereas it was positively linked to basal-like and triple negative breast cancer status. Ectopic expression of CLIP4 was related with poor prognosis. In the analysis of genes co-expressed with CLIP4, GSEA showed that the Hedgehog (Hh), JAK-STAT, ERBB, Wnt signaling pathway, cell adhesion molecules, and pathways in cancer were dissimilarly enriched in the CLIP4 expression high phenotype. Analysis of the genetics and epigenetics of CLIP4 indicated that its expression was negatively correlated with DNA methylation.

**Conclusion**: Methylated CLIP4 may be a novel prognostic and therapeutic biomarker for breast cancer.

**Keywords: DNA methylation, CAP-Gly domain containing linker protein family member 4, breast cancer, prognosis, biomarker, integrated analysis**

OPEN ACCESS

***Edited by:***
*Matteo Becatti,*
*University of Florence, Italy*

***Reviewed by:***
*Rifat Hamoudi,*
*University of Sharjah, United Arab Emirates*
*DuanBo Shi,*
*Shandong University, China*
*Zhang Fan,*
*The People's Hospital of Jianyang City, China*

****Correspondence:***
*Yu Fan*
*yufan@swmu.edu.cn*

***Specialty section:***
*This article was submitted to Molecular Diagnostics and Therapeutics, a section of the journal Frontiers in Molecular Biosciences*

***Received:*** *11 October 2020*
***Accepted:*** *18 December 2020*
***Published:*** *26 January 2021*

***Citation:***
*Fan Y, He L, Wang Y, Fu S, Han Y, Fan J and Wen Q (2021) CLIP4 Shows Putative Tumor Suppressor Characteristics in Breast Cancer: An Integrated Analysis. Front. Mol. Biosci. 7:616190. doi: 10.3389/fmolb.2020.616190*

## INTRODUCTION

Breast cancer is the most common female malignancy in China and is the main cause of mortality in Western countries (Chen et al., 2016; Siegel et al., 2018). Moreover, the incidence of breast cancer is gradually rising in most countries (DeSantis et al., 2019). Despite advances in early screening, diagnosis, and treatment of breast cancer, the overall prognosis for patients remains poor. Thus, it is urgent to find sensitive and specific biomarkers for breast cancer.

Microtubules have a dynamic structure that continuously changes during growth and shrinkage (Mitchison and Kirschner, 1984). Microtubule-associated proteins (MAPs) influence microtubule properties. One group of MAPs, the plus end binding proteins (or +TIPs), bind to and stabilize microtubule plus ends. Mammalian cytoplasmic linker protein (CLIP)-170, links microtubule plus ends to kinomeres, endocytosis vesicles, and the leading edge of migrating cells (Howard and Hyman, 2003), is a prototypical +TIP (Perez et al., 1999). The CLIP-170 family (CLIP1, CLIP2, CLIP3, and CLIP4) associates microtubules with cellular organelles through a cytoskeleton-associated protein glycine rich (CAP-Gly) domain. The CAP-Gly domain, which is conserved among organisms, is a small 80-residue protein module (Riehemann and Sorg, 1993). CAP-Gly domains are important to the function of CLIPs and many other proteins, and are implicated in cell polarity maintenance, intracellular transport, cell migration, and oncogenesis (Galjart and Perez, 2003; Akhmanova and Hoogenraad, 2005; Galjart, 2005). Recent research on CLIP4 uncovered its potential functions in cancers. However, the role of CLIP4 in breast cancer remains unknown.

Here, we first evaluated the expression profile of CLIP4 in breast cancer by data mining. The prognostic value of CLIP4 was also analyzed. To gain further insight into the molecular mechanisms involved in breast cancer-related CLIP4 regulatory networks, GSEA was used. Finally, the regulation of the expression of CLIP4 in breast cancer was investigated by genetic and epigenetic analyses.

# METHODS

## Expression profile analysis

The expression pattern of CLIP4 was analyzed using Oncomine and TCGA. First, the expression profile of CLIP4 was analyzed with Oncomine, which facilitates investigation of cancer microarray databases and genome-wide expression analysis (Rhodes et al., 2004). The cut-off of p-value, fold change, and gene rank were defined as 0.05, 2, and 10% (Fan et al., 2019), respectively. The gene expression (1,098 cases) and corresponding clinical data were downloaded from TCGA official website for Breast Invasive Carcinoma (TCGA-BRCA). All statistical analyses were performed using R (v.3.6.3). The association with clinical features and CLIP4 was analyzed with the Wilcoxon signed-rank and logistic regression test.

bc-GenExMiner (Jezequel et al., 2012) was used to assess relationships among CLIP4 expression and clinicopathological features including age, nodal status, hormone receptor status (ER and PR), HER2, pathological subtype, NPI, and SBR grade. A value of $p$ <0.05 was statistically significant.

## Survival analysis

The Kaplan-Meier Plotter (http://kmplot.com/analysis/), an online tool established from gene expression and survival data of cancer patients originated from the GEO database (Gyorffy et al., 2010), was used to evaluate the prognostic value of CLIP4 in breast cancer. The survival plot, hazards ratio (HR), 95% confidence interval (CI), and log-rank p were displayed on the web page. The prognostic significance are available from Human Protein Atlas (https://www.proteinatlas.org/) (Uhlen et al., 2005). A log-rank $p < 0.05$ was statistically significant.

## Analysis of Co-Expression and Protein-Protein Interaction Networks

The genes co-expressed with CLIP4 were analyzed using UALCAN (Chandrashekar et al., 2017). A total of 687 genes positively and negatively correlated with CLIP4 in breast cancer were downloaded. Genes with a Pearson's correlation coefficient ≥0.3 (absolute value) were included. The protein-protein interaction network was established using STRING v11.0 and was based on co-expressed genes (https://string-db.org/cgi/input.pl/) (Szklarczyk et al., 2019). The confidence score was defined as 0.4 (Fan et al., 2019).

## Metascape and Gene Set Enrichment Analysis

Gene ontology (GO) and pathway enrichment analysis of CLIP4-associated genes were performed using Metascape (http://metascape.org/) (Zhou et al., 2019). A computational method GSEA was used to determine whether a prior defined set of genes shows statistically significant, concordant differences between two biological states (Subramanian et al., 2005). In this study, an ordered list of genes was first generated by GSEA based on correlation with CLIP4 expression. The significant survival difference observed between high and low CLIP4 was elucidated. Gene set permutations were performed 1,000 times each analysis. The expression level of CLIP4 was used as a phenotype label. The nominal p-value and normalized enrichment score (NES) were used to classify the pathways enriched in each phenotype.

## Analysis of DNA Methylation and Genetic Alterations

To further investigate the regulatory effect of DNA methylation modification on CLIP4 mRNA expression, we used DiseaseMeth, version 2.0, which was updated along with the increased DNA methylation data and associations between diseases and genes. These datasets were collected from revolutionary large international disease projects such as TCGA and GEO among others (Xiong et al., 2017). Then, 871 breast invasive carcinoma samples in MEXPRESS (https://mexpress.be/) (Koch et al., 2015) datasets were analyzed to evaluate the CLIP4 gene. The genetic alterations of CLIP4 were identified by a web portal (http://www.cbioportal.org/) (Cerami et al., 2012) evaluated from breast invasive carcinoma (TCGA, Firehose Legacy, 1108 samples).

# RESULTS

## The Expression of CLIP4 in Breast Cancer

To identify the roles of CLIP4 in cancers, we searched the Oncomine dataset for CLIP4 mRNA expression in common

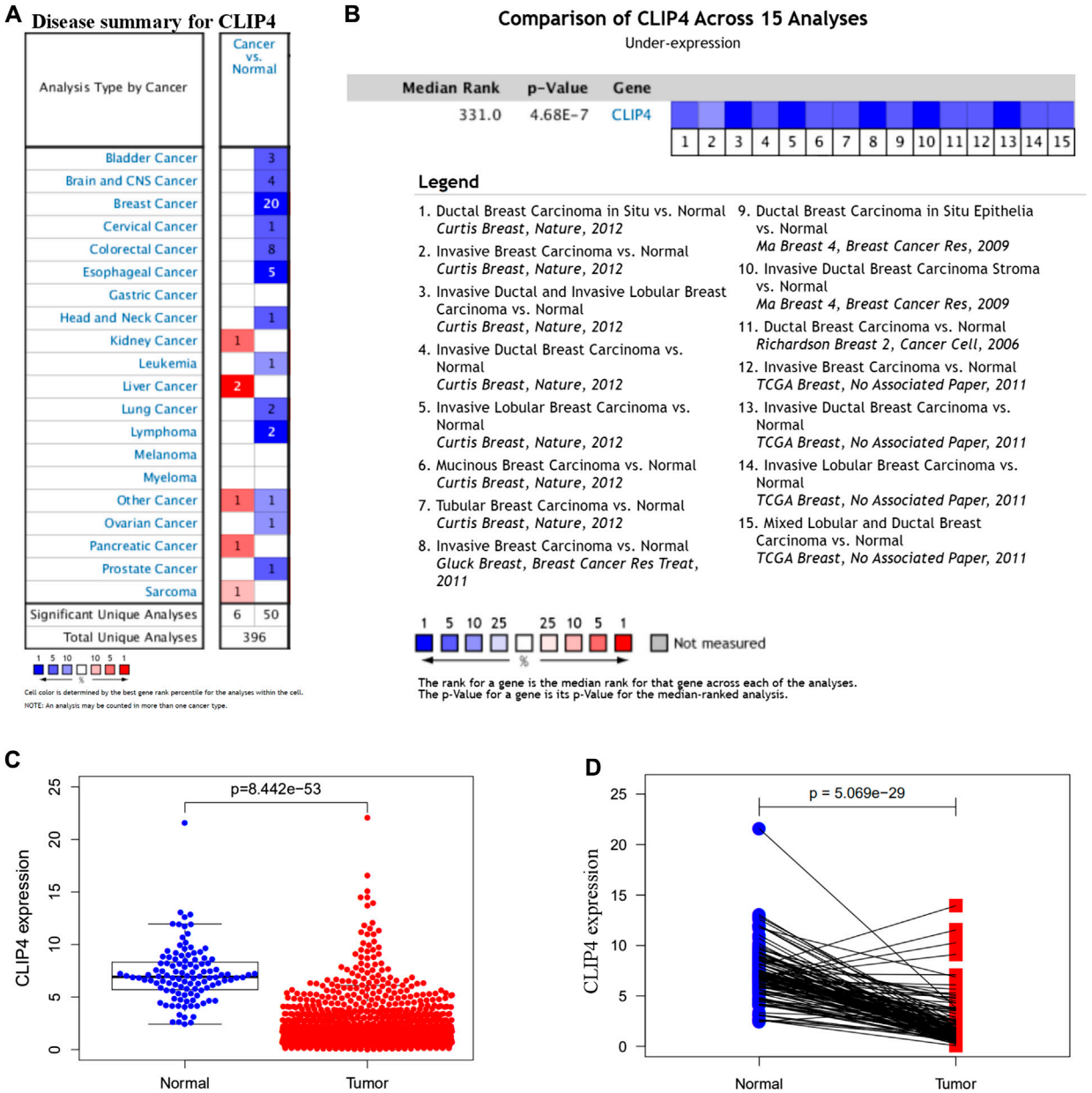


**FIGURE 1 |** Expression pattern of CLIP4 in breast cancer. **(A)** Expression of CLIP4 in different human cancers by analysis of cancer and normal tissue based on Oncomine; **(B)** Oncomine meta-analysis for the expression of CLIP4 in breast cancer; **(C)** CLIP4 mRNA expression in breast cancer and normal tissue (TCGA datasets); and **(D)** CLIP4 mRNA expression in breast cancer and adjacent normal tissue (TCGA datasets).

cancer types. Comparison of cancer and normal samples was performed to analyze the expression pattern of CLIP4 in breast cancer (**Figure 1A**). The meta-analysis based on Oncomine was used to evaluate the integrated and median expression of CLIP4 across 15 analyses ($p$ = 4.68E−7, <0.001) (**Figure 1B**). As shown in **Table 1**, the CLIP4 expression was significantly decreased in invasive breast carcinoma, invasive lobular breast carcinoma, invasive ductal breast carcinoma, tubular breast carcinoma, mucinous breast carcinoma, ductal breast carcinoma *in situ*, and mixed lobular and ductal breast carcinoma (Richardson et al., 2006; Ma et al., 2009; Curtis et al., 2012; Gluck et al., 2012). For further validation, we also investigated the expression of CLIP4 from TCGA datasets. As shown in **Figure 1C**, CLIP4 expression was dramatically lower in breast cancer than in normal tissues ($p$ = 8.44E−53, <0.001). Furthermore, the paired plot for CLIP4 showed that the expression in breast cancer was significantly downregulated compared with adjacent normal samples ($p$ = 5.07E−29, <0.001) (**Figure 1D**). Taken together, the combination of bioinformatic analyses demonstrated that CLIP4 was significantly downregulated in breast cancer.

**TABLE 1 |** The significant changes of CLIP4 in breast cancer from oncomine datasets.

| Types of cancer vs normal tissues | Fold change (>2) | *t*-test | *p*-value (<1E-4) | Reporter ID |
|---|---|---|---|---|
| Invasive ductal breast carcinoma | −2.268 | −33.329 | 4.48E−79 | ILMN_1759792 |
| Invasive lobular breast carcinoma | −2.215 | −23.245 | 2.12E−68 | ILMN_1759792 |
| Invasive ductal and invasive lobular breast carcinoma | −2.253 | −19.951 | 8.72E−47 | ILMN_1759792 |
| Tubular breast carcinoma | −2.130 | −16.210 | 2.42E−31 | ILMN_1759792 |
| Mucinous breast carcinoma | −2.187 | −14.080 | 9.84E−22 | ILMN_1759792 |
| Ductal breast carcinoma in situ | −2.187 | −9.924 | 4.68E−7 | ILMN_1759792 |
| Invasive breast carcinoma | −2.158 | −6.366 | 1.15E−6 | ILMN_1759792 |
| Invasive ductal breast carcinoma | −5.492 | −27.864 | 4.28E−70 | A_23_P209230 |
| Invasive breast carcinoma | −3.581 | −12.411 | 1.09E−22 | A_23_P209230 |
| Invasive lobular breast carcinoma | −3.466 | −11.370 | 1.22E−15 | A_23_P209230 |
| Mixed lobular and ductal breast carcinoma | −2.242 | −7.247 | 1.15E−5 | A_23_P209230 |
| Invasive breast carcinoma | −3.053 | −14.220 | 4.71E−9 | 27167 |
| Ductal breast carcinoma | −3.054 | −5.849 | 3.36E−7 | 226425_at |
| Invasive ductal breast carcinoma stroma | −2.615 | −5.451 | 4.71E−5 | Hs.56123.0.S1_3p_at |
| Ductal breast carcinoma in situ epithelia | −5.191 | −5.361 | 9.44E−5 | |

We further evaluated the associations between CLIP4 expression and clinicopathological characteristics using the bc-GenExMiner tool (**Figure 2**). There was no significant difference of CLIP4 expression between the nodal-positive and -negative groups ($p = 0.1797$, >0.05). Age, ER, PR, HER2 status, NPI, and SBR grade were negatively related to CLIP4 expression (Age: $p = 0.0015$, <0.01; ER status: $p < 0.0001$; PR status: $p < 0.0001$; HER2 status: $p < 0.0001$; NPI: $p = 0.0003$, <0.001; SBR grade: $p < 0.0001$). However, the expression of CLIP4 was markedly upregulated in basal-like and triple-negative breast cancer (TNBC) (basal-like status: $p < 0.0001$; triple-negative status: $p < 0.0001$). To further evaluate the association between TNM stage and CLIP4 expression, we performed analysis using R (v.3.6.3) based on TCGA datasets. The results showed that the T, N, and stage were negatively associated with CLIP4 expression (T3-4 vs. T1-2: $p = 0.008$, <0.01; nodal-positive vs. -negative: $p = 0.046$, <0.05; stage III-IV vs. stage I-II: p = 0.027, <0.05) (**Supplementary Figure S1**). However, logistic regression analysis showed no significant differences between T, N, stage and CLIP4 expression ($p > 0.05$) (**Supplementary Table S1**). In short, these results indicated that CLIP4 expression may play a favorable role in breast cancer patients.

## Prognostic Significance of CLIP4 in Breast Cancer

The analysis using the Kaplan-Meier plotter based on 626 breast cancer patients showed that CLIP4 upregulation was significantly associated with better overall survival (OS) [HR: 0.71 (0.50–0.99); $p = 0.043$, <0.05, **Figure 3A**]. High expression of CLIP4 was associated with better relapse-free survival (RFS) in 1,764 breast cancer patients [HR: 0.64 (0.55–0.76); $p = 1.30E-07$, **Figure 3B**]. Furthermore, CLIP4 was also positively associated with distant metastasis-free survival (DMFS) in breast cancer, although statistical significance was not reached [HR: 0.77 (0.54–1.10); $p = 0.150$, >0.05, **Figure 3C**]. Based on TCGA dataset and the optimal cutoff value, the survival rate was significantly better in breast cancer patients ($n = 726$) with high expression of CLIP4 than in those with low expression ($n = 349$) ($p = 0.020$, <0.05) (https://www.proteinatlas.org/) (**Figure 3D**). In summary, CLIP4 may be a novel prognostic indicator in breast cancer patients. Meanwhile, the value of CLIP4 in different intrinsic subtypes of breast cancer was evaluated using the Kaplan-Meier plotter. High CLIP4 expression in three intrinsic subtypes (Luminal A, Luminal B, and HER2 positive) but not in the basal-like subtype was correlated with better OS [Luminal A: HR: 0.63 (0.37–1.07), $p = 0.085$; Luminal B: HR: 0.46 (0.21–1.01), $p = 0.047$; HER2 positive: HR: 0.46 (0.21–1.02), $p = 0.050$] (**Supplementary Figure S2**).

## Genes Co-Expressed with CLIP4 and Potential Biomolecular Networks

To find the potential role and regulatory mechanism of CLIP4 in breast cancer, genes co-expressed with CLIP4 were predicted using the UALCAN database, and 687 genes were identified (**Supplementary Table S2**). A PPI network for CLIP4 co-expressed genes, based on experimental evidence, was constructed using the STRING database (**Supplementary Figure S3**). We further performed GO and pathway enrichment analysis for these genes using Metascape (**Figure 4**). The top 20 clusters with their enriched terms, which originated from two categories, were included: GO biological process (BP) and Reactome gene sets. The representative enriched GO functions for these co-expressed genes included Wnt signaling pathway (GO: 0016055), actin cytoskeleton organization (GO: 0030036), developmental growth (GO: 0048589), transmembrane receptor protein tyrosine kinase signaling pathway (GO: 0007169), regulation of GTPase activity (GO: 0043087), toll-like receptor 2 signaling pathway (GO: 0034134), and regulation of epidermal growth factor receptor signaling pathway (GO: 0042058). To further identify molecular signaling pathways differentially activated in breast cancer, GSEA between CLIP4 low and high expression datasets was performed (**Supplementary Table S3, S4**). GSEA identified significant differences (FDR *q*-value

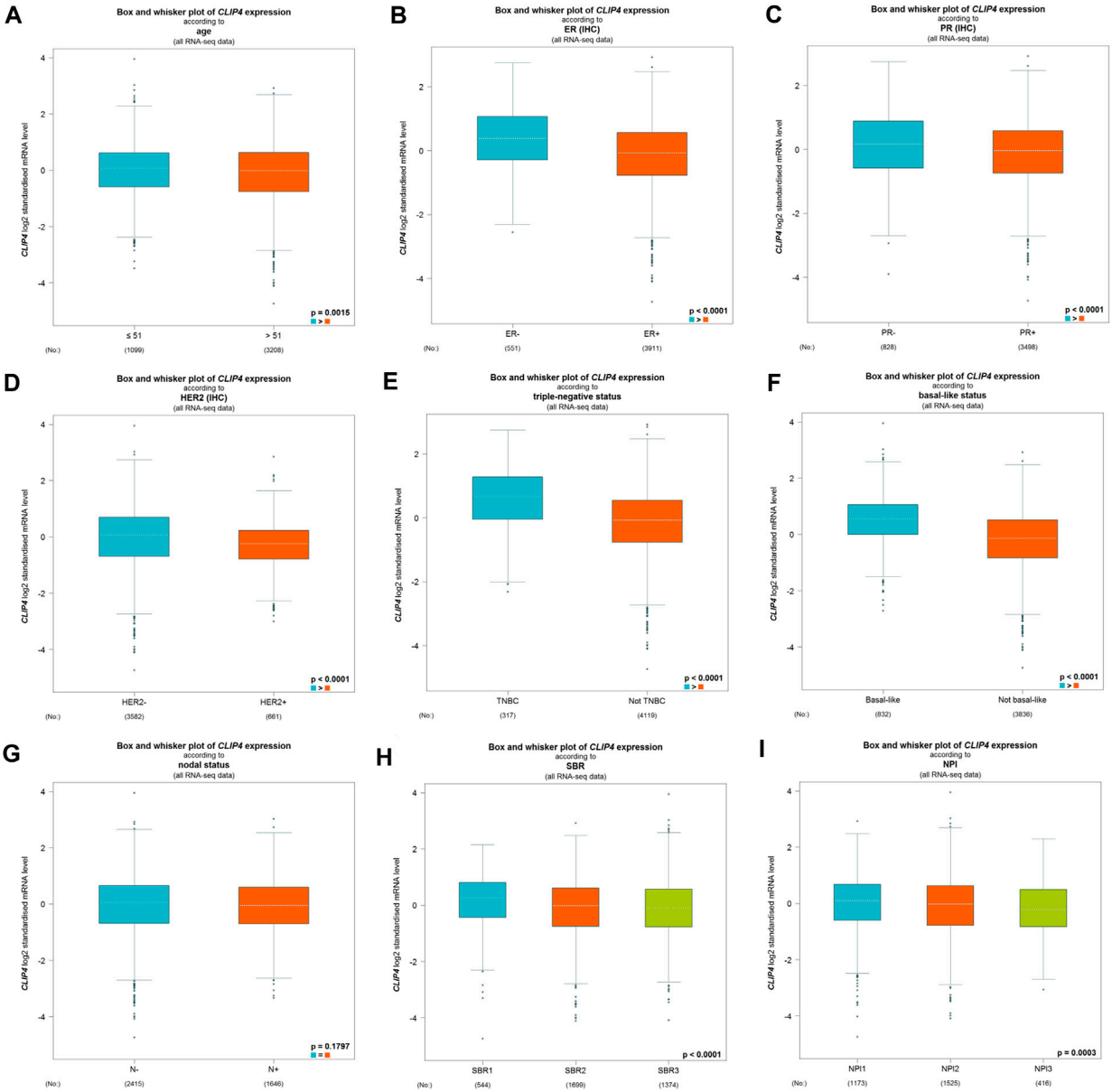


**FIGURE 2 |** Relationships among CLIP4 expression and clinicopathological features of breast cancer based on the bc-GenExMiner database. **(A)** Box plot for the association of CLIP4 mRNA expression and age; **(B)** box plot for the association of CLIP4 mRNA expression and ER; **(C)** box plot for the association of CLIP4 mRNA expression and PR; **(D)** box plot for the association of CLIP4 mRNA expression and HER2; **(E)** box plot for the association of CLIP4 mRNA expression and triple-negative status; **(F)** box plot for the association of CLIP4 mRNA expression and basal-like status; **(G)** box plot for the association of CLIP4 mRNA expression and nodal status; **(H)** box plot for the association of CLIP4 mRNA expression and SBR; and **(I)** box plot for the association of CLIP4 mRNA expression and NPI.

<0.25, NOM $p$-value <0.05) in enrichment of the MSigDB Collection (c2.cp.kegg.v6.2.symbols.gmt). The most enriched tumor-associated signaling pathways were selected based on their NES values (Wu and Zhang, 2018) (**Figure 5**; **Table 2**). As shown in **Figure 5**, Hh signaling pathway, JAK-STAT signaling pathway, cell adhesion molecules, ERBB signaling pathway, Wnt signaling pathway, and pathways in cancer were differentially enriched in the CLIP4-high expression phenotype. These results demonstrated that upregulation of CLIP4 in breast cancer may involve the Wnt, ERBB, or other tumor-associated signaling pathways. Another result based on multiple GSEA analysis is shown in **Supplementary Figure S4**.

## Promoter Methylation of CLIP4 in Breast Cancer

To assess whether CLIP4 downregulation was related with DNA methylation in breast cancer, the DiseaseMeth database was

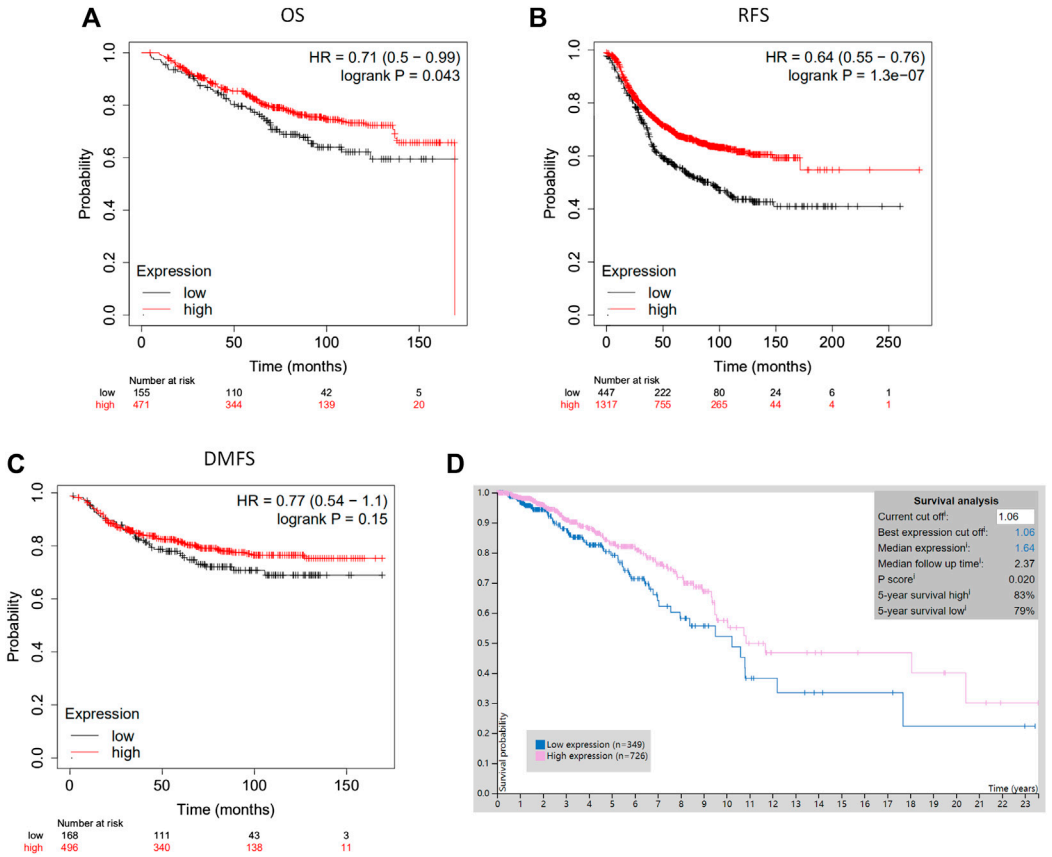


**FIGURE 3 |** The prognostic significance of CLIP4 for breast cancer determined by Kaplan-Meier Plotter and TCGA datasets. **(A)** High CLIP4 expression shows a better OS for breast cancer; **(B)** high CLIP4 expression shows a better RFS for breast cancer; **(C)** high CLIP4 expression shows a better DMFS for breast cancer; **(D)** the 5-year survival rate for patients with breast cancer ($n$ = 726) with greater CLIP4 mRNA expression (83%) better for patients ($n$ = 349) than low expression (79%) (TCGA datasets).

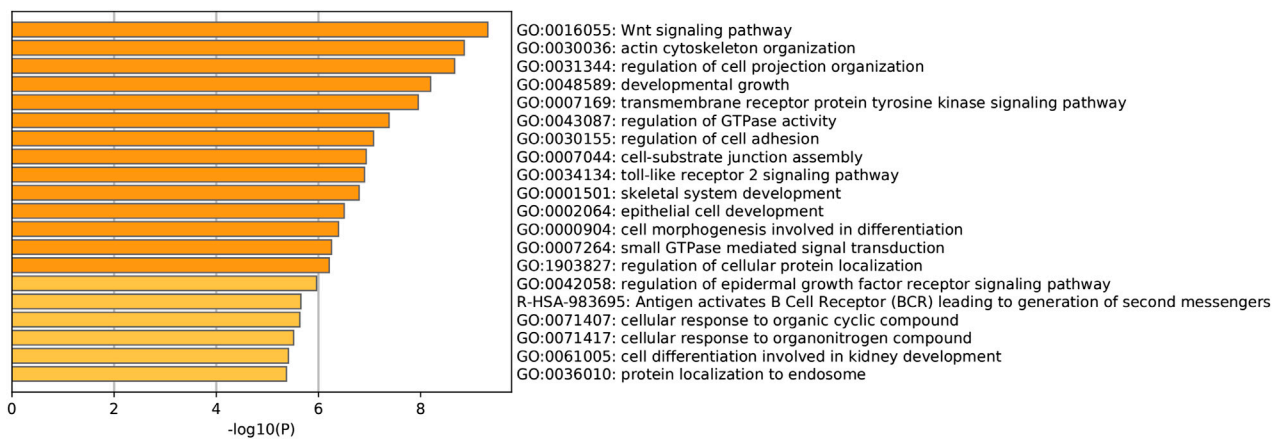


**FIGURE 4 |** Pathway enrichment analysis of CLIP4 co-expressed genes. The top 20 pathway enrichment clusters based on Metascape analysis of CLIP4 co-expressed genes carried out with GO Biological Processes and Reactome Gene Sets. Length of bars represent $\log_{10}$ ($p$-value) determined by the best-scoring term within each cluster.

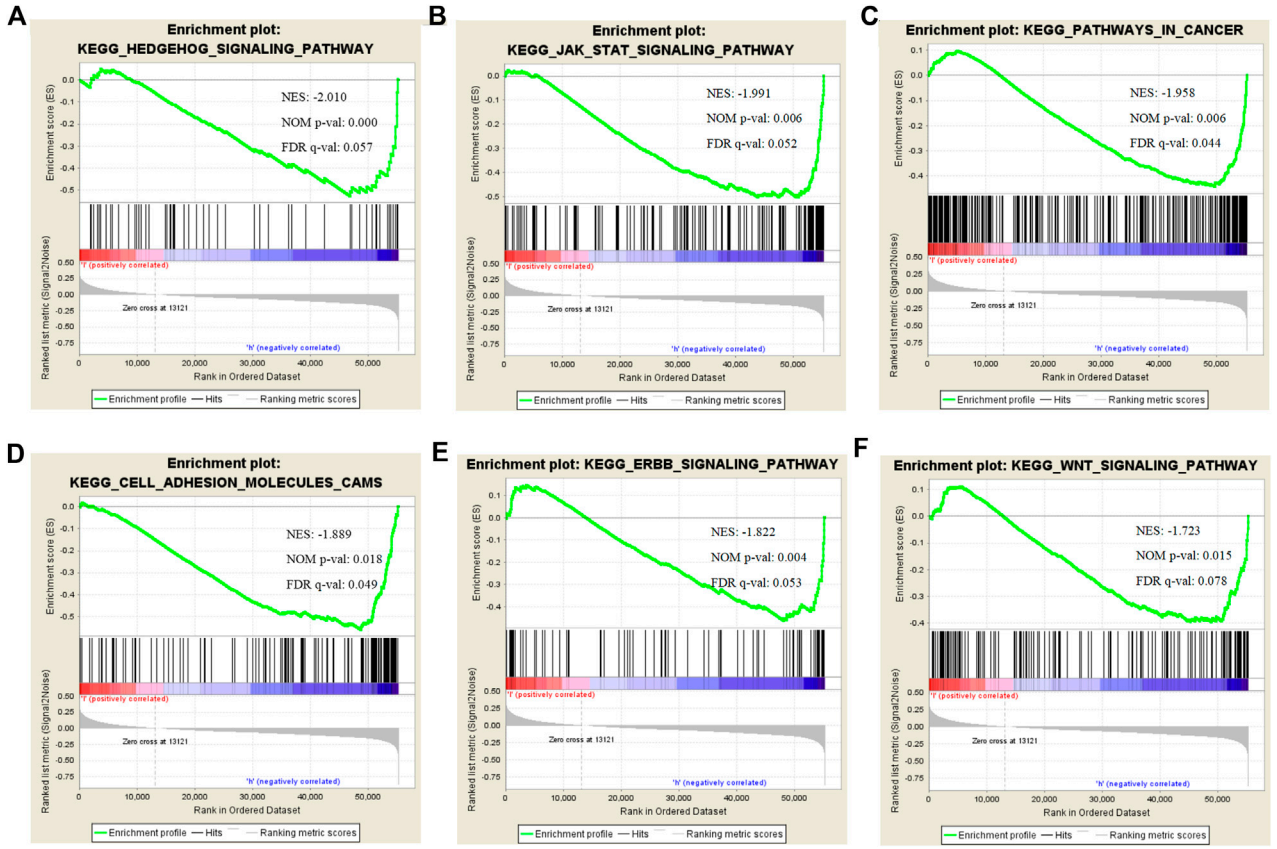


**FIGURE 5 |** Enrichment plots for CLIP4 in breast cancer obtained by GSEA. GSEA results showing Hedgehog signaling pathway **(A)**, JAK-STAT signaling pathway **(B)**, pathways in cancer **(C)**, cell adhesion molecules **(D)**, ERBB signaling pathway **(E)**, and Wnt signaling pathway **(F)** are differentially enriched in CLIP4-related breast cancer. NES, normalized ES; NOM *p*-value, normalized *p*-value; FDR *q*-value, false discovery rate *q*-value.

**TABLE 2 |** The most enriched and tumor-associated signaling pathways in phenotype high.

| MSigDB collection | Gene set name | ES | NES | NOM *p*-value | FDR *q*-value |
|---|---|---|---|---|---|
| c2.cp.kegg.v6.2.symbols.gmt | HEDGEHOG_SIGNALING_PATHWAY | −0.528 | −2.010 | 0.000 | 0.057 |
| | JAK_STAT_SIGNALING_PATHWAY | −0.504 | −1.991 | 0.006 | 0.052 |
| | PATHWAYS_IN_CANCER | −0.442 | −1.958 | 0.006 | 0.044 |
| | CELL_ADHESION_MOLECULES_CAMS | −0.561 | −1.889 | 0.018 | 0.049 |
| | ERBB_SIGNALING_PATHWAY | −0.463 | −1.822 | 0.004 | 0.053 |
| | WNT_SIGNALING_PATHWAY | −0.396 | −1.723 | 0.015 | 0.077 |

*Note: NES, normalized enrichment score; NOM, nominal; FDR, false discovery rate. Gene sets with NOM p-val < 0.05 and FDR q-val < 0.25 are considered as significant.*

analyzed. The results showed that the CLIP4 promoter was hypermethylated in patients compared with normal controls ($p$ = 4.533E−11, <0.001) (**Figure 6A**). MEXPRESS was used to confirm the promoter methylation status of CLIP4 in breast cancer. The samples were presented in ascending order according to the level of expression, and CLIP4 expression was negatively associated with DNA methylation based on Pearson's correlation analyses (**Supplementary Figure S5**). The results indicated that promoter hypermethylation of CLIP4 was related to the downregulation of mRNA expression. Furthermore, we investigated whether CLIP4 downregulation was caused by genetic alterations. Copy number alterations and gene mutations of CLIP4 were analyzed using the cBioPortal online tool. Genetic alterations of CLIP4 were mutually exclusive and only found in 11 (1.1%) of 963 invasive breast carcinoma patients, of which six samples had DNA amplification, two had deep deletion, two had a truncating mutation, and one had a missense mutations (**Figure 6B**). These results supported the significant role of DNA methylation in the regulation of CLIP4 expression.

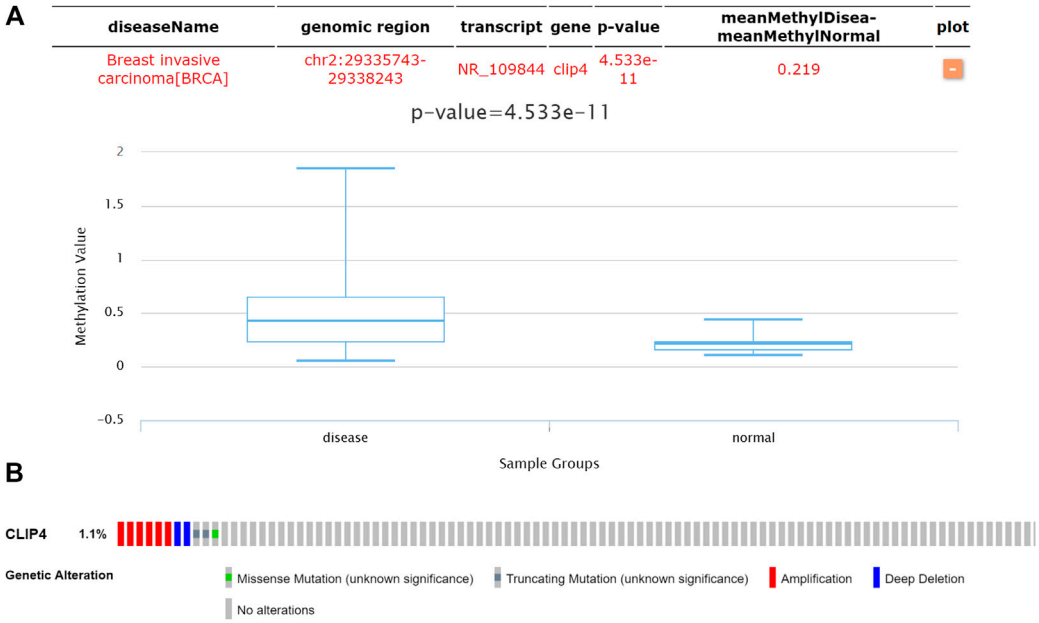


**FIGURE 6 |** Genetic features of CLIP4 in breast cancer. **(A)** The DNA methylation status of CLIP4 in 1299 breast invasive carcinomas and in normal tissue obtained from DiseaseMeth datasets. **(B)** CLIP4 gene alterations in 963 breast cancers based on OncoPrint. Tumor tissues are shown in columns.

## DISCUSSION

In the present study, the expression of CLIP4 was investigated in breast cancer by bioinformatics analysis. Oncomine and TCGA analysis revealed mRNA expression of CLIP4 to be significantly decreased in breast cancer, when compared to normal samples. CLIP4 expression was negatively correlated with HER2 status, NPI, SBR grade, nodal status, and tumor stage. However, the basal-like and TNBC types were positively associated with CLIP4 expression. The prognostic role of CLIP4 in breast cancer was then investigated using the Kaplan-Meier Plotter, and the results demonstrated that higher expression of CLIP4 was associated with better RFS and OS, especially in Luminal B and HER2 positive breast cancers. Analysis of epigenetic and genetic alterations of CLIP4 in breast cancer indicated that promoter methylation was the main mechanism underlying the regulation of CLIP4 gene expression. These findings suggested that promoter methylation-mediated loss of CLIP4 expression may be a novel prognostic biomarker for breast cancer.

Cytoskeletal proteins play important effects in cellular functions such as opposing compression, invasion, migration, and transport. The cytoskeleton also provides an optimal scaffold for the process of signal transduction (Balikov et al., 2017). However, the role of the cytoskeleton and microtubule-associated protein CLIP4 in human cancer has not been studied extensively. The methylation of XKR6, CCDC57, MAML3, SDC2, and CLIP4 is associated with age and tumor location in gastric cancer (Chong et al., 2014). The promoter methylation of IRF4, ELMO1, CLIP4, and MSC is related with increasing seriousness from gastritis with no metaplasia to gastritis with metaplasia and gastric cancer (Pirini et al., 2017). Contrary to the results of this study, increased expression of four genes (CLIP4, NOX4, LAMP5, and MATN3) is related to poor prognosis, and the expression of these genes is higher in stromal components than in epithelial cancer cells in gastric cancer (Lee et al., 2014). CLIP4 shows high expression levels in kidney cancer cell lines compared with normal cell lines, and CLIP4 significantly increases cell migration and viability (Ahn et al., 2016). In clear cell renal cell carcinoma (ccRCC), CLIP4 mutations are three-fold higher in patients with aggressive tumors than in those without aggressive ccRCC, and high expression levels of MOCOS, BAIAP2L1, DDX11, and CLIP4 are markedly associated with poor OS (Park et al., 2020). Interestingly, potentially pathogenic mutations of CLIP4 and other genes may state a subset of lung adenocarcinoma among never-smoking women (Donner et al., 2018). In line with this study, 43 genes (including CLIP4) were downregulated in ovarian cancer tumor samples and reactivated after treatment with 5-Aza-2'-deoxycytidine (5-aza-dC); CLIP4, GULP1, BAMBI, NT5E, and TGFB2 showed a pattern of cancer-specific methylation (Maldonado et al., 2018). Three DNA methylation markers, C9orf50, KCNQ5, and CLIP4, can discriminate between the plasma from colorectal cancer patients and that of healthy individuals (Jensen et al., 2019). Furthermore, CLIP4 has been considered a promising epigenetic biomarker by analysis of differentially methylated genes and differentially expressed genes between matched tumor and non-tumor tissues of the colon (Wu et al., 2020). Of note, CLIP4 was associated with better OS in Luminal B and HER2 positive breast cancers but not TNBC type in this study, the result revealed that CLIP4 may be used as a target to overcome the drug resistance, incomplete responders, and relapsed in individualized treatment of Luminal B and HER2 breast cancer. Despite many

studies providing important data and tumor-specific roles for CLIP4 in human cancer, its biological function and molecular mechanism remain unclear. Another CAP-Gly domain containing linker protein, CLIP1 is a mRNA stemness index-related key gene associated with a better lung adenocarcinoma prognosis, which is involved in tumor metastasis, relapse, and drug resistance (Zhao et al., 2020). A report showed that cells expressing FGFR2-CLIP1 fusion were sensitive to INCB054828 (a pan-FGFR inhibitor) in cholangiocarcinoma while the FGFR2 N549H mutation was resistant to this inhibitor (Krook et al., 2019).

Unlike previous reports, analyzing gastric cancer and ccRCC, this study showed that high CLIP4 expression was associated with a better prognosis, suggesting that CLIP4 had a suppressive function in breast cancer. To elucidate the molecular mechanism underlying the function of CLIP4 in breast cancer, we constructed a CLIP4-associated regulatory network. The present findings supported the important role of CLIP4 upregulation in tumor-associated signaling pathways such as Hh, JAK-STAT, Wnt, and ERBB, and suggested that it acted as a tumor suppressor in breast cancer. GSEA and Metascape analysis indicated that CLIP4 was related to the Wnt signaling pathway. Wnt signaling plays a critical role in normal development as well as tumorigenesis (Yin et al., 2018). Overactivation of Wnt signaling is implicated in human diseases including breast cancer. However, the association of CLIP4 with Wnt signaling and cytoskeletal proteins in human cancers has not been reported to date. Tankyrases, which are multifunctional poly (ADP-ribose) polymerase (PARP) superfamily members with features of both signaling and cytoskeletal proteins, antagonize the Wnt/β-catenin signaling (Kuusela et al., 2016). In addition, the Wnt/β-catenin pathway can influence the distribution of microtubules and neurofilaments (Tian et al., 2019). As a therapeutic target to overcome drug resistance in breast cancer (Tabassum et al., 2019), the JAK-STAT signaling pathway was associated with CLIP4 in this study. However, only one previous study has shown that another cytoskeletal protein, CLIP3, plays an essential role in astrocyte activation, and is associated with STAT3 pathway activation induced by spinal cord injury (Chen et al., 2018). Therefore, there is lack of other evidence in human cancers that identifies the role of CLIPs in JAK-STAT signaling. Similarly, one study reported that the cytoskeletal protein Zyxin is involved in fine tuning the neural plate patterning in *Xenopus laevis* embryos by modulating the activity of an effector of Hh signaling, the transcription factor glioma-associated oncogene 1 (GLI1) (Martynova et al., 2018). Hh signaling, which results in activation of GLI transcription factors and correlates with worse outcomes of breast cancer, is activated in human mammary stem cells (Bhateja et al., 2019). Although therapeutic agents such as Herceptin, which are designed to inhibit ERBB activity, have dramatically improved the survival of patients with HER2 positive breast cancer, approximately 50% of patients acquire drug resistance within 1 year (Zahnow, 2006). Therefore, it is important to identify gene targets associated with ERBB signaling. The present findings on the association between CLIP4 and ERBB signaling in breast cancer may provide a novel research direction.

In summary, the cytoplasmic linker protein CLIP4 may act as a novel prognostic and epigenetic biomarker for breast cancer patients. There were limitations to this study. First, the analysis was based on mRNA levels from public datasets, which requires confirmation at the mRNA and protein level. Second, some of the bioinformatics tools used had only limited functionality, such as hierarchical analysis without multivariable Cox regression analysis. Finally, there was a lack of in vivo and in vitro direct evidence to confirm the biological function and molecular mechanism of CLIP4 in breast cancer. Additional basic studies and clinical trials are urgently needed to validate the findings of this study. For the future, we plan to confirm and evaluate the value of CLIP4 as a potential biomarker for breast cancer.

## DATA AVAILABILITY STATEMENT

The datasets presented in this study can be found in online repositories. The names of the repository/repositories and accession number(s) can be found in the article/ **Supplementary Material**.

## AUTHOR CONTRIBUTIONS

Study deign: YF and LH; investigation and resources: YF; data collection: YF, SF, YH, and JF; writing-original draft preparation: YF and YW; writing-review and editing: YF and YW; data interpretation and visualization: LH and QW; supervision: YF; project administration: YF; funding acquisition: YF; statistical analysis: LH, YW, and SF. All authors have read and agreed to the published version of the manuscript.

## FUNDING

This work was supported by the Funded Project of Affiliated Hospital of Southwest Medical University for Doctors (grant no. 17135), and the Luzhou-Southwest Medical University Applied Basic Research Project (grant no. 2019LZXNYDJ07).

## SUPPLEMENTARY MATERIAL

The Supplementary Material for this article can be found online at: https://www.frontiersin.org/articles/10.3389/fmolb.2020.616190/full#supplementary-material.

## REFERENCES


Ahn, J., Han, K. S., Heo, J. H., Bang, D., Kang, Y. H., Jin, H. A., et al. (2016). FOXC2 and CLIP4 : a potential biomarker for synchronous metastasis of ≤7-cm clear cell renal cell carcinomas. *Oncotarget* 7 (32), 51423–51434. doi:10.18632/oncotarget.9842

Akhmanova, A., and Hoogenraad, C. C. (2005). Microtubule plus-end-tracking proteins: mechanisms and functions. *Curr Opin Cell Biol* 17 (1), 47–54. doi:10.1016/j.ceb.2004.11.001

Balikov, D. A., Brady, S. K., Ko, U. H., Shin, J. H., De Pereda, J. M., Sonnenberg, A., et al. (2017). The nesprin-cytoskeleton interface probed directly on single nuclei is a mechanically rich system. *Nucleus* 8 (5), 534–547. doi:10.1080/19491034.2017.1322237

Bhateja, P., Cherian, M., Majumder, S., and Ramaswamy, B. (2019). The hedgehog signaling pathway: a viable target in breast cancer?. *Cancers* 11 (8), 1126. doi:10.3390/cancers11081126

Cerami, E., Gao, J., Dogrusoz, U., Gross, B. E., Sumer, S. O., Aksoy, B. A., et al. (2012). The cBio cancer genomics portal: an open platform for exploring multidimensional cancer genomics data. *Cancer Discov* 2 (5), 401–404. doi:10.1158/2159-8290.CD-12-0095

Chandrashekar, D. S., Bashel, B., Balasubramanya, S. A. H., Creighton, C. J., Ponce-Rodriguez, I., Chakravarthi, B. V. S. K., et al. (2017). UALCAN: a portal for facilitating tumor subgroup gene expression and survival analyses. *Neoplasia* 19 (8), 649–658. doi:10.1016/j.neo.2017.05.002

Chen, W., Zheng, R., Baade, P. D., Zhang, S., Zeng, H., Bray, F., et al. (2016). Cancer statistics in China, 2015. *CA Cancer J Clin* 66 (2), 115–132. doi:10.3322/caac.21338

Chen, X., Chen, C., Hao, J., Zhang, J., and Zhang, F. (2018). Effect of CLIP3 upregulation on astrocyte proliferation and subsequent glial scar formation in the rat spinal cord via STAT3 pathway after injury. *J Mol Neurosci* 64 (1), 117–128. doi:10.1007/s12031-017-0998-6

Chong, Y., Mia-Jan, K., Ryu, H., Abdul-Ghafar, J., Munkhdelger, J., Lkhagvadorj, S., et al. (2014). DNA methylation status of a distinctively different subset of genes is associated with each histologic Lauren classification subtype in early gastric carcinogenesis. *Oncol Rep* 31 (6), 2535–2544. doi:10.3892/or.2014.3133

Curtis, C., Shah, S. P., Chin, S. F., Turashvili, G., Rueda, O. M., Dunning, M. J., et al. (2012). The genomic and transcriptomic architecture of 2,000 breast tumours reveals novel subgroups. *Nature* 486 (7403), 346–352. doi:10.1038/nature10983

DeSantis, C. E., Ma, J., Gaudet, M. M., Newman, L. A., Miller, K. D., Goding Sauer, A., et al. (2019). Breast cancer statistics, 2019. *CA A Cancer J Clin.* 69 (6), 438–451. doi:10.3322/caac.21583

Donner, I., Katainen, R., Sipilä, L. J., Aavikko, M., Pukkala, E., and Aaltonen, L. A. (2018). Germline mutations in young non-smoking women with lung adenocarcinoma. *Lung Canc* 122, 76–82. doi:10.1016/j.lungcan.2018.05.027

Fan, Y., Mu, J., Huang, M., Imani, S., Wang, Y., Lin, S., et al. (2019). Epigenetic identification of ADCY4 as a biomarker for breast cancer: an integrated analysis of adenylate cyclases. *Epigenomics* 11 (14), 1561–1579. doi:10.2217/epi-2019-0207

Galjart, N. (2005). CLIPs and CLASPs and cellular dynamics. *Nat Rev Mol Cell Biol* 6 (6), 487–98. doi:10.1038/nrm1664

Galjart, N., and Perez, F. (2003). A plus-end raft to control microtubule dynamics and function. *Curr Opin Cell Biol.* 15 (1), 48–53. doi:10.1016/s0955-0674(02)00007-8

Glück, S., Ross, J. S., Royce, M., McKenna, E. F., Jr., Perou, C. M., Avisar, E, et al. (2012). TP53 genomics predict higher clinical and pathologic tumor response in operable early-stage breast cancer treated with docetaxel-capecitabine ± trastuzumab. *Breast Cancer Res Treat* 132 (3), 781–791. doi:10.1007/s10549-011-1412-7

Győrffy, B., Lanczky, A., Eklund, A. C., Denkert, C., Budczies, J., Li, Q., et al. (2010). An online survival analysis tool to rapidly assess the effect of 22,277 genes on breast cancer prognosis using microarray data of 1,809 patients. *Breast Cancer Res Treat* 123 (3), 725–731. doi:10.1007/s10549-009-0674-9

Howard, J., and Hyman, A. A. (2003). Dynamics and mechanics of the microtubule plus end. *Nature* 422 (6933), 753–758. doi:10.1038/nature01600

Jensen, S. Ø., Øgaard, N., Ørntoft, M.-B. W., Rasmussen, M. H., Bramsen, J. B., Kristensen, H., et al. (2019). Novel DNA methylation biomarkers show high sensitivity and specificity for blood-based detection of colorectal cancer-a clinical biomarker discovery and validation study. *Clin Epigenet* 11 (1), 158. doi:10.1186/s13148-019-0757-3

Jézéquel, P., Campone, M., Gouraud, W., Guérin-Charbonnel, C., Leux, C., Ricolleau, G., et al. (2012). bc-GenExMiner: an easy-to-use online platform for gene prognostic analyses in breast cancer. *Breast Cancer Res Treat* 131 (3), 765–775. doi:10.1007/s10549-011-1457-7

Koch, A., De Meyer, T., Jeschke, J., and Van Criekinge, W. (2015). MEXPRESS: visualizing expression, DNA methylation and clinical TCGA data. *BMC Genom.* 16, 636. doi:10.1186/s12864-015-1847-z

Krook, M. A., Bonneville, R., Chen, H. Z., Reeser, J. W., Wing, M. R., Martin, D. M., et al. (2019). Tumor heterogeneity and acquired drug resistance in FGFR2-fusion-positive cholangiocarcinoma through rapid research autopsy. *Cold Spring Harb Mol Case Stud* 5 (4), a004002. doi:10.1101/mcs.a004002

Kuusela, S, Wang, H, Wasik, AA, Suleiman, H, and Lehtonen, S (2016). Tankyrase inhibition aggravates kidney injury in the absence of CD2AP. *Cell Death Dis* 7, e2302. doi:10.1038/cddis.2016.217

Lee, J., Sohn, I., Do, I. G., Kim, K. M., Park, S. H., Park, J. O., et al. (2014). Nanostring-based multigene assay to predict recurrence for gastric cancer patients after surgery. *PLoS One* 9 (3), e90133. doi:10.1371/journal.pone.0090133

Ma, X. J., Dahiya, S., Richardson, E., Erlander, M., and Sgroi, D. C. (2009). Gene expression profiling of the tumor microenvironment during breast cancer progression. *Breast Cancer Res* 11 (1), R7. doi:10.1186/bcr2222

Maldonado, L., Brait, M., Izumchenko, E., Begum, S., Chatterjee, A., Sen, T., et al. (2018). Integrated transcriptomic and epigenomic analysis of ovarian cancer reveals epigenetically silenced GULP1. *Cancer Lett* 433, 242–251. doi:10.1016/j.canlet.2018.06.030

Martynova, N. Y., Parshina, E. A, Ermolina, L. V., and Zaraisky, A. G. (2018). The cytoskeletal protein Zyxin interacts with the zinc-finger transcription factor Zic1 and plays the role of a scaffold for Gli1 and Zic1 interactions during early development of Xenopus laevis. *Biochem Biophys Res Commun* 504 (1), 251–256. doi:10.1016/j.bbrc.2018.08.164

Mitchison, T., and Kirschner, M. (1984). Dynamic instability of microtubule growth. *Nature* 312 (5991), 237–242. doi:10.1038/312237a0

Park, J. S., Pierorazio, P. M., Lee, J. H., Lee, H. J., Lim, Y. S., Jang, W. S., et al. (2020). Gene expression analysis of aggressive clinical t1 stage clear cell renal cell carcinoma for identifying potential diagnostic and prognostic biomarkers. *Cancers* 12 (1), 222. doi:10.3390/cancers12010222

Perez, F., Diamantopoulos, G. S., Stalder, R., and Kreis, T. E. (1999). CLIP-170 highlights growing microtubule ends in vivo. *Cell* 96 (4), 517–527. doi:10.1016/s0092-8674(00)80656-x

Pirini, F., Noazin, S., Jahuira-Arias, M. H., Rodriguez-Torres, S., Friess, L., Michailidi, C., et al. (2017). Early detection of gastric cancer using global, genome-wide and IRF4, ELMO1, CLIP4 and MSC DNA methylation in endoscopic biopsies. *Oncotarget* 8 (24), 38501–38516. doi:10.18632/oncotarget.16258

Rhodes, D. R., Yu, J., Shanker, K., Deshpande, N., Varambally, R., Ghosh, D., et al. (2004). ONCOMINE: a cancer microarray database and integrated data-mining platform. *Neoplasia* 6 (1), 1–6. doi:10.1016/s1476-5586(04)80047-2

Richardson, A. L., Wang, Z. C., De Nicolo, A., Lu, X., Brown, M., Miron, A., et al. (2006). X chromosomal abnormalities in basal-like human breast cancer. *Canc. Cell* 9 (2), 121–132. doi:10.1016/j.ccr.2006.01.013

Riehemann, K., and Sorg, C. (1993). Sequence homologies between four cytoskeleton-associated proteins. *Trends Biochem Sci* 18 (3), 82–83. doi:10.1016/0968-0004(93)90159-k

Siegel, R. L., Miller, K. D., and Jemal, A. (2018). Cancer statistics, 2018. *CA: A Cancer Journal for Clinicians* 68 (1), 7–30. doi:10.3322/caac.21442

Subramanian, A., Tamayo, P., Mootha, V. K., Mukherjee, S., Ebert, B. L., Gillette, M. A., et al. (2005). Gene set enrichment analysis: a knowledge-based approach for interpreting genome-wide expression profiles. *Proc Natl Acad Sci USA* 102 (43), 15545–15550. doi:10.1073/pnas.0506580102

Szklarczyk, D., Gable, A. L., Lyon, D., Junge, A., Wyder, S., Huerta-Cepas, J., et al. (2019). STRING v11: protein-protein association networks with increased coverage, supporting functional discovery in genome-wide experimental datasets. *Nucleic Acids Res* 47 (D1), D607–D613. doi:10.1093/nar/gky1131

Tabassum, S., Abbasi, R., Ahmad, N., and Farooqi, A. A. (2019). Targeting of JAK-STAT signaling in breast cancer: therapeutic strategies to overcome drug resistance. *Adv Exp Med Biol.* 1152, 271–281. doi:10.1007/978-3-030-20301-6_14

Tian, Z., Zhang, X., Zhao, Z., Zhang, F., and Deng, T. (2019). The Wnt/β-catenin signaling pathway affects the distribution of cytoskeletal proteins in Aβ treated PC12 cells. *J Integr Neurosci* 18 (3), 309–312. doi:10.31083/j.jin.2019.03.168

Uhlén, M., Björling, E., Agaton, C., Szigyarto, C. A., Amini, B., Andersen, E., et al. (2005). A human protein atlas for normal and cancer tissues based on antibody proteomics. *Mol Cell Proteomics* 4 (12), 1920-1932. doi:10.1074/mcp.M500279-MCP200

Pontén, H., and Zhang, J. (2018). Decreased expression of TFAP2B in endometrial cancer predicts poor prognosis: a study based on TCGA data. *Gynecol Oncol* 149 (3), 592–597. doi:10.1016/j.ygyno.2018.03.057

Wu, Y., Wan, X., Jia, G., Xu, Z., Tao, Y., Song, Z., et al. (2020). aberrantly methylated and expressed genes as prognostic epigenetic biomarkers for colon cancer. *DNA Cell Biol* 39 (11), 1961–1969. doi:10.1089/dna.2020.5591

Xiong, Y., Wei, Y., Gu, Y., Zhang, S., Lyu, J., Zhang, B., et al. (2017). DiseaseMeth version 2.0: a major expansion and update of the human disease methylation database. *Nucleic Acids Res* 45 (D1), D888–D895. doi:10.1093/nar/gkw1123

Yin, P., Wang, W., Zhang, Z., Bai, Y., Gao, J., and Zhao, C. (2018). Wnt signaling in human and mouse breast cancer: Focusing on Wnt ligands, receptors and antagonists. *Cancer Sci* 109 (11), 3368–3375. doi:10.1111/cas.13771

Zahnow, C. A. (2006). ErbB receptors and their ligands in the breast. *Expert Rev. Mol. Med.* 8 (23), 1–21. doi:10.1017/S146239940600010X

Zhao, M., Chen, Z., Zheng, Y., Liang, J., Hu, Z., Bian, Y., et al. (2020). Identification of cancer stem cell-related biomarkers in lung adenocarcinoma by stemness index and weighted correlation network analysis. *J Cancer Res Clin Oncol* 146 (6), 1463–1472. doi:10.1007/s00432-020-03194-x

Zhou, Y., Zhou, B., Pache, L., Chang, M., Khodabakhshi, A. H., Tanaseichuk, O., et al. (2019). Metascape provides a biologist-oriented resource for the analysis of systems-level datasets. *Nat Commun* 10 (1), 1523. doi:10.1038/s41467-019-09234-6

**Conflict of Interest:** The authors declare that the research was conducted in the absence of any commercial or financial relationships that could be construed as a potential conflict of interest.

frontiers in Molecular Biosciences

ORIGINAL RESEARCH
published: 23 March 2021
doi: 10.3389/fmolb.2021.659168

# Transcriptomic Profiling Identifies DCBLD2 as a Diagnostic and Prognostic Biomarker in Pancreatic Ductal Adenocarcinoma

*Zengyu Feng*[1,2,3], *Kexian Li*[1,2], *Yulian Wu*[3]* and *Chenghong Peng*[1,2]*

[1] Department of General Surgery, Pancreatic Disease Center, Ruijin Hospital, Shanghai Jiao Tong University School of Medicine, Shanghai, China, [2] Research Institute of Pancreatic Diseases, Shanghai Jiao Tong University School of Medicine, Shanghai, China, [3] Department of General Surgery, The Second Affiliated Hospital, School of Medicine, Zhejiang University, Hangzhou, China

OPEN ACCESS

**Edited by:**
Saber Imani,
Affiliated Hospital of Southwest Medical University, China

**Reviewed by:**
Youcai Deng,
Army Medical University, China
Parham Jabbarzadeh Kaboli,
Southwest Medical University, China

***Correspondence:**
Chenghong Peng
chhpeng@yeah.net
Yulian Wu
yulianwu@zju.edu.cn

**Specialty section:**
This article was submitted to Molecular Diagnostics and Therapeutics, a section of the journal Frontiers in Molecular Biosciences

**Received:** 27 January 2021
**Accepted:** 05 March 2021
**Published:** 23 March 2021

**Citation:**
Feng Z, Li K, Wu Y and Peng C (2021) Transcriptomic Profiling Identifies DCBLD2 as a Diagnostic and Prognostic Biomarker in Pancreatic Ductal Adenocarcinoma. Front. Mol. Biosci. 8:659168. doi: 10.3389/fmolb.2021.659168

Background: Accumulating evidence shows that the elevated expression of DCBLD2 (discoidin, CUB and LCCL domain-containing protein 2) is associated with unfavorable prognosis of various cancers. However, the correlation of DCBLD2 expression value with the diagnosis and prognosis of pancreatic ductal adenocarcinoma (PDAC) has not yet been elucidated. Methods: Univariate Cox regression analysis was used to screen robust survival-related genes. Expression pattern of selected genes was investigated in PDAC tissues and normal tissues from multiple cohorts. Kaplan–Meier (K–M) survival curves, ROC curves and calibration curves were employed to assess prognostic performance. The relationship between DCBLD2 expression and immune cell infiltrates was conducted by CIBERSORT software. Biological processes and KEGG pathway enrichment analyses were adopted to clarify the potential function of DCBLD2 in PDAC. Results: Univariate analysis, K–M survival curves and calibration curves indicated that DCBLD2 was a robust prognostic factor for PDAC with cross-cohort compatibility. Upregulation of DCBLD2 was observed in dissected PDAC tissues as well as extracellular vesicles from both plasma and serum samples of PDAC patients. Both DCBLD2 expression in tissue and extracellular vesicles had significant diagnostic value. Besides, DCBLD2 expression was correlated with infiltrating level of $CD8^+$ T cells and macrophage M2 cells. Functional enrichment revealed that DCBLD2 might be involved in cell motility, angiogenesis, and cancer-associated pathways. Conclusion: Our study systematically analyzed the potential diagnostic, prognostic and therapeutic value of DCBLD2 in PDAC. All the findings indicated that DCBLD2 might play a considerably oncogenic role in PDAC with diagnostic, prognostic and therapeutic potential. These preliminary results of bioinformatics analyses need to be further validated in more prospective studies.

**Keywords: DCBLD2, pancreatic ductal adenocarcinoma, prognosis, diagnosis, extracellular vesicles, immune infiltrates**

## INTRODUCTION

Pancreatic ductal adenocarcinoma (PDAC) is one of the deadliest cancers in the world with a 5-year survival rate lower than 9% (Siegel et al., 2020). Curative resection is the only established treatment and it remarkably improves the 5-year survival rate to 20–30% (Kamisawa et al., 2016). Unfortunately, only minority of PDAC patients have surgical indication since over 80% patients are diagnosed with unresectable, advanced-stage tumors (Wong and Raman, 2010). Accumulating evidences have demonstrated that diagnosis of PDAC at an earlier, resectable stage is likely to result in dramatic improvement of patient outcome (Ideno et al., 2020). Thus, novel diagnostic and prognostic biomarkers of PDAC with satisfactory sensitivity and specificity is urgently needed.

The discoidin, CUB and LCCL domain-containing protein 2 (DCBLD2) is a type-I transmembrane protein which has been discovered to have considerable tumor-specific functions (Schmoker et al., 2019). DCBLD2 is upregulated in lung cancer and promotes cell motility (Koshikawa et al., 2002). In colorectal cancer, high DCBLD2 expression is associated with poor patient survival, as well as tumorigenesis, invasion and metastasis of cancer cells (He et al., 2020). In gastric cancer, DCBLD2 is downregulated by epigenetic modification, and it exhibits a suppressive role in cancer cell proliferation and invasion (Kim et al., 2008). In the context of PDAC, the elevated expression of DCBLD2 is correlated with poor clinical outcome (Raman et al., 2018; Feng et al., 2020). However, the prognostic value of DCBLD2 was evaluated solely in microarray data (Feng et al., 2020), which does not capture mRNA expression as accurately as RNA-Sequencing (Zhao et al., 2014). Compared with clinical predictors such as age and histological grade, the superiority of DCBLD2 expression for survival prediction is largely unclarified. In addition, although DCBLD2 was frequently reported to be upregulated in PDAC, its diagnostic value is rarely studied, especially in extracellular vesicles.

In this study, we aim to integrate transcriptome data and survival data from multiple cohorts and platforms in order to comprehensively and systematically analysis the diagnostic and prognostic potential of DCBLD2 in PDAC. The prognostic performance was validated in both microarray data and RNA-sequencing data to ensure compatibility and reliability. The diagnostic value was investigated in both PDAC tissues and extracellular vesicles from serum and plasma samples. The considerable clinical relevance of DCBLD2 may facilitate early detection and personalized treatment of PDAC.

## MATERIALS AND METHODS

### PDAC Cohorts

The ten PDAC cohorts included in this study for survival analyses were the MTAB-6134 cohort ($N$ = 288), PACA-AU cohort ($N$ = 62), PACA-CA cohort ($N$ = 181), TCGA cohort ($N$ = 139), and six microarray cohorts, GSE21501 ($N$ = 97), GSE28735 ($N$ = 42), GSE57495 ($N$ = 63), GSE62452 ($N$ = 64), GSE71729 ($N$ = 123), and GSE85916 ($N$ = 79). Eleven cohorts including GSE15471, GSE16515, GSE28735, GSE32676, GSE41368, GSE55643, GSE60979, GSE62165, GSE62452, GSE71729, and GSE71989 were employed to evaluate the expression of genes. All these cohorts contained both PDAC tissue samples and normal tissue samples. In addition, GSE133684 cohort, which provided expression profiles of extracellular vesicles in human plasma samples from PDAC, chronic pancreatitis (CP) and healthy individuals, was chosen to investigate the potential implication of genes in liquid biopsy. The normalized gene expression data and clinical information of all GSE cohorts were downloaded from the Gene Expression Omnibus[1] (GEO). Data of MTAB-6134 cohort was downloaded from ArrayExpress database[2]. All data of PACA-AU and PACA-CA cohorts was obtained from the International Cancer Genome Consortium[3] (ICGC). The TCGA data was obtained from the TCGA hub at UCSC Xena[4]. In each cohort, patients with incomplete clinical data or with a histopathological type other than PDAC were removed from this study. Patients with a survival time of <1 month were excluded. The baseline characteristics of all PDAC patients with global clinical information are detailed in **Supplementary Table S1**.

### In-House Serum Samples

Serum samples from patients with CP ($n$ = 5), PDAC ($n$ = 73), and from healthy donors ($n$ = 42) were collected at the Department of General Surgery of Ruijin Hospital from March 2018 to December 2018 and frozen at −80°C. None of the patients received preoperative chemotherapy or radiotherapy. Written informed consent was obtained from all patients. The Ethics Committee of Ruijin Hospital affiliated with Shanghai Jiao Tong University approved the study (No. 121 in 2017).

### Survival-Related Genes Screening

The univariate Cox regression analysis was conducted to identify the survival-related genes in six independent microarray cohorts (GSE21501, GSE28735, GSE57495, GSE62452, GSE71729, and GSE85916 cohorts). Venn diagram[5] was used to screen common prognostic genes with $P < 0.05$ in all six cohorts. The identified genes were deemed as robust survival-related genes.

### Prognostic Validation of Robust Survival-Related Genes

Patients in each cohort were divided into low- and high-expression groups according to the optimal cut-off value calculated by X-Tile software (Camp et al., 2004). Kaplan–Meier (K–M) survival curves were utilized to assess the survival differences between low- and high-expression groups. Calibration plots comparing the predicted and observed clinical outcome were adopted to evaluate the predictive performance. ROC curves were used to compare the efficiency of genes with that of clinical indicators for prognosis prediction.

[1]https://www.ncbi.nlm.nih.gov/geo/

[2]https://www.ebi.ac.uk/arrayexpress/

[3]https://icgc.org/

[4]https://tcga.xenahubs.net

[5]https://www.omicshare.com/tools/Home/Soft/venn

## Estimation of Tumor Immune Infiltrates

We estimated the relative proportions of the 22 subtype immune cells in each sample by the software CIBERSORT. Samples with a $P < 0.05$ were included. The CIBERSORT software can use the deconvolution algorithm to estimate the composition of immune infiltrating cells according to gene expression matrix (Chen et al., 2018). We further used the Pearson correlation analyses to determine the correlation of gene expression level with the immune infiltrates.

## Functional Enrichment Analysis

To shed light on the biological function, co-expressed genes ($P < 0.05$) were screened by Pearson correlation analysis in MTAB-6134 cohort and TCGA cohort respectively. Top 1,000 positively correlated genes were subjected to biological process and The Kyoto Encyclopedia of Genes and Genomes (KEGG) pathway enrichment analysis on DAVID online website (Huang et al., 2009).

## Isolation of Extracellular Vesicles and Extracellular Vesicular RNA

For each case, 1.2 mL of serum was used, and an exoRNeasy Serum/Plasma Kit (Qiagen, Hilden, Germany) was used to extract extracellular vesicles following the manufacturer's instructions. Extracellular vesicles were eluted with 100 μL phosphate-buffered saline (PBS), and half of them were used for characterization and the rest for RNA isolation. Morphology of extracellular vesicles was observed by transmission electron microscopy (TEM, JEOL, Japan) on a JEOL-1230 instrument. The density and size distribution of the extracellular vesicles were measured by nanoparticle tracking analysis (NTA) using a ZetaView PMX 110 (Particle Metrix, Germany). Extracellular vesicular RNA was extracted using QIAzol (Qiagen, Hilden, Germany).

## Quantitative Real-Time Polymerase Chain Reaction (qRT-PCR)

The extracellular vesicular RNAs of total 120 samples (Ruijin cohort) were reverse-transcribed using an Evo M-MLV RT Kit (Accurate Biology, China). Real-time PCR was conducted with an ABI 7900 instrument using ChamQ SYBR qPCR Master Mix (Vazyme, Nanjing, China). Quantitation was performed in triplicate and expression was computed using the $2^{-\Delta\Delta CT}$ method. Glyceraldehyde-3-phosphate dehydrogenase (GAPDH) was used as an internal reference. The primer sequences for amplified mRNAs are as follows: DCBLD2-Forward: 5′-GCTCCAACTCCTCCTCCTTCTCC-3′; DCBLD2-Reverse: 5′-GTGTCCACATCCATCACCTTGCTG-3′; GPADH-Forward: 5′- GCACCGTCAAGGCTGAGAAC-3′; GAPDH-Reverse: 5′-TGGTGAAGACGCCAGTGGA-3′.

## Statistical Analysis

The statistical analysis and graphical work were carried out in the R environment (version 3.5.2). Cox regression analyses and K–M survival curves were plotted by the "survival" package. The ROC curves for diagnosis were derived from the "pROC" package while the ROC curves for prognosis were generated from the "survivalROC" package. Boxplots were depicted using the "ggpubr" package. Calibration curves were produced by the "rms" package. Correlation curves were plotted by the "ggstatsplot" package. The enriched pathways and biological processes were illustrated by the "ggplot2" package. A two-sided log-rank $P < 0.05$ was considered significant.

# RESULTS

## DCBLD2 Was Associated With Unfavorable Survival in PDAC

**Figure 1** shows the research workflow of this study. Univariate Cox regression analysis was first applied to screen survival-related genes and hundreds of prognostic genes in each cohort were identified. Subsequently Venn diagram revealed that only DCBLD2 was consistently correlated with patient survival in six independent microarray cohorts. We then evaluated the prognostic value of DCBLD2 in four RNA-sequencing cohorts. The results showed that in all these abovementioned cohorts, DCBLD2 was significantly associated with overall survival (OS) of patients (GSE21501: HR = 1.21, 95% CI = 1.06–1.39, $P = 0.0065$; GSE28735: HR = 1.98, 95% CI = 1.24–3.14, $P = 0.004$; GSE57495: HR = 1.53, 95% CI = 1.16–2.01, $P = 0.0029$; GSE62452: HR = 1.68, 95% CI = 1.24–2.29, $P = 0.0009$; GSE71729: HR = 1.28, 95% CI = 1.00–1.64, $P = 0.0457$; GSE85916: HR = 1.89, 95% CI = 1.43–2.51, $P < 0.0001$; MTAB-6134: HR = 1.39, 95% CI = 1.19–1.56, $P < 0.0001$; PACA-AU: HR = 1.52, 95% CI = 1.13–2.05, $P = 0.0056$; PACA-CA: HR = 1.14, 95% CI = 1.03–1.25, $P = 0.0098$; TCGA: HR = 1.24, 95% CI = 1.03–1.49, $P = 0.0199$).

## DCBLD2 Is Upregulated in PDAC With Diagnostic Potential

As illustrated in **Figure 2A**, DCBLD2 was remarkably overexpressed in PDAC tissues compared with unpaired normal tissues in seven independent GEO cohorts. According to the Gene Expression Profiling Interactive Analysis (GEPIA) database (Tang et al., 2017), DCBLD2 expression was significantly elevated in PDAC tissues (**Figure 2B**). **Figures 2C–F** demonstrated that DCBLD2 expression was also significantly increased in PDAC tissues compared with paired normal tissues. Furthermore, we explored the diagnostic potential of DCBLD2 in four GEO cohorts (GSE32676, GSE60979, GSE62165, and GSE71729). The area under the curve (AUC) values of DCBLD2 for diagnosis were 0.800, 0.874, 0.984, and 0.818, respectively (**Figures 2G–J**). This finding suggested that diagnostic accuracy of DCBLD2 was comparable to that of an established diagnostic marker, CA19-9, whose AUC value was approximately 0.84 (Xing et al., 2018). In addition, the expression of DCBLD2 was markedly increased in patients with high grade ($P < 0.05$), suggesting that DCBLD2 was related to high tumor malignancy (**Supplementary Figure 1**).

## Prognostic Performance of DCBLD2

We next assessed the prognostic efficiency of DCBLD2 in 10 independent PDAC cohorts. K–M survival curves illustrated

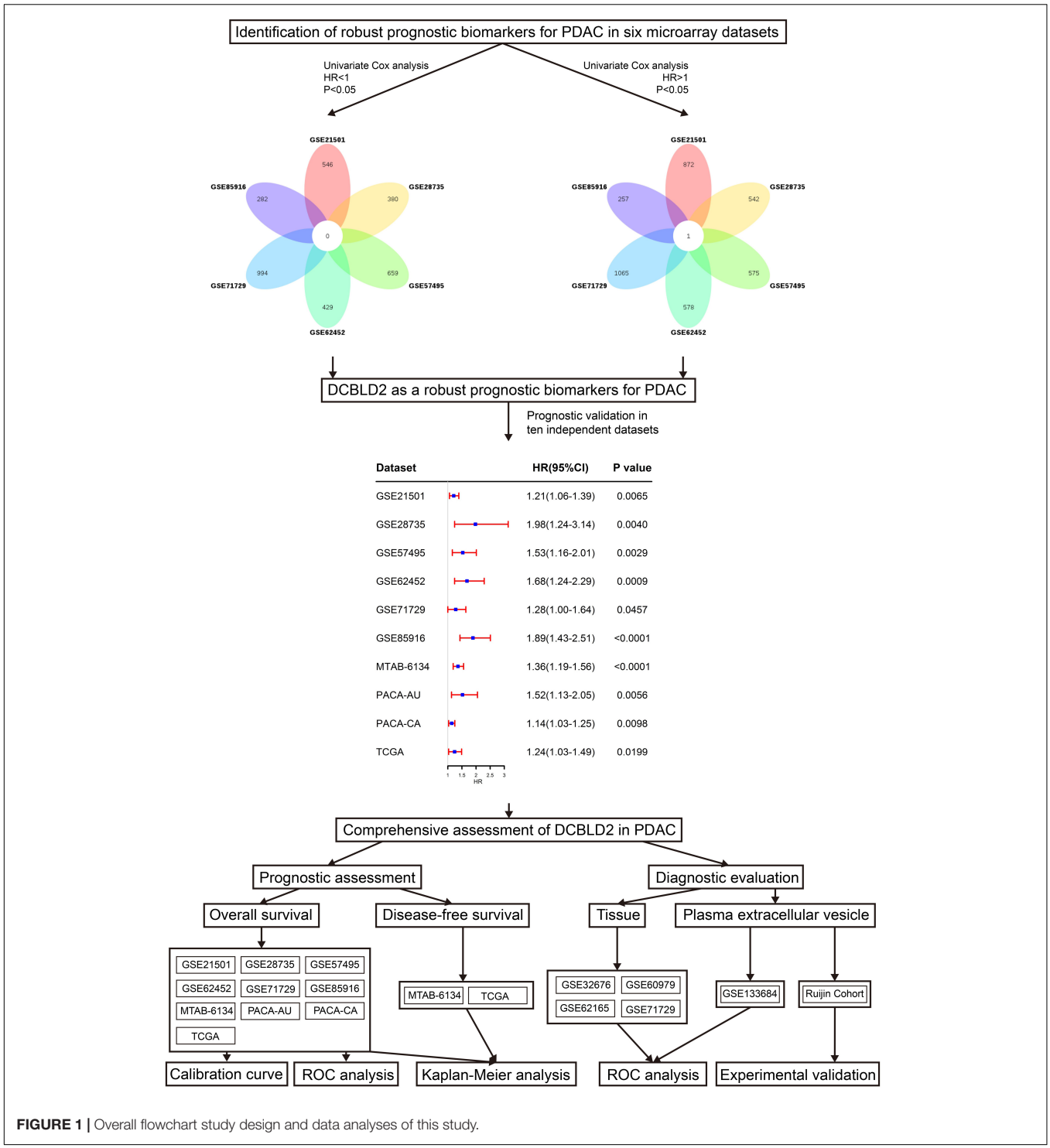


**FIGURE 1 |** Overall flowchart study design and data analyses of this study.

that patients in the high-expression group of DCBLD2 had a significant shorter OS than patients in the low-expression group (**Figures 3A–J**). The calibration curves revealed that the predicted survival probabilities by DCBLD2 were in good accordance with the observed survival probabilities (**Figures 4A–J**).

We further compared the robustness of DCBLD2 with clinical indicators, including histological grade, N stage and T stage, in MTAB-6134, PACA-AU, and TCGA cohorts. The AUC values of DCBLD2 for 1-year OS prediction were 0.708, 0.753, and 0.690, respectively, which were higher than those of clinical factors in all three cohorts (**Figures 5A–C**). This finding suggested that DCBLD2 outperformed traditional indicators in predicting PDAC survival. Moreover, patients in the high-expression group had a significantly decreased disease-free survival (DFS)

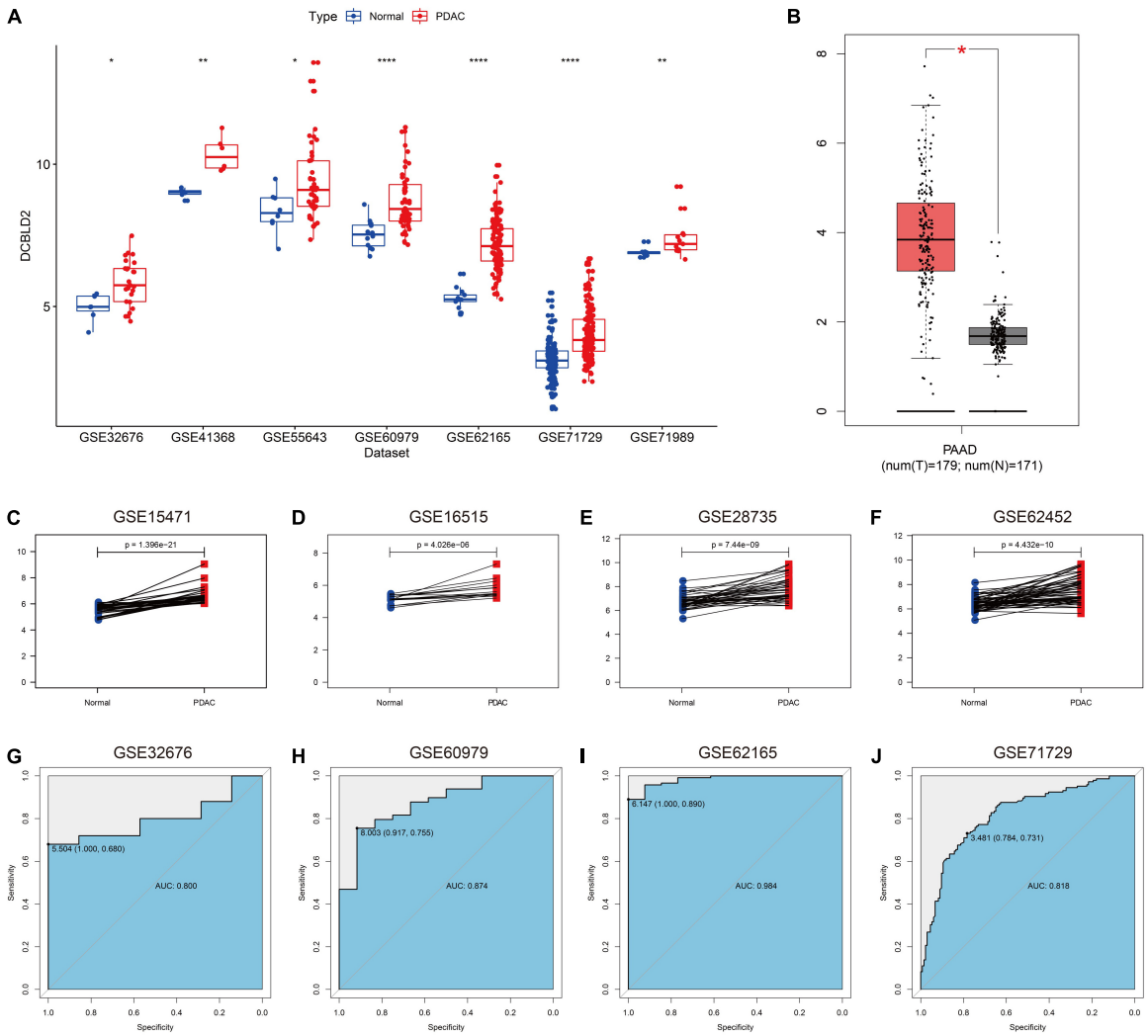


**FIGURE 2 |** Expression of DCBLD2 in PDAC tissues and its diagnostic value. **(A)** The expression of DCBLD2 in unpaired PDAC tissues and normal tissues in seven independent PDAC cohorts. **(B)** Expression profile of DCBLD2 based on the GEPIA database. **(C–F)** Expression pattern of DCBLD2 in PDAC tissues and matched adjacent normal tissues in four independent PDAC cohorts. **(G–J)** ROC curves illustrated the value of DCBLD2 in the diagnosis of PDAC in four independent PDAC cohorts. The statistical significance of differential expression was assessed by Wilcoxon test (*$p < 0.05$, **$p < 0.01$ and ****$p < 0.0001$).

compared with patients in the low-expression group in MTAB-6134 and TCGA cohorts, indicating that DCBLD2 may also serve as a prognostic indicator of DFS (**Supplementary Figure 2**).

## Relationship Between Immune Cell Infiltration and DCBLD2 Expression

The infiltration level of immune cells is strongly associated with the clinical effects of immunotherapy and the prognosis of PDAC patients (Inman et al., 2014). Consequently, we investigated the relationship between DCBLD2 expression and immune cell infiltration and explored the possibility of DCBLD2 as the precise predictor of response to immunotherapy. The abundance of macrophage M0 and M2 was positively related to DCBLD2 expression, while $CD8^+$ T cell infiltration had a negative correlation with DCBLD2 expression in MTAB-6134 cohort ($P < 0.05$, **Figures 6A–C**). Similar trends were observed in TCGA cohort ($P < 0.05$, **Figures 6D–F**).

## Biological Function and Pathway of DCBLD2

In order to preliminarily illuminate the function of DCBLD2, we performed biological process analysis and KEGG pathway enrichment analysis on top 1,000 positively co-expressed genes of DCBLD2. For biological process, DCBLD2 was found to be primarily involved in angiogenesis, cell adhesion, cell motility, and cell migration in both cohorts (**Figures 7A,B**). For pathway enrichment, DCBLD2 was mainly associated with PI3K-AKT signaling pathway, Hippo signaling pathway, Rap1 signaling pathway and pancreatic cancer in both cohorts (**Figures 7C,D**).

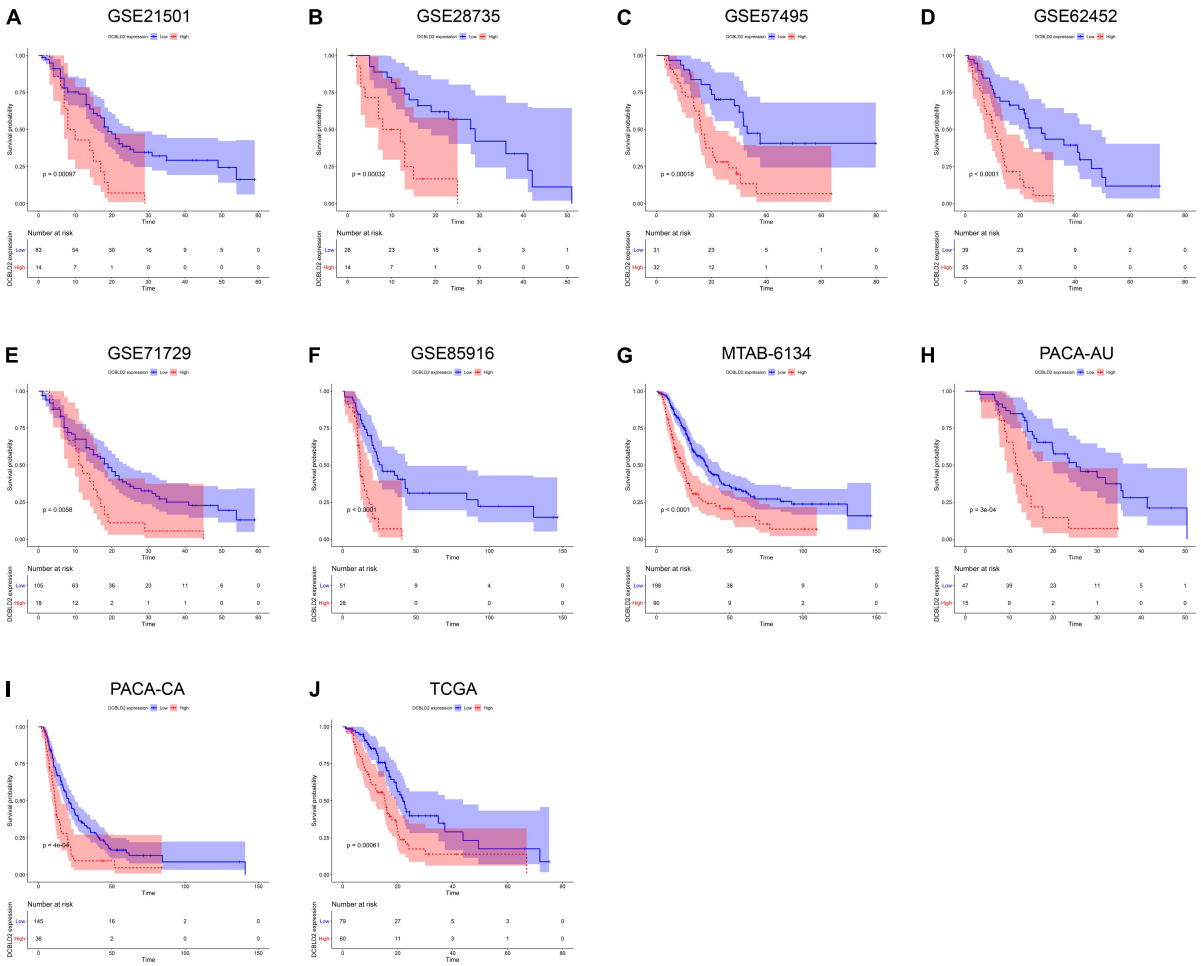


**FIGURE 3 |** Prognostic validation of DCBLD2 in PDAC. **(A–J)** K–M curves estimated the OS difference between low- and high-expression groups in ten independent PDAC cohorts. The statistical significance of differential survival was evaluated by log-rank test.

## Expression of DCBLD2 in Extracellular Vesicles From Human Plasma Samples

Early diagnosis of PDAC remains challengeable, and extracellular vesicles have emerged as attractive diagnostic biomarkers for early detection of PDAC (Yee et al., 2020). Since DCBLD2 was upregulated in PDAC tissues, we wondered whether DCBLD2 was also highly expressed in extracellular vesicles from plasma samples of PDAC patients. As **Figure 8A** illustrated, expression of DCBLD2 in extracellular vesicles from plasma samples of PDAC patients was significantly higher than that from normal donors ($P = 0.0029$) or CP patients ($P < 0.0001$). In addition, DCBLD2 in extracellular vesicles could serve as a moderate diagnostic biomarker for PDAC as the AUC value was 0.627 (**Figure 8B**).

## Validation of DCBLD2 Expression in Extracellular Vesicles From Human Serum Samples

Extracellular vesicles can be isolated from both plasma and serum of whole blood, and we had proved that DCBLD2 in extracellular vesicles from plasma samples had diagnostic potential based on the public data. We next analyzed our own data to evaluate the diagnostic value of DCBLD2 in extracellular vesicles from serum samples. The results of NTA analysis and TEM demonstrated typical characteristics of isolated extracellular vesicles (**Figures 9A,B**). **Figure 9C** showed that the expression of DCBLD2 in extracellular vesicles from serum samples was markedly elevated in PDAC patients compared with healthy donors ($P < 0.0001$) or CP patients ($P = 0.0018$). Similarly, DCBLD2 in extracellular vesicles from serum samples also bore moderate diagnostic accuracy for PDAC as the AUC value was 0.756 (**Figure 9D**).

# DISCUSSION

For PDAC patients, early detection is laudable and beneficial for long-term survival, but it is challenging. New strategies and better biomarkers are urgently needed to achieve early detection, especially for potentially curable PDAC (Singhi et al., 2019).

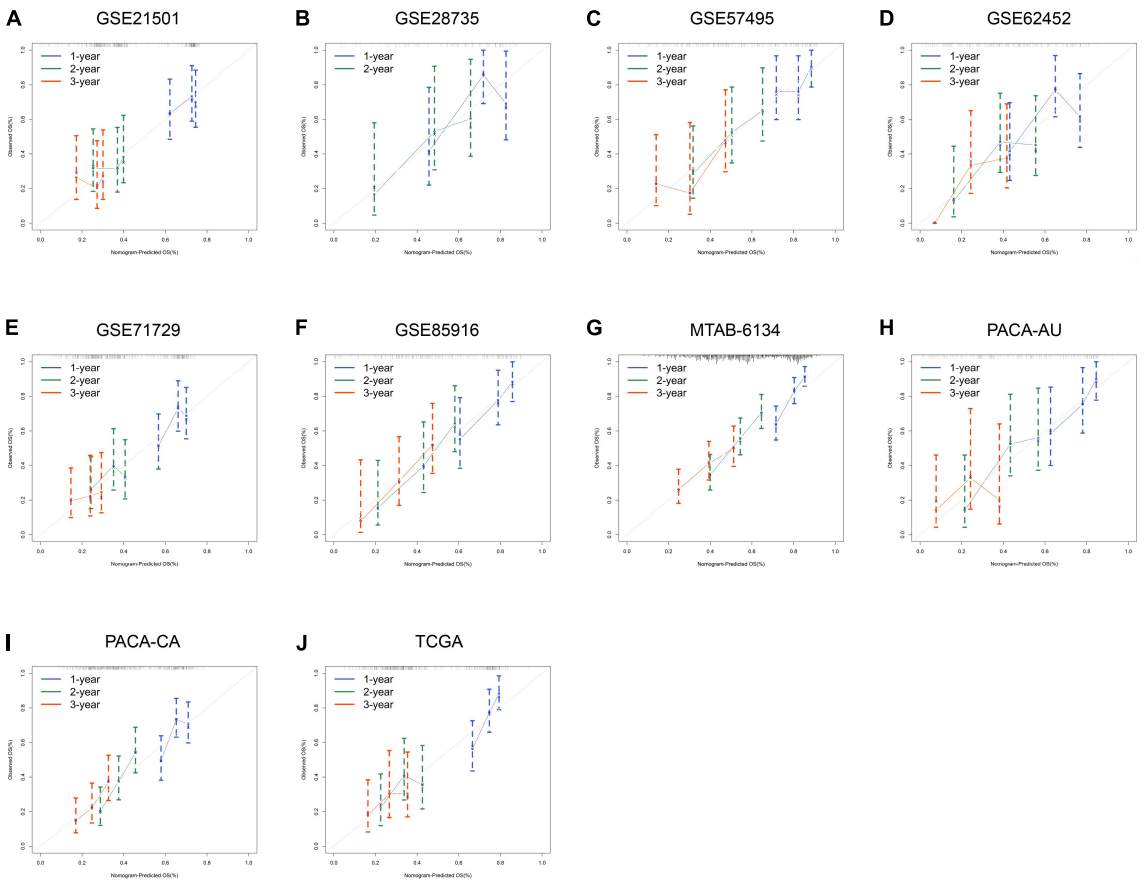


**FIGURE 4 |** Prognostic performance of DCBLD2 in PDAC. **(A–J)** Calibration curves for DCBLD2 in ten independent PDAC cohorts.

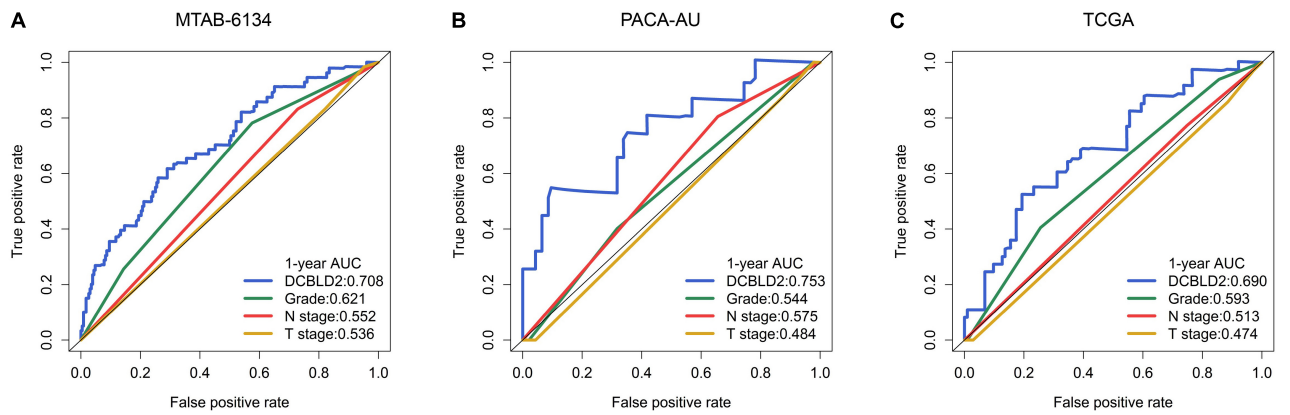


**FIGURE 5 |** Comparison of predictive accuracy of DCBLD2 and clinical parameters. **(A–C)** ROC curves compared the predictive abilities of DCBLD2 and clinical parameters for OS in the MTAB-6134, PACA-AU, and TCGA cohorts, respectively.

In the current study, we identified a robust diagnostic and prognostic biomarker, DCBLD2, with cross-platform compatibility through bioinformatic analyses. The proposed gene exhibited satisfactory predictive performance and could be detected in extracellular vesicles from both human plasma and human serum samples. Mechanistically, DCBLD2 was correlated with immune infiltrates, cell motility and several essential oncogenic pathways.

DCBLD2 is a neuropilin-like transmembrane scaffolding receptor and participates in the regulation of receptor tyrosine kinase (RTK) signaling pathway (Nie et al., 2013; Feng et al., 2014; Li et al., 2016). Elevated expression of DCBLD2 was

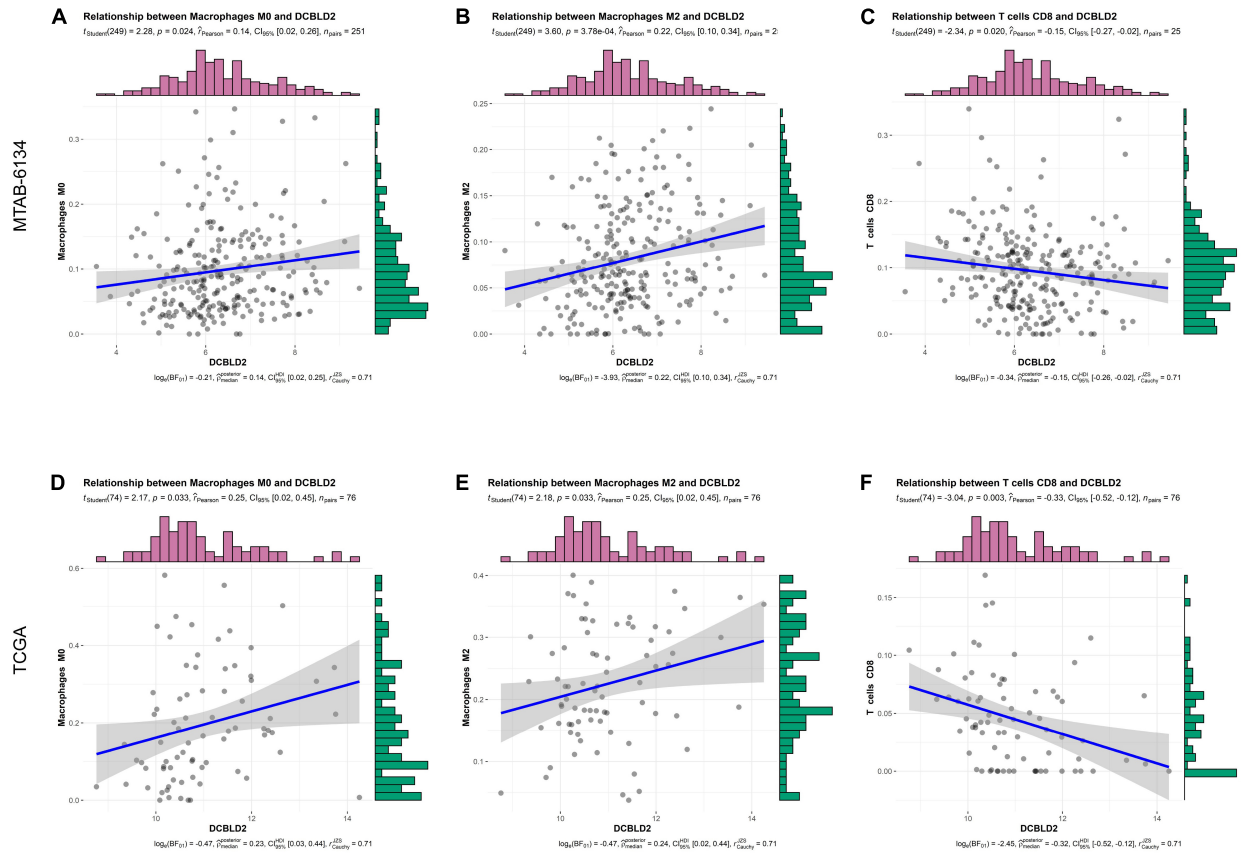


**FIGURE 6 |** Correlation analysis between DCBLD2 expression and immune infiltrates. **(A–C)** The correlation between DCBLD2 expression and the abundance of macrophage M0, macrophage M2, and $CD8^+$ T cell in MTAB-6134 cohort, respectively. **(D–F)** The correlation between DCBLD2 expression and the infiltration of macrophage M0, macrophage M2 and $CD8^+$ T cell in TCGA cohort, respectively. The correlation coefficients and *p* value were derived from Pearson correlation analysis.

significantly associated with decreased OS time in various cancers including PDAC (Raman et al., 2018), colorectal cancer (Martinez-Romero et al., 2018), hypopharyngeal squamous cell carcinoma (Fukumoto et al., 2014) and melanoma (Osella-Abate et al., 2012). Apart from OS, we found that high expression of DCBLD2 was also indicative of short DFS. We previously reported that DCBLD2 was overexpressed in pancreatic cancer stem cells (Feng et al., 2020), a small population of cancer cells with an indispensable role for tumor metastasis and recurrence (Hermann et al., 2007; Simeone, 2008). These results suggested that DCBLD2 was potentially involved in the regulation of cell stemness and might serve as a promising therapeutic target for PDAC. Function analysis of DCBLD2 revealed that this gene was positively associated with several pathways participating in stemness regulation, such as PI3K-AKT signaling pathway (Qin et al., 2021; Yoon et al., 2021) and Hippo signaling pathway (Cordenonsi et al., 2011; Park et al., 2018). These findings could provide new insight into biological implications and clinical relevance of DCBLD2 in PDAC.

In addition to prognostic potential, we also attempted to characterize the diagnostic potential of DCBLD2 in tissue samples, plasma samples and serum samples. DCBLD2 expression could be a useful diagnostic biomarker to evaluate invasive properties of myxofibrosarcoma (Kikuta et al., 2017), but its diagnostic value in PDAC remained unclear. We profiled DCBLD2 expression in several cohorts containing either matched or unmatched PDAC tissues and adjacent normal tissues. Compared with normal tissues, DCBLD2 expression increased in PDAC tissues, which revealed an oncogenic role of DCBLD2. The diagnostic ability of DCBLD2 in tissues was satisfactory, as the AUC value was close to or no less than CA19-9, an established diagnostic biomarker for PDAC (Luo et al., 2020). Extracellular vesicles contain proteins, lipids and RNA from donor cells and can be an attractive source of diagnostic biomarkers for human cancers (Yu et al., 2020). More and more researches have focused on the application of extracellular vesicular protein markers in the diagnosis of human cancers (Melo et al., 2015; Yang et al., 2017). Based on the RNA-seq data from GSE133684 dataset, we found that DCBLD2 existed in extracellular vesicles from plasma samples and could serve as a moderate marker in the early diagnosis of PDAC. We also experimentally verified the diagnostic value of DCBLD2 in extracellular vesicles from serum samples. These findings highlighted the clinical utility of DCBLD2 in liquid biopsy.

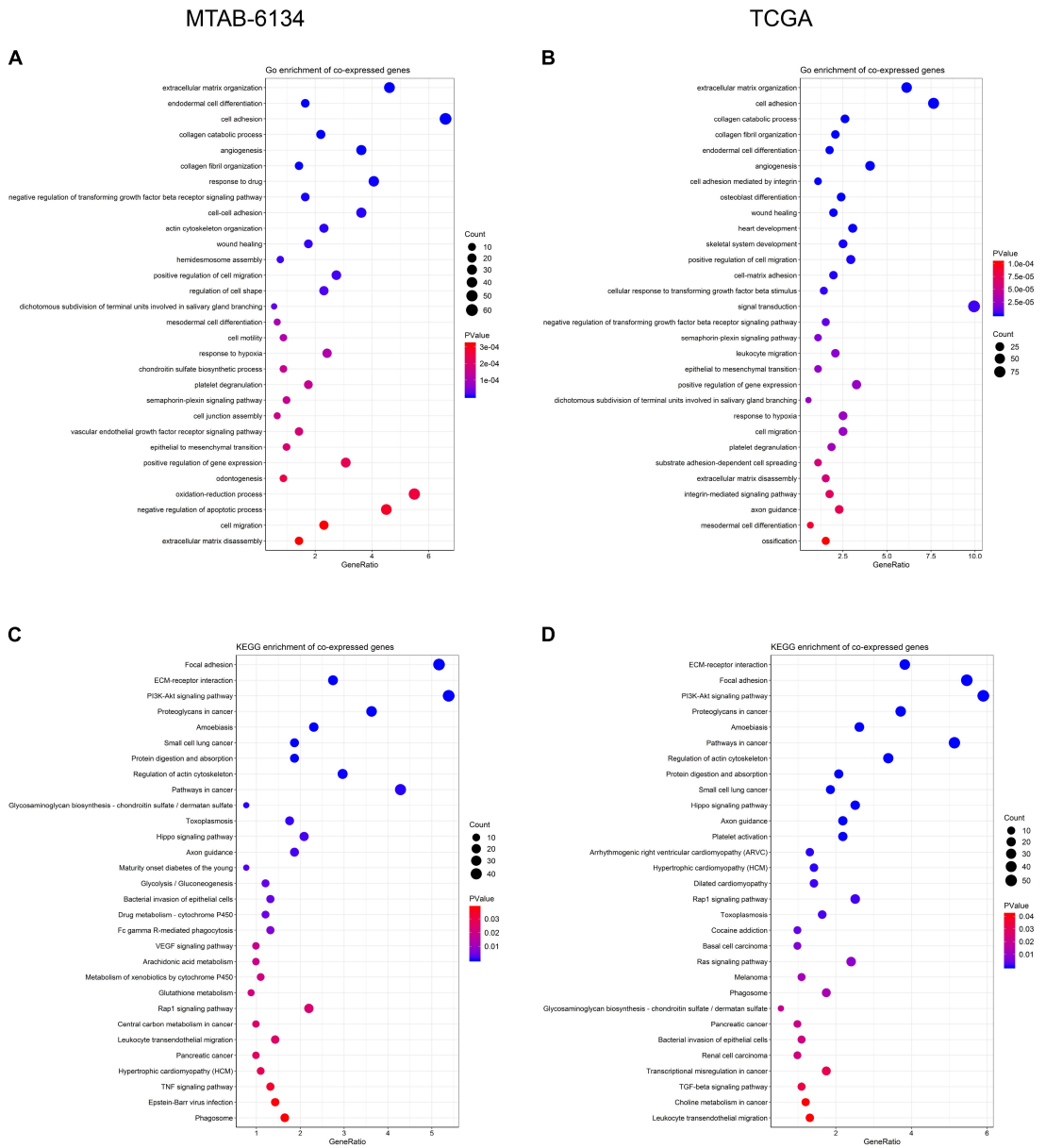


**FIGURE 7 |** Biological function of DCBLD2. **(A,B)** Biological process analysis of top 1,000 positively co-expressed genes of DCBLD2. **(C,D)** KEGG pathway enrichment analysis of top 1,000 positively co-expressed genes of DCBLD2.

Researchers recently reported two prognostic gene signatures constructed using DCBLD2 in PDAC (Raman et al., 2018; Feng et al., 2020). The prognostic accuracy of DCBLD2 was certainly inferior to that of gene models, because accumulating evidence had demonstrated that multi-gene signatures achieved higher prognostic accuracy compared with a single gene (Beane et al., 2009; Sim et al., 2017; Schmidt et al., 2018; Huang et al., 2020; Ahluwalia et al., 2021). However, we found that the diagnostic accuracy of DCBLD2 was close to or no less than that of gene models. The diagnostic AUC values of DCBLD2 were 0.800, 0.874, 0.984, and 0.818 while those of a four gene signature containing DCBLD2 (Feng et al., 2020) were 0.806, 0.881, 0.997, and 0.724 in GSE32676, GSE60979, GSE62165, and GSE71729 cohorts, respectively (**Supplementary Figure 3**). High diagnostic accuracy of DCBLD2 might facilitate novel development of a single-marker qPCR approach for PDAC detection with a reduced cost and widespread applicability.

To preliminarily elucidate the underlying mechanism of DCBLD2-resulted poor prognosis, we investigated the biological function and immune infiltrates associated with DCBLD2 expression. Co-expressed genes with DCBLD2 were mainly enriched in cell motility and multiple classic oncogenic pathways. We observed that the DCBLD2 expression was negatively correlated with the $CD8^+$ T cells infiltration while it was

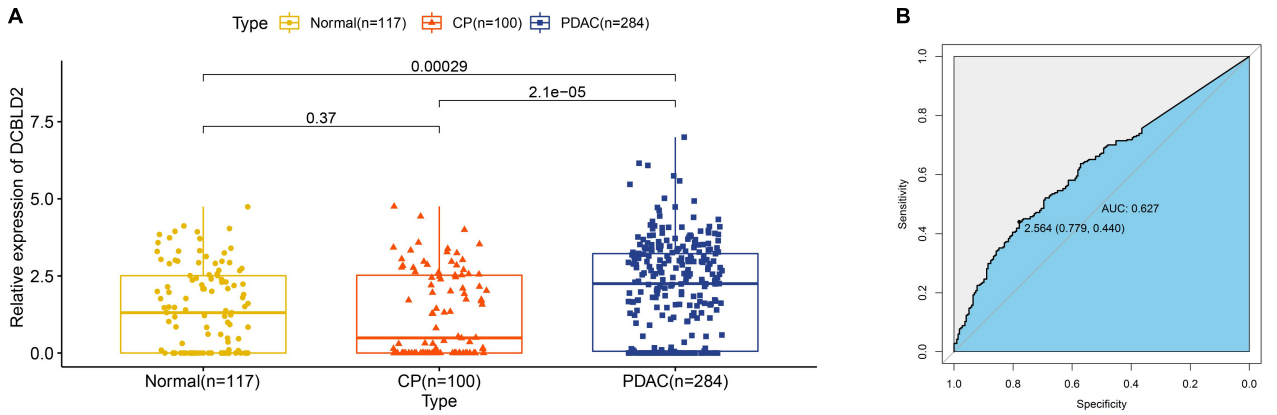


**FIGURE 8 |** Expression of DCBLD2 in extracellular vesicles from human plasma samples. **(A)** Boxplots show the distribution of extracellular vesicular DCBLD2 expression in plasma samples from healthy donors, CP patients and PDAC patients. **(B)** ROC curve showed the diagnostic value of extracellular vesicular DCBLD2 (PDAC vs Normal + CP). The statistical significance in comparing DCBLD2 expression between the two groups was determined by Wilcoxon test.

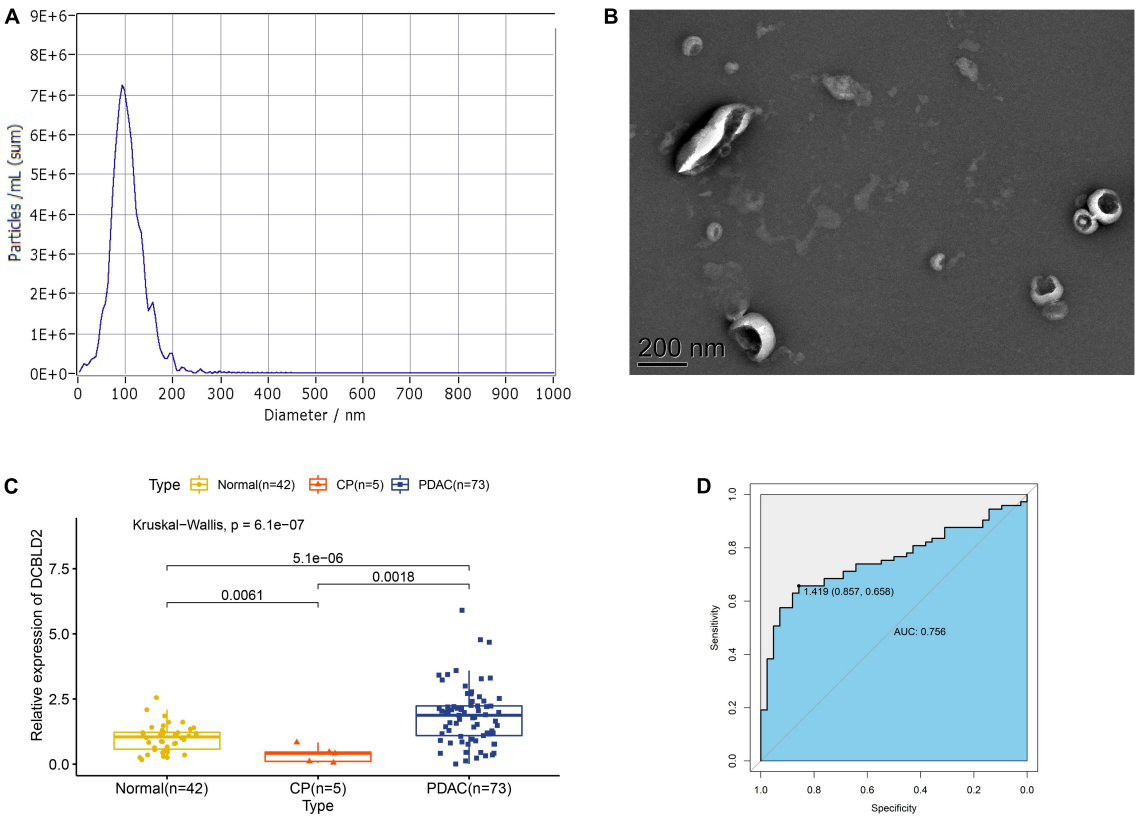


**FIGURE 9 |** Expression of DCBLD2 in extracellular vesicles from human serum samples. **(A)** NTA analysis and **(B)** TEM analysis to assess characteristics of extracellular vesicles. **(C)** Boxplots show the distribution of extracellular vesicular DCBLD2 expression in serum samples from healthy donors, CP patients and PDAC patients. **(D)** ROC curve showed the diagnostic value of extracellular vesicular DCBLD2 (PDAC vs Normal + CP). The statistical significance in comparing DCBLD2 expression between the two groups was determined by Wilcoxon test. The statistical significance in comparing DCBLD2 expression between the three groups was investigated by Kruskal–Wallis test.

positively correlated with the infiltrating level of M2 macrophage cells. Above findings further confirmed the oncogenic role of DCBLD2 and indicated that DCBLD2 had a potential impact on cell immunity. Multiple pathways related to DCBLD2 were implicated in immunological function. For instance, inhibition of PI3K-dependent phosphorylation of Akt and its transcription

factor target Foxo1 resulted in defective T cell immunity (Xu et al., 2021). Hippo signaling pathway was also involved in T cell immunity (Bouchard et al., 2020) and TGF-beta signaling pathway were known to induce M2-like macrophage polarization (Gratchev, 2017). Above findings could partly explain how DCBLD2 affects the infiltration of immune cells. Therefore, this study provided the reference for clarifying the potential biological role of DCBLD2 in tumor immunology and PDAC progression.

However, this study, after all, is a retrospective study and has several limitations. First, the clinical application of DCBLD2 in PDAC management should be tested and validated in more prospective studies. Second, more *in vivo* and *in vitro* experiments are needed to verify the abovementioned bioinformatic findings, especially the biological function of DCBLD2 in PDAC tumorigenesis. Finally, we fail to adequately assess the relationship between DCBLD2 expression and clinical factors due to the lack of significant data. With the development of follow-up research, we hope to supplement them in future studies.

In conclusion, we integrated and analyzed genomic data and clinical data of multiple PDAC cohorts to demonstrate that expression value of DCBLD2 was a reliable diagnostic and prognostic factor and was significantly associated with immune and oncogenic signaling pathways in PDAC. DCBLD2 might facilitate tumor progression and bore strong diagnostic, prognostic and therapeutic value in PDAC.

Abbreviations: AUC, area under the curve; CP, chronic pancreatitis; DCBLD2, discoidin, CUB and LCCL domain-containing protein 2; DFS, disease-free survival; GEO, Gene Expression Omnibus; GEPIA, Gene Expression Profiling Interactive Analysis; KEGG, The Kyoto Encyclopedia of Genes and Genomes; K–M, Kaplan-Meier; OS, overall survival; PDAC, pancreatic ductal adenocarcinoma; ROC, receiver operating characteristic; RTK, receptor tyrosine kinase; QRT-PCR, quantitative real-time polymerase chain reaction.

## DATA AVAILABILITY STATEMENT

Processed gene expression data and clinical data of TCGA cohort were obtained from the TCGA hub at UCSC Xena (https://tcga.xenahubs.net). Microarray data and clinical information of GSE21501, GSE28735, GSE57495, GSE62452, GSE71729, and GSE85916 cohorts were downloaded from the Gene Expression Omnibus (GEO) database (https://www.ncbi.nlm.nih.gov/geo/), while those of MTAB-6134 cohort were downloaded from the Arrayexpress database (https://www.ebi.ac.uk/arrayexpress/). Gene expression data of GSE15471, GSE16515, GSE32676, GSE41368, GSE55643, GSE60979, GSE62165, and GSE71989 was also downloaded from the GEO database. Normalized RNA-sequencing data and survival data of PACA-CA and PACA-AU cohorts were obtained from the International Cancer Genome Consortium (ICGC) database (https://icgc.org/).

## ETHICS STATEMENT

The studies involving human participants were reviewed and approved by the Ethics Committee of Ruijin Hospital affiliated with Shanghai Jiao Tong University. The patients/participants provided their written informed consent to participate in this study.

## AUTHOR CONTRIBUTIONS

ZF and CP were involved in conception and design of the study and wrote the manuscript. ZF and KL participated in data analysis, discussion, and language editing. ZF collected the serum samples. YW reviewed the manuscript. All authors contributed to the article and approved the submitted version.

## FUNDING

This work was supported by grants from the National Natural Science Foundation of China (81672325 and 81802316).

## ACKNOWLEDGMENTS

We acknowledge the contributions from GEO, GEPIA, ICGC, UCSC, and ArrayExpress databases.

## SUPPLEMENTARY MATERIAL

The Supplementary Material for this article can be found online at: https://www.frontiersin.org/articles/10.3389/fmolb.2021.659168/full#supplementary-material

## REFERENCES

Ahluwalia, P., Kolhe, R., and Gahlay, G. K. (2021). The clinical relevance of gene expression based prognostic signatures in colorectal cancer. *Biochim. Biophys. Acta Rev. Cancer* 1875:188513. doi: 10.1016/j.bbcan.2021.188513

Beane, J., Spira, A., and Lenburg, M. E. (2009). Clinical impact of high-throughput gene expression studies in lung cancer. *J. Thorac. Oncol.* 4, 109–118. doi: 10.1097/JTO.0b013e31819151f8

Bouchard, A., Witalis, M., Chang, J., Panneton, V., Li, J., Bouklouch, Y., et al. (2020). Hippo signal transduction mechanisms in T cell immunity. *Immune Netw.* 20:e36. doi: 10.4110/in.2020.20.e36

Camp, R. L., Dolled-Filhart, M., and Rimm, D. L. (2004). X-tile: a new bio-informatics tool for biomarker assessment and outcome-based cut-point optimization. *Clin. Cancer Res.* 10, 7252–7259. doi: 10.1158/1078-0432.Ccr-04-0713

Chen, B., Khodadoust, M. S., Liu, C. L., Newman, A. M., and Alizadeh, A. A. (2018). Profiling tumor infiltrating immune cells with CIBERSORT. *Methods Mol. Biol.* 1711, 243–259. doi: 10.1007/978-1-4939-7493-1_12

Cordenonsi, M., Zanconato, F., Azzolin, L., Forcato, M., Rosato, A., Frasson, C., et al. (2011). The hippo transducer TAZ confers cancer stem cell-related traits on breast cancer cells. *Cell* 147, 759–772. doi: 10.1016/j.cell.2011.09.048

Feng, H., Lopez, G. Y., Kim, C. K., Alvarez, A., Duncan, C. G., Nishikawa, R., et al. (2014). EGFR phosphorylation of DCBLD2 recruits TRAF6 and stimulates

AKT-promoted tumorigenesis. *J. Clin. Invest.* 124, 3741–3756. doi: 10.1172/jci73093

Feng, Z., Shi, M., Li, K., Ma, Y., Jiang, L., Chen, H., et al. (2020). Development and validation of a cancer stem cell-related signature for prognostic prediction in pancreatic ductal adenocarcinoma. *J. Transl. Med.* 18:360. doi: 10.1186/s12967-020-02527-1

Fukumoto, I., Kinoshita, T., Hanazawa, T., Kikkawa, N., Chiyomaru, T., Enokida, H., et al. (2014). Identification of tumour suppressive microRNA-451a in hypopharyngeal squamous cell carcinoma based on microRNA expression signature. *Br. J. Cancer* 111, 386–394. doi: 10.1038/bjc.2014.293

Gratchev, A. (2017). TGF-β signalling in tumour associated macrophages. *Immunobiology.* 222, 75–81. doi: 10.1016/j.imbio.2015.11.016

He, J., Huang, H., Du, Y., Peng, D., Zhou, Y., Li, Y., et al. (2020). Association of DCBLD2 upregulation with tumor progression and poor survival in colorectal cancer. *Cell. Oncol. (Dordr.)* 43, 409–420. doi: 10.1007/s13402-020-00495-8

Hermann, P. C., Huber, S. L., Herrler, T., Aicher, A., Ellwart, J. W., Guba, M., et al. (2007). Distinct populations of cancer stem cells determine tumor growth and metastatic activity in human pancreatic cancer. *Cell Stem Cell* 1, 313–323. doi: 10.1016/j.stem.2007.06.002

Huang, D. W., Sherman, B. T., and Lempicki, R. A. (2009). Systematic and integrative analysis of large gene lists using DAVID bioinformatics resources. *Nat. Protoc.* 4, 44–57. doi: 10.1038/nprot.2008.211

Huang, W., Yan, Y. G., Wang, W. J., Ouyang, Z. H., Li, X. L., Zhang, T. L., et al. (2020). Development and validation of a 6-miRNA prognostic signature in spinal chordoma. *Front. Oncol.* 10:556902. doi: 10.3389/fonc.2020.556902

Ideno, N., Mori, Y., Nakamura, M., and Ohtsuka, T. (2020). Early detection of pancreatic cancer: role of biomarkers in pancreatic fluid samples. *Diagnostics (Basel)* 10:1056. doi: 10.3390/diagnostics10121056

Inman, K. S., Francis, A. A., and Murray, N. R. (2014). Complex role for the immune system in initiation and progression of pancreatic cancer. *World J. Gastroenterol.* 20, 11160–11181. doi: 10.3748/wjg.v20.i32.11160

Kamisawa, T., Wood, L. D., Itoi, T., and Takaori, K. (2016). Pancreatic cancer. *Lancet* 388, 73–85. doi: 10.1016/s0140-6736(16)00141-0

Kikuta, K., Kubota, D., Yoshida, A., Qiao, Z., Morioka, H., Nakamura, M., et al. (2017). Discoidin, CUB and LCCL domain-containing protein 2 (DCBLD2) is a novel biomarker of myxofibrosarcoma invasion identified by global protein expression profiling. *Biochim. Biophys. Acta Proteins Proteom.* 1865, 1160–1166. doi: 10.1016/j.bbapap.2017.06.023

Kim, M., Lee, K. T., Jang, H. R., Kim, J. H., Noh, S. M., Song, K. S., et al. (2008). Epigenetic down-regulation and suppressive role of DCBLD2 in gastric cancer cell proliferation and invasion. *Mol. Cancer Res.* 6, 222–230. doi: 10.1158/1541-7786.Mcr-07-0142

Koshikawa, K., Osada, H., Kozaki, K., Konishi, H., Masuda, A., Tatematsu, Y., et al. (2002). Significant up-regulation of a novel gene, CLCP1, in a highly metastatic lung cancer subline as well as in lung cancers in vivo. *Oncogene* 21, 2822–2828. doi: 10.1038/sj.onc.1205405

Li, X., Jung, J. J., Nie, L., Razavian, M., Zhang, J., Samuel, V., et al. (2016). The neuropilin-like protein ESDN regulates insulin signaling and sensitivity. *Am. J. Physiol. Heart Circ. Physiol.* 310, H1184–H1193. doi: 10.1152/ajpheart.00782.2015

Luo, G., Jin, K., Deng, S., Cheng, H., Fan, Z., Gong, Y., et al. (2020). Roles of CA19-9 in pancreatic cancer: biomarker, predictor and promoter. *Biochim. Biophys. Acta Rev. Cancer* 1875:188409. doi: 10.1016/j.bbcan.2020.188409

Martinez-Romero, J., Bueno-Fortes, S., Martín-Merino, M., Ramirez de Molina, A., and De Las Rivas, J. (2018). Survival marker genes of colorectal cancer derived from consistent transcriptomic profiling. *BMC Genomics* 19:857. doi: 10.1186/s12864-018-5193-9

Melo, S. A., Luecke, L. B., Kahlert, C., Fernandez, A. F., Gammon, S. T., Kaye, J., et al. (2015). Glypican-1 identifies cancer exosomes and detects early pancreatic cancer. *Nature* 523, 177–182. doi: 10.1038/nature14581

Nie, L., Guo, X., Esmailzadeh, L., Zhang, J., Asadi, A., Collinge, M., et al. (2013). Transmembrane protein ESDN promotes endothelial VEGF signaling and regulates angiogenesis. *J. Clin. Invest.* 123, 5082–5097. doi: 10.1172/jci67752

Osella-Abate, S., Novelli, M., Quaglino, P., Orso, F., Ubezio, B., Tomasini, C., et al. (2012). Expression of AP-2α, AP-2γ and ESDN in primary melanomas: correlation with histopathological features and potential prognostic value. *J. Dermatol. Sci.* 68, 202–204. doi: 10.1016/j.jdermsci.2012.09.008

Park, J. H., Shin, J. E., and Park, H. W. (2018). The role of hippo pathway in cancer stem cell biology. *Mol. Cells* 41, 83–92. doi: 10.14348/molcells.2018.2242

Qin, Y., Hou, Y., Liu, S., Zhu, P., Wan, X., Zhao, M., et al. (2021). A novel long non-coding RNA lnc030 maintains breast cancer stem cell stemness by stabilizing SQLE mRNA and increasing cholesterol synthesis. *Adv. Sci. (Weinh.)* 8:2002232. doi: 10.1002/advs.202002232

Raman, P., Maddipati, R., Lim, K. H., and Tozeren, A. (2018). Pancreatic cancer survival analysis defines a signature that predicts outcome. *PLoS One* 13:e0201751. doi: 10.1371/journal.pone.0201751

Schmidt, L., Fredsøe, J., Kristensen, H., Strand, S. H., Rasmussen, A., Høyer, S., et al. (2018). Training and validation of a novel 4-miRNA ratio model (MiCaP) for prediction of postoperative outcome in prostate cancer patients. *Ann. Oncol.* 29, 2003–2009. doi: 10.1093/annonc/mdy243

Schmoker, A. M., Ebert, A. M., and Ballif, B. A. (2019). The DCBLD receptor family: emerging signaling roles in development, homeostasis and disease. *Biochem. J.* 476, 931–950. doi: 10.1042/bcj20190022

Siegel, R. L., Miller, K. D., and Jemal, A. (2020). Cancer statistics, 2020. *CA Cancer J. Clin.* 70, 7–30. doi: 10.3322/caac.21590

Sim, W., Lee, J., and Choi, C. (2017). Robust method for identification of prognostic gene signatures from gene expression profiles. *Sci. Rep.* 7:16926. doi: 10.1038/s41598-017-17213-4

Simeone, D. M. (2008). Pancreatic cancer stem cells: implications for the treatment of pancreatic cancer. *Clin. Cancer Res.* 14, 5646–5648. doi: 10.1158/1078-0432.Ccr-08-0584

Singhi, A. D., Koay, E. J., Chari, S. T., and Maitra, A. (2019). Early detection of pancreatic cancer: opportunities and challenges. *Gastroenterology* 156, 2024–2040. doi: 10.1053/j.gastro.2019.01.259

Tang, Z., Li, C., Kang, B., Gao, G., Li, C., and Zhang, Z. (2017). GEPIA: a web server for cancer and normal gene expression profiling and interactive analyses. *Nucleic Acids Res.* 45, W98–W102. doi: 10.1093/nar/gkx247

Wong, J. C., and Raman, S. (2010). Surgical resectability of pancreatic adenocarcinoma: CTA. *Abdom. Imaging* 35, 471–480. doi: 10.1007/s00261-009-9539-2

Xing, H., Wang, J., Wang, Y., Tong, M., Hu, H., Huang, C., et al. (2018). Diagnostic value of CA 19-9 and carcinoembryonic antigen for pancreatic cancer: a meta-analysis. *Gastroenterol. Res. Pract.* 2018:8704751. doi: 10.1155/2018/8704751

Xu, K., Yin, N., Peng, M., Stamatiades, E. G., Shyu, A., Li, P., et al. (2021). Glycolysis fuels phosphoinositide 3-kinase signaling to bolster T cell immunity. *Science* 371, 405–410. doi: 10.1126/science.abb2683

Yang, K. S., Im, H., Hong, S., Pergolini, I., Del Castillo, A. F., Wang, R., et al. (2017). Multiparametric plasma EV profiling facilitates diagnosis of pancreatic malignancy. *Sci. Transl. Med.* 9:eaal3226. doi: 10.1126/scitranslmed.aal3226

Yee, N. S., Zhang, S., He, H. Z., and Zheng, S. Y. (2020). Extracellular vesicles as potential biomarkers for early detection and diagnosis of pancreatic cancer. *Biomedicines* 8:581. doi: 10.3390/biomedicines8120581

Yoon, C., Lu, J., Yi, B. C., Chang, K. K., Simon, M. C., Ryeom, S., et al. (2021). PI3K/Akt pathway and Nanog maintain cancer stem cells in sarcomas. *Oncogenesis* 10:12. doi: 10.1038/s41389-020-00300-z

Yu, S., Li, Y., Liao, Z., Wang, Z., Wang, Z., Li, Y., et al. (2020). Plasma extracellular vesicle long RNA profiling identifies a diagnostic signature for the detection of pancreatic ductal adenocarcinoma. *Gut* 69, 540–550. doi: 10.1136/gutjnl-2019-318860

Zhao, S., Fung-Leung, W. P., Bittner, A., Ngo, K., and Liu, X. (2014). Comparison of RNA-Seq and microarray in transcriptome profiling of activated T cells. *PLoS One* 9:e78644. doi: 10.1371/journal.pone.0078644

**Conflict of Interest:** The authors declare that the research was conducted in the absence of any commercial or financial relationships that could be construed as a potential conflict of interest.

frontiers in Molecular Biosciences

MINI REVIEW
published: 07 May 2021
doi: 10.3389/fmolb.2021.643824

# Oxaliplatin-Induced Neuropathy: Genetic and Epigenetic Profile to Better Understand How to Ameliorate This Side Effect

*Jacopo Junio Valerio Branca[1], Donatello Carrino[1], Massimo Gulisano[1], Carla Ghelardini[2], Lorenzo Di Cesare Mannelli[2†] and Alessandra Pacini[1*†]*

[1] Histology and Anatomy Section, Department of Experimental and Clinical Medicine, University of Firenze, Firenze, Italy, [2] Pharmacology and Toxicology Section, Department of Neuroscience, Psychology, Drug Research and Child Health (NEUROFARBA), University of Firenze, Firenze, Italy

OPEN ACCESS

**Edited by:**
Md. Asaduzzaman Khan,
Southwest Medical University, China

**Reviewed by:**
Snehal M. Gaikwad,
National Cancer Institute,
United States
Yu-Hui Liu,
Third Military Medical University,
China

***Correspondence:**
Alessandra Pacini
alessandra.pacini@unifi.it

† These authors have contributed equally to this work and share senior authorship

**Specialty section:**
This article was submitted to Molecular Diagnostics and Therapeutics, a section of the journal Frontiers in Molecular Biosciences

**Received:** 18 December 2020
**Accepted:** 24 February 2021
**Published:** 07 May 2021

**Citation:**
Branca JJV, Carrino D, Gulisano M, Ghelardini C, Di Cesare Mannelli L and Pacini A (2021) Oxaliplatin-Induced Neuropathy: Genetic and Epigenetic Profile to Better Understand How to Ameliorate This Side Effect. Front. Mol. Biosci. 8:643824. doi: 10.3389/fmolb.2021.643824

In the most recent decades, oxaliplatin has been used as a chemotherapeutic agent for colorectal cancer and other malignancies as well. Oxaliplatin interferes with tumor growth predominantly exerting its action in DNA synthesis inhibition by the formation of DNA-platinum adducts that, in turn, leads to cancer cell death. On the other hand, unfortunately, this interaction leads to a plethora of systemic side effects, including those affecting the peripheral and central nervous system. Oxaliplatin therapy has been associated with acute and chronic neuropathic pain that induces physicians to reduce the dose of medication or discontinue treatment. Recently, the capability of oxaliplatin to alter the genetic and epigenetic profiles of the nervous cells has been documented, and the understanding of gene expression and transcriptional changes may help to find new putative treatments for neuropathy. The present article is aimed to review the effects of oxaliplatin on genetic and epigenetic mechanisms to better understand how to ameliorate neuropathic pain in order to enhance the anti-cancer potential and improve patients' quality of life.

**Keywords: oxaliplatin, neuropathic pain, glial cells, genetic mechanisms, epigenetic mechanisms**

## INTRODUCTION

### The Anti-cancer Features of Oxaliplatin

In the last decades, despite early cancer diagnosis, cancer deaths rapidly increased (Kanavos, 2006). Among the most common cancer types, colorectal cancer is one of the most diffuse cancer in both genders worldwide. Indeed, it has been recently reported that more than 1.8 million new cases and about 0.9 million deaths were estimated in 2018, ranking the colorectal cancer third in terms of incidence and second in terms of mortality in both male and female (Bray et al., 2018). Therefore, the researchers are making great efforts in order to counteract this debilitating and mortal health concern.

The platinum-derived drugs are widely used as chemotherapeutic agents and, among these compounds, cisplatin was the first one patented (Rosenberg et al., 1969). However, the poor effects of cisplatin against different cancer types (Taylor and Filby, 2017), its side effects (Lokich, 2001),

and the cancer resistance (Stordal and Davey, 2007) limited its use in chemotherapy leading physicians and researchers to explore new paths in order to improve the quality of life of patients.

Within this framework, new platinum analogs have been developed. Although other new platinum-derived drugs are under study (Johnstone et al., 2016; Dai and Wang, 2020), nowadays, carboplatin and oxaliplatin are the most widely used in clinical practice (Fischer and Ganellin, 2006).

Oxaliplatin, a third generation 1,2-diaminocyclohexane platinum compound patented in 1976, shows high efficacy against colorectal cancer (Wiseman et al., 1999). Recently, its efficacy has been found also in other cancer types including lung (Raez et al., 2010), gastric (Cunningham, 2006; Zhang et al., 2019), ovarian, and prostate cancer (Zhou et al., 2017).

The primary anti-cancer effect exerted by oxaliplatin therapy, as well as for the other platinum-derived drugs, is due to DNA damage. Indeed, it has been largely demonstrated that oxaliplatin forms intra-strand crosslinks with DNA, as the main mechanism for the induction of DNA lesions, inhibiting the proliferation of neoplastic cells (Culy et al., 2000). Furthermore, another intriguing anti-cancer effect of oxaliplatin was discovered by Tesniere and colleagues, demonstrating that oxaliplatin-treated CT26 colorectal cancer cells were able to release immunogenic signals that trigger an immune response, thus leading to an enhanced anti-cancer effect promoted by the immune system (Tesniere et al., 2010).

With respect to oxaliplatin pharmacokinetics, it has been reported that the platinum compound can interact with and bind to plasma proteins. In patients affected by cancer, the platinum-plasma protein binding increased around 70% after 2 h of infusion, growing up to 95% 5 days after infusion. However, it can be considered that the maximum platinum concentration is achieved during the first cycle of oxaliplatin administration and no accumulation was reported after single or multiple doses, except for erythrocytes where an accumulation has been found (Culy et al., 2000; Lévi et al., 2000). On the other hand, the main excretion of platinum products occurs mainly by the renal route, consisting in about 50% after 72 h, whereas the excretion by defecation is very low, ranging about 2% after 5 days (Culy et al., 2000).

However, even if the antineoplastic efficacy of oxaliplatin is overt, it also unfortunately generates a series of undesired side effects.

## The Side Effects of Oxaliplatin Administration

Among the DNA-interfering chemotherapeutic agents, platinum-derived drugs can potentially interact with normal cells with high proliferating turnover, thus altering their physiological features and leading to adverse side effects (Oun et al., 2018).

Over the years, many researchers have highlighted the deleterious events in different organs and tissues resulting from oxaliplatin treatment. For instance, it has been shown that oxaliplatin exhibits irritant properties that may lead to the occurrence of vesicant lesions (Foo et al., 2003; Kennedy et al., 2003; Kretzschmar et al., 2003).

In contrast to cisplatin, oxaliplatin is not nephrotoxic or ototoxic, but it produces various adverse effects, the main one is neurotoxicity. Oxaliplatin-dependent neurotoxicity can be acute and/or chronic, but both types give rise to neuropathic pain (Sałat, 2020). The acute type elicits a transient neuropathy that occurs in 90% of patients within a few hours of chemotherapy administration, lasts for a few days, and recurs with subsequent administrations. The main signs and symptoms of acute neuropathy are exacerbated by cold and consist of dysesthesia and paresthesia of the hands and feet. Motor symptoms may also occur, such as tetanic spasms, fasciculations, and prolonged muscular contractions. It has been demonstrated that acute neuropathy is caused by a $Na_v$ channel activation that transiently induces nerve hyperexcitability (Gebremedhn et al., 2018). In 70% of cases, prolonged exposure to oxaliplatin induces a severe chronic peripheral neuropathy, with symptoms very similar to those of acute form that force patients to discontinue the treatment (Miaskowski et al., 2017). Among all, the most relevant mechanism that trigger neuropathic pain (extensively reviewed by Kanat et al., 2017), is the binding of oxaliplatin to the mitochondrial DNA of sensory neurons, thus causing their death. This oxaliplatin-dependent neuronal loss also accounts for the persistence of symptoms for up to years following treatment discontinuation (Kokotis et al., 2016). The loss of sensory neurons is further confirmed by alterations in taste and smell frequently observed in patients who underwent oxaliplatin treatment (reviewed in Gamper et al., 2012). Other relevant side effects consist of fever (Saif, 2007), thrombocytopenia (Jardim et al., 2012), anemia (Cobo et al., 2007), nausea (Fleishman et al., 2012), liver function abnormalities (Lu et al., 2019), and gastro-intestinal dysfunction (Boussios et al., 2012).

This latter side effects, such as diarrhea or constipation, might be ascribed to enteric neuronal loss. In this regard, McQuade and colleagues demonstrated that the use of antioxidant molecules, such as the novel BPF-15, ameliorated the oxidative stress-dependent gastrointestinal symptoms (McQuade et al., 2016, 2018). Also, oxaliplatin can induce cognitive impairment. This debilitating condition was observed in a rat model (Fardell et al., 2012) and in patients who experienced an oxaliplatin-dependent impairment of verbal memory (Cruzado et al., 2014).

Another side effect of oxaliplatin treatment was observed by Okamoto in a Japanese patient who reported the Lhermitte's sign, a sudden sensation resembling an electric shock that passes down the back of the neck and into the spine and may then radiate out into the arms and legs. This symptom mainly occurs in multiple sclerosis and is believed to be due to a demyelination of the posterior columns of the spinal cord induced by chemotherapy (Okamoto et al., 2020).

Finally, in a very recent study a high increase of serum neurofilament light chain level was observed in patients who referred an oxaliplatin-dependent neuropathic pain. The serological increase of neurofilament light chain has been previously reported in patient with Alzheimer's disease, frontotemporal dementia, and multiple sclerosis. However, even if the authors concluded that a major part of the serum neurofilament light chain originates from the peripheral nervous

system, it is not excluded that something has happened in the CNS, but more insights are needed (Kim et al., 2020).

## OXALIPLATIN-INDUCED NEUROPATHY

Many authors have underlined the main effects exerted by oxaliplatin (**Table 1**) and have evidenced that one of the main causes of the neuropathy onset is its accumulation inside the cells. Within the nervous system, oxaliplatin preferentially accumulates in those cells that express specific membrane transporters such as the multidrug and toxin extrusion proteins (MATEs), the organic anion-transporting polypeptides (OATPs), and the organic cation transporter (OCT) (Huang et al., 2020). The expression of OCT-type transporters by sensory neurons of the dorsal root ganglia (DRG) (Fujita et al., 2019) not only demonstrates the accumulation of the chemotherapy mainly in these cell type, but also that this event could trigger a peripheral neurotoxicity. These data were corroborated by other results demonstrating the oxaliplatin-dependent detrimental effect on DRG neurons causing a reduced volume of the neuronal soma and an increase in the number of multinucleated neuronal nuclei (Di Cesare Mannelli et al., 2017).

The OCT transporter is also expressed on the luminal surface of the blood-brain barrier (BBB) micro-vessel endothelial cells, the OCT role in transporting oxaliplatin inside the cells has been demonstrated (Lin et al., 2010). In this regard, recently it has been reported that in a rat brain endothelial cell line expressing OCT protein (Friedrich et al., 2003), oxaliplatin elicits a dislocation of the Zonula Occludens-1 (ZO-1), one of the tight junction proteins that contribute to constitute the BBB (Branca et al., 2018). The increased permeability of the BBB allows the chemotherapy agent to enter the brain parenchyma, affecting both the neuronal (Park et al., 2009) and glial compartment (Lee and Kim, 2020).

As for the effects of oxaliplatin on neurons, an increase in oxidative stress is the most remarkable event. *In vitro* experiments have demonstrated that oxaliplatin is able to increase the reactive oxygen species (ROS) and the superoxide anion levels as well as protein carbonylation (Di Cesare Mannelli et al., 2013b), thus suggesting that oxidative stress could be responsible for oxaliplatin-induced neuropathic pain.

*In vivo* analysis carried out on plasma, sciatic nerves, and lumbar portion of the spinal cord obtained from oxaliplatin-treated rats strengthened the role of oxidative stress in the onset of neuropathic pain (Di Cesare Mannelli et al., 2012).

Analysis of the signaling pathway that triggers neuropathy highlighted the involvement of activating transcription factor 3 (ATF3) protein. This protein is a member of the cAMP-responsive element binding protein family (Li et al., 2019) that, following the activation of the Toll Like receptors (TLRs), regulates a signaling cascade involved in the onset of neuropathy. Also, its expression has been found significatively increased in oxaliplatin-treated nerves and DRGs (Di Cesare Mannelli et al., 2013a) that should be achieved by cAMP-increased levels, as reported by *in vitro* analysis on oxaliplatin-treated neuronal cells (Morucci et al., 2015). Moreover, an oxaliplatin-dependent alteration of the cell viability and of the expression of the growth associated protein 43 (GAP-43), a well-known marker of axon development (Morucci et al., 2015), was also reported.

With respect to the glial compartment, neuropathic pain has been linked to changes in the gene expression and secretory profile of microglia that elicits a signaling cascade resulting in neuroinflammation (Ji et al., 2016).

As demonstrated by *in vitro* analysis both in human and murine cells, oxaliplatin induced an increase in pro-inflammatory marker expression such as clusters of differentiation 86 (CD86), and morphological changes shifting from resting to activating shape (Branca et al., 2015). These effects are in accordance with *ex vivo* experiments carried

**TABLE 1 |** Main signaling pathways involved in oxaliplatin-dependent alterations.

| | Effects | Literature |
|---|---|---|
| ABCs (ATP-binding cassettes) | Single nucleotide polymorphisms (e.g., rs717620, rs8187710, rs2231142 and rs1045642) inhibit the oxaliplatin efflux increasing its accumulation | Nichetti et al., 2019 |
| OCTs (organic cation transporters) | Epigenetic modification increases the oxaliplatin influx in resistant cells | Liu et al., 2016 |
| ROS (oxidative stress) | Overproduction/activation following mitochondrial impairment | Di Cesare Mannelli et al., 2012, 2013b, 2016; Massicot et al., 2013; De Monaco et al., 2014; Stankovic et al., 2020 |
| ATF3 (activating transcription factor 3) | Significant increase in the DRG neurons in oxaliplatin-treated rats | Di Cesare Mannelli et al., 2013a |
| cAMP | Increased production after oxaliplatin-treated SH-SY5Y | Morucci et al., 2015 |
| GAP-43 (growth associated protein 43) | Expression level down-regulation after oxaliplatin-treated SH-SY5Y | Morucci et al., 2015 |
| CD86 | Increased levels of protein expression after oxaliplatin-treated microglial cells | Branca et al., 2015 |
| CX3CL1 | Histone H4 acetylation in the *CX3CL1* promoter region induces the up-regulation of the cytokine | Huang et al., 2016 |
| GFAP (glial fibrillary acidic protein) | Cell number increases both in spinal cord (dorsal horn) and brain cortex | Di Cesare Mannelli et al., 2013a, 2015 |
| Iba1 (ionized calcium-binding adapter molecule 1) | Cell number increases both in spinal cord (dorsal horn) and brain cortex | Di Cesare Mannelli et al., 2013a, 2015 |
| Resting → Activating state | Morphological shift from ramified/resting to activating microglia | Branca et al., 2015 |

out in oxaliplatin-treated rats, showing an increase in the number of cells expressing the microglial marker Iba-1 (ionized calcium-binding adapter molecule 1) in the spinal cord as well as in the basal ganglia and "pain matrix" brain areas (Di Cesare Mannelli et al., 2013a).

The onset of microglia-dependent neuroinflammation also induces the recruitment of astrocytes. Indeed, it has been demonstrated that oxaliplatin treatment causes an increase in the expression levels of glial fibrillary acidic protein (GFAP) and a modification of astrocytic shape, both in the spinal cord and in some brain areas (Di Cesare Mannelli et al., 2015).

Microglia and astrocyte activation is strictly related to pain sensitivity since the selective inhibition of one or the other cellular type prevented pain development (Di Cesare Mannelli et al., 2014). On the other hand, an indiscriminate glial cell silencing impaired the neurorestorative mechanisms promoted by these cell types (Di Cesare Mannelli et al., 2014).

Another important target of oxaliplatin-dependent toxicity is the mitochondrion whose dysfunction leads to the generation of reactive oxygen species (ROS). Although the research on the mechanisms underlying mitochondrial toxicity and ROS generation are only beginning to be analyzed, some studies have fully demonstrated that the antioxidant properties of different molecules are able to mitigate the oxaliplatin-dependent neuropathy (Di Cesare Mannelli et al., 2016). These results suggest that ROS generation and mitochondrial impairment are early events in the oxaliplatin-triggered signaling pathway that results in the onset of neuropathy.

## GENETIC AND EPIGENETIC ROLE IN OXALIPLATIN-INDUCED NEUROPATHIC PAIN

Over the last 10 years research has highlighted a very important role of epigenetics in determining variations that induce lasting or permanent changes in neuronal function (Borrelli et al., 2008). Also, it is now evident that drug exposure leads to epigenomic changes that are the basis of the different individual responses to chemotherapy. Indeed, the focus is now centered on improving the chemotherapeutic efficacy of anticancer molecules through pharmacogenetic and pharmacoepigenetic approaches (Mohelnikova-Duchonova, 2014).

Pharmacogenetics, recently changed to the term pharmacogenomics, is the field of research that encompasses all genes in the genome that may determine drug response (Pirmohamed, 2001). Indeed, especially for what may concern drug resistance and chemotherapy, the study of genetic polymorphisms is essential to choose the optimal personalized therapeutic treatment, minimizing the side effects produced by chemotherapy (Lesko, 2007). On the other hand, epigenetic modifications can influence the drug response and a decisive role in personalized medicine is assigned to pharmacoepigenetics (Majchrzak-Celińska, 2017).

In view of these fascinating scenarios, it has been recently hypothesized that the pivotal role of single nucleotide polymorphisms (SNPs) affects the gene coding for oxaliplatin transporters. The alteration of the expression levels and the functioning of these transporters, in particular, the SNPs occurring in ATP-binding cassette (ABCs) transporters (such as rs717620, rs8187710, rs2231142, and rs1045642), causes an increase in the oxaliplatin concentration inside the cells (in particular, the DRG neurons) that may account for an higher risk to develop an oxaliplatin-dependent neuropathy as previously reported (Nichetti et al., 2019).

It has been reported that a prolonged and high oxaliplatin intracellular accumulation, induced ROS overproduction mediated by mitochondrial impairment (Massicot et al., 2013). Thus, even if specific transporter polymorphisms are not beneficial for patients that unfortunately do not correctly excrete oxaliplatin leading to its accumulation, the simultaneous use of antioxidant molecules during a chemotherapy regimen could help to retrieve and ameliorate the oxaliplatin-induced neuropathic pain (De Monaco et al., 2014; Stankovic et al., 2020).

However, there are many other elements that influence chemotherapeutic drug sensitivity, such as the glutathione S transferase P1 (GSTP1), involved in the inactivation of platinum-DNA adducts (Kweekel et al., 2005). For example, the 105Val allele variant at exon 5 of the GSTP1 gene confers a significantly decreased risk of developing severe oxaliplatin-related neuropathy (Lecomte et al., 2006; Chen et al., 2010, p. 201; McLeod et al., 2010; Hong et al., 2011).

Moreover, genetic polymorphisms play a key role also in adjuvant therapies where opioid drugs are used in order to ameliorate oxaliplatin-induced neuropathic pain (Wang, 2014).

Despite a clear correlation between oxaliplatin-based neuropathy and individual genetic polymorphisms, pharmacotherapy based on genetic profile is not yet routinely introduced, perhaps because different polymorphisms can correlate and a wide range of genomic analysis in a larger population is needed (Peng et al., 2013; Ruzzo et al., 2015).

In the attempt to find the molecular basis for neuropathy induction and maintenance, attention has recently been turned to epigenetic mechanisms. Epigenetic-dependent alterations of gene expression are independent of DNA sequence alterations, but they are heritable and reversible. Recently, environmental stimuli have been observed to induce long-term epigenetic modifications of the gene expression profile that characterizes neuropathic pain (extensively reviewed by Penas and Navarro, 2018).

If SNPs represent a risk of developing neuropathy, epigenetic regulation of the ABC transporters expression levels may lead to a decreased risk. Indeed, these transporters regulate the oxaliplatin efflux from cells (Sparreboom et al., 2003), thus reducing its accumulation (Huo et al., 2010).

A similar fascinating result in this field was obtained by the epigenetic modification of the OCT2 transporter both *in vitro* and in xenografts. Some authors have promoted the epigenetic expression of this oxaliplatin transporter in renal cancer cells in order to increase the oxaliplatin sensitization of these cells (Liu et al., 2016). It could be argued that the OCT2 epigenetic modification could induce an oxaliplatin accumulation also into other cell compartments, including the brain, thus leading to the induction of neuropathy.

Epigenetic modifications of glial cells have also been shown to play a role in neuropathic pain. Astrocytic DNA methylation and histone modifications, two of the major epigenetic modifications, induce the production of pro-inflammatory cytokines triggering a microglia neuroinflammatory activation that, in turn, contributes to the development of neuropathy (McMahon et al., 2005; Descalzi et al., 2015; Machelska and Celik, 2016).

It has also been demonstrated that oxaliplatin treatment significantly increased the histone H4 acetylation in the *CX3CL1* promoter region in spinal cord neurons (Huang et al., 2016), inducing the up-regulation of this cytokine. *In vivo* studies have demonstrated involvement in the induction of central sensitization and acute pain behavior after oxaliplatin administration (Huang et al., 2016; Zhang et al., 2018). More recently, it has been evidenced that oxaliplatin treatment is able to increase the expression of 10–11 translocation methylcytosine dioxygenase 1 (TET1), a well-known enzyme involved in DNA demethylation. The researchers found that TET1 up-regulation indirectly acts on Homeobox A6 protein (*HOX-A6*) expression in neurons, thus becoming a pivotal target in ameliorating oxaliplatin-induced neuropathy (Deng et al., 2020).

## CONCLUDING REMARKS

The oxaliplatin-induced neuropathic pain is a deleterious side effect for patient healthcare that could lead to therapy interruption. In recent years many efforts have been made in order to both increase the oxaliplatin anti-cancer effects and ameliorate neuropathy. Hopefully, genetic and epigenetic information can help physicians toward a personalized therapeutic strategy. However, many other analyses of pharmacogenetics and epigenetics should be performed in order to corroborate and obtain useful data to seriously improve the benefit from chemotherapeutic treatment.

## AUTHOR CONTRIBUTIONS

JB, LD, and AP conceived the structure of the manuscript and drafted the manuscript. DC, MG, and CG critically revised the manuscript. All authors contributed to the article and approved the submitted version.

## ACKNOWLEDGMENTS

LD would like to acknowledge support from the Innovative Medicines Initiative 2 Joint Undertaking under grant agreement No. 821528 (NeuroDeRisk: Neurotoxicity De-Risking in Preclinical Drug Discovery). This Joint Undertaking is sustained by the European Union's Horizon 2020 Research and Innovation Programme and the European Federation of Pharmaceutical Industries and Associations (EFPIA).

## REFERENCES

Borrelli, E., Nestler, E. J., Allis, C. D., and Sassone-Corsi, P. (2008). Decoding the epigenetic language of neuronal plasticity. *Neuron* 60, 961–974. doi: 10.1016/j.neuron.2008.10.012

Boussios, S., Pentheroudakis, G., Katsanos, K., and Pavlidis, N. (2012). Systemic treatment-induced gastrointestinal toxicity: incidence, clinical presentation and management. *Nausea Vomit.* 25, 106–118.

Branca, J. J. V., Maresca, M., Morucci, G., Becatti, M., Paternostro, F., Gulisano, M., et al. (2018). Oxaliplatin-induced blood brain barrier loosening: a new point of view on chemotherapy-induced neurotoxicity. *Oncotarget* 9, 23426–23438. doi: 10.18632/oncotarget.25193

Branca, J. J. V., Morucci, G., Malentacchi, F., Gelmini, S., Ruggiero, M., and Pacini, S. (2015). Effects of oxaliplatin and oleic acid Gc-protein-derived macrophage-activating factor on murine and human microglia: effects of oxaliplatin and GcMAF on microglia. *J. Neurosci. Res.* 93, 1364–1377. doi: 10.1002/jnr.23588

Bray, F., Ferlay, J., Soerjomataram, I., Siegel, R. L., Torre, L. A., and Jemal, A. (2018). Global cancer statistics 2018: GLOBOCAN estimates of incidence and mortality worldwide for 36 cancers in 185 countries. *CA Cancer J. Clin.* 68, 394–424. doi: 10.3322/caac.21492

Chen, Y.-C., Tzeng, C.-H., Chen, P.-M., Lin, J.-K., Lin, T.-C., Chen, W.-S., et al. (2010). Influence of GSTP1 I105V polymorphism on cumulative neuropathy and outcome of FOLFOX-4 treatment in Asian patients with colorectal carcinoma. *Cancer Sci.* 101, 530–535. doi: 10.1111/j.1349-7006.2009.01418.x

Cobo, F., Celis, G. D., Pereira, A., Latorre, X., Pujadas, J., and Albiol, S. (2007). Oxaliplatin-induced immune hemolytic anemia: a case report and review of the literature. *Anticancer. Drugs* 18, 973–976.

Cruzado, J. A., López-Santiago, S., Martínez-Marín, V., José-Moreno, G., Custodio, A. B., and Feliu, J. (2014). Longitudinal study of cognitive dysfunctions induced by adjuvant chemotherapy in colon cancer patients. *Support Care Cancer* 22, 1815–1823. doi: 10.1007/s00520-014-2147-x

Culy, C. R., Clemett, D., and Wiseman, L. R. (2000). Oxaliplatin: a review of its pharmacological properties and clinical efficacy in metastatic colorectal cancer and its potential in other malignancies. *Drugs* 60, 895–924. doi: 10.2165/00003495-200060040-200060045

Cunningham, D. (2006). Is oxaliplatin the optimal platinum agent in gastric cancer? *Eur. J. Cancer Suppl.* 4, 10–13. doi: 10.1016/S1359-6349(06)70003-70009

Dai, Z., and Wang, Z. (2020). Photoactivatable platinum-based anticancer drugs: mode of photoactivation and mechanism of action. *Molecules* 25: 5167.

De Monaco, A., Valente, D., Di Paolo, M., Troisi, A., D'Orta, A., and Del Buono, A. (2014). Oxaliplatin-based therapy: strategies to prevent or minimize neurotoxicity. *World Cancer Res. J.* 1:e232.

Deng, J., Ding, H., Long, J., Lin, S., Liu, M., Zhang, X., et al. (2020). Oxaliplatin-induced neuropathic pain involves HOXA6 via a TET1 -dependent demethylation of the SOX10 promoter. *Int. J. Cancer* 147, 2503–2514. doi: 10.1002/ijc.33106

Descalzi, G., Ikegami, D., Ushijima, T., Nestler, E. J., Zachariou, V., and Narita, M. (2015). Epigenetic mechanisms of chronic pain. *Trends Neurosci.* 38, 237–246. doi: 10.1016/j.tins.2015.02.001

Di Cesare Mannelli, L., Pacini, A., Bonaccini, L., Zanardelli, M., Mello, T., et al. (2013a). Morphologic features and glial activation in rat oxaliplatin-dependent neuropathic pain. *J. Pain* 14, 1585–1600. doi: 10.1016/j.jpain.2013.08.002

Di Cesare Mannelli, L., Zanardelli, M., Failli, P., and Ghelardini, C. (2013b). Oxaliplatin-induced oxidative stress in nervous system-derived cellular models: could it correlate with in vivo neuropathy? *Free Radical Biol. Med.* 61, 143–150. doi: 10.1016/j.freeradbiomed.2013.03.019

Di Cesare Mannelli, L., Pacini, A., Corti, F., Boccella, S., Luongo, L., et al. (2015). Antineuropathic profile of N-Palmitoylethanolamine in a rat model of oxaliplatin-induced neurotoxicity. *PLoS One* 10:e0128080. doi: 10.1371/journal.pone.0128080

Di Cesare Mannelli, L., Pacini, A., Micheli, L., Femia, A. P., Maresca, M., et al. (2017). Astragali radix: could it be an adjuvant for oxaliplatin-induced neuropathy? *Sci. Rep.* 7:42021. doi: 10.1038/srep42021

Di Cesare Mannelli, L., Pacini, A., Micheli, L., Tani, A., Zanardelli, M., et al. (2014). Glial role in oxaliplatin-induced neuropathic pain. *Exp. Neurol.* 261, 22–33.

Di Cesare Mannelli, L., Zanardelli, M., Failli, P., and Ghelardini, C. (2012). Oxaliplatin-Induced neuropathy: oxidative stress as pathological mechanism. protective effect of silibinin. *J. Pain* 13, 276–284. doi: 10.1016/j.jpain.2011.11.009

Di Cesare Mannelli, L., Zanardelli, M., Landini, I., Pacini, A., Ghelardini, C., et al. (2016). Effect of the SOD mimetic MnL4 on in vitro and in vivo oxaliplatin toxicity: possible aid in chemotherapy induced neuropathy. *Free Radical Biol. Med.* 93, 67–76. doi: 10.1016/j.freeradbiomed.2016.01.023

Fardell, J. E., Vardy, J., Shah, J. D., and Johnston, I. N. (2012). Cognitive impairments caused by oxaliplatin and 5-fluorouracil chemotherapy are ameliorated by physical activity. *Psychopharmacology* 220, 183–193. doi: 10.1007/s00213-011-2466-2462

Fischer, J., and Ganellin, C. R. (2006). *Analogue-based Drug Discovery*. Weinheim: Wiley-VCH.

Fleishman, S. B., Mahajan, D., Rosenwald, V., Nugent, A. V., and Mirzoyev, T. (2012). Prevalence of delayed nausea and/or vomiting in patients treated with oxaliplatin-based regimens for colorectal Cancer. *JOP* 8, 136–140. doi: 10.1200/JOP.2010.000151

Foo, K. F., Michael, M., Toner, G., and Zalcberg, J. (2003). A case report of oxaliplatin extravasation. *Ann. Oncol.* 14, 961–962. doi: 10.1093/annonc/mdg252

Friedrich, A., Prasad, P. D., Freyer, D., Ganapathy, V., and Brust, P. (2003). Molecular cloning and functional characterization of the OCTN2 transporter at the RBE4 cells, an in vitro model of the blood–brain barrier. *Brain Res.* 968, 69–79.

Fujita, S., Hirota, T., Sakiyama, R., Baba, M., and Ieiri, I. (2019). Identification of drug transporters contributing to oxaliplatin-induced peripheral neuropathy. *J. Neurochem.* 148, 373–385. doi: 10.1111/jnc.14607

Gamper, E.-M., Zabernigg, A., Wintner, L. M., Giesinger, J. M., Oberguggenberger, A., Kemmler, G., et al. (2012). Coming to your senses: detecting taste and smell alterations in chemotherapy patients. a systematic review. *J. Pain Symptom Manag.* 44, 880–895. doi: 10.1016/j.jpainsymman.2011.11.011

Gebremedhn, E. G., Shortland, P. J., and Mahns, D. A. (2018). The incidence of acute oxaliplatin-induced neuropathy and its impact on treatment in the first cycle: a systematic review. *BMC Cancer* 18:410. doi: 10.1186/s12885-018-4185-4180

Hong, J., Han, S. W., Ham, H. S., Kim, T. Y., Choi, I. S., Kim, B.-S., et al. (2011). Phase II study of biweekly S-1 and oxaliplatin combination chemotherapy in metastatic colorectal cancer and pharmacogenetic analysis. *Cancer Chemother. Pharmacol.* 67, 1323–1331. doi: 10.1007/s00280-010-1425-1427

Huang, K. M., Leblanc, A. F., Uddin, M. E., Kim, J. Y., Chen, M., Eisenmann, E. D., et al. (2020). Neuronal uptake transporters contribute to oxaliplatin neurotoxicity in mice. *J. Clin. Investigat.* 130, 4601–4606. doi: 10.1172/JCI136796

Huang, Z.-Z., Li, D., Ou-Yang, H.-D., Liu, C.-C., Liu, X.-G., Ma, C., et al. (2016). Cerebrospinal fluid oxaliplatin contributes to the acute pain induced by systemic administration of oxaliplatin. *Anesthesiology* 124, 1109–1121. doi: 10.1097/ALN.0000000000001084

Huo, H., Magro, P. G., Pietsch, E. C., Patel, B. B., and Scotto, K. W. (2010). Histone methyltransferase MLL1 regulates MDR1 transcription and chemoresistance. *Cancer Res.* 70, 8726–8735.

Jardim, D. L., Rodrigues, C. A., Novis, Y. A. S., Rocha, V. G., and Hoff, P. M. (2012). Oxaliplatin-related thrombocytopenia. *Ann. Oncol.* 23, 1937–1942. doi: 10.1093/annonc/mds074

Ji, R. R., Chamessian, A., and Zhang, Y. Q. (2016). Pain regulation by non-neuronal cells and inflammation. *Science* 354, 572–577. doi: 10.1126/science.aaf8924

Johnstone, T. C., Suntharalingam, K., and Lippard, S. J. (2016). The next generation of platinum drugs: targeted Pt(II) agents, nanoparticle delivery, and Pt(IV) prodrugs. *Chem. Rev.* 116, 3436–3486.

Kanat, O., Ertas, H., and Caner, B. (2017). Platinum-induced neurotoxicity: a review of possible mechanisms. *WJCO* 8, 329–335. doi: 10.5306/wjco.v8.i4.329

Kanavos, P. (2006). The rising burden of cancer in the developing world. *Ann. Oncol.* 17:9.

Kennedy, J. G., Donahue, J. P., Hoang, B., and Boland, P. J. (2003). Vesicant characteristics of oxapliplatin following antecubital extravasation. *Clin. Oncol.* 15, 237–239. doi: 10.1016/S0936-6555(02)00338-332

Kim, S.-H., Choi, M. K., Park, N. Y., Hyun, J.-W., Lee, M. Y., Kim, H. J., et al. (2020). Serum neurofilament light chain levels as a biomarker of neuroaxonal injury and severity of oxaliplatin-induced peripheral neuropathy. *Sci. Rep.* 10:7995. doi: 10.1038/s41598-020-64511-64515

Kokotis, P., Schmelz, M., Kostouros, E., Karandreas, N., and Dimopoulos, M.-A. (2016). Oxaliplatin-Induced neuropathy: a long-term clinical and neurophysiologic follow-up study. *Clin. Colorectal Cancer* 15, e133–e140. doi: 10.1016/j.clcc.2016.02.009

Kretzschmar, A., Pink, D., Thuss-Patience, P., Dörken, B., Reichart, P., and Eckert, R. (2003). Extravasations of oxaliplatin. *JCO* 21, 4068–4069. doi: 10.1200/JCO.2003.99.095

Kweekel, D., Gelderblom, H., and Guchelaar, H. (2005). Pharmacology of oxaliplatin and the use of pharmacogenomics to individualize therapy. *Cancer Treat. Rev.* 31, 90–105. doi: 10.1016/j.ctrv.2004.12.006

Lecomte, T., Landi, B., Beaune, P., Laurent-Puig, P., and Loriot, M. A. (2006). Glutathione S-Transferase P1 polymorphism (Ile105Val) predicts cumulative neuropathy in patients receiving oxaliplatin-based chemotherapy. *Clin. Cancer Res.* 12, 3050–3056.

Lee, J. H., and Kim, W. (2020). The role of satellite glial cells, astrocytes, and microglia in oxaliplatin-induced neuropathic pain. *Biomedicines* 8:324. doi: 10.3390/biomedicines8090324

Lesko, L. J. (2007). Personalized medicine: elusive dream or imminent reality? *Clin. Pharmacol. Ther.* 81, 807–816. doi: 10.1038/sj.clpt.6100204

Lévi, F., Metzger, G., Massari, C., and Milano, G. (2000). Oxaliplatin: pharmacokinetics and chronopharmacological aspects. *Clin. Pharmacokinet* 38, 1–21. doi: 10.2165/00003088-200038010-200038011

Li, X., Zang, S., Cheng, H., Li, J., and Huang, A. (2019). Overexpression of activating transcription factor 3 exerts suppressive effects in HepG2 cells. *Mol. Med. Rep.* 19, 869–876.

Lin, C. J., Tai, Y., Huang, M.-T., Tsai, Y.-F., Hsu, H.-J., Tzen, K.-Y., et al. (2010). Cellular localization of the organic cation transporters, OCT1 and OCT2, in brain microvessel endothelial cells and its implication for MPTP transport across the blood-brain barrier and MPTP-induced dopaminergic toxicity in rodents: OCT-mediated transport of MPTP across the BBB in rodents. *J. Neurochem.* 114, 717–727. doi: 10.1111/j.1471-4159.2010.06801.x

Liu, Y., Zheng, X., Yu, Q., Wang, H., Tan, F., Zhu, Q., et al. (2016). Epigenetic activation of the drug transporter OCT2 sensitizes renal cell carcinoma to oxaliplatin. *Sci. Transl. Med.* 8:348ra97. doi: 10.1126/scitranslmed.aaf3124

Lokich, J. (2001). What is the "Best" platinum: cisplatin, carboplatin, or oxaliplatin? *Cancer Investigat.* 19, 756–760. doi: 10.1081/CNV-100106152

Lu, Y., Lin, Y., Huang, X., Wu, S., Wei, J., and Yang, C. (2019). Oxaliplatin aggravates hepatic oxidative stress, inflammation and fibrosis in a non-alcoholic fatty liver disease mouse model. *Int. J. Mol. Med.* 43, 2398–2408. doi: 10.3892/ijmm.2019.4154

Machelska, H., and Celik, M. Ö (2016). Recent advances in understanding neuropathic pain: glia, sex differences, and epigenetics. *F1000Res* 5:2743. doi: 10.12688/f1000research.9621.1

Majchrzak-Celińska, A. (2017). Pharmacoepigenetics: an element of personalized therapy? *Expert Opin. Drug Metab. Toxicol.* 13, 387–398. doi: 10.1080/17425255.2017.1260546

Massicot, F., Hache, G., David, L., Chen, D., Leuxe, C., Garnier-Legrand, L., et al. (2013). P2X7 cell death receptor activation and mitochondrial impairment in oxaliplatin-induced apoptosis and neuronal injury: cellular mechanisms and in vivo approach. *PLoS One* 8:e66830. doi: 10.1371/journal.pone.0066830

McLeod, H. L., Sargent, D. J., Marsh, S., Green, E. M., King, C. R., Fuchs, C. S., et al. (2010). Pharmacogenetic predictors of adverse events and response to chemotherapy in metastatic colorectal cancer: results from north american gastrointestinal intergroup trial N9741. *JCO* 28, 3227–3233. doi: 10.1200/JCO.2009.21.7943

McMahon, S. B., Cafferty, W. B. J., and Marchand, F. (2005). Immune and glial cell factors as pain mediators and modulators. *Exp. Neurol.* 192, 444–462. doi: 10.1016/j.expneurol.2004.11.001

McQuade, R. M., Carbone, S. E., Stojanovska, V., Rahman, A., Gwynne, R. M., Robinson, A. M., et al. (2016). Role of oxidative stress in oxaliplatin-induced enteric neuropathy and colonic dysmotility in mice. *Br. J. Pharmacol.* 173, 3502–3521. doi: 10.1111/bph.13646

McQuade, R. M., Stojanovska, V., Stavely, R., Timpani, C., Petersen, A. C., Abalo, R., et al. (2018). Oxaliplatin-induced enteric neuronal loss and intestinal dysfunction is prevented by co-treatment with BGP-15: BGP-15 prevents

oxaliplatin-induced side effects. *Br. J. Pharmacol.* 175, 656–677. doi: 10.1111/bph.14114

Miaskowski, C., Mastick, J., Paul, S. M., Topp, K., Smoot, B., Abrams, G., et al. (2017). Chemotherapy-Induced neuropathy in Cancer survivors. *J. Pain Symptom Manage* 54, 204–218.e2. doi: 10.1016/j.jpainsymman.2016.12.342

Mohelnikova-Duchonova, B. (2014). FOLFOX/FOLFIRI pharmacogenetics: the call for a personalized approach in colorectal cancer therapy. *WJG* 20:10316. doi: 10.3748/wjg.v20.i30.10316

Morucci, G., Branca, J. J. V., Gulisano, M., Ruggiero, M., Paternostro, F., Pacini, A., et al. (2015). Gc-protein-derived macrophage activating factor counteracts the neuronal damage induced by oxaliplatin. *Anti-Cancer Drugs* 26, 197–209. doi: 10.1097/CAD.0000000000000177

Nichetti, F., Falvella, F. S., Miceli, R., Cheli, S., Gaetano, R., Fucà, G., et al. (2019). Is a pharmacogenomic panel useful to estimate the risk of oxaliplatin-related neurotoxicity in colorectal cancer patients? *Pharmacogenomics J.* 19, 465–472. doi: 10.1038/s41397-019-0078-70

Okamoto, T., Takagi, K., and Fukuda, K. (2020). Oxaliplatin-Induced lhermitte's sign in gastric Cancer. *Case Rep. Oncol. Med.* 2020:8826657. doi: 10.1155/2020/8826657

Oun, R., Moussa, Y. E., and Wheate, N. J. (2018). The side effects of platinum-based chemotherapy drugs: a review for chemists. *Dalton Trans.* 47, 6645–6653. doi: 10.1039/C8DT00838H

Park, S. B., Lin, C. S. Y., Krishnan, A. V., Goldstein, D., Friedlander, M. L., and Kiernan, M. C. (2009). Oxaliplatin-induced neurotoxicity: changes in axonal excitability precede development of neuropathy. *Brain* 132, 2712–2723. doi: 10.1093/brain/awp219

Penas, C., and Navarro, X. (2018). Epigenetic modifications associated to neuroinflammation and neuropathic pain after neural trauma. *Front. Cell. Neurosci.* 12:158. doi: 10.3389/fncel.2018.00158

Peng, Z., Wang, Q., Gao, J., Ji, Z., Yuan, J., Tian, Y., et al. (2013). Association between GSTP1 Ile105Val polymorphism and oxaliplatin-induced neuropathy: a systematic review and meta-analysis. *Cancer Chemother. Pharmacol.* 72, 305–314. doi: 10.1007/s00280-013-2194-x

Pirmohamed, M. (2001). Pharmacogenetics and pharmacogenomics. *Br. J. Clin. Pharmacol.* 52, 345–347. doi: 10.1046/j.0306-5251.2001.01498.x

Raez, L. E., Kobina, S., and Santos, E. S. (2010). Oxaliplatin in first-line therapy for advanced non–small-cell lung Cancer. *Clin. Lung Cancer* 11, 18–24. doi: 10.3816/CLC.2010.n.003

Rosenberg, B., VanCamp, L., Trosko, J. E., and Mansour, V. H. (1969). Platinum compounds: a new class of potent antitumour agents. *Nature* 222, 385–386. doi: 10.1038/222385a0

Ruzzo, A., Graziano, F., Galli, F., Giacomini, E., Floriani, I., Galli, F., et al. (2015). Genetic markers for toxicity of adjuvant oxaliplatin and fluoropyrimidines in the phase III TOSCA trial in high-risk colon cancer patients. *Sci. Rep.* 4:6828. doi: 10.1038/srep06828

Saif, M. W. (2007). Fever as the only manifestation of hypersensitivity reactions associated with oxaliplatin in a patient with colorectal Cancer oxaliplatin-induced hypersensitivity reaction. *WJG* 13:5277. doi: 10.3748/wjg.v13.i39.5277

Sałat, K. (2020). Chemotherapy-induced peripheral neuropathy—part 2: focus on the prevention of oxaliplatin-induced neurotoxicity. *Pharmacol. Rep.* 72, 508–527. doi: 10.1007/s43440-020-00106-101

Sparreboom, A., Danesi, R., Ando, Y., Chan, J., and Figg, W. D. (2003). Pharmacogenomics of ABC transporters and its role in cancer chemotherapy. *Drug Resist. Update* 6, 71–84. doi: 10.1016/S1368-7646(03)00005-0

Stankovic, J. S. K., Selakovic, D., Mihailovic, V., and Rosic, G. (2020). Antioxidant supplementation in the treatment of neurotoxicity induced by platinum-based chemotherapeutics—a review. *Int. J. Mol. Sci.* 21:7753.

Stordal, B., and Davey, M. (2007). Understanding cisplatin resistance using cellular models. *TBMB* 59, 696–699. doi: 10.1080/15216540701636287

Taylor, M., and Filby, A. (2017). Health impact analysis of cisplatin, carboplatin and oxaliplatin. *Johnson Matthey Technol. Rev.* 61, 32–39.

Tesniere, A., Schlemmer, F., Boige, V., Kepp, O., Martins, I., Ghiringhelli, F., et al. (2010). Immunogenic death of colon cancer cells treated with oxaliplatin. *Oncogene* 29, 482–491. doi: 10.1038/onc.2009.356

Wang, W. S. (2014). Advances in the management of oxaliplatin-induced neuropathy: focus on glutamine and using pharmacogenomics to predict the effectiveness of opioid drugs. *J. Cancer Res. Pract.* 1, 175–185. doi: 10.6323/JCRP.2014.1.3.01

Wiseman, L. R., Adkins, J. C., Plosker, G. L., and Goa, K. L. (1999). Oxaliplatin: a review of its use in the management of metastatic colorectal Cancer. *Drugs Aging* 14, 459–475. doi: 10.2165/00002512-199914060-19991 4066

Zhang, F., Zhang, Y., Jia, Z., Wu, H., and Gu, K. (2019). Oxaliplatin-Based regimen is superior to cisplatin-based regimen in tumour remission as first-line chemotherapy for advanced gastric Cancer: a meta-analysis. *J. Cancer* 10, 1923–1929. doi: 10.7150/jca.28896

Zhang, M., Zhi, Y., Xie, H., Li, P., Jiao, D., He, J., et al. (2018). The role of chemokine CX3CL1 in the anterior cingulate cortex in a rat model of chronic pathological pain. *Int J. Clin. Exp. Med.* 11, 11988–11994.

Zhou, J., Yang, T., Liu, L., and Lu, B. (2017). Chemotherapy oxaliplatin sensitizes prostate cancer to immune checkpoint blockade therapies via stimulating tumor immunogenicity. *Mol. Med. Rep.* 16, 2868–2874. doi: 10.3892/mmr.2017.6908

**Conflict of Interest:** The authors declare that the research was conducted in the absence of any commercial or financial relationships that could be construed as a potential conflict of interest.

frontiers in Molecular Biosciences

REVIEW
published: 14 June 2021
doi: 10.3389/fmolb.2021.694141

# The Role of Notch3 Signaling in Cancer Stemness and Chemoresistance: Molecular Mechanisms and Targeting Strategies

*Mengxi Xiu*[1,2], *Yongbo Wang*[1,2], *Baoli Li*[1,2], *Xifeng Wang*[3], *Fan Xiao*[1,2], *Shoulin Chen*[1,2], *Lieliang Zhang*[1,2], *Bin Zhou*[1,2] *and Fuzhou Hua*[1,2]*

[1]*Department of Anesthesiology, The Second Affiliated Hospital of Nanchang University, Nanchang, China,* [2]*Key Laboratory of Anesthesiology of Jiangxi Province, Nanchang, China,* [3]*Department of Gastroenterology, The First Affiliated Hospital of Nanchang University, Nanchang, China*

Aberrant Notch signaling profoundly affects cancer progression. Especially the Notch3 receptor was found to be dysregulated in cancer, where its expression is correlated with worse clinicopathological features and poor prognosis. The activation of Notch3 signaling is closely related to the activation of cancer stem cells (CSCs), a small subpopulation in cancer that is responsible for cancer progression. In addition, Notch3 signaling also contributes to tumor chemoresistance against several drugs, including doxorubicin, platinum, taxane, epidermal growth factor receptor (EGFR)–tyrosine kinase inhibitors (TKIs) and gemcitabine, through complex mechanisms. In this review, we mainly focus on discussing the molecular mechanisms by which Notch3 modulates cancer stemness and chemoresistance, as well as other cancer behaviors including metastasis and angiogenesis. What's more, we propose potential treatment strategies to block Notch3 signaling, such as non-coding RNAs, antibodies and antibody-drug conjugates, providing a comprehensive reference for research on precise targeted cancer therapy.

**Keywords: cancer, Notch3, mechanism, targeted therapy, cancer biology**

OPEN ACCESS

***Edited by:***
*Matteo Becatti,*
*University of Firenze, Italy*

***Reviewed by:***
*Parham Jabbarzadeh Kaboli,*
*Southwest Medical University, China*
*Shanchun Guo,*
*Xavier University of Louisiana, United States*

***Correspondence:**
*Fuzhou Hua*
*huafuzhou@126.com*

***Specialty section:***
*This article was submitted to Molecular Diagnostics and Therapeutics, a section of the journal Frontiers in Molecular Biosciences*

***Received:*** *12 April 2021*
***Accepted:*** *27 May 2021*
***Published:*** *14 June 2021*

***Citation:***
*Xiu M, Wang Y, Li B, Wang X, Xiao F, Chen S, Zhang L, Zhou B and Hua F (2021) The Role of Notch3 Signaling in Cancer Stemness and Chemoresistance: Molecular Mechanisms and Targeting Strategies. Front. Mol. Biosci. 8:694141. doi: 10.3389/fmolb.2021.694141*

## INTRODUCTION

Notch signaling is a highly conserved among multicellular organisms, and it is involved in cell fate decision, cell proliferation/differentiation, as well as cell lineage specification (Bray, 2006; Bray, 2016). The activation of Notch signaling is mediated by cell-to-cell interactions with a Notch ligand. In mammals, there are four Notch receptors (Notch1-4) and five ligands [Jagged (JAG)1, 2 and

**Abbreviations:** CSL, CBF-1 (RBPJ)/suppressor of hairless/Lag1; TNM, tumor node metastasis; ZIP4, zinc transporter 4; LSD1, lysine-specific demethylase 1; SIRT1, Sirtuin1; akt, AKT serine/threonine kinase; PBX1, PBX homeobox 1; SUSD2, sushi domain containing 2; PI3K, phosphatidylinositol 3-kinase; PD-L1, programmed death ligand 1; mTOR, mammalian target of rapamycin; IL6, interleukin 6; HIF1α, hypoxia inducible factor 1 subunit alpha; COX-2, cyclooxygenase 2; ERK1/2, extracellular-regulated kinase 1/2; MSI-1, musashi RNA binding protein 1; NUMB, NUMB endocytic adaptor protein; TGF-β, transforming growth factor beta; ZEB1, zinc finger E-box binding homeobox 1; GATA3, GATA binding protein 3; KIBRA, kidney and BRAin; NR2F6, nuclear receptor subfamily 2 group F member 6; MUC4, mucin 4, cell surface associated; VEGF-A, vascular endothelial growth factor a; ANG-2, angiogenin 2; CHAC1, cation transport regulator-like protein 1; JNK1, c-jun N-terminal kinase 1; CCND1, cyclin D1; NF-κB, nuclear factor kappa B; OCT-4, organic cation/carnitine transporter 4.

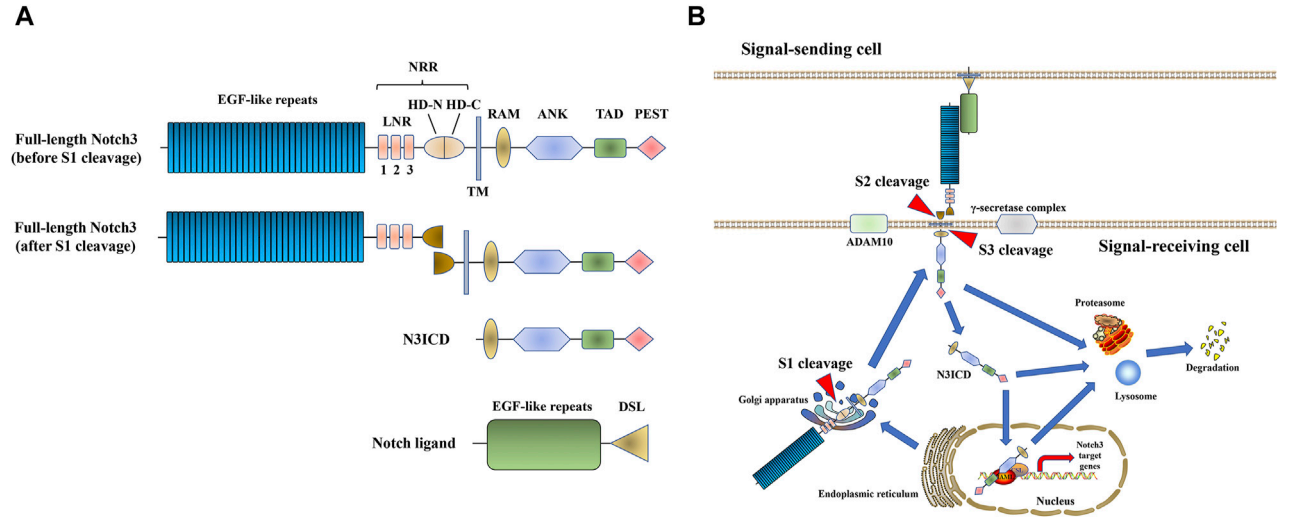


**FIGURE 1 |** Notch3 signaling. **(A)** The structure of Notch3 and its ligand. The full-length Notch3 protein consists of 34 epidermal growth factor (EGF) repeats, a negative regulatory region (NRR) [composed of three Lin-Notch repeats (LNRs) and a heterodimerization domain (HD)], a transmembrane domain, an RBPJ-association module (RAM) domain, seven ankyrin (ANK) repeats, two nuclear localization signals (NLS), a transactivation domain (TAD) and a C-terminal domain rich in proline, glutamic acid, serine, and threonine (PEST domain) (Xiu and Liu, 2019). The Notch ligand consists of EGF repeats and a Delta/Serrate/LAG-2 (DSL) domain. **(B)** Notch3 signal transduction process.

Delta-like ligand (DLL)1, 3 and 4]. Before it is trafficked to the cell membrane, the full-length Notch receptor undergoes initial cleavage, also called S1 cleavage, in the Golgi apparatus. When a Notch ligand (JAG or DLL) in the cell membrane of an adjacent signal-sending cell interacts with a Notch receptor in the cell membrane of the signal-receiving cell, the Notch receptor is activated and undergoes another proteolytic cleavage. This so-called S2 and S3 cleavage steps are induced by A Disintegrin And Metalloprotease domain 10 (ADAM10) and the $\gamma$-secretase complex, respectively (Bray, 2006; Kopan and Ilagan, 2009; Bray, 2016). Subsequently, the Notch intracellular domain (NICD) is released and translocated into the nucleus, where it binds to the effector DNA-binding transcription factor CSL. The latter then recruits the transcription co-activator mastermind-like protein (MAML) to induce the transcription of downstream target genes. Finally, the Notch receptor or NICD undergoes proteasomal/lysosome degradation (Bray, 2006; Kopan and Ilagan, 2009; Bray, 2016; Xiu and Liu, 2019) (**Figure 1**, shown on the example of Notch3 signaling).

The Notch3 receptor is encoded on chromosome 19p13.12 (19: 15159038-15200995), spanning 33 exons (https://www.ncbi.nlm.nih.gov/gene/4854). The aberrant high expression of Notch3 is common in human cancer tissues, as shown in several studies (Giovannini et al., 2009; Park et al., 2010; Zhang et al., 2011; Rahman et al., 2012; Hu et al., 2013; Ye et al., 2013; Ozawa et al., 2014; Liu et al., 2016b; Zhang et al., 2017; Tang et al., 2019; Xu et al., 2019), as well as the Cancer Genome Atlas (TCGA) and Oncomine database (**Figure 2**). High Notch3 expression in cancer tissues is correlated with a series of clinicopathological features, such as large tumor size, advanced TNM stage, high pathological grade and tumor metastasis, as well as a diminished prognosis of cancer patients, such as poor overall survival (OS), disease-free survival (DFS), relapse-free survival (RFS) and progression-free survival (PFS) (**Table 1**) (Park et al., 2010; Zhang et al., 2011; Mann et al., 2012; Rahman et al., 2012; Alqudah et al., 2013; Hu et al., 2013; Ye et al., 2013; Zhou et al., 2013; Ozawa et al., 2014; Yuan et al., 2015; Liu et al., 2016a; Liu et al., 2016b; Ma et al., 2016; Zhou et al., 2016; Kim et al., 2017a; Xue et al., 2017; Yu et al., 2017; Zhang et al., 2017; Lin et al., 2018; Tang et al., 2019; Xu et al., 2019; Zhang et al., 2019).

Notch3 overexpression in cancer is mainly caused by alterations of the Notch3 gene. According to TCGA, the Notch3 gene was altered in 5% of cancer samples, mainly via amplification and mutation (**Figure 3**). Notch3 has been reported to be amplified in 10–25% of ovarian carcinoma (OC) (Park et al., 2006; Etemadmoghadam et al., 2009; Cancer Genome Atlas Research Network, 2011; Hu et al., 2014). Among all cancer types in the TCGA database, OC has the highest Notch3 amplification rate (11.64%, 68 of 584 cases) (**Figure 3**). In addition to amplification, mutations in the negative regulatory region (NRR) and proline (P), glutamic acid (E), serine (S), threonine (T)-rich (PEST) domains of Notch3 gene can cause Notch3 activation (gain-of-function/activating mutations), as seen in human T-cell acute lymphoblastic leukemia (T-ALL) (Bernasconi-Elias et al., 2016).

Notch signaling plays complex roles in regulating cellular behaviors during cancer progression, and each Notch receptor has its specific pattern (Majumder et al., 2021). A major role of Notch3 is maintaining the stemness of cancer stem cells (CSCs). As a population of self-renewing cells with high tumorigenic potency, CSCs are found to be activated by Notch3 signaling in several kinds of cancer and contribute to cancer progression through complex mechanisms (See *Notch3 and Cancer Stem Cell Properties*). Another main feature of Notch3 signaling is to induce

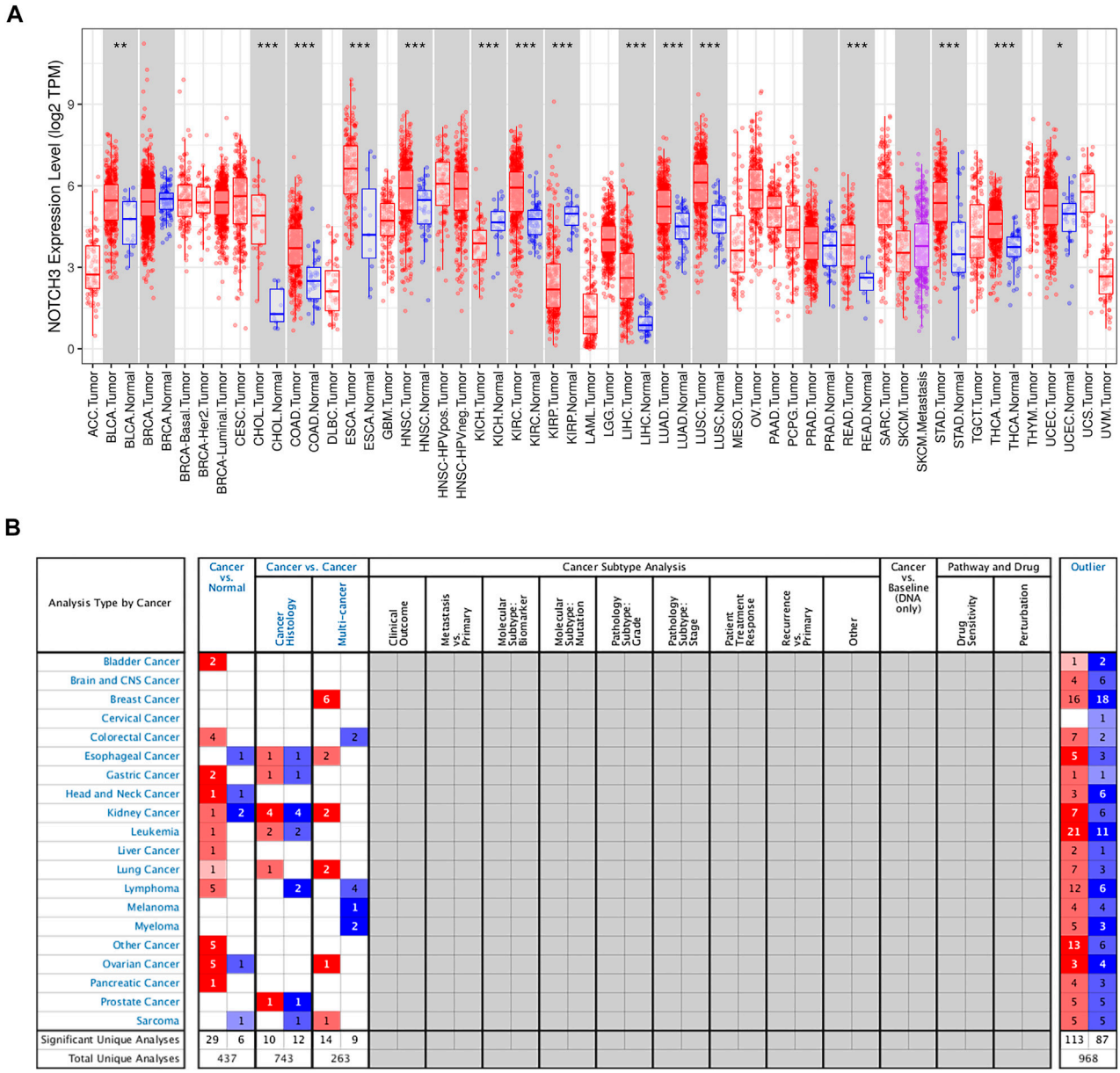


**FIGURE 2 |** The expression of Notch3 in human cancers. **(A)** The Notch3 expression levels of different cancer types in TCGA were determined using TIMER (https://cistrome.shinyapps.io/timer/) (*$p < 0.05$, **$p < 0.01$, ***$p < 0.001$). **(B)**. Notch3 expression levels in different cancer types from the Oncomine database (www.oncomine.org/).

tumor resistance against several kinds of chemotherapeutic drugs, including doxorubicin, platinum, taxane, epidermal growth factor receptor (EGFR)–tyrosine kinase inhibitors (TKIs) and gemcitabine (See in *Notch3 and Drug Resistance*). Of note, Notch3-supported CSC activity is also involved in the mechanisms of tumor chemoresistance, as well as tumor metastasis and angiogenesis, indicating the key role of Notch3 signaling in cancer (Sullivan et al., 2010; Xiao et al., 2011; McAuliffe et al., 2012; Cheung et al., 2016a; Sansone et al., 2016; Kim et al., 2017a; Kim et al., 2017b; Jeong et al., 2017; Wang et al., 2018a; Leontovich et al., 2018; Liu et al., 2018; Papadakos et al., 2019; Fan et al., 2020; Fang et al., 2020; Mansour et al., 2020).

There are numerous published review articles on the effects of Notch signaling in cancer treatment (Giovannini et al., 2016; Bellavia et al., 2018; Giuli et al., 2019; Katoh and Katoh, 2020). By contrast, this review mainly focuses on the underlying Notch3-related molecular mechanisms that regulate cancer stemness and chemoresistance. In addition, the relationships between Notch3 and other tumor biological characteristics, including metastasis and angiogenesis are also discussed. Finally, we summarize known Notch3-targeting strategies/methods for cancer therapy.

**TABLE 1 |** The clinical significance of Notch3 in different types of cancer.

| Cancer type | Sample count | Clinicopathological and prognostic significance of high Notch3 expression in cancer | References |
|---|---|---|---|
| Lung adenocarcinoma | 20 | Predicts poor OS | Zhang et al. (2019) |
| Non-small-cell lung carcinoma | 104 | Predicts poor OS and DFS | Ma et al. (2016) |
| | 3663 (Meta-analysis) | Predicts poor OS | Yuan et al. (2015) |
| | 131 | Predicts poor OS<br>Correlated with advanced TNM stage and lymph node metastasis | Ye et al. (2013) |
| Hepatocellular carcinoma | 86 | Predicts poor OS<br>Correlated with metastasis, venous invasion and satellite lesions | Zhou et al. (2013) |
| | 95 | Predicts poor OS<br>Correlated with large tumor size, multiple tumors and advanced TNM stage | Hu et al. (2013) |
| Hepatitis B virus-related hepatocellular carcinoma | 465 | Predicts poor OS and RFS | Yu et al. (2017) |
| Colorectal carcinoma | 305 | Predicts poor relapse-free survival and distant metastasis<br>Correlated with low differentiation degree and venous invasion | Ozawa et al. (2014) |
| Breast carcinoma | 72 | Correlated with positive expression of ERα and PR, with reduced lymph node metastasis | Lin et al. (2018) |
| Triple-negative breast carcinoma | 105 | Correlated with advanced TNM stage and lymph node metastasis | Xue et al. (2017) |
| Tongue carcinoma | 74 | Correlated with advanced TNM stage | Zhang et al. (2011) |
| Pancreatic adenocarcinoma | 42 | Predicts poor OS and DFS<br>Correlated with lymph node metastasis | Mann et al. (2012) |
| | 101 | Predicts poor OS<br>Correlated with advanced TNM stage, high pathological grade, lymph node metastasis and venous invasion | Zhou et al. (2016) |
| Gliomas | 60 | Predicts poor OS | Alqudah et al. (2013) |
| Ovarian carcinoma | 42 | Predicts poor OS and PFS | Park et al. (2010) |
| | 61 | Predicts poor OS and PFS | Rahman et al. (2012) |
| | 86 | Predicts poor OS<br>Correlated with advanced TNM stage, lymph node metastasis, distant metastasis, and chemoresistance | Kim et al. (2017a) |
| | 120 | Predicts poor OS<br>Correlated with advanced TNM stage, high pathological grade, advanced histological type, lymph node metastasis, and ascites | Liu et al. (2016b) |
| | 266 | Predicts poor OS and PFS | Xu et al. (2019) |
| Urothelial carcinoma | 59 | Predicts poor OS<br>Correlated with distant metastasis | Zhang et al. (2017) |
| Gallbladder carcinoma | 126 | Predicts poor OS<br>Correlated with large tumor size, advanced TNM stage, invasion, lymph node metastasis, and inability of surgical resection | Liu et al. (2016a) |
| Osteosarcoma | 70 | Predicts poor OS<br>Correlated with tumor metastasis | Tang et al. (2019) |

*Notes: OS: overall survival; DFS: disease-free survival; TNM: tumor node metastasis; RFS: relapse-free survival; ERα: estrogen receptor α; PR: progesterone receptor; PFS: progression-free survival.*

Overall, this review provides comprehensive information on the role of Notch3 signaling in cancer and its value as a therapeutic target.

## NOTCH3 AND CANCER STEM CELL PROPERTIES

Tumor initiation and progression is driven by a small population of cancer cells with self-renewal and tumor-formation capacity, known as CSCs (Dawood et al., 2014). The activation of Notch3 signaling is widely found in CSCs, where it regulates their abundance and activity through several molecular mechanisms (**Figure 4**). The expression of aldehyde dehydrogenase (ALDH), a recognized CSC marker, is significantly positively correlated with Notch3 expression, as seen in OC, lung carcinoma (LC), hepatocellular carcinoma (HCC) and breast carcinoma (BC) (Sullivan et al., 2010; Xiao et al., 2011; Zhang et al., 2015; Kim et al., 2017a). Suppression of Notch3 signaling in LC cells by treatment with either a γ-secretase inhibitor (GSI) or short hairpin RNA (shRNA) against Notch3 resulted in a significant decrease of $ALDH^+$ CSCs, indicating that Notch3 is critical for ALDH expression (Sullivan et al., 2010).

In OC, the zinc transporter ZIP4 was identified as a novel CSC marker that physically interacts with Notch3 and activates Notch3 signaling (Fan et al., 2020). Several studies also found that the activation of Notch3 signaling enhances CSC activity, especially in chemoresistant OC tumors (Kim et al., 2017b; Jeong et al., 2017; Fang et al., 2020), and the relevant mechanisms are discussed in *Platinum and Taxane*.

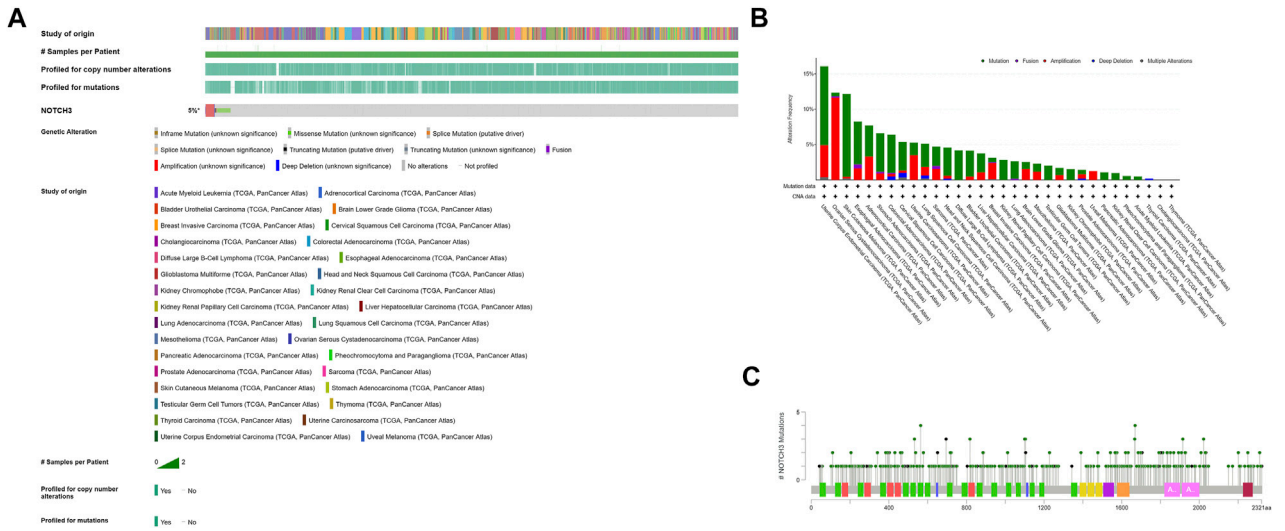


**FIGURE 3 |** Alterations of Notch3 gene in human cancers from TCGA were determined using the cBio Cancer Genomics Portal (http://cbioportal.org). **(A)** Types of Notch3 gene alterations found in cancer. **(B)** Cancer-specific Notch3 gene alterations. **(C)** Cancer-related mutations of Notch3, including 354 missense mutations (green dots) and 55 truncation mutations (black dots).

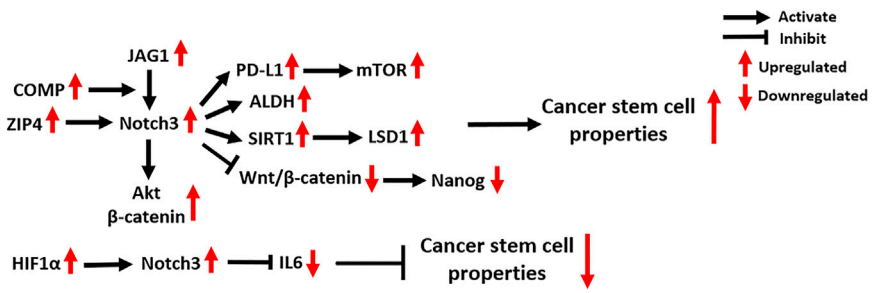


**FIGURE 4 |** Notch3-related molecular mechanisms in cancer stem cells. COMP: Cartilage Oligomeric Matrix Protein; Akt: AKT Serine/Threonine Kinase; PD-L1: Programmed Death Ligand 1; ALDH: Aldehyde dehydrogenase; SIRT1: Sirtuin 1; LSD1: Lysine-specific demethylase 1; HIF1α : Hypoxia Inducible Factor 1 Subunit Alpha; IL6: Interleukin 6.

In HCC, the activation of Notch3 signaling was found to inhibit Wnt/β-catenin signaling and increase the expression of the stemness-related protein Nanog, which promotes the maintenance of the CSC population, thereby contributing to the pathogenesis of HCC (Zhang et al., 2015). In addition, Notch3 signaling in liver CSCs is supported by cancer-associated fibroblasts in the tumor microenvironment and maintains tumor cell self-renewal (Liu et al., 2018). Mechanistically, Notch3 signaling activates LSD1, a histone-modifying enzyme that promotes cancer stemness, by inducing its deacetylation by activating the class-III histone deacetylase (HDAC) SIRT1 (Liu et al., 2018).

In the tumor microenvironment of BC, a secreted protein named Cartilage Oligomeric Matrix Protein (COMP) physically bridges Notch3 and JAG1 on the cell membrane of CSCs, thus driving JAG1/Notch3 signaling and subsequently activating the β-catenin and Akt signaling pathways to maintain CSC status (Papadakos et al., 2019). A recent study showed that Notch3 signaling contributes to the overexpression of the T-cell inhibitory molecule PD-L1 in breast CSCs by activating mTOR signaling (Mansour et al., 2020). Specific knockdown of Notch3 can downregulate PD-L1 expression on CSCs and reduce CSC activity, providing a novel strategy for anti-PD-L1 combination therapies (Mansour et al., 2020). In addition to the mechanisms that promote CSC activity, Notch3 signaling is also found to reduce the population of breast CSCs by negatively regulating IL6 (Wang et al., 2018a). Furthermore, the activation of HIF1α in response to hypoxia is involved in Notch3-mediated IL6 inhibition in breast CSCs via direct binding to the Notch3 promoter. The combination of Notch and IL6 inhibitors significantly decreases the abundance of breast CSCs and inhibits BC growth, suggesting it might serve as a novel therapeutic strategy for treating Notch3-expressing BC (Wang et al., 2018a).

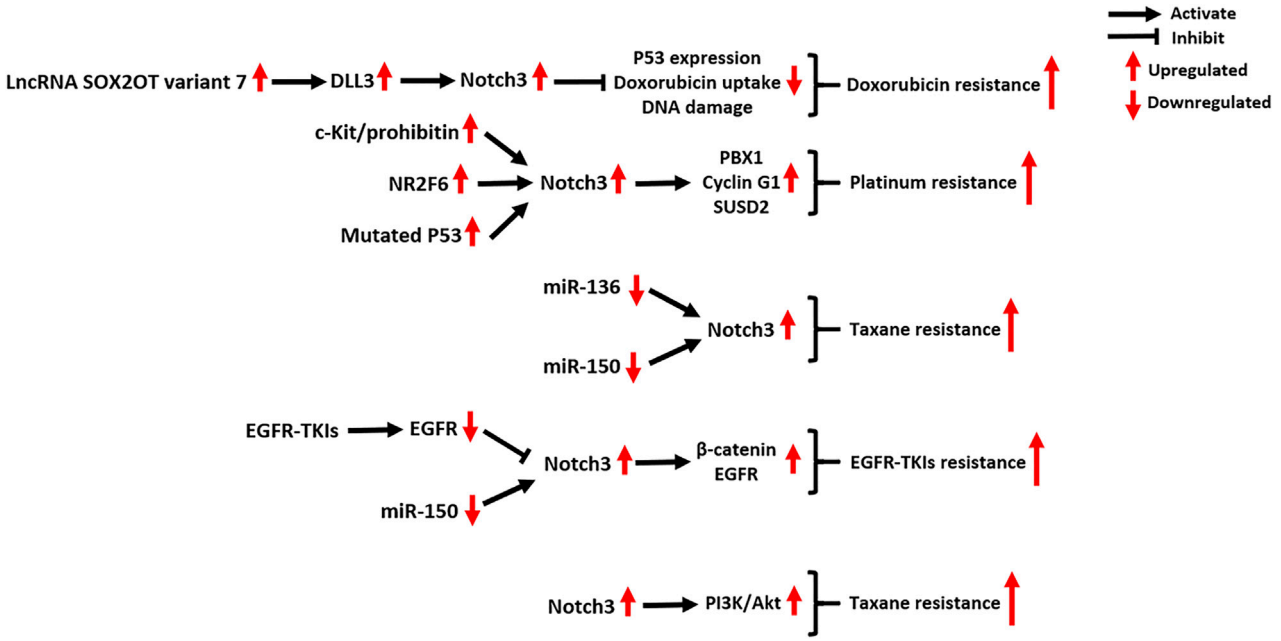


**FIGURE 5 |** Notch3-related molecular mechanisms in cancer drug resistance. NR2F6: Nuclear Receptor Subfamily 2 Group F Member 6; PBX1: PBX Homeobox 1; SUSD2: Sushi Domain Containing two; EGFR-TKIs: epidermal growth factor receptor–tyrosine kinase inhibitors; PI3K: phosphatidylinositol 3-kinase; Akt: AKT Serine/Threonine Kinase.

## NOTCH3 AND DRUG RESISTANCE

A large number of studies have shown that Notch3 signaling is closely related to the ability of tumors to chemotherapy. Here, we mainly introduce the roles of Notch3 in the resistance of tumors to five kinds of chemotherapeutic drugs (doxorubicin, platinum, taxane, EGFR-TKIs and gemcitabine), whose mechanisms are comparatively well-understood (**Figure 5**).

### Doxorubicin

The resistance of tumor cells to doxorubicin, a DNA topoisomerase II inhibitor, is associated with the activation of Notch3 signaling (Giovannini et al., 2009; Michishita et al., 2011; Wang et al., 2018b). In HCC cells, Notch3 signaling contributes to doxorubicin resistance by inhibiting p53 expression, doxorubicin uptake and DNA damage, which can be reversed by Notch3 depletion (Giovannini et al., 2009). In osteosarcoma, both *in vivo* and *in vitro* experiments indicate that the lncRNA SOX2OT variant seven can activate DLL3/Notch3 signaling, maintaining the stemness and doxorubicin-resistance of tumor cells (Wang et al., 2018b). Treatment of osteosarcoma cells with epigallocatechin gallate, a polyphenol from green tea, can counteract the SOX2OT-7/DLL3/Notch3 axis, thus inhibiting cancer progression (Wang et al., 2018b).

### Platinum and Taxane

Notch3 signaling plays a critical role in tumor resistance to platinum, taxane, or their combination chemotherapy regimens, especially in OC. In a clinical study of 61 OC patients, the high expression of Notch3 was correlated with shorter PFS and OS in patients with stage III and IV disease treated with a standard platinum and taxane chemotherapy regimen (Rahman et al., 2012). *In vitro* experiments in OC cell lines also confirmed that Notch3 was significantly overexpressed in cisplatin-resistant A2780cis cells (2.5-fold) and paclitaxel (PTX)-resistant SKpac cells (25.5-fold) compared to chemo-sensitive A2780 cells (Kim et al., 2017a).

In cisplatin-resistant OC, Notch3 signaling was found to be induced by the activation of the c-Kit/prohibitin axis and the nuclear orphan receptor NR2F6, as well as P53 mutations (Li et al., 2019; Xu et al., 2019; Fang et al., 2020). The activation of Notch3 signaling activates the stem cell reprogramming factor PBX1, which supports the activity of CSCs contributing to platinum chemoresistance (Fang et al., 2020). In addition, Notch3 signaling also upregulates the expression of Cyclin G1 and SUSD2, which contributes to both tumor metastasis and cisplatin resistance of OC (Xu et al., 2018; Xu et al., 2019). As seen in OC, Epstein-Barr virus (EBV)-associated nasopharyngeal carcinoma and colorectal carcinoma (CRC), inhibition of Notch3 signaling can significantly enhance the cisplatin chemosensitivity of tumor cells, indicating the value of Notch3-targeted therapy (Man et al., 2012; McAuliffe et al., 2012; Tzeng et al., 2014; Xie et al., 2016).

In PTX-resistant OC, the decreased expression of the tumor-suppressive miRNAs miR-136 and miR-150 contributes to the overexpression of Notch3 (Kim et al., 2017b; Jeong et al., 2017). Ectopic expression of miR-136 and miR-150 was found to inhibit Notch3 expression, which suppressed the stemness and angiogenesis of SKpac cells (Kim et al., 2017b; Jeong et al., 2017). In addition, several pre-clinical studies indicated that

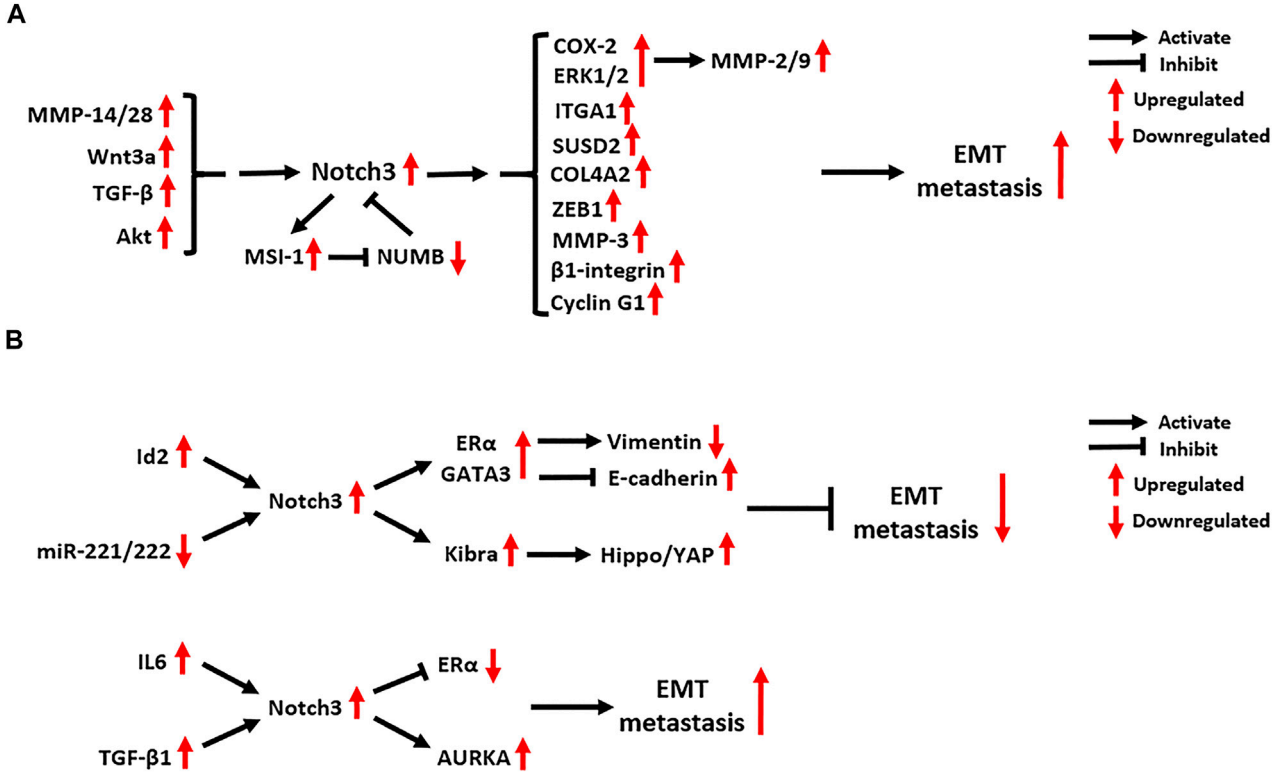


**FIGURE 6 |** Notch3-related EMT molecular mechanisms in **(A)** tumors other than breast carcinoma and **(B)** breast carcinoma. EMT: Epithelial-Mesenchymal Transition; MMP: Matrix Metalloproteinase; Wnt3a: Wnt Family Member 3A; TGF-β: Transforming Growth Factor Beta; MSI-1: Musashi RNA Binding Protein 1; NUMB: NUMB Endocytic Adaptor Protein; COX-2: Cyclooxygenase 2; ERK1/2: Extracellular-regulated Kinase 1/2; ITGA1: Integrin Subunit Alpha 1; SUSD2: Sushi Domain Containing 2; COL4A2: Collagen Type IV Alpha 2 Chain; ZEB1: Zinc Finger E-Box Binding Homeobox 1; Id2: Inhibitor Of DNA Binding 2; ERα: Estrogen Receptor α; GATA3: GATA Binding Protein 3; IL6: Interleukin 6; KIBRA: KIdney and BRAin; AURKA: Aurora Kinase A.

concomitant treatment with PTX and Notch3-specific inhibitors, including GSI, Small interfering RNA (siRNA) or antibody drugs, can enhance the efficacy of PTX treatment in several tumors, including OC, pancreatic carcinoma (PC), and LC (Groeneweg et al., 2014; Yen et al., 2015; Kang et al., 2016; He et al., 2017; Morgan et al., 2017).

## EGFR-TKIs

Studies have revealed novel mechanisms by which Notch3 induces EGFR-TKI resistance in EGFR-mutated tumors. Notch3 receptor was identified as a substrate for EGFR-mediated tyrosine phosphorylation, and EGFR kinase activity induces tyrosine phosphorylation of Notch3, thus inhibiting Notch3 signaling (Arasada et al., 2014). Unfortunately, EGFR-TKI therapy relieves this inhibition, resulting in Notch3 activation and subsequent CSC enrichment (Arasada et al., 2014). In response to EGFR-TKI therapy of non-small-cell lung carcinoma (NSCLC), Notch3 physically binds to β-catenin in the cytoplasm of tumor cells to activate β-catenin signaling (Arasada et al., 2018). The combination of EGFR-TKIs and a β-catenin inhibitor abrogates the Notch3-dependent activation of β-catenin, which strongly attenuates tumor onset, improving the OS and RFS of NSCLC xenograft mice (Arasada et al., 2018). Zhang et al. found that recovering the expression of miR-150 can directly downregulate Notch3 in TKI-resistant NSCLC cell lines, providing another method for reversing Notch3-mediated TKI resistance (Zhang et al., 2019).

In gliomas and triple-negative BC (TNBC), it was found that Notch3 signaling can promote EGFR expression (Alqudah et al., 2013; Diluvio et al., 2018). Notch3 silencing in TKI-resistant TNBC cells induces EGFR dephosphorylation and promotes its intracellular arrest, which increases tumor cell sensitivity to TKI–gefitinib treatment (Diluvio et al., 2018).

## Gemcitabine

In a clinical study of 71 PC patients, Notch3 was identified as a novel biomarker for predicting the efficacy of gemcitabine (GEM), whereby low Notch3 expression was associated with better GEM treatment efficacy and longer OS of PC patients (Eto et al., 2013). Mechanistically, Notch3 increases the activity of PI3K/Akt signaling in PC cells in response to GEM treatment, and this effect can be reversed by Notch3-specific siRNAs (Yao and Qian, 2010). In addition, Notch3 signaling also contributes to GEM resistance in NSCLC cells. Treatment with GEM and GSI significantly enhances GEM sensitivity and leads to tumor cell apoptosis, but the underlying molecular mechanisms remain unclear (Hu et al., 2018).

# NOTCH3 IN OTHER ASPECTS OF CANCER BIOLOGY

## Notch3 in Cancer Epithelial-Mesenchymal Transition and Metastasis

Notch3 has a close relationship with tumor metastasis (**Figure 6**). In clinical studies, high expression of Notch3 was found to be associated with tumor metastasis in OC, NSCLC, prostate carcinoma (PCa), HCC, PC and gallbladder carcinoma (Ye et al., 2013; Zhou et al., 2013; Liu et al., 2016a; Liu et al., 2016b; Zhou et al., 2016; Kim et al., 2017a; Lin et al., 2018; Kim and Gu, 2019). Matrix metalloproteinases (MMPs) cascade with Notch3 signaling and promote tumor metastasis. The Notch3-MMP-3 axis contributes to bone metastasis of PC by promoting the formation of osteoblastic lesions and decreasing osteoblastogenesis (Ganguly et al., 2020). In HCC and pancreatic ductal adenocarcinoma (PDAC), Notch3 signaling activates the COX-2 and ERK1/2 pathways, which subsequently enhance the migration and invasion of tumor cells by upregulating the expression of MMP-2 and MMP-9 (Zhou et al., 2013; Zhou et al., 2016). In addition, MMP-14 and MMP-28 were found to promote tumor metastasis by inducing Notch3 signaling. The MMP-14-Notch3-β1-integrin axis can be activated by interactions between lymphatic endothelial cells and melanoma cells, leading to the transformation of non-metastatic melanoma cells into invasively sprouting melanoma cells (Pekkonen et al., 2018). The MMP-28-Notch3 axis promotes the Epithelial-Mesenchymal Transition (EMT), migration and invasion of HCC cells *in vivo* and *in vitro* (Zhou et al., 2019).

In advanced CRC, Notch3 expression is positively correlated with lymph node as well as distant metastasis, and its expression is dependent on the activation of Akt signaling (Varga et al., 2020). Additionally, DLL4/Notch3 signaling was found to upregulate the expression of the RNA-binding protein MSI-1 in metastatic CRC tumors. Active MSI-1 can inhibit the expression of NUMB, a negative regulator of Notch signaling, which maintains the activation of oncogenic Notch1 and Notch3 signaling pathways (Pastò et al., 2014).

As a key component of Wnt signaling, Wnt3a can activate Notch3 signaling to promote the EMT and metastasis of NSCLC (Li et al., 2015). In bone metastasis of NSCLC, Notch3 signaling is also involved in TGF-β signaling-induced EMT by activating the EMT regulator ZEB1 (Liu et al., 2014a). In metastatic OC tumors, several downstream targets of Notch3 signaling were found to be activated, including type IV collagen (COL4A2), sushi domain containing 2 (SUSD2), Cyclin G1 and integrin subunit alpha 1 (ITGA1) (Brown et al., 2015; Xu et al., 2018; Xu et al., 2019; Price et al., 2020). Blocking Notch3 signaling in metastatic OC can inhibit the adhesion, migration and metastasis of tumor cells, while also enhancing their chemo-sensitivity (Brown et al., 2015; Xu et al., 2018; Xu et al., 2019; Price et al., 2020).

The role of Notch3 in BC metastasis is controversial. A study of 72 BC cases reported that Notch3 expression is correlated with a lower risk of lymph node metastasis, as well as the expression of estrogen receptor α (ERα), progesterone receptor (PR) and GATA3 (Lin et al., 2018). N3ICD in the nucleus of BC cells can bind to the promotors of ERα and GATA3 to promote their expression. ERα and GATA3 activated by Notch3 signaling upregulate vimentin expression and repress E-cadherin expression, which then suppresses the EMT and metastasis of BC by maintaining a luminal phenotype (Dou et al., 2017; Lin et al., 2018). Another Notch3-mediated EMT-suppression mechanism in BC relies on the activation of Hippo/YAP signaling by upregulating the transcription of KIBRA, an upstream factor of Hippo signaling (Zhang et al., 2016b). The inhibitor of DNA binding 2 (Id2), a transcription factor belonging to the bHLH family, can promote the transcription of Notch3, thus attenuating the EMT in BC (Wen et al., 2018). By contrast, microRNAs 221 and 222 were found to target the 3' UTR of Notch3 and suppress its protein translation in BC cells, which reverses EMT inhibition by Notch3 signaling (Liang et al., 2018).

Although the inhibitory effect of Notch3 on BC metastasis has been confirmed in several studies, a pro-EMT function of Notch3 has been also identified. It was found that the activation of Notch3 signaling is linked to BC seeding and lung/brain metastasis, while abrogation of Notch3 reduces the self-renewal and invasion ability of BC cells, restoring a luminal $CD44^{low}/CD24^{high}/ERα^{high}$ phenotype (Leontovich et al., 2018). Mechanistically, aberrant Aurora A kinase activity activates Notch3 in breast CSCs and contributes to metastatic growth (Leontovich et al., 2018). In addition, IL6 was found to activate Notch3 signaling in $CD133^{high}/ERα^{low}/IL6^{high}$ breast CSCs, where it promotes endocrine resistance and metastatic progression (Sansone et al., 2016). In bone-metastatic BC, the activation of JAG1/Notch3 signaling induced by osteoblasts and osteoblast-derived TGF-β1 contributes to aggressive osteolytic metastasis and bone destruction *in vivo* (Zhang et al., 2010). These findings indicate that the relationship between Notch3 and BC metastasis should be explored further.

## Notch3 and Tumor Angiogenesis

The functions of Notch signaling in tumor vasculature are mainly determined by Notch ligands. JAG1-mediated Notch signaling induces neovascularization and sprouting angiogenesis, while DLL4-mediated Notch signaling inhibits tumor angiogenesis (Xiu et al., 2020b; Xiu et al., 2020a). Notch3 is also involved in the regulation of tumor angiogenesis (**Figure 7**). Immunohistochemistry for Notch3 expression in 105 TNBC tissues showed that its expression is positively correlated with tumor microvascular density (MVD), which suggests a potential pro-angiogenic role of Notch3 (Xue et al., 2017). MUC4, a large membrane-anchored glycoprotein, can facilitate tumor angiogenesis and increase tumor MVD in PC by activating Notch3 signaling and downstream pro-angiogenic genes, including VEGF-A and ANG-2 (Tang et al., 2016). In addition, Notch3 signaling can be activated by interactions between tumor cells and cells in the tumor microenvironment, which contribute to tumor angiogenesis in several cancers. The interactions between tumor cells and cancer-associated fibroblasts activate Notch3 signaling, thus promoting angiogenesis in oral squamous cell carcinoma (Kayamori et al.,

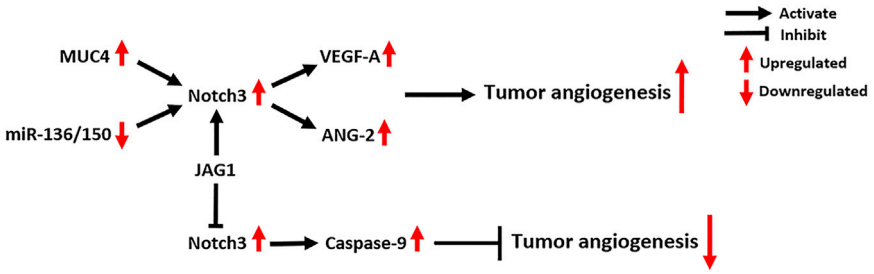


**FIGURE 7 |** Notch3-related molecular mechanisms in tumor angiogenesis. MUC4: Mucin 4, Cell Surface Associated; VEGF-A: Vascular Endothelial Growth Factor A; ANG-2: Angiogenin 2.

2016). Similarly, the interactions between CSCs and endothelial cells (ECs) activate Notch3 signaling to promote angiogenesis in OC, which can be inhibited by Notch3-targeting miRNAs, including miR-136 and miR-150 (Kim et al., 2017b; Jeong et al., 2017). Additionally, the interactions between CSCs and ECs activate Notch3 signaling to promote angiogenesis and vasculogenic mimicry in melanoma (Hsu et al., 2017).

Notch3 signaling promotes tumor angiogenesis in a canonical CSL-dependent manner, which requires cell-cell interactions and is driven by Notch ligands. However, Notch3 was also found to act as a dependent receptor in tumor ECs to negatively regulate tumor angiogenesis, circumventing CSL (Lin et al., 2017). Mechanistically, Notch3 receptors on the surface of tumor ECs can directly activate caspase-9, which induces the caspase-dependent cell death of ECs (Lin et al., 2017). Interestingly, overexpression of JAG1 ligand can abrogate this effect and promote tumor neovascularization. This indicates that the effects of Notch3 on tumor angiogenesis depend on the cellular context, such as the availability and amounts of Notch ligands in tumors (Lin et al., 2017).

## NOTCH3-TARGETING STRATEGIES FOR CANCER THERAPY

GSIs that prevent the S3 cleavage of Notch receptor are the most commonly used therapeutic option for blocking Notch signaling in cancer (Shih Ie and Wang, 2007). However, they lack specificity and may interfere with the processing of other transmembrane proteins. What's more, pre-clinical studies have shown that the use of GSIs is associated with severe side effects, such as gastrointestinal tract toxicity (Milano et al., 2004; van Es et al., 2005). Therefore, it is essential to propose other potential methods/strategies that target Notch3 signaling.

### Small Interfering RNAs and Short Hairpin RNAs

siRNAs and shRNAs are powerful molecules that can directly knock down the expression of target genes (Rao et al., 2009). In pre-clinical experiments, Notch3-specific siRNAs or shRNAs were able to prevent Notch3 activation and potently inhibit tumor cell growth *in vivo* and *in vitro* (Yao and Qian, 2010; Serafin et al., 2011; Hassan et al., 2016; Kang et al., 2016; Diluvio et al., 2018). However, the low efficiency of traditional siRNA/shRNA delivery vehicles remains a significant obstacle for their clinical application. To overcome this, researchers developed a novel aptamer-siRNA chimera-based delivery system to inhibit Notch3 expression (Cheng et al., 2017). The chimera consisting of an aptamer and Notch3-specific siRNA was bonded with cationic Au-$Fe_3O_4$ nanoparticles (NPs). This chimera exhibited a high Notch3 silencing efficiency in OC cell lines, as well as potent anti-tumor effects (Cheng et al., 2017). However, there are still no reports on the *in vivo* use of this Au-$Fe_3O_4$ NP-chimera, and its potential value also needs evaluation in clinical studies.

### Non-Coding RNAs

Many non-coding RNAs (ncRNAs), including microRNAs (miRNAs), long noncoding RNAs (lncRNAs) and circular RNAs (circRNAs), play oncogenic or tumor-suppressor roles by regulating Notch3 expression (**Table 2**) (Song et al., 2009; Furukawa et al., 2013; Liu et al., 2014b; Wang et al., 2015; Cheung et al., 2016a; Zhang et al., 2016a; Kim et al., 2017b; Kim et al., 2017b; Cai et al., 2017; Jeong et al., 2017; Liang et al., 2018; Zhang et al., 2018; Yao et al., 2019; Zhang et al., 2019; Zhu et al., 2019; Cai et al., 2020; Chen et al., 2020; Pei et al., 2020; Zhang et al., 2020; Zong et al., 2020; Kang et al., 2021). MiRNAs are small noncoding nucleotides that directly interact with the 3′-untranslated region (3′-UTR) to degrade a targeted mRNA or inhibit its translation (Vishnoi and Rani, 2017). Most Notch3-targeting miRNAs are tumor-suppressive, and are downregulated in tumor tissues compared to normal tissues. Several lncRNAs and circRNAs were found to "sponge" Notch3-targeting miRNAs, thus resulting in Notch3 overexpression and forming competing endogenous RNA (ceRNA) networks in cancer, including the RUSC1-AS1-miR-7-Notch3 axis (Chen et al., 2020), Circ_PUM1-miR-136-Notch3 axis (Zong et al., 2020), LINC00707-miR-206-Notch3 axis (Zhu et al., 2019), Circ_0058124-miR-218-Notch3 axis (Yao et al., 2019), LINC00210-miR-328-Notch3 axis (Zhang et al., 2018), FAM225A/HOTAIR-miR-613-Notch3 axis (Cai et al., 2017; Zhang et al., 2020), and TUG1-miR-1299-Notch3 axis (Pei et al., 2020). Treatment strategies based on inhibiting the expression of these lncRNAs and circRNAs or recovering the expression of miRNAs have been confirmed to suppress Notch3 expression and block Notch3-controlled oncogenic mechanisms

**TABLE 2 |** Non-coding RNAs that target Notch3 in cancer.

| Non-coding RNA | Role | Cancer type/cell line | Observations | References |
|---|---|---|---|---|
| miR-1 | Tumor-suppressive | CRC | MiR-1 inhibits *in vitro* tumor cell migration by targeting Notch3 | Furukawa et al. (2013) |
| LncRNA RUSC1-AS1 | Oncogenic | HCC | LncRNA RUSC1-AS1 sponges miR-7 to upregulate Notch3 and promotes tumor cell proliferation *in vitro* | Chen et al. (2020) |
| miR-7 | Tumor-suppressive | | | |
| Circ_PUM1 | Oncogenic | Endometrial carcinoma | Circ_PUM1 sponges miR-136 to upregulate Notch3, and promotes the proliferation, migration and invasion of tumor cells *in vitro* and *in vivo* | Zong et al. (2020) |
| miR-136 | Tumor-suppressive | OC | MiR-136 inhibits the stemness, angiogenesis and chemoresistance of tumor cells *in vitro* by targeting Notch3 | Jeong et al. (2017) |
| miR-150 | Tumor-suppressive | OC | MiR-150 inhibits the stemness, angiogenesis and chemoresistance of tumor cells *in vitro* by targeting Notch3 | Kim et al. (2017b) |
| | | Lung adenocarcinoma | MiR-150 inhibits tumor cell proliferation *in vitro* by targeting Notch3 | Zhang et al. (2019) |
| miR-96/183 | Tumor-suppressive | EBV-associated NPC | MiR-96/183 inhibit stem cell-like properties of tumor cells *in vitro* and inhibit tumor growth *in vivo* by downregulating the expression of NICD3 and NICD4 | Cheung et al. (2016b) |
| miR-206 | Tumor-suppressive | HCC, CRC, osteosarcoma and HeLa cells | MiR-206 inhibits the proliferation and migration of tumor cells *in vitro* by targeting Notch3 | Song et al. (2009); Liu et al. (2014b); Wang et al. (2015); Cai et al. (2020) |
| LncRNA 00707 | Oncogenic | CRC | LINC00707 sponges miR-206 to upregulate Notch3 and promotes the proliferation and metastasis of tumor cells *in vitro* | Zhu et al. (2019) |
| Circ_0058124 | Oncogenic | Papillary thyroid carcinoma | Circ_0058124 sponges miR-218 to upregulate Notch3, and promotes the proliferation, migration and invasion of tumor cells *in vitro* and *in vivo* | Yao et al. (2019) |
| miR-218 | Tumor-suppressive | | | |
| miR-221/222 | Oncogenic | BC | MiR-221/222 promote the epithelial-mesenchymal transition of tumor cells *in vitro* by targeting Notch3 | Liang et al. (2018) |
| LncRNA 00210 | Oncogenic | NPC | LINC00210 sponges miR-328 to upregulate Notch3 and promotes the proliferation and migration of tumor cells *in vivo* and *in vitro* | Zhang et al. (2018) |
| miR-328 | Tumor-suppressive | | | |
| miR-491 | Tumor-suppressive | NPC | MiR-491 inhibits the proliferation, migration and invasion of tumor cells *in vitro* and inhibits tumor growth *in vivo* by targeting Notch3 | Zhang et al. (2016a) |
| miR-491/875 | Tumor-suppressive | GC | MiR-491/875 inhibit the proliferation, migration and invasion of tumor cells *in vitro* and *in vivo* by targeting Notch3 | Kang et al. (2021) |
| LncRNA FAM225A | Oncogenic | CRC | LncRNA FAM225A sponges miR-613 to upregulate Notch3 and promotes the proliferation, migration and invasion of tumor cells *in vitro* | Zhang et al. (2020) |
| miR-613 | Tumor-suppressive | | | |
| LncRNA HOTAIR | Oncogenic | PC | LncRNA HOTAIR sponges miR-613 to upregulate Notch3 and inhibits the proliferation, migration and invasion of tumor cells *in vitro* and *in vivo* | Cai et al. (2017) |
| LncRNA TUG1 | Oncogenic | OC | LncRNA TUG1 sponges miR-1299 to upregulate Notch3 and inhibits tumor cell proliferation *in vitro* and *in vivo* | Pei et al. (2020) |
| miR-1299 | Tumor-suppressive | | | |

*Notes: CRC: colorectal carcinoma; HCC: hepatocellular carcinoma; OC: ovarian carcinoma; EBV: Epstein-Barr virus; NPC: nasopharyngeal carcinoma; BC: breast carcinoma; GC: gastric carcinoma; PC: pancreatic carcinoma.*

*in vivo* and/or *in vitro* (Song et al., 2009; Furukawa et al., 2013; Liu et al., 2014b; Wang et al., 2015; Cheung et al., 2016a; Zhang et al., 2016a; Cheung et al., 2016b; Kim et al., 2017b; Cai et al., 2017; Jeong et al., 2017; Liang et al., 2018; Zhang et al., 2018; Yao et al., 2019; Zhang et al., 2019; Zhu et al., 2019; Cai et al., 2020; Chen et al., 2020; Pei et al., 2020; Zhang et al., 2020; Zong et al., 2020; Kang et al., 2021).

## Antibodies

Antibodies that target Notch receptors/ligands have been confirmed to effectively modulate Notch signaling activity (Xiu et al., 2020b; Gharaibeh et al., 2020). The monoclonal antibodies (mAbs) named A4, A8, MOR20350 and MOR20358, were designed to bind the NRR domain (Lin-Notch repeat (LNR) and heterodimerization domain (HD) domain) of Notch3 protein, which prevents the exposure of the S2 cleavage site and blocks Notch3 activation (Li et al., 2008; Tiyanont et al., 2013; Bernasconi-Elias et al., 2016). In T-ALL harboring Notch3 gain-of-function mutations, anti-Notch3 NRR mAbs show potent anti-leukemic activity in T-ALL cell lines and tumor xenografts (Bernasconi-Elias et al., 2016).

In addition to anti-Notch3 NRR mAbs, another mAb against epidermal growth factor (EGF) repeats of Notch2/3 named tarextumab (also called OMP-59R5) has been used to block Notch2/3 signaling in pre- and clinical studies (O'Reilly et al., 2015; Yen et al., 2015; Hu et al., 2019; Smith et al., 2019). Tarextumab was found to significantly inhibit the growth of PC, BC, OC and small-cell lung carcinoma (SCLC) xenograft tumors, partly by reducing the abundance of CSCs. Additionally, the combination of tarextumab with GEM plus nab-paclitaxel exhibited more potent anti-tumor effects (Yen et al., 2015). In the phase 1b clinical study NCT01647828, tarextumab in combination with gemcitabine plus nab-PTX was evaluated in 38 untreated metastatic PDAC patients, and the overall response rate (ORR) was 29% (O'Reilly et al., 2015). The recommended phase 2 dose was 15 mg/kg with standard doses of the cytotoxic agents. The frequent tarextumab-related emergent adverse events (TEAEs) were diarrhea (60%) and fatigue (43%), which were mostly grade 1 or 2 (O'Reilly et al., 2015). In another phase 1 study (NCT01277146) dose escalation and expansion of tarextumab was evaluated in 42 patients with solid tumors (Smith et al., 2019). Tarextumab was well tolerated at doses of 2.5 mg/kg weekly, as well as 7.5 mg/kg every 14 or 21 days. Diarrhea (81%) was the most common TEAE, followed by fatigue (48%), nausea (45%) and decreased appetite (38%) (Smith et al., 2019). Unfortunately, the results of a phase 2 study (NCT01859741) indicated that tarextumab treatment in combination with platinum-based therapy in 145 untreated SCLC patients did not improve PFS, OS, or ORR of patients (Daniel et al., 2017). In another phase 2 study (NCT01647828) of 177 untreated metastatic PDAC patients, tarextumab treatment in combination with GEM plus nab-paclitaxel also did not improve the OS, PFS, or ORR, while PFS was even statistically worse in tarextumab-treated patients (Hu et al., 2019). Due to the adverse effects of tarextumab shown in phase 2 clinical trials, its clinical development was discontinued.

As mentioned in *EGFR-TKIs*, co-blockage of EGFR and Notch receptors is necessary in some cases. In recent studies, bispecific mAbs targeting both Notch2/3 (tarextumab) and EGFR/HER3 (panitumumab/RG7116/MEHD7945A) have been established using the "Knobs into holes" and "CrossMAb" technologies (Hu et al., 2017; Fu et al., 2019). *In vivo* and *in vitro* experiments on NSCLC and TNBC showed that EGFR/Notch-bispecific mAbs exhibit potent anti-tumor effects, especially decreasing the abundance of CSCs, which limits tumor resistance to EGFR-TKIs and has potential value for clinical applications (Hu et al., 2017; Fu et al., 2019).

## Antibody-Drug Conjugates

Antibody-drug conjugates (ADCs) are mAbs conjugated to small-molecule chemotherapeutic agents via a chemical linker. ADCs can selectively bind to specific targets on the surface of cancer cells and directly deliver the ultra-toxic payload, thus killing cancer cells (Chau et al., 2019). PF06650808, a novel Notch3-targeting ADC, contains a humanized anti-Notch3 IgG1 antibody, a cleavable maleimidocapronic-valinecitruline-p-aminobenzylooxycarbonyl peptide linker, and an auristatin-based cytotoxic payload (Geles et al., 2015). Pre-clinical experiments revealed that PF06650808 can effectively inhibit the growth of TNBC, OC and NSCLC xenograft tumors (Geles et al., 2015). In a recent phase 1, dose-escalation study with 40 solid tumor patients, PF-06650808 was well tolerated at doses ≤2.0 mg/kg, and the maximum tolerated dose was 2.4 mg/kg (Rosen et al., 2020). The most common TEAEs were fatigue (40.0%), decreased appetite (37.5%), nausea (35.0%) and alopecia (32.5%). The ORR and clinical benefit response in the 31 response-evaluable patients was 9.7 and 35.5%, respectively (Rosen et al., 2020). However, the study has been terminated due to a change in sponsor prioritization.

## Histone Deacetylase Inhibitors

Histone deacetylases (HDACs) regulate gene transcription by removing active histone marks such as acetyl groups from ε-N-acetyl lysine on a histone, allowing the histones to wrap the DNA more tightly (Jenke et al., 2021). Several reports indicate that impairing the acetylation/deacetylation balance of Notch3 using HDAC inhibitors (HDACi) that favor hyperacetylation can negatively affect the stability and function of Notch3 in cancer cells and tumor xenograft mouse models (Palermo et al., 2012; Jaskula-Sztul et al., 2015; Zhang et al., 2017; Pinazza et al., 2018). Mechanistically, HDACi such as trichostatin A (TSA), suberoylanilide hydroxamic acid (SAHA) and AB3 increase the ubiquitination and proteasomal/lysosomal degradation of Notch3, which reduces its abundance at the cell surface and impairs Notch3 signaling (Palermo et al., 2012; Jaskula-Sztul et al., 2015; Zhang et al., 2017; Pinazza et al., 2018).

## Other Drugs/Compounds

Temozolomide (TMZ) is an alkylating chemotherapeutic agent that can penetrate the blood-brain barrier and is clinically used in the treatment of glioblastoma (GBM). One study demonstrated that the inhibition of Notch3 expression contributes to TMZ-induced GBM cytotoxicity (Chen et al., 2017). Mechanistically, TMZ enhances the expression of the ER stress protein CHAC1 by activating JNK1/c-JUN signaling. Subsequently, CHAC1 binds to Notch3 protein, which reduces the generation of N3ICD, thus preventing Notch3 signaling (Chen et al., 2017). However, a recent study found that TMZ can also activate DLL4/Notch3 signaling to maintain CSC properties in GBM by upregulating MMP14 expression (Ulasov et al., 2020). Thus, the effect of TMZ on Notch3 signaling needs further exploration.

In HCC chemotherapy, a well-tolerated combination of sorafenib and valproic acid was found to synergistically inhibit tumor growth by downregulating Notch3 and p-Akt (Zhu et al., 2017). Mangiferin, a C-glucosyl xanthone (1,3,6,7-tetrahydroxy-xanthone-C2-β-D-glucoside), can specifically repress Notch3 signaling, which increases apoptosis and inhibits OC tumor growth both *in vitro* and *in vivo* (Zou et al., 2017). In spite of these success stories, more drugs/compounds that potentially target Notch3 should be screened in the future.

# DISCUSSION AND CONCLUSION

Notch3 signaling plays critical roles in cancer progression, and the related molecular mechanisms have been studied in some detail. Stem cell-like properties are a primary feature of Notch3-positive cancer

**TABLE 3 |** The associations between Notch3 signaling and other signaling pathways.

| Pathway | Cancer type | Function | References |
|---|---|---|---|
| Wnt/β-catenin/Notch3 | OC | Not shown | Chen et al. (2010) |
| | NSCLC | Promotes tumor cell cycle progression | Li et al. (2011) |
| | | Promotes tumor cell proliferation and survival | Li et al. (2013) |
| | | Promotes tumor cell invasion and EMT. | Li et al. (2015) |
| | | Promotes tumor cell drug resistance | Arasada et al. (2018) |
| Notch3/Wnt/β-catenin | HCC | Promotes tumor cell stemness | Zhang et al. (2015) |
| | BC | — | Papadakos et al. (2019) |
| Akt/Notch3 | CRC | Promotes tumor cell invasion and metastasis | Varga et al. (2020) |
| | CC | Promotes tumor cell survival | Guest et al. (2016) |
| Notch3/Akt | BC | Promotes tumor cell stemness | Papadakos et al. (2019) |
| | GC | Promotes the proliferation, invasion and metastasis of tumor cells | Kang et al. (2021) |
| | PC | Promotes tumor cell drug resistance | Yao and Qian (2010) |
| IL6/Notch3 | BC | Promotes the stemness, metastasis and drug resistance of tumor cells | Sansone et al. (2016) |
| Notch3/IL6 | BC | Inhibits tumor cell stemness | Wang et al. (2018a) |
| | NSCLC | Promotes tumor cell EMT and metastasis | Liu et al. (2014a) |
| EGFR/Notch3 | BC | Inhibits tumor cell stemness | Arasada et al. (2014) |
| Notch3/EGFR | BC | Promotes tumor cell drug resistance | Diluvio et al. (2018) |
| | Gliomas | Promotes the proliferation, migration and invasion of tumor cells | Alqudah et al. (2013) |
| TGF-β/Notch3 | NSCLC | Promotes tumor cell EMT and metastasis | Liu et al. (2014a) |
| | BC | | Zhang et al. (2010) |
| Notch3/NF-κB | EBV-associated NPC | Promotes tumor cell proliferation | Man et al. (2012) |
| | T-cell malignancies | Promotes tumor cell survival | Bellavia et al. (2000); Vacca et al. (2006) |
| | HCC | — | Qiao et al. (2016) |

*Notes: OC: ovarian carcinoma; NSCLC: non-small-cell lung carcinoma; EMT: epithelial-mesenchymal transition; HCC: hepatocellular carcinoma; BC: breast carcinoma; CRC: colorectal carcinoma; Akt: AKT Serine/Threonine Kinase; CC: cholangiocarcinoma; GC: gastric carcinoma; PCa: pancreatic carcinoma; IL6: Interleukin 6; EGFR: Epidermal Growth Factor Receptor; TGF-β: Transforming Growth Factor Beta; NF-κB: Nuclear Factor kappa B; EBV: Epstein-Barr virus; NPC: nasopharyngeal carcinoma.*

cells, and the overexpression of Notch3 may act as a biomarker for CSCs (See *Notch3 and Cancer Stem Cell Properties*). Notch3 signaling can regulate tumor resistance to chemotherapeutic drugs including doxorubicin, platinum, taxane, EGFR-TKIs, and gemcitabine, which is also dependent on CSCs (See *Notch3 and Drug Resistance*).

To maintain the stemness and proliferation of tumor cells, Notch3 signaling can activate the expression of downstream genes, such as cell cycle-related genes (CCND1, C-MYC and NF-kB1), antiapoptotic genes (SURVIVIN and BCL2), as well as stemness-related genes (OCT-4, ALDH1, NANOG, PBX1, CD44 and CD133) (Park et al., 2010; Man et al., 2012; McAuliffe et al., 2012; Alqudah et al., 2013; Jeong et al., 2017). In addition, there are several associations and cross-talk interactions between Notch3 signaling and other signaling pathways, mainly including the Wnt/β-catenin, Akt, IL6, EGFR, TGF-β and NF-κB signaling pathways, which affect several aspects of cancer cell behavior (**Table 3**). In tumor metastasis, Notch3 signaling was found to cascade the MMP, Wnt, Akt, IL6 and TGF-β signaling pathways, thereby promoting the invasion and EMT of tumor cells (See *Notch3 in Cancer EMT and Metastasis*). However, anti-EMT properties and mechanisms of Notch3 signaling were also found in BC, suggesting a controversial role of Notch3 in BC metastasis (Zhang et al., 2016b; Dou et al., 2017; Liang et al., 2018; Lin et al., 2018; Wen et al., 2018). Moreover, Notch3 signaling activated by cell-cell interactions between tumor cells and tumor ECs can promote tumor angiogenesis and vasculogenic mimicry (See *Notch3 and Tumor Angiogenesis*). These findings suggest that Notch3 has diverse, complex and wide-ranging roles in tumor cells.

To prevent the abnormal activation of Notch3 signaling in cancer, key Notch3-targeting strategies have been proposed and confirmed effective in pre-clinical studies, including the application of siRNAs/shRNAs, ncRNAs, antibodies, ADCs, and HDACi (See *Notch3-Targeting Strategies for Cancer Therapy*). Different mAbs against Notch3 can specially block Notch3 signaling. However, phase 2 clinical trials of the anti-Notch2/3 mAb drug tarextumab have showed poor efficacy, and the relevant clinical trials have been terminated (Daniel et al., 2017; Hu et al., 2019). Recently, bispecific mAbs targeting both Notch2/3 and EGFR/HER3 have been developed. The main advantage of these bispecific mAbs is that they can target/block both Notch3 and EGFR signaling, which reverses the activation of Notch3 signaling in response to EGFR-TKIs (Hu et al., 2017; Fu et al., 2019). The efficacy of bispecific mAbs may be worth testing in future clinical trials.

ADCs are novel drugs that can kill tumor cells which express specific target molecules. The first Notch3-targeting ADC drug PF06650808 has been evaluated in pre-clinical experiments and a phase 1 clinical trial. Although preliminary, the results demonstrate a manageable safety profile and early signs of anti-tumor activity in cancer patients (Geles et al., 2015; Rosen et al., 2020). Other Notch3-targeting strategies, such as siRNAs/shRNAs, non-coding RNAs and HDACi, have not been tested in clinical trials, so that their efficacy and safety in the treatment of cancer patients need to be evaluated in the future.

In order to develop Notch3-targeting methods/drugs for cancer treatment, the following potential strategies should be considered: 1) Inhibiting Notch3 gene expression using siRNAs, shRNAs, or ncRNAs. 2) Preventing the cleavage of Notch3 protein using small molecules such as using ADAM10 inhibitors (prevent S2 cleavage) and GSIs (prevent S3 cleavage). 3) Antibodies targeting

Notch3 protein. 4) Killing Notch3-positive tumor cells by ADCs. 5) Promoting Notch3 degradation by HDACi. Notably, Notch3-specific inhibitors such as antibodies and ADCs are more specific than pan-Notch inhibitors such as GSIs, which may merit further pre- and clinical evaluation.

In summary, Notch3 signaling affects cancer progression through complex molecular mechanisms. Future studies should investigate the relevant mechanisms and exact roles of Notch3 signaling in regulating different cancer behaviors (such as CSC properties, Epithelial-Mesenchymal Transition (EMT), metastasis, drug resistance and angiogenesis) in different tumor types. Furthermore, it is necessary to propose, establish and evaluate more potential Notch3-targeting methods/strategies for cancer treatment.

## AUTHOR CONTRIBUTIONS

MX wrote the manuscript. YW, BL, XW, FX, SC, LZ, BZ, and FH directed the project. All authors read and approved the manuscript.

## FUNDING

This work was supported by grants from the National Natural Science Foundation of China (81860259); Provincal Science foudation of Jiangxi (20202BABL206016); Youth Team Project of the Second Affiliated Hospital of Nanchang University (2019YNTD12003).

## REFERENCES

Alqudah, M. A. Y., Agarwal, S., Al-Keilani, M. S., Sibenaller, Z. A., Ryken, T. C., and Assem, M. (2013). NOTCH3 Is a Prognostic Factor that Promotes Glioma Cell Proliferation, Migration and Invasion via Activation of CCND1 and EGFR. *PLoS One* 8 (10), e77299, doi:10.1371/journal.pone.0077299

Arasada, R. R., Amann, J. M., Rahman, M. A., Huppert, S. S., and Carbone, D. P. (2014). EGFR Blockade Enriches for Lung Cancer Stem-like Cells through Notch3-dependent Signaling. *Cancer Res.* 74 (19), 5572–5584. doi:10.1158/0008-5472.Can-13-3724

Arasada, R. R., Shilo, K., Yamada, T., Zhang, J., Yano, S., Ghanem, R., et al. (2018). Notch3-dependent β-catenin Signaling Mediates EGFR TKI Drug Persistence in EGFR Mutant NSCLC. *Nat. Commun.* 9 (1), 3198. doi:10.1038/s41467-018-05626-2

Bellavia, D., Campese, A. F., Alesse, E., Vacca, A., Felli, M. P., Balestri, A., et al. (2000). Constitutive Activation of NF-kappaB and T-Cell Leukemia/lymphoma in Notch3 Transgenic Mice. *Embo j* 19 (13), 3337–3348. doi:10.1093/emboj/19.13.3337

Bellavia, D., Checquolo, S., Palermo, R., and Screpanti, I. (2018). The Notch3 Receptor and its Intracellular Signaling-dependent Oncogenic Mechanisms. *Adv. Exp. Med. Biol.* 1066, 205–222. doi:10.1007/978-3-319-89512-3_10

Bernasconi-Elias, P., Hu, T., Jenkins, D., Firestone, B., Gans, S., Kurth, E., et al. (2016). Characterization of Activating Mutations of NOTCH3 in T-Cell Acute Lymphoblastic Leukemia and Anti-leukemic Activity of NOTCH3 Inhibitory Antibodies. *Oncogene* 35 (47), 6077–6086. doi:10.1038/onc.2016.133

Bray, S. J. (2016). Notch Signalling in Context. *Nat. Rev. Mol. Cel Biol* 17 (11), 722–735. doi:10.1038/nrm.2016.94

Bray, S. J. (2006). Notch Signalling: a Simple Pathway Becomes Complex. *Nat. Rev. Mol. Cel Biol* 7 (9), 678–689. doi:10.1038/nrm2009

Brown, C. W., Brodsky, A. S., and Freiman, R. N. (2015). Notch3 Overexpression Promotes Anoikis Resistance in Epithelial Ovarian Cancer via Upregulation of COL4A2. *Mol. Cancer Res.* 13 (1), 78–85. doi:10.1158/1541-7786.Mcr-14-0334

Cai, H., Yao, J., An, Y., Chen, X., Chen, W., Wu, D., et al. (2017). LncRNA HOTAIR Acts as Competing Endogenous RNA to Control the Expression of Notch3 via Sponging miR-613 in Pancreatic Cancer. *Oncotarget* 8 (20), 32905–32917. doi:10.18632/oncotarget.16462

Cai, W. T., Guan, P., Lin, M. X., Fu, B., Wu, B., and Wu, J. (2020). MiRNA-206 Suppresses the Metastasis of Osteosarcoma via Targeting Notch3. *J. Biol. Regul. Homeost Agents* 34 (3), 775–783. doi:10.23812/20-72-a-26

Cancer Genome Atlas Research Network (2011). Integrated Genomic Analyses of Ovarian Carcinoma. *Nature* 474 (7353), 609–615. 10.1038/nature10166

Chau, C. H., Steeg, P. S., and Figg, W. D. (2019). Antibody-drug Conjugates for Cancer. *The Lancet* 394 (10200), 793–804. doi:10.1016/s0140-6736(19)31774-x

Chen, P.-H., Shen, W.-L., Shih, C.-M., Ho, K.-H., Cheng, C.-H., Lin, C.-W., et al. (2017). The CHAC1-Inhibited Notch3 Pathway Is Involved in Temozolomide-Induced Glioma Cytotoxicity. *Neuropharmacology* 116, 300–314. doi:10.1016/j.neuropharm.2016.12.011

Chen, X., Stoeck, A., Lee, S. J., Shih, I.-M., Wang, M. M., and Wang, T.-L. (2010). Jagged1 Expression Regulated by Notch3 and Wnt/β-Catenin Signaling Pathways in Ovarian Cancer. *Oncotarget* 1 (3), 210–218. doi:10.18632/oncotarget.127

Chen, Y. A., Cheng, L., Zhang, Y., Peng, L., and Yang, H. G. (2021). LncRNA RUSC1-AS1 Promotes the Proliferation of Hepatocellular Carcinoma Cells through Modulating NOTCH Signaling. *neo* 67 (6), 1204–1213. doi:10.4149/neo_2020_191010N1024

Cheng, R., Cai, X.-r., Ke, K., and Chen, Y.-l. (2017). Notch4 Inhibition Suppresses Invasion and Vasculogenic Mimicry Formation of Hepatocellular Carcinoma Cells. *Curr. Med. Sci.* 37 (5), 719–725. doi:10.1007/s11596-017-1794-9

Cheung, C. C.-M., Lun, S. W.-M., Chung, G. T.-Y., Chow, C., Lo, C., Choy, K.-W., et al. (2016a). MicroRNA-183 Suppresses Cancer Stem-like Cell Properties in EBV-Associated Nasopharyngeal Carcinoma. *BMC Cancer* 16, 495. doi:10.1186/s12885-016-2525-5

Cheung, C. M., Lun, W. M., Chung, T. Y., Chow, C., Lo, C., Choy, K. W., et al. (2016b). MicroRNA-183 Suppresses Cancer Stem-like Cell Properties in EBV-Associated Nasopharyngeal Carcinoma. *Bmc Cancer* 16 (1), 495. doi:10.1186/s12885-016-2525-5

Daniel, D. B., Rudin, C. M., Hart, L., Spigel, D. R., Edelman, M. J., Goldschmidt, J., et al. (2017). Results of a Randomized, Placebo-Controlled, Phase 2 Study of Tarextumab (TRXT, Anti-notch2/3) in Combination with Etoposide and Platinum (EP) in Patients (Pts) with Untreated Extensive-Stage Small-Cell Lung Cancer (ED-SCLC). *Ann. Oncol.* 28, v540–v542. doi:10.1093/annonc/mdx386.004

Dawood, S., Austin, L., and Cristofanilli, M. (2014). Cancer Stem Cells: Implications for Cancer Therapy. *Oncology (Williston Park)* 28 (12), 1101–1110. 25510809

Diluvio, G., Del Gaudio, F., Giuli, M. V., Franciosa, G., Giuliani, E., Palermo, R., et al. (2018). NOTCH3 Inactivation Increases Triple Negative Breast Cancer Sensitivity to Gefitinib by Promoting EGFR Tyrosine Dephosphorylation and its Intracellular Arrest. *Oncogenesis* 7 (5), 42. doi:10.1038/s41389-018-0051-9

Dou, X.-W., Liang, Y.-K., Lin, H.-Y., Wei, X.-L., Zhang, Y.-Q., Bai, J.-W., et al. (2017). Notch3 Maintains Luminal Phenotype and Suppresses Tumorigenesis and Metastasis of Breast Cancer via Trans-activating Estrogen Receptor-α. *Theranostics* 7 (16), 4041–4056. doi:10.7150/thno.19989

Etemadmoghadam, D., deFazio, A., Beroukhim, R., Mermel, C., George, J., Getz, G., et al. (2009). Integrated Genome-wide DNA Copy Number and Expression Analysis Identifies Distinct Mechanisms of Primary Chemoresistance in Ovarian Carcinomas. *Clin. Cancer Res.* 15 (4), 1417–1427. doi:10.1158/1078-0432.Ccr-08-1564

Eto, K., Kawakami, H., Kuwatani, M., Kudo, T., Abe, Y., Kawahata, S., et al. (2013). Human Equilibrative Nucleoside Transporter 1 and Notch3 Can Predict Gemcitabine Effects in Patients with Unresectable Pancreatic Cancer. *Br. J. Cancer* 108 (7), 1488–1494. doi:10.1038/bjc.2013.108

Fan, Q., Zhang, W., Emerson, R. E., and Xu, Y. (2020). ZIP4 Is a Novel Cancer Stem Cell Marker in High-Grade Serous Ovarian Cancer. *Cancers* 12 (12), 3692. doi:10.3390/cancers12123692

Fang, C.-H., Lin, Y.-T., Liang, C.-M., and Liang, S.-M. (2020). A Novel C-Kit/phospho-Prohibitin axis Enhances Ovarian Cancer Stemness and Chemoresistance via Notch3-PBX1 and β-catenin-ABCG2 Signaling. *J. Biomed. Sci.* 27 (1), 42. doi:10.1186/s12929-020-00638-x

Fu, W., Lei, C., Yu, Y., Liu, S., Li, T., Lin, F., et al. (2019). EGFR/Notch Antagonists Enhance the Response to Inhibitors of the PI3K-Akt Pathway by Decreasing Tumor-Initiating Cell Frequency. *Clin. Cancer Res.* 25 (9), 2835–2847. doi:10.1158/1078-0432.Ccr-18-2732

Furukawa, S., Kawasaki, Y., Miyamoto, M., Hiyoshi, M., Kitayama, J., and Akiyama, T. (2013). The miR-1-NOTCH3-Asef Pathway Is Important for Colorectal Tumor Cell Migration. *PLoS One* 8 (11), e80609. doi:10.1371/journal.pone.0080609

Ganguly, S. S., Hostetter, G., Tang, L., Frank, S. B., Saboda, K., Mehra, R., et al. (2020). Notch3 Promotes Prostate Cancer-Induced Bone Lesion Development via MMP-3. *Oncogene* 39 (1), 204–218. doi:10.1038/s41388-019-0977-1

Geles, K. G., Gao, Y., Sridharan, L., Giannakou, A., Yamin, T.-T., Golas, J., et al. (2015). Abstract 1697: Therapeutic Targeting the NOTCH3 Receptor with Antibody Drug Conjugates. *Cancer Res.* 75, 1697. doi:10.1158/1538-7445.AM2015-1697

Gharaibeh, L., Elmadany, N., Alwosaibai, K., and Alshaer, W. (2020). Notch1 in Cancer Therapy: Possible Clinical Implications and Challenges. *Mol. Pharmacol.* 98 (5), 559–576. doi:10.1124/molpharm.120.000006

Giovannini, C., Bolondi, L., and Gramantieri, L. (2016). Targeting Notch3 in Hepatocellular Carcinoma: Molecular Mechanisms and Therapeutic Perspectives. *Ijms* 18 (1), 56. doi:10.3390/ijms18010056

Giovannini, C., Gramantieri, L., Chieco, P., Minguzzi, M., Lago, F., Pianetti, S., et al. (2009). Selective Ablation of Notch3 in HCC Enhances Doxorubicin's Death Promoting Effect by a P53 Dependent Mechanism. *J. Hepatol.* 50 (5), 969–979. doi:10.1016/j.jhep.2008.12.032

Giuli, M. V., Giuliani, E., Screpanti, I., Bellavia, D., and Checquolo, S. (2019). Notch Signaling Activation as a Hallmark for Triple-Negative Breast Cancer Subtype. *J. Oncol.* 2019, 1–15. doi:10.1155/2019/8707053

Groeneweg, J. W., DiGloria, C. M., Yuan, J., Richardson, W. S., Growdon, W. B., Sathyanarayanan, S., et al. (2014). Inhibition of Notch Signaling in Combination with Paclitaxel Reduces Platinum-Resistant Ovarian Tumor Growth. *Front. Oncol.* 4, 171. doi:10.3389/fonc.2014.00171

Guest, R. V., Boulter, L., Dwyer, B. J., Kendall, T. J., Man, T.-Y., Minnis-Lyons, S. E., et al. (2016). Notch3 Drives Development and Progression of Cholangiocarcinoma. *Proc. Natl. Acad. Sci. USA* 113 (43), 12250–12255. doi:10.1073/pnas.1600067113

Hassan, W. A., Yoshida, R., Kudoh, S., Motooka, Y., and Ito, T. (2016). Evaluation of Role of Notch3 Signaling Pathway in Human Lung Cancer Cells. *J. Cancer Res. Clin. Oncol.* 142 (5), 981–993. doi:10.1007/s00432-016-2117-4

He, F., Du, T., Jiang, Q., and Zhang, Y. (2017). Synergistic Effect of Notch-3-specific Inhibition and Paclitaxel in Non-small Cell Lung Cancer (NSCLC) Cells via Activation of the Intrinsic Apoptosis Pathway. *Med. Sci. Monit.* 23, 3760–3769. doi:10.12659/msm.902641

Hsu, M.-Y., Yang, M. H., Schnegg, C. I., Hwang, S., Ryu, B., and Alani, R. M. (2017). Notch3 Signaling-Mediated Melanoma-Endothelial Crosstalk Regulates Melanoma Stem-like Cell Homeostasis and Niche Morphogenesis. *Lab. Invest.* 97 (6), 725–736. doi:10.1038/labinvest.2017.1

Hu, B. D., Guo, J., Ye, Y. Z., Du, T., Cheng, C. S., Jiang, Q., et al. (2018). Specific Inhibitor of Notch-3 Enhances the Sensitivity of NSCLC Cells to Gemcitabine. *Oncol. Rep.* 40 (1), 155–164. doi:10.3892/or.2018.6448

Hu, L., Xue, F., Shao, M., Deng, A., and Wei, G. (2013). Aberrant Expression of Notch3 Predicts Poor Survival for Hepatocellular Carcinomas. *Biosci. Trends* 7 (3), 152–156.

Hu, S., Fu, W., Li, T., Yuan, Q., Wang, F., Lv, G., et al. (2017). Antagonism of EGFR and Notch Limits Resistance to EGFR Inhibitors and Radiation by Decreasing Tumor-Initiating Cell Frequency. *Sci. Transl. Med.* 9 (380), eaag0339. doi:10.1126/scitranslmed.aag0339

Hu, W., Liu, T., Ivan, C., Sun, Y., Huang, J., Mangala, L. S., et al. (2014). Notch3 Pathway Alterations in Ovarian Cancer. *Cancer Res.* 74 (12), 3282–3293. doi:10.1158/0008-5472.Can-13-2066

Hu, Z. I., Bendell, J. C., Bullock, A., LoConte, N. K., Hatoum, H., Ritch, P., et al. (2019). A Randomized Phase II Trial of Nab-paclitaxel and Gemcitabine with Tarextumab or Placebo in Patients with Untreated Metastatic Pancreatic Cancer. *Cancer Med.* 8 (11), 5148–5157. doi:10.1002/cam4.2425

Jaskula-Sztul, R., Eide, J., Tesfazghi, S., Dammalapati, A., Harrison, A. D., Yu, X.-M., et al. (2015). Tumor-suppressor Role of Notch3 in Medullary Thyroid Carcinoma Revealed by Genetic and Pharmacological Induction. *Mol. Cancer Ther.* 14 (2), 499–512. doi:10.1158/1535-7163.Mct-14-0073

Jenke, R., Reßing, N., Hansen, F. K., Aigner, A., and Büch, T. (2021). Anticancer Therapy with HDAC Inhibitors: Mechanism-Based Combination Strategies and Future Perspectives. *Cancers* 13 (4), 634. doi:10.3390/cancers13040634

Jeong, J.-Y., Kang, H., Kim, T. H., Kim, G., Heo, J.-H., Kwon, A.-Y., et al. (2017). MicroRNA-136 Inhibits Cancer Stem Cell Activity and Enhances the Anti-tumor Effect of Paclitaxel against Chemoresistant Ovarian Cancer Cells by Targeting Notch3. *Cancer Lett.* 386, 168–178. doi:10.1016/j.canlet.2016.11.017

Kang, H., Jeong, J.-Y., Song, J.-Y., Kim, T. H., Kim, G., Huh, J. H., et al. (2016). Notch3-specific Inhibition Using siRNA Knockdown or GSI Sensitizes Paclitaxel-Resistant Ovarian Cancer Cells. *Mol. Carcinog.* 55 (7), 1196–1209. doi:10.1002/mc.22363

Kang, W., Zhang, J., Huang, T., Zhou, Y., Wong, C. C., Chan, R. C. K., et al. (2021). NOTCH3, a Crucial Target of miR-491-5p/miR-875-5p, Promotes Gastric Carcinogenesis by Upregulating PHLDB2 Expression and Activating Akt Pathway. *Oncogene* 40, 1578–1594. doi:10.1038/s41388-020-01579-3

Katoh, M., and Katoh, M. (2020). Precision Medicine for Human Cancers with Notch Signaling Dysregulation (Review). *Int. J. Mol. Med.* 45 (2), 279–297. doi:10.3892/ijmm.2019.4418

Kayamori, K., Katsube, K.-i., Sakamoto, K., Ohyama, Y., Hirai, H., Yukimori, A., et al. (2016). NOTCH3 Is Induced in Cancer-Associated Fibroblasts and Promotes Angiogenesis in Oral Squamous Cell Carcinoma. *PLoS One* 11 (4), e0154112. doi:10.1371/journal.pone.0154112

Kim, A. R., and Gu, M. J. (2019). The Clinicopathologic Significance of Notch3 Expression in Prostate Cancer. *Int. J. Clin. Exp. Pathol.* 12 (9), 3535–3541. 31934201

Kim, M. J., Kim, A.-R., Jeong, J.-Y., Kim, K.-i., Kim, T.-H., Lee, C., et al. (2017a). Correlation of ALDH1 and Notch3 Expression: Clinical Implication in Ovarian Carcinomas. *J. Cancer* 8 (16), 3331–3342. doi:10.7150/jca.18955

Kim, T. H., Jeong, J.-Y., Park, J.-Y., Kim, S.-W., Heo, J. H., Kang, H., et al. (2017b). miR-150 Enhances Apoptotic and Anti-tumor Effects of Paclitaxel in Paclitaxel-Resistant Ovarian Cancer Cells by Targeting Notch3. *Oncotarget* 8 (42), 72788–72800. doi:10.18632/oncotarget.20348

Kopan, R., and Ilagan, M. X. G. (2009). The Canonical Notch Signaling Pathway: Unfolding the Activation Mechanism. *Cell* 137 (2), 216–233. doi:10.1016/j.cell.2009.03.045

Leontovich, A. A., Jalalirad, M., Salisbury, J. L., Mills, L., Haddox, C., Schroeder, M., et al. (2018). NOTCH3 Expression Is Linked to Breast Cancer Seeding and Distant Metastasis. *Breast Cancer Res.* 20 (1), 105. doi:10.1186/s13058-018-1020-0

Li, C., Song, G., Zhang, S., Wang, E., and Cui, Z. (2015). Wnt3a Increases the Metastatic Potential of Non-small Cell Lung Cancer Cells *In Vitro* in Part via its Upregulation of Notch3. *Oncol. Rep.* 33 (3), 1207–1214. doi:10.3892/or.2014.3700

Li, C., Zhang, S., Lu, Y., Zhang, Y., Wang, E., and Cui, Z. (2013). The Roles of Notch3 on the Cell Proliferation and Apoptosis Induced by CHIR99021 in NSCLC Cell Lines: a Functional Link between Wnt and Notch Signaling Pathways. *PLoS One* 8 (12), e84659. doi:10.1371/journal.pone.0084659

Li, C., Zhang, Y., Lu, Y., Cui, Z., Yu, M., Zhang, S., et al. (2011). Evidence of the Cross Talk between Wnt and Notch Signaling Pathways in Non-small-cell Lung Cancer (NSCLC): Notch3-siRNA Weakens the Effect of LiCl on the Cell Cycle of NSCLC Cell Lines. *J. Cancer Res. Clin. Oncol.* 137 (5), 771–778. doi:10.1007/s00432-010-0934-4

Li, H., Zhang, W., Niu, C., Lin, C., Wu, X., Jian, Y., et al. (2019). Nuclear Orphan Receptor NR2F6 Confers Cisplatin Resistance in Epithelial Ovarian Cancer Cells by Activating the Notch3 Signaling Pathway. *Int. J. Cancer* 145 (7), 1921–1934. doi:10.1002/ijc.32293

Li, K., Li, Y., Wu, W., Gordon, W. R., Chang, D. W., Lu, M., et al. (2008). Modulation of Notch Signaling by Antibodies Specific for the Extracellular Negative Regulatory Region of NOTCH3. *J. Biol. Chem.* 283 (12), 8046–8054. doi:10.1074/jbc.M800170200

Liang, Y.-K., Lin, H.-Y., Dou, X.-W., Chen, M., Wei, X.-L., Zhang, Y.-Q., et al. (2018). MiR-221/222 Promote Epithelial-Mesenchymal Transition by

Targeting Notch3 in Breast Cancer Cell Lines. *NPJ Breast Cancer* 4, 20. doi:10.1038/s41523-018-0073-7

Lin, H.-Y., Liang, Y.-K., Dou, X.-W., Chen, C.-F., Wei, X.-L., Zeng, D., et al. (2018). Notch3 Inhibits Epithelial-Mesenchymal Transition in Breast Cancer via a Novel Mechanism, Upregulation of GATA-3 Expression. *Oncogenesis* 7 (8), 59. doi:10.1038/s41389-018-0069-z

Lin, S., Negulescu, A., Bulusu, S., Gibert, B., Delcros, J.-G., Ducarouge, B., et al. (2017). Non-canonical NOTCH3 Signalling Limits Tumour Angiogenesis. *Nat. Commun.* 8, 16074. doi:10.1038/ncomms16074

Liu, C., Liu, L., Chen, X., Cheng, J., Zhang, H., Zhang, C., et al. (2018). LSD1 Stimulates Cancer-Associated Fibroblasts to Drive Notch3-dependent Self-Renewal of Liver Cancer Stem-like Cells. *Cancer Res.* 78 (4), 938–949. doi:10.1158/0008-5472.Can-17-1236

Liu, L., Chen, X., Wang, Y., Qu, Z., Lu, Q., Zhao, J., et al. (2014a). Notch3 Is Important for TGF-β-Induced Epithelial-Mesenchymal Transition in Non-small Cell Lung Cancer Bone Metastasis by Regulating ZEB-1. *Cancer Gene Ther.* 21 (9), 364–372. doi:10.1038/cgt.2014.39

Liu, L., Yang, Z.-l., Wang, C., Miao, X., Liu, Z., Li, D., et al. (2016a). The Expression of Notch 1 and Notch 3 in Gallbladder Cancer and Their Clinicopathological Significance. *Pathol. Oncol. Res.* 22 (3), 483–492. doi:10.1007/s12253-015-0019-4

Liu, W., Xu, C., Wan, H., Liu, C., Wen, C., Lu, H., et al. (2014b). MicroRNA-206 Overexpression Promotes Apoptosis, Induces Cell Cycle Arrest and Inhibits the Migration of Human Hepatocellular Carcinoma HepG2 Cells. *Int. J. Mol. Med.* 34 (2), 420–428. doi:10.3892/ijmm.2014.1800

Liu, Z., Yun, R., Yu, X., Hu, H., Huang, G., Tan, B., et al. (2016b). Overexpression of Notch3 and pS6 Is Associated with Poor Prognosis in Human Ovarian Epithelial Cancer. *Mediators Inflamm.* 2016, 1–6. doi:10.1155/2016/5953498

Ma, Y., Li, M., Si, J., Xiong, Y., Lu, F., Zhang, J., et al. (2016). Blockade of Notch3 Inhibits the Stem-like Property and Is Associated with ALDH1A1 and CD44 via Autophagy in Non-small Lung Cancer. *Int. J. Oncol.* 48 (6), 2349–2358. doi:10.3892/ijo.2016.3464

Majumder, S., Crabtree, J. S., Golde, T. E., Minter, L. M., Osborne, B. A., and Miele, L. (2021). Targeting Notch in Oncology: the Path Forward. *Nat. Rev. Drug Discov.* 20 (2), 125–144. doi:10.1038/s41573-020-00091-3

Man, C.-H., Wei-Man Lun, S., Wai-Ying Hui, J., To, K.-F., Choy, K.-W., Wing-Hung Chan, A., et al. (2012). Inhibition of NOTCH3 Signalling Significantly Enhances Sensitivity to Cisplatin in EBV-Associated Nasopharyngeal Carcinoma. *J. Pathol.* 226 (3), 471–481. doi:10.1002/path.2997

Mann, C. D., Bastianpillai, C., Neal, C. P., Masood, M. M., Jones, D. J. L., Teichert, F., et al. (2012). Notch3 and HEY-1 as Prognostic Biomarkers in Pancreatic Adenocarcinoma. *PLoS One* 7 (12), e51119. doi:10.1371/journal.pone.0051119

Mansour, F. A., Al-Mazrou, A., Al-Mohanna, F., Al-Alwan, M., and Ghebeh, H. (2020). PD-L1 Is Overexpressed on Breast Cancer Stem Cells through notch3/mTOR axis. *Oncoimmunology* 9 (1), 1729299. doi:10.1080/2162402x.2020.1729299

McAuliffe, S. M., Morgan, S. L., Wyant, G. A., Tran, L. T., Muto, K. W., Chen, Y. S., et al. (2012). Targeting Notch, a Key Pathway for Ovarian Cancer Stem Cells, Sensitizes Tumors to Platinum Therapy. *Proc. Natl. Acad. Sci.* 109 (43), E2939–E2948. doi:10.1073/pnas.1206400109

Michishita, M., Akiyoshi, R., Yoshimura, H., Katsumoto, T., Ichikawa, H., Ohkusu-Tsukada, K., et al. (2011). Characterization of Spheres Derived from Canine Mammary Gland Adenocarcinoma Cell Lines. *Res. Vet. Sci.* 91 (2), 254–260. doi:10.1016/j.rvsc.2010.11.016

Milano, J., McKay, J., Dagenais, C., Foster-Brown, L., Pognan, F., Gadient, R., et al. (2004). Modulation of Notch Processing by γ-Secretase Inhibitors Causes Intestinal Goblet Cell Metaplasia and Induction of Genes Known to Specify Gut Secretory Lineage Differentiation. *Toxicol. Sci.* 82 (1), 341–358. doi:10.1093/toxsci/kfh254

Morgan, K. M., Fischer, B. S., Lee, F. Y., Shah, J. J., Bertino, J. R., Rosenfeld, J., et al. (2017). Gamma Secretase Inhibition by BMS-906024 Enhances Efficacy of Paclitaxel in Lung Adenocarcinoma. *Mol. Cancer Ther.* 16 (12), 2759–2769. doi:10.1158/1535-7163.Mct-17-0439

O'Reilly, E. M., Smith, L. S., Bendell, J. C., Strickler, J. H., Zalupski, M., Gluck, W., et al. (2015). Final Results of Phase Ib of Anticancer Stem Cell Antibody Tarextumab (OMP-59R5, TRXT, Anti-notch 2/3) in Combination with Nab-Paclitaxel and Gemcitabine (Nab-P+Gem) in Patients (Pts) with Untreated Metastatic Pancreatic Cancer (mPC). *Jco* 33 (3_Suppl. l), 278. doi:10.1200/jco.2015.33.3_suppl.278

Ozawa, T., Kazama, S., Akiyoshi, T., Murono, K., Yoneyama, S., Tanaka, T., et al. (2014). Nuclear Notch3 Expression Is Associated with Tumor Recurrence in Patients with Stage II and III Colorectal Cancer. *Ann. Surg. Oncol.* 21 (8), 2650–2658. doi:10.1245/s10434-014-3659-9

Palermo, R., Checquolo, S., Giovenco, A., Grazioli, P., Kumar, V., Campese, A. F., et al. (2012). Acetylation Controls Notch3 Stability and Function in T-Cell Leukemia. *Oncogene* 31 (33), 3807–3817. doi:10.1038/onc.2011.533

Papadakos, K. S., Bartoschek, M., Rodriguez, C., Gialeli, C., Jin, S.-B., Lendahl, U., et al. (2019). Cartilage Oligomeric Matrix Protein Initiates Cancer Stem Cells through Activation of Jagged1-Notch3 Signaling. *Matrix Biol.* 81, 107–121. doi:10.1016/j.matbio.2018.11.007

Park, J. T., Chen, X., Tropè, C. G., Davidson, B., Shih, I.-M., and Wang, T.-L. (2010). Notch3 Overexpression Is Related to the Recurrence of Ovarian Cancer and Confers Resistance to Carboplatin. *Am. J. Pathol.* 177 (3), 1087–1094. doi:10.2353/ajpath.2010.100316

Park, J. T., Li, M., Nakayama, K., Mao, T.-L., Davidson, B., Zhang, Z., et al. (2006). Notch3 Gene Amplification in Ovarian Cancer. *Cancer Res.* 66 (12), 6312–6318. doi:10.1158/0008-5472.Can-05-3610

Pastò, A., Serafin, V., Pilotto, G., Lago, C., Bellio, C., Trusolino, L., et al. (2014). NOTCH3 Signaling Regulates MUSASHI-1 Expression in Metastatic Colorectal Cancer Cells. *Cancer Res.* 74 (7), 2106–2118. doi:10.1158/0008-5472.Can-13-2022

Pei, Y., Li, K., Lou, X., Wu, Y., Dong, X., Wang, W., et al. (2020). miR-1299/NOTCH3/TUG1 Feedback Loop Contributes to the Malignant Proliferation of Ovarian Cancer. *Oncol. Rep.* 44 (2), 438–448. doi:10.3892/or.2020.7623

Pekkonen, P., Alve, S., Balistreri, G., Gramolelli, S., Tatti-Bugaeva, O., Paatero, I., et al. (2018). Lymphatic Endothelium Stimulates Melanoma Metastasis and Invasion via MMP14-dependent Notch3 and β1-integrin Activation. *Elife* 7, e32490. doi:10.7554/eLife.32490

Pinazza, M., Ghisi, M., Minuzzo, S., Agnusdei, V., Fossati, G., Ciminale, V., et al. (2018). Histone Deacetylase 6 Controls Notch3 Trafficking and Degradation in T-Cell Acute Lymphoblastic Leukemia Cells. *Oncogene* 37 (28), 3839–3851. doi:10.1038/s41388-018-0234-z

Price, J. C., Azizi, E., Naiche, L. A., Parvani, J. G., Shukla, P., Kim, S., et al. (2020). Notch3 Signaling Promotes Tumor Cell Adhesion and Progression in a Murine Epithelial Ovarian Cancer Model. *PLoS One* 15 (6), e0233962. doi:10.1371/journal.pone.0233962

Qiao, J., Liu, J., Jia, K., Li, N., Liu, B., Zhang, Q., et al. (2016). Diosmetin Triggers Cell Apoptosis by Activation of the p53/Bcl-2 Pathway and Inactivation of the Notch3/NF-Kb Pathway in HepG2 Cells. *Oncol. Lett.* 12 (6), 5122–5128. doi:10.3892/ol.2016.5347

Rahman, M. T., Nakayama, K., Rahman, M., Katagiri, H., Katagiri, A., Ishibashi, T., et al. (2012). Notch3 Overexpression as Potential Therapeutic Target in Advanced Stage Chemoresistant Ovarian Cancer. *Am. J. Clin. Pathol.* 138 (4), 535–544. doi:10.1309/ajcpkdlrq8f3ewns

Rao, D. D., Vorhies, J. S., Senzer, N., and Nemunaitis, J. (2009). siRNA vs. shRNA: Similarities and Differences. *Adv. Drug Deliv. Rev.* 61 (9), 746–759. doi:10.1016/j.addr.2009.04.004

Rosen, L. S., Wesolowski, R., Baffa, R., Liao, K.-H., Hua, S. Y., Gibson, B. L., et al. (2020). A Phase I, Dose-Escalation Study of PF-06650808, an Anti-notch3 Antibody-Drug Conjugate, in Patients with Breast Cancer and Other Advanced Solid Tumors. *Invest. New Drugs* 38 (1), 120–130. doi:10.1007/s10637-019-00754-y

Sansone, P., Ceccarelli, C., Berishaj, M., Chang, Q., Rajasekhar, V. K., Perna, F., et al. (2016). Self-renewal of CD133hi Cells by IL6/Notch3 Signalling Regulates Endocrine Resistance in Metastatic Breast Cancer. *Nat. Commun.* 7, 10442. doi:10.1038/ncomms10442

Serafin, V., Persano, L., Moserle, L., Esposito, G., Ghisi, M., Curtarello, M., et al. (2011). Notch3 Signalling Promotes Tumour Growth in Colorectal Cancer. *J. Pathol.* 224 (4), 448–460. doi:10.1002/path.2895

Shih, I.-M., and Wang, T.-L. (2007). Notch Signaling, γ-Secretase Inhibitors, and Cancer Therapy: Figure 1. *Cancer Res.* 67 (5), 1879–1882. doi:10.1158/0008-5472.Can-06-3958

Smith, D. C., Chugh, R., Patnaik, A., Papadopoulos, K. P., Wang, M., Kapoun, A. M., et al. (2019). A Phase 1 Dose Escalation and Expansion Study of

Tarextumab (OMP-59R5) in Patients with Solid Tumors. *Invest. New Drugs* 37 (4), 722–730. doi:10.1007/s10637-018-0714-6

Song, G., Zhang, Y., and Wang, L. (2009). MicroRNA-206 Targets Notch3, Activates Apoptosis, and Inhibits Tumor Cell Migration and Focus Formation. *J. Biol. Chem.* 284 (46), 31921–31927. doi:10.1074/jbc.M109.046862

Sullivan, J. P., Spinola, M., Dodge, M., Raso, M. G., Behrens, C., Gao, B., et al. (2010). Aldehyde Dehydrogenase Activity Selects for Lung Adenocarcinoma Stem Cells Dependent on Notch Signaling. *Cancer Res.* 70 (23), 9937–9948. doi:10.1158/0008-5472.Can-10-0881

Tang, J., Zhu, Y., Xie, K., Zhang, X., Zhi, X., Wang, W., et al. (2016). The Role of the AMOP Domain in MUC4/Y-Promoted Tumour Angiogenesis and Metastasis in Pancreatic Cancer. *J. Exp. Clin. Cancer Res.* 35 (1), 91. doi:10.1186/s13046-016-0369-0

Tang, X., Cao, Y., Peng, D., Zhao, G., Zeng, Y., Gao, Z., et al. (2019). Overexpression of Notch3 Is Associated with Metastasis and Poor Prognosis in Osteosarcoma Patients. *Cmar* 11, 547–559. doi:10.2147/cmar.S185495

Tiyanont, K., Wales, T. E., Siebel, C. W., Engen, J. R., and Blacklow, S. C. (2013). Insights into Notch3 Activation and Inhibition Mediated by Antibodies Directed against its Negative Regulatory Region. *J. Mol. Biol.* 425 (17), 3192–3204. doi:10.1016/j.jmb.2013.05.025

Tzeng, T. J., Cao, L., Fu, Y., Zeng, H., and Cheng, W.-H. (2014). Methylseleninic Acid Sensitizes Notch3-Activated OVCA429 Ovarian Cancer Cells to Carboplatin. *PLoS One* 9 (7), e101664. doi:10.1371/journal.pone.0101664

Ulasov, I. V., Mijanovic, O., Savchuk, S., Gonzalez-Buendia, E., Sonabend, A., Xiao, T., et al. (2020). TMZ Regulates GBM stemnessviaMMP14-DLL4-Notch3 Pathway. *Int. J. Cancer* 146 (8), 2218–2228. doi:10.1002/ijc.32636

Vacca, A., Felli, M. P., Palermo, R., Di Mario, G., Calce, A., Di Giovine, M., et al. (2006). Notch3 and Pre-TCR Interaction Unveils Distinct NF-Kb Pathways in T-Cell Development and Leukemia. *Embo j* 25 (5), 1000–1008. doi:10.1038/sj.emboj.7600996

van Es, J. H., van Gijn, M. E., Riccio, O., van den Born, M., Vooijs, M., Begthel, H., et al. (2005). Notch/γ-secretase Inhibition Turns Proliferative Cells in Intestinal Crypts and Adenomas into Goblet Cells. *Nature* 435 (7044), 959–963. doi:10.1038/nature03659

Varga, J., Nicolas, A., Petrocelli, V., Pesic, M., Mahmoud, A., Michels, B. E., et al. (2020). AKT-dependent NOTCH3 Activation Drives Tumor Progression in a Model of Mesenchymal Colorectal Cancer. *J. Exp. Med.* 217 (10). e20191515. doi:10.1084/jem.20191515

Vishnoi, A., and Rani, S. (2017). MiRNA Biogenesis and Regulation of Diseases: An Overview. *Methods Mol. Biol.* 1509, 1–10. doi:10.1007/978-1-4939-6524-3_1

Wang, D., Xu, J., Liu, B., He, X., Zhou, L., Hu, X., et al. (2018a). IL6 Blockade Potentiates the Anti-tumor Effects of γ-secretase Inhibitors in Notch3-Expressing Breast Cancer. *Cell Death Differ* 25 (2), 330–339. doi:10.1038/cdd.2017.162

Wang, W., Chen, D., and Zhu, K. (2018b). SOX2OT Variant 7 Contributes to the Synergistic Interaction between EGCG and Doxorubicin to Kill Osteosarcoma via Autophagy and Stemness Inhibition. *J. Exp. Clin. Cancer Res.* 37 (1), 37. doi:10.1186/s13046-018-0689-3

Wang, X.-W., Xi, X.-Q., Wu, J., Wan, Y.-Y., Hui, H.-X., and Cao, X.-F. (2015). MicroRNA-206 Attenuates Tumor Proliferation and Migration Involving the Downregulation of NOTCH3 in Colorectal Cancer. *Oncol. Rep.* 33 (3), 1402–1410. doi:10.3892/or.2015.3731

Wen, X.-F., Chen, M., Wu, Y., Chen, M.-N., Glogowska, A., Klonisch, T., et al. (2018). Inhibitor of DNA Binding 2 Inhibits Epithelial-Mesenchymal Transition via Up-Regulation of Notch3 in Breast Cancer. *Translational Oncol.* 11 (5), 1259–1270. doi:10.1016/j.tranon.2018.07.015

Xiao, Y., Ye, Y., Zou, X., Jones, S., Yearsley, K., Shetuni, B., et al. (2011). The Lymphovascular Embolus of Inflammatory Breast Cancer Exhibits a Notch 3 Addiction. *Oncogene* 30 (3), 287–300. doi:10.1038/onc.2010.405

Xie, T., Li, Y., Li, S.-L., and Luo, H.-F. (2016). Astragaloside IV Enhances Cisplatin Chemosensitivity in Human Colorectal Cancer via Regulating NOTCH3. *Oncol. Res.* 24 (6), 447–453. doi:10.3727/096504016x14685034103590

Xiu, M.-x., Liu, Y.-m., and Kuang, B.-h. (2020a). The Oncogenic Role of Jagged1/Notch Signaling in Cancer. *Biomed. Pharmacother.* 129, 110416. doi:10.1016/j.biopha.2020.110416

Xiu, M.-X., Liu, Y.-M., and Kuang, B.-h. (2020b). The Role of DLLs in Cancer: A Novel Therapeutic Target. *Ott* 13, 3881–3901. doi:10.2147/ott.S244860

Xiu, M. X., and Liu, Y. M. (2019). The Role of Oncogenic Notch2 Signaling in Cancer: a Novel Therapeutic Target. *Am. J. Cancer Res.* 9 (5), 837–854.

Xu, Y., Miao, C., Jin, C., Qiu, C., Li, Y., Sun, X., et al. (2018). SUSD2 Promotes Cancer Metastasis and Confers Cisplatin Resistance in High Grade Serous Ovarian Cancer. *Exp. Cel Res.* 363 (2), 160–170. doi:10.1016/j.yexcr.2017.12.029

Xu, Y., Zhang, Q., Miao, C., Dongol, S., Li, Y., Jin, C., et al. (2019). CCNG1 (Cyclin G1) Regulation by Mutant-P53 via Induction of Notch3 Expression Promotes High-Grade Serous Ovarian Cancer (HGSOC) Tumorigenesis and Progression. *Cancer Med.* 8 (1), 351–362. doi:10.1002/cam4.1812

Xue, S., He, L., Zhang, X., Zhou, J., Li, F., and Wang, X. (2017). Expression of Jagged1/Notch3 Signaling Pathway and Their Relationship with the Tumor Angiogenesis in TNBC. *Arch. Med. Res.* 48 (2), 169–179. doi:10.1016/j.arcmed.2017.03.014

Yao, J., and Qian, C. (2010). Inhibition of Notch3 Enhances Sensitivity to Gemcitabine in Pancreatic Cancer through an Inactivation of PI3K/Akt-dependent Pathway. *Med. Oncol.* 27 (3), 1017–1022. doi:10.1007/s12032-009-9326-5

Yao, Y., Chen, X., Yang, H., Chen, W., Qian, Y., Yan, Z., et al. (2019). Hsa_circ_0058124 Promotes Papillary Thyroid Cancer Tumorigenesis and Invasiveness through the NOTCH3/GATAD2A axis. *J. Exp. Clin. Cancer Res.* 38 (1), 318. doi:10.1186/s13046-019-1321-x

Ye, Y.-z., Zhang, Z.-h., Fan, X.-y., Xu, X.-l., Chen, M.-l., Chang, B.-w., et al. (2013). Notch3 Overexpression Associates with Poor Prognosis in Human Non-small-cell Lung Cancer. *Med. Oncol.* 30 (2), 595. doi:10.1007/s12032-013-0595-7

Yen, W.-C., Fischer, M. M., Axelrod, F., Bond, C., Cain, J., Cancilla, B., et al. (2015). Targeting Notch Signaling with a Notch2/Notch3 Antagonist (Tarextumab) Inhibits Tumor Growth and Decreases Tumor-Initiating Cell Frequency. *Clin. Cancer Res.* 21 (9), 2084–2095. doi:10.1158/1078-0432.Ccr-14-2808

Yu, T., Han, C., Zhu, G., Liao, X., Qin, W., Yang, C., et al. (2017). Prognostic Value of Notch Receptors in Postsurgical Patients with Hepatitis B Virus-Related Hepatocellular Carcinoma. *Cancer Med.* 6 (7), 1587–1600. doi:10.1002/cam4.1077

Yuan, X., Wu, H., Xu, H., Han, N., Chu, Q., Yu, S., et al. (2015). Meta-analysis Reveals the Correlation of Notch Signaling with Non-small Cell Lung Cancer Progression and Prognosis. *Sci. Rep.* 5, 10338. doi:10.1038/srep10338

Zhang, H., Liu, L., Liu, C., Pan, J., Lu, G., Zhou, Z., et al. (2017). Notch3 Overexpression Enhances Progression and Chemoresistance of Urothelial Carcinoma. *Oncotarget* 8 (21), 34362–34373. doi:10.18632/oncotarget.16156

Zhang, Q., Li, Q., Xu, T., Jiang, H., and Xu, L.-G. (2016a). miR-491-5p Suppresses Cell Growth and Invasion by Targeting Notch3 in Nasopharyngeal Carcinoma. *Oncol. Rep.* 35 (6), 3541–3547. doi:10.3892/or.2016.4713

Zhang, Q., Lu, C., Fang, T., Wang, Y., Hu, W., Qiao, J., et al. (2015). Notch3 Functions as a Regulator of Cell Self-Renewal by Interacting with the β-catenin Pathway in Hepatocellular Carcinoma. *Oncotarget* 6 (6), 3669–3679. doi:10.18632/oncotarget.2898

Zhang, S., Li, P., Zhao, L., and Xu, L. (2018). LINC00210 as a miR-328-5p Sponge Promotes Nasopharyngeal Carcinoma Tumorigenesis by Activating NOTCH3 Pathway. *Biosci. Rep.* 38 (6). doi:10.1042/bsr20181168

Zhang, T.-H., Liu, H.-C., Zhu, L.-J., Chu, M., Liang, Y.-J., Liang, L.-Z., et al. (2011). Activation of Notch Signaling in Human Tongue Carcinoma. *J. Oral Pathol. Med.* 40 (1), 37–45. doi:10.1111/j.1600-0714.2010.00931.x

Zhang, X., Liu, X., Luo, J., Xiao, W., Ye, X., Chen, M., et al. (2016b). Notch3 Inhibits Epithelial-Mesenchymal Transition by Activating Kibra-Mediated Hippo/YAP Signaling in Breast Cancer Epithelial Cells. *Oncogenesis* 5 (11), e269. doi:10.1038/oncsis.2016.67

Zhang, X., Shi, H., Yao, J., Li, Y., Gao, B., Zhang, Y., et al. (2020). FAM225A Facilitates Colorectal Cancer Progression by Sponging miR-613 to Regulate NOTCH3. *Cancer Med.* 9 (12), 4339–4349. doi:10.1002/cam4.3053

Zhang, Y., Chen, B., Wang, Y., Zhao, Q., Wu, W., Zhang, P., et al. (2019). NOTCH3 Overexpression and Posttranscriptional Regulation by miR-150 Were Associated with EGFR-TKI Resistance in Lung Adenocarcinoma. *Oncol. Res.* 27 (7), 751–761. doi:10.3727/096504018x15372657298381

Zhang, Z., Wang, H., Ikeda, S., Fahey, F., Bielenberg, D., Smits, P., et al. (2010). Notch3 in Human Breast Cancer Cell Lines Regulates Osteoblast-Cancer Cell Interactions and Osteolytic Bone Metastasis. *Am. J. Pathol.* 177 (3), 1459–1469. doi:10.2353/ajpath.2010.090476

Zhou, J.-X., Zhou, L., Li, Q.-J., Feng, W., Wang, P.-M., Li, E.-F., et al. (2016). Association between High Levels of Notch3 Expression and High Invasion and Poor Overall Survival Rates in Pancreatic Ductal Adenocarcinoma. *Oncol. Rep.* 36 (5), 2893–2901. doi:10.3892/or.2016.5079

Zhou, J., Zheng, X., Feng, M., Mo, Z., Shan, Y., Wang, Y., et al. (2019). Upregulated MMP28 in Hepatocellular Carcinoma Promotes Metastasis via Notch3 Signaling and Predicts Unfavorable Prognosis. *Int. J. Biol. Sci.* 15 (4), 812–825. doi:10.7150/ijbs.31335

Zhou, L., Zhang, N., Song, W., You, N., Li, Q., Sun, W., et al. (2013). The Significance of Notch1 Compared with Notch3 in High Metastasis and Poor Overall Survival in Hepatocellular Carcinoma. *PLoS One* 8 (2), e57382. doi:10.1371/journal.pone.0057382

Zhu, H., He, G., Wang, Y., Hu, Y., Zhang, Z., Qian, X., et al. (2019). Long Intergenic Noncoding RNA 00707 Promotes Colorectal Cancer Cell Proliferation and Metastasis by Sponging miR-206. *Ott* 12, 4331–4340. doi:10.2147/ott.S198140

Zhu, W., Liang, Q., Yang, X., Yu, Y., Shen, X., and Sun, G. (2017). Combination of Sorafenib and Valproic Acid Synergistically Induces Cell Apoptosis and Inhibits Hepatocellular Carcinoma Growth via Down-Regulating Notch3 and pAkt. *Am. J. Cancer Res.* 7 (12), 2503–2514. 29312803

Zong, Z. H., Liu, Y., Chen, S., and Zhao, Y. (2020). Circ_PUM1 Promotes the Development of Endometrial Cancer by Targeting the miR-136/NOTCH3 Pathway. *J. Cel Mol Med* 24 (7), 4127–4135. doi:10.1111/jcmm.15069

Zou, B., Wang, H., Liu, Y., Qi, P., Lei, T., Sun, M., et al. (2017). Mangiferin Induces Apoptosis in Human Ovarian Adenocarcinoma OVCAR3 Cells via the Regulation of Notch3. *Oncol. Rep.* 38 (3), 1431–1441. doi:10.3892/or.2017.5814

**Conflict of Interest:** The authors declare that the research was conducted in the absence of any commercial or financial relationships that could be construed as a potential conflict of interest.

frontiers in Molecular Biosciences

ORIGINAL RESEARCH
published: 19 August 2021
doi: 10.3389/fmolb.2021.654387

# Evaluation of NTRK Gene Fusion by Five Different Platforms in Triple-Negative Breast Carcinoma

*Shafei Wu†, Xiaohua Shi†, Xinyu Ren, Kaimi Li, Junyi Pang and Zhiyong Liang**

*Department of Pathology, State Key Laboratory of Complex Severe and Rare Disease, Molecular Pathology Research Center, Peking Union Medical College Hospital, Chinese Academy of Medical Sciences and Peking Union Medical College, Beijing, China*

Triple-negative breast carcinoma (TNBC) is an aggressive disease that has a poor prognosis since it lacks effective treatment methods. Neurotrophic tyrosine receptor kinase (NTRK) fusion genes are excellent candidates for targeted RTK inhibitor therapies and there are available targeted therapy drugs for the treatment of TRK fusion-positive tumors in a tumor agnostic pattern. Our study was designed to investigate the NTRK gene fusion status in TNBC patients and to determine whether RTK-targeted therapies are suitable for TNBC patients. A total of 305 TNBC patients were enrolled in our study. IHC was employed as a prescreening method, and IHC positive cases were further submitted for evaluation by FISH, RT-PCR, and NGS methods. NTRK IHC was evaluated successfully in 287 of the 305 cases, and there were 32 (11.15%) positive cases. FISH was carried out in the 32 IHC positive cases. There were 13 FISH-positive cases if the threshold was set as >15% of the 100 counted tumor cells having a split orange and green signal with more than one signal diameter. There were only 2 FISH-positive cases if the cutoff value was defined as >15% of the counted tumor cells having a split signal with more than two signal diameter widths. One of the FISH-positive cases had a separate NTRK3 FISH signal in 88% of the tumor cells, and its IHC result was strong nuclear staining in all the tumor cells. After evaluation of the morphology, it was re-diagnosed as secretory breast carcinoma, and the NGS result confirmed that it had a NTRK3-ETV6 fusion gene. The other FISH-positive cases were all negative for NTRK gene fusion in the NGS or RT-PCR examination. The NTRK gene fusion rate was low in our TNBC cohort. NTRK gene fusion may be a rare event in TNBC. The high false-positive rate of NTRK gene fusion detected by IHC questions its role as a prescreening method in TNBC. More data may be needed to determine a suitable threshold for NTRK FISH in TNBC in the future. More studies are needed to confirm whether RTK-targeted therapies are appropriate treatments for TNBC patients.

**Keywords: IHC, NGS, RT-PCR, FISH, NTRK fusion gene, triple-negative breast carcinoma**

OPEN ACCESS

***Edited by:***
*Md. Asaduzzaman Khan, Southwest Medical University, China*

***Reviewed by:***
*Michael Hummel, Charité – Universitätsmedizin Berlin, Germany*
*Marzieh Dehghan, University of Zanjan, Iran*

***Correspondence:**
*Zhiyong Liang*
*liangzhiyong1220@yahoo.com*

*† These authors have contributed equally to this work*

***Specialty section:***
*This article was submitted to Molecular Diagnostics and Therapeutics, a section of the journal Frontiers in Molecular Biosciences*

***Received:*** *16 January 2021*
***Accepted:*** *19 April 2021*
***Published:*** *19 August 2021*

***Citation:***
*Wu S, Shi X, Ren X, Li K, Pang J and Liang Z (2021) Evaluation of NTRK Gene Fusion by Five Different Platforms in Triple-Negative Breast Carcinoma. Front. Mol. Biosci. 8:654387. doi: 10.3389/fmolb.2021.654387*

## INTRODUCTION

Breast carcinoma is the most common carcinoma in females. It had an incidence of approximately 2.1 million new cases worldwide in 2018 (Ahmad, 2019). Treatment decision is mainly determined by the hormone and HER2 status when a patient presents in an advanced clinical stage. Triple-negative breast carcinoma (TNBC) is a subtype of breast carcinoma with hormone receptor

immunohistochemistry (IHC) stains of less than 1% for estrogen receptors (ER) and progesterone receptors (PR) and is devoid of HER2 protein overexpression or *HER2* gene amplification (or both) (Bergin and Loi, 2019). TNBC is a special subgroup of breast carcinoma which has a poor prognosis, early recurrence, and high metastasis rates. TNBC patients usually present with advanced clinical stage, large tumor size, and poor Nottingham prognostic index when evaluated using pathological criteria at diagnosis (Li et al., 2013). Systemic chemotherapy is the mainstay treatment since TNBC lacks effective targeted therapies. TNBC is always a hotspot of investigation owing to the above-mentioned characteristics, and our study focuses on it too.

The neurotrophic tyrosine receptor kinase (NTRK) gene encodes three different tropomyosin receptor kinases, TRKA, TRKB, and TRKC. These proteins play an important role in the physiology of the development and function of the nervous system (Stephen, 2008). The proteins are structured into three components: the extracellular ligand-binding domain, the transmembrane part, and the intracellular kinase domain. The intracellular domain can undergo homodimerization upon ligand binding or gene fusion caused by chromosomal translocation. Aberrant fusion of the NTRK 3′ kinase domain with the other genes can lead to ligand-independent activation of the NTRK gene and constitutively cause an increase in proliferation and decreased apoptosis of the tumor cells (Nakagawara, 2001). Patients with a positive NTRK fusion gene are excellent candidates for targeted RTK inhibitor therapies. To date, two drugs (entrectinib and larotrectinib) have been approved by the FDA for the treatment of TRK fusion-positive tumors in a tumor agnostic pattern. Secretory breast carcinoma patients who have a high incidence of NTRK fusion gene have shown an excellent clinical response to these targeted drugs in clinical trials (Drilon et al., 2018; Scott, 2019). Secretory breast carcinoma is characterized by NTRK3-ETV6 gene fusion (Vasudev and Onuma, 2011). However, the incidence of NTRK gene fusion in other types of breast carcinoma is low, ranging from 0 to 0.08% (Remoué et al., 2019; Vranic et al., 2019; Rosen et al., 2020). But then again, few reports have been focusing on exploring the NTRK fusion rate in TNBC until now.

Tumors harboring NTRK fusion genes can be divided into two groups: one is a special type of tumor that has a high frequency of NTRK fusion genes, including secretory carcinoma of the breast and salivary glands, congenital mesoblastic nephroma, and infant fibrosarcoma (Stransky et al., 2014; Kheder and Hong, 2018). The other is the common tumor in which NTRK fusion is a rare event (Gatalica et al., 2019). There are different methods for the detection of NTRK fusion, such as immunohistochemistry (IHC), fluorescence *in situ* hybridization (FISH), reverse transcription-polymerase chain reaction (RT-PCR), and next-generation sequencing (NGS). The clinical trials did not employ a specific or uniform diagnostic test, and there are no approved companion diagnostic assays. There are recommendations for the methods of identifying NTRK fusion-positive patients in the common tumor types, such as the ESMO and the Japan Society of Clinical Oncology, and the Japanese Society of Medical Oncology (Marchio et al., 2019; Naito et al., 2020). The IHC method can be used as a prescreening method in common tumors with a low incidence of NTRK fusion. Although targeted therapy drugs are histologically agnostic, whether the IHC methods are also histology-based triage needs to be evaluated.

In our study, we evaluated NTRK gene fusion in TNBC patient samples using the NTRK IHC method as a prescreening method. Other methods, including FISH, RT-PCR, and NGS, were carried out in the IHC positive samples to determine the final NTRK fusion status in TNBC.

## MATERIALS AND METHODS

### Patient Selection

Three hundred and five patients who underwent surgery between January 2011 and December 2014 at Peking Union Medical College Hospital (Beijing, China) were enrolled in our study. All cases had an IHC profile of less than 1% for ER and PR and were devoid of HER2 protein overexpression or *HER2* gene amplification (or both). The average age of the TNBC patients were 49 years old. None of the patients under evaluation had a history of taking NTRK targeted therapy drugs.

This study was approved by the Institutional Review Board of Peking Union Medical College Hospital.

### Tissue Microarray Construction

The selective areas of representative morphology of the hematoxylin-eosin staining slides were labeled. The corresponding formalin-fixed paraffin-embedded (FFPE) primary tumor samples were obtained from the Department of Pathology. A tissue microarray construction machine (Quick-Ray UT-06, UNITMA) was used, and two core-tissue biopsies of 2.0 mm diameter were collected for each sample.

### Immunohistochemistry

NTRK immunohistochemical staining was performed using the antibody clone EPR17341 (Roche, Tusan, United States) to assess NTRK1, NTRK2, and NTRK3 protein expression in the FFPE samples. Positive results were defined as staining above background in at least 1% of tumor cells in any pattern, including membranous, cytoplasmic, perinuclear, or nuclear.

## FISH

Representative FFPE samples were cut into 4-um thick slides, and FISH was performed using the Thermo-Brite Elite automated FISH slide prep system (Leica, Richmond, CA, United States). The FISH break-apart probes used in our study included NTRK1, NTRK2, and NTRK3 Break Apart FISH Probe (ZytoVision GmbH, Bremerhaven, Germany). The results were evaluated using the cytoVision DM6000B fluorescent microscope system (Leica, Biosystem, Buffalo Grove, IL). One hundred tumor nuclei per case were calculated and the percentage of the positive signals was calculated in each case using two different criteria. One was a split of two or more signal widths apart between the orange and green signals in more than 15% of the tumor cells, and the

other was a split of more than one signal width apart between the orange and green signals in more than 15% of the tumor cells.

## NGS

DNA was extracted from FFPE tissues using the QIAamp DNA FFPE Tissue Kit (Qiagen) according to the manufacturer's instructions. After fragmentation with a Covaris S2 ultrasonicator (Covaris, United States) to generate fragments with a 300-bp peak, we performed library construction reactions to generate sequencing libraries using the NEBNext® Ultra™ DNA Library Prep Kit for Illumina® (NEB) according to the manufacturer's instructions. Then, we enriched the library DNA for targeted regions using customized probe sets (Integrated DNA Technologies, IDT) according to the manufacturer's instructions. The DNA libraries were then sequenced with a paired-end 2 × 100 bp protocol aiming for an average coverage of 20 × and 100 × for the tumor DNA, respectively. All the final DNA libraries were subsequently sequenced on the Gene + Seq-2000 to generate approximately 6.2 Gb data. MuTect2 (3.4-46-gbc02625) was used to call single nucleotide variants (SNVs), while GATK was employed to call small insertions and deletions (indels). Copy number variations (CNVs) were detected using Contra (2.0.8). Structure variations (SVs) were detected with BreakDancer. All final candidate variants were verified with an integrative genomics viewer browser. After annotation, the variants were cross-referenced with those in the 1000 Genomes Project, GAD, dbSNP, and ExAC.

The DNA-based NGS assay used at Geneplus interrogates whole exon region in NTRK1/2/3, and introns 8–11 in NTRK1, intron 12 in NTRK2, and introns 4–6 in ETV6, the most common NTRK3 fusion partner. However, because of the aforementioned issues involving coverage of the NTRK3 introns, NTRK3 fusion coverage selected the breakpoint region.

For RNA-seq, total RNA was isolated from FFPE using an RNeasy Mini Kit (Qiagen) and RNeasy FFPE Kit (Qiagen), respectively. cDNA synthesis and NGS library preparation were performed using NEBNext® Ultra™ II Directional RNA Library Prep Kit (NEB) following the manufacturer's protocol, but a substituted adaptor and an index primer were used in Gene + Seq-2000. The library was quantitated using Qubit 3.0 (Life Invitrogen, United States) and quality was assessed using the LabChip GX Touch (PerkinElmer, United States). The libraries were sequenced on the Gene + Seq-2000 with a paired-end 2 × 100 bp protocol resulting in 20 Gb per sample. After removal of terminal adaptor sequences and low-quality data using fastp (version: 0.19.5), and rRNA reads were removed by aligning clean reads to the rRNA database (downloaded from NCBI) by using bowtie2 (version:2.2.8), clean reads without known rRNA were aligned to the reference human genome (hg19) through STAR (version 020201). Fusions were detected using a customized version of Arriba 1.1.0. and annotated using the in-house software annoFilterArriba (version:1.0.0) with the NCBI release 104 database. All final candidate fusions were manually verified with an integrative genomics viewer browser. A series of quality control metrics were computed using RNA-SeQC (Gatalica et al., 2019) assessment. A threshold of ≥ 80 million mapped reads and ≥ 10 million junction reads per sample was set.

## RT-PCR

The NTRK Gene Fusions Detection Kit (AmoyDx) was used in this study. The kit can qualitatively detect 109 fusions in NTRK1, NTRK2, and NTRK3. There were three major steps, including RNA extraction, reverse PCR, and DNA amplification. There are eight NTRK PCR mix tubes that contain fusion detection and internal control systems. The fusion detection system includes primers and FAM-labeled probes specific for NTRK1/2/3 gene fusions. The internal control system contained primers and a VIC-labeled probe for detection of reference genes to reveal the RNA quality and presence of PCR inhibitors that may lead to false-negative results. Reverse transcription and amplification PCR were run on an ABI 7500 PCR machine. For the NTRK PCR mix, FAM Ct values ≤25 were considered positive. Detailed information on the NTRK fusion types examined by the RT-PCR kit is summarized in **Table 1**.

## RESULTS

A total of 305 TNBC patients were enrolled in our study. NTRK IHC was evaluated successfully in 287 cases, of which 32 (11.15%) were positive. Six cases showed strong NTRK immunostaining with an average staining percentage of 47% (ranging from 2 to 100%), and the stain was located either in the cytoplasm (5 cases) or nucleus (1 case). There were 15 cases with moderate staining intensity in the tumor cell cytoplasm or nucleus, and the average stain percentage of the tumor cells was 21.67% (ranging from 5 to 40%). The remaining 11 patients had weak cytoplasmic staining in the tumor cells, with an average percentage of 10.27%. Detailed information on IHC staining is summarized in **Table 2**.

All IHC positive cases were subjected to FISH testing. If the evaluation threshold was set to be >15% of the tumor cells with a separation width of more than one signal diameter, there were 13(4.5%) positive cases with an average ratio of 28.46%. The highest proportion of the separated signals was 88%, followed by 36% and 28%. If the evaluation threshold was set to be > 15% of the tumor cells with a separation width of more than two signal diameters, there were 2 (0.70%) positive cases with an average ratio of 55%. One of the FISH positive cases had a positive NTRK1 separation signal in 22% of the tumor cells (**Figure 1A**), while its IHC result showed a strong cytoplasmic stain in 80% of the tumor cells (**Figure 1B**). The other FISH positive case identified an NTRK3 separation signal in 88% of the tumor cells (**Figure 1C**), and IHC results indicated a strong and diffuse nuclear stain in almost all tumor cells (**Figure 1D**). After further evaluation of the HE slides, the latter case was modified from breast carcinoma, no special type to secretory breast carcinoma (**Figure 1E**).

DNA-based NGS was carried out in 13 cases in which the IHC was positive and FISH could identify separated orange and green

**TABLE 1 |** The detailed information on the NTRK fusion types examined by the RT-PCR kit.

| Tube | Detected target | Fusion type |
|---|---|---|
| ① | NTRK1 Fusion | TP53 exon8;ins6 NTRK1 exon8 |
| | | TP53 exon9;ins6 NTRK1 exon8 |
| | | TP53 exon10;ins6 NTRK1 exon8 |
| | | TP53 exon11;ins6 NTRK1 exon8 |
| | | CTRC exon2;NTRK1 exon8 |
| | | IRF2BP2 exon1;NTRK1 exon8 |
| | | LRRC71 exon1;NTRK1 exon8 |
| | | LMNA exon2;NTRK1 exon11 |
| | | LMNA exon3;NTRK1 exon11 |
| | | LMNA exon5;NTRK1 exon11 |
| | | LMNA exon10;NTRK1 exon11 |
| | | LMNA exon11 del150;NTRK1 exon11 |
| | | PPL exon21;NTRK1 exon11 |
| | | GRIPAP1 exon22;NTRK1 exon11 |
| | | BCAN exon13;NTRK1 exon11 |
| ② | NTRK1 Fusion | TFG exon5;NTRK1 exon9 |
| | | TPR exon21;NTRK1 exon9 |
| | | TFG exon4;NTRK1 exon9 |
| | | TPM3 exon10;NTRK1 exon9 |
| | | AFAP1 exon4;NTRK1 exon9 |
| | | TRIM63 exon8;NTRK1 exon9 |
| | | TPM3 exon8;NTRK1 exon10 |
| | | SQSTM1 exon2;NTRK1 exon10 |
| | | SQSTM1 exon5;NTRK1 exon10 |
| | | TPR exon10;NTRK1 exon10 |
| | | TPR exon16 del54;NTRK1 ins13 exon10 |
| | | TPR exon21;NTRK1 exon10 |
| | | CD74 exon8;NTRK1 exon10 |
| | | IRF2BP2 exon1;NTRK1 exon10 |
| | | IRF2BP2 exon1 del48;NTRK1 exon10 |
| | | PPL exon21;NTRK1 exon10 |
| | | PEAR1 exon15;NTRK1 exon10 |
| | | TFG exon5;NTRK1 exon10 |
| | | GRIPAP1 exon22;NTRK1 exon10 |
| | | TFG exon6;NTRK1 exon10 |
| | | F11R exon4;NTRK1 exon10 |
| | | F11 exon4;NTRK1 exon10 |
| | | SQSTM1 exon6;NTRK1 exon10 |
| | | ARHGEF2 exon21;NTRK1 exon10 |
| | | CHTOP exon5;NTRK1 exon10 |
| | | NFASC exon21;NTRK1 exon10 |
| | | TPM3 exon7 del39;NTRK1 exon10 |
| | | BCAN exon12;NTRK1 exon10 |
| | | PPL exon11;NTRK1 exon13 |
| ③ | NTRK1 Fusion | TPM3 exon8;NTRK1 exon12 |
| | | LMNA exon6 del172;NTRK1 exon12 |
| | | MPRIP exon21;NTRK1 exon12 |
| | | SSBP2 exon12;NTRK1 exon12 |
| | | LMNA exon2;NTRK1 exon12 |
| | | LMNA exon4;NTRK1 exon12 |
| | | LMNA exon8;NTRK1 exon12 |
| | | LMNA exon10;NTRK1 exon12 |
| | | LMNA exon12;NTRK1 exon12 |
| | | MPRIP exon14;NTRK1 exon12 |
| | | MPRIP exon18;NTRK1 exon12 |
| | | TPR exon6;NTRK1 exon12 |
| | | GRIPAP1 exon22;NTRK1 exon12 |
| | | SCYL3 exon11;NTRK1 exon12 |
| | | MEF2D exon9;NTRK1 exon12 |
| | | AMOTL2 exon6;NTRK1 exon12 |
| | | PRDX1 exon5;NTRK1 exon12 |
| ④ | NTRK1 Fusion | MPRIP exon21;NTRK1 exon14 |
| | | LMNA exon2;NTRK1 exon16 |
| ⑤ | NTRK2 Fusion | VCL exon16;NTRK2 exon12 |
| | | AFAP1 exon13;NTRK2 exon12 |
| | | VCAN exon6; NTRK2 exon12 |
| | | NCAA2 exon5;NTRK2 exon13 |
| | | NOS1AP exon9; NTRK2 exon13 |
| | | TBC1D2 exon6; NTRK2 exon14 |
| ⑥ | NTRK2 Fusion | TRIM24 exon12;NTRK2 exon15 |
| | | TRAF2 exon9;NTRK2 exon15 |
| | | SQSTM1 exon4;NTRK2 exon15 |
| | | ETV6 exon5;NTRK2 exon15 |
| | | TLE4 exon7;NTRK2 exon15 |
| | | TRIM24 exon12;NTRK2 exon16 |
| | | AGBL4 exon6;NTRK2 exon16 |
| | | SQSTM1 exon5;NTRK2 exon16 |
| | | STRN3 exon7;NTRK2 exon16 |
| | | WNK2 exon24;NTRK2 exon16 |
| | | QKI exon6;NTRK2 exon16 |
| | | STRN exon3;NTRK2 exon16 |
| | | GKAP1 exon9; NTRK2 exon16 |
| | | KCTD8 exon1;NTRK2 exon16 |
| | | PRKAR2A exon2;NTRK2 exon16 |
| | | PAN3 exon1;NTRK2 exon17 |
| | | SQSTM1 exon5;NTRK2 exon17 |
| | | BCR exon1;NTRK2 exon17 |
| ⑦ | NTRK3 Fusion | ETV6 exon4;NTRK3 exon14 |
| | | ETV6 exon5;NTRK3 exon14 |
| | | EML4 exon2;NTRK3 exon14 |
| | | SQSTM1 exon5;NTRK3 exon14 |
| | | TFG exon6;NTRK3 exon14 |
| | | MYH9 exon31;NTRK3 exon14 |
| | | RBPMS exon5;NTRK3 exon14 |
| | | BTBD1 exon4; NTRK3 exon14 |
| | | SPECC1L exon5;NTRK3 exon14 |
| | | VIM exon8;NTRK3 exon14 |
| | | STRN exon3;NTRK3 exon14 |
| | | STRN3 exon3;NTRK3 exon14 |
| | | HNRNPA2B1 exon7;NTRK3 exon14 |
| | | AKAP13 exon3;NTRK3 exon14 |
| | | ETV6 exon5;NTRK3 exon15 |
| | | ETV6 exon4;NTRK3 exon15 |
| | | SQSTM1 exon6;NTRK3 exon15 |
| | | ETV6 exon6;NTRK3 exon15 |

*(Continued)*

**TABLE 1** | Continued

| Tube | Detected target | Fusion type |
|---|---|---|
| ⑧ | NTRK3 Fusion | ETV6 exon4;NTRK3 exon12 |
| | | ETV6 exon5;NTRK3 exon13 |
| | | ETV6 exon4;NTRK3 exon13 |
| | | ETV6 exon5;NTRK3 exon16 |

signals of more than one diameter width in over 15% of the tumor cells. Besides the one which is confirmed to be secretory breast carcinoma (**Figure 1F**), the rest of them are all negative for NTRK rearrangement. RNA-based NGS was further evaluated in 7 cases that were negative for NTRK fusion examined by DNA-based NGS and had a good quality of RNA for further analysis. The final results were also negative for NTRK gene rearrangement at the RNA level.

RT-PCR was also carried out in the 7 cases that had been evaluated by RNA-based NGS, and the results were also negative for NTRK rearrangement (**Figure 1G**).

## DISCUSSION

In our study, we used five different platforms to evaluate NTRK gene rearrangement in TNBC. IHC was used as a pre-screening method with a high false-positive result. DNA-based NGS, RNA-based NGS, and RT-PCR methods did not identify positive NTRK gene rearrangements except in one secretory breast carcinoma case with NTRK3 gene fusion, which was misdiagnosed as TBNC. Different FISH evaluation criteria yield diverse positive results for NTRK gene fusion. Only the NTRK FISH result with a high proportion of split signals in the tumor cells can achieve positive NGS or RT-PCR results.

NTRK gene fusion is reported to be a rare event in common cancer types, such as pancreatic carcinoma and lung cancer, with a reported incidence below 1% (Rosen et al., 2020). There are several massive sequencing results showing that NTRK gene fusion in breast carcinoma ranges from 0 to 0.34%, most of which are focused on breast carcinoma (NOS). As we know, TNBC is a special type of breast carcinoma that lacks effective treatment methods, and at diagnosis, is always at an advanced clinical stage, with high recurrence and metastasis rates. Therefore, exploring new targeted therapy methods for this type of tumor is meaningful. Unfortunately, our preliminary results show that the NTRK fusion rate in TNBC is low. To our knowledge, there is only one report focusing on investigating NTRK gene fusion in TNBC, and its conclusion is similar to ours (Remoué et al., 2019).

Secretory breast carcinomas are a rare type of breast carcinoma, accounting for less than 0.15% of the invasive breast cancers (Lee et al., 2014; Del Castillo et al., 2015). They are characterized by NTRK3-ETV6 gene rearrangement (Vasudev and Onuma, 2011). Secretory breast carcinoma usually presents as a phenotype of triple-negative breast carcinoma with typical features of intracellular and extracellular eosinophilic secretion material. One secretory breast carcinoma was wrongly included in TNBC because of its negative expression of ER, PR, and HER-2 in our study. NTRK IHC showed strong nuclear staining in all the tumor cells and positive NTRK FISH signals in 88% of the tumor cells. NGS also identified NTRK3 fusion signals in this peculiar case. Correct diagnosis of secretory breast carcinoma is important because it is morphologically and immunohistologically different from TNBC. Second, it has targeted therapy for advanced-stage patients because of the high prevalence of characteristic NTRK3-ETV6 gene fusion.

There are different methods to detect the fusion status of NTRK genes, including NGS, RT-PCR, FISH, and IHC (Solomon and Hechtman, 2019). Each one has its own advantages and disadvantages. NGS methods, which include DNA-based NGS and RNA-based NGS, are a massive sequencing method that can tell the corresponding fusion partners. Their disadvantage is the long turnaround time and requirement of a high amount of DNA input and good quality of RNA. Although RT-PCR has a short turnaround time compared to the NGS method, it can only detect the known fusion types of NTRK, and there are currently no commercial testing kits available on the market. The FISH method is limited by the experience of the pathologists and may produce false-negative results if the breakpoints involve non-canonical sites. The IHC method is a labor and time saving method that can be carried out in most pathology labs. However, the absence of a standardized scoring method limits its application in clinical practice. Since there are no uniform examination methods in clinical trials, there is no consensus method for the detection of NTRK gene fusion.

Recently, the ESMO working group proposed a two-step method to detect NTRK fusions in daily practice, and IHC can be used as a pre-screening method in common cancers that have a low prevalence of NTRK fusion (Marchio et al., 2019). In our study, we used the IHC method to screen for NTRK fusion patients in TNBC. The final results showed that the fusion rate of TNBC in our cohort was 11.15%, which is high above the reported level. Further NGS analysis showed that the IHC positive cases were all negative for NTRK rearrangement at the DNA and RNA levels, except for one secretory breast carcinoma case. Our preliminary results question the role of IHC as a prescreening method in TNBC because of its high false positivity rate. This phenomenon was not observed in lung cancer, gallbladder carcinoma, or pancreatic cancer in our parallel study (data not published). Several studies have investigated the sensitivity and specificity of the pan-TRK IHC method vs. the FISH or NGS method, and the results showed that the positive predictive value and negative predictive value are high between the various methods in infant fibrosarcoma, lipofibromatosis-like neural tumor, colorectal cancer, and lung adenocarcinoma (Hechtman et al., 2017; Rudzinski et al., 2018). In Solomen's report, NTRK IHC specificity was 100% for carcinomas of the colon, lung, thyroid, pancreas, and biliary tract, while decreased specificity was seen in breast and salivary gland carcinomas (82 and 52%, respectively) (Solomon et al., 2019). Some research result indicated that the pan-TRK antibody can predict the NTRK fusion partners according to the staining patterns. For example the ETV6-NTRK3 positive cases were prone to have nuclear staining, like the secretory carcinoma in our study

**TABLE 2 |** The detail information of the NTRK immunohistochemistry positive cases.

| No | Intensity | Percentage | Location | FISH (one diameter) | FISH (two diameter) | NGS DNA | NGS RNA | PCR |
|---|---|---|---|---|---|---|---|---|
| 1 | S | 100 | Nu | Pos (88%) | Pos (88%) | pos | pos | pos |
| 2 | S | 80 | C | Pos (24%) | Pos (22%) | neg | neg | neg |
| 3 | S | 60 | C | Pos (20%) | Neg | neg | neg | neg |
| 4 | S | 20 | C | Pos (16%) | Neg | neg | neg | neg |
| 5 | S | 20 | C | Neg | Neg | NA | NA | NA |
| 6 | S | 2 | C | Neg | Neg | NA | NA | NA |
| 7 | M | 40 | C | Neg | Neg | NA | NA | NA |
| 8 | M | 40 | C | Neg | Neg | NA | NA | NA |
| 9 | M | 40 | Nu | Neg | Neg | NA | NA | NA |
| 10 | M | 40 | C | Pos (20%) | Neg | neg | NA | NA |
| 11 | M | 30 | C | Pos (22%) | Neg | neg | NA | NA |
| 12 | M | 30 | C | Neg | Neg | NA | NA | NA |
| 13 | M | 25 | C | Neg | Neg | NA | NA | NA |
| 14 | M | 20 | C | Neg | Neg | NA | NA | NA |
| 15 | M | 10 | C | Neg | Neg | NA | NA | NA |
| 16 | M | 10 | C | Neg | Neg | NA | NA | NA |
| 17 | M | 10 | C | Pos (24%) | Neg | neg | neg | neg |
| 18 | M | 10 | C | Pos (26%) | Neg | neg | NA | NA |
| 19 | M | 10 | C | Pos (28%) | Neg | neg | NA | NA |
| 20 | M | 5 | C | Neg | Neg | NA | NA | NA |
| 21 | M | 5 | C | Neg | Neg | NA | NA | NA |
| 22 | W | 40 | C | Neg | Neg | NA | NA | NA |
| 23 | W | 20 | C | Pos (20%) | Neg | neg | NA | NA |
| 24 | W | 10 | C | Neg | Neg | NA | neg | neg |
| 25 | W | 10 | C | Neg | Neg | NA | NA | NA |
| 26 | W | 5 | C | Neg | Neg | NA | NA | NA |
| 27 | W | 5 | C | Neg | Neg | NA | NA | NA |
| 28 | W | 5 | C | Neg | Neg | NA | NA | NA |
| 29 | W | 5 | C | Neg | Neg | NA | NA | NA |
| 30 | W | 5 | C | Pos (18%) | Neg | neg | neg | neg |
| 31 | W | 5 | C | Pos (28%) | Neg | neg | neg | neg |
| 32 | W | 3 | C | Pos (36%) | Neg | neg | NA | NA |

*S, strong; M, moderate; W, weak; C, cytoplasm; Nu, nuclear; Neg, negative; Pos, positive; NA, not available. FISH, fluorescence in situ hybridization; NGS, next generation sequencing; PCR, polymease chain reaction.*

which showed diffuse and strong nuclear stain. While LMNA-NTRK1 fusion positive samples displayed perinuclear expression pattern and TPM-NTRK1 fusions showed membranous staining (Gatalica et al., 2019).

Together with our study results, we found that although the NTRK treatment relies on the specific molecular alteration instead of the histological classification, the prescreening IHC method should be histology-triaged, and IHC is not a suitable prescreening method in TNBC tumor type.

FISH is regarded as the gold standard method for the detection of gene fusion because it can visualize the separation or fusion signals under a microscope, even in poorly preserved FFPE samples. There are currently no consensus criteria for the evaluation of NTRK FISH results. Different criteria have been applied in research papers, for example, a threshold of > 15% of tumor nuclei with a positive signal (i.e., a split signal of a single 3′ orange signal, or a split pattern with 3′ and 5′ signals separated by a distance superior to the diameter of the largest signal) within 100 tumor nuclei (George et al., 2018; Remoué et al., 2019), or cases can be considered positive for gene fusion if >10% or >15% of nuclei display "split-apart signals" (red and green signals should be separated by a distance greater than the size of two hybridization probe signals) (Del Castillo et al., 2015; Marchio et al., 2019). In our study, if the split signal proportion was below 50% of the tumor cells, regardless of the separation signal width (more than one signal diameter or two signal diameters), the NGS or RT-PCR method could not identify NTRK gene fusion in the tumor cells. Only cases with a high proportion of NTRK gene split signals in the FISH examination had positive NGS and RT-PCR results. There have been few reports describing the detailed FISH positive signal proportion in context. One study showed that an average of 55, 75, 70, and 55% of the tumor cells were positive in the FISH examination within the known fusion-positive cases tested by NGS (Kirchner et al., 2020). Taken together, the FISH positive threshold of the NTRK gene needs to be further evaluated to reach a suitable cutoff value.

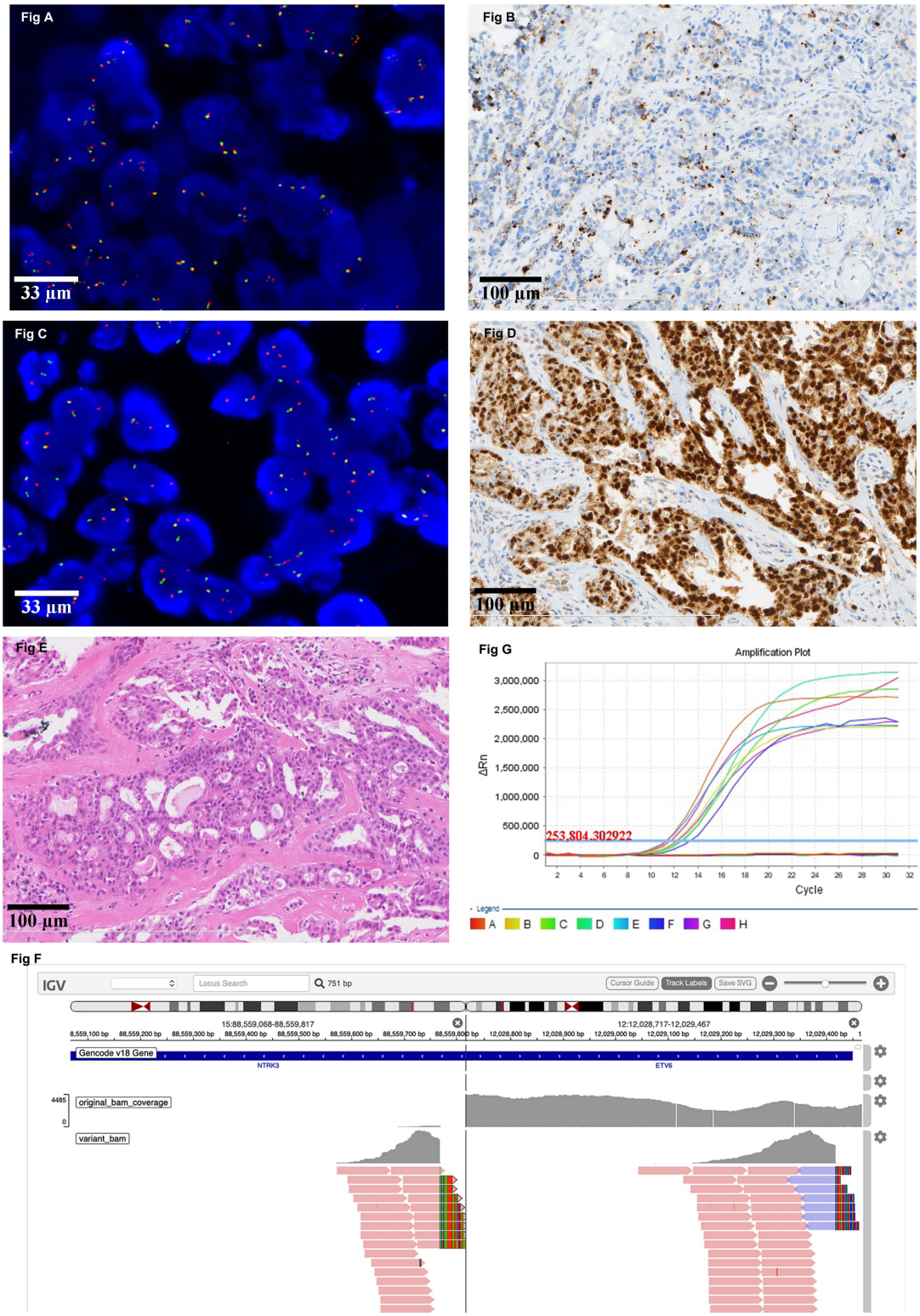


**FIGURE 1 |** Representative image of NTRK result detected by different platforms. **(A)** There is a positive NTRK1 FISH signal in 22% of the tumor cells (630X). **(B)** The corresponding IHC result of the case in Figure A showed a strong cytoplasmic stain in 80% of the tumor cells (200X). **(C)** There is a positive NTRK3 FISH signal in 88% of the tumor cells (630X). **(D)** The corresponding IHC result of the case in Figure C indicated a strong and diffuse nuclear stain in almost all tumor cells (200X). **(E)** The morphology of the case which the diagnosis was modified from breast carcinoma, no special type, to secretory breast carcinoma (100X). **(F)** Positive NTRK3 result detected by DNA-based NGS. **(G)** Representative image of negative NTRK result detected by RT-PCR.

The retrospective nature of our study is one of its limitations. We lacked information on the available targeted drugs. The specimens included in our study were at least 5-year-old archived FFPE samples, which were not suitable for NGS analysis because of the limitation of DNA and RNA quality. Finally, since not all the cases underwent NGS analysis, there was no accurate false-negative predictive value in our study.

In conclusion, NTRK gene fusion may be a rare event in TNBC. The high false-positive rate of NTRK gene fusion detected by IHC questions its role as a prescreening method in TNBC. More data may be needed to determine a suitable threshold for NTRK FISH in TNBC in the future. More studies are needed to confirm whether RTK-targeted therapies are appropriate treatments for TNBC patients.

## DATA AVAILABILITY STATEMENT

The authors declare that the datasets presented in this article are not readily available because of the restriction of uploading human genetic resources. Requests to access the datasets should be directed to the corresponding author ZL, liangzhiyong1220@yahoo.com.

## ETHICS STATEMENT

The studies involving human participants were reviewed and approved by the Medical Ethical Committee of the Peking Union Medical College Hospital. Written informed consent for participation was not required for this study in accordance with the national legislation and the institutional requirements.

## AUTHOR CONTRIBUTIONS

SW and XS performed experiments and data analysis and wrote manuscript. XR and KL performed experiments and data analysis. JP performed IHC staining. ZL conceptualized the study design and manuscript writing. All authors contributed to the article and approved the submitted version.

## FUNDING

This study was supported by the foundation from Chinese Academy of Medical Sciences (CAMS) and the Innovation Fund for Medical Sciences (CIFMS) (Project No. 2016-I2M-1-002).

## REFERENCES

Ahmad, A. (2019). Breast Cancer Statistics: recent Trends. *Adv. Exp. Med. Biol.* 1152, 1–7. doi: 10.1007/978-3-030-20301-6_1

Bergin, A. R. T., and Loi, S. (2019). Triple-negative breast cancer: recent treatment advances. *F1000 Res.* 8:342. doi: 10.12688/f1000research.18888.1

Del Castillo, M., Chibon, F., Arnould, L., Croce, S., Ribeiro, A., and Perot, G. (2015). Secretory Breast Carcinoma: a Histopathologic and Genomic Spectrum Characterized by a Joint Specific ETV6-NTRK3 Gene Fusion. *Am. J. Surg. Pathol.* 39, 1458–1467. doi: 10.1097/pas.0000000000000487

Drilon, A., Laetsch, T. W., Kummar, S., DuBois, S. G., Lassen, U. N., and Demetri, G. D. (2018). Efficacy of Larotrectinib in TRK Fusion-Positive Cancers in Adults and Children. .*N. Engl. J. Med.* 378, 731–739.

Gatalica, Z., Xiu, J., Swensen, J., and Vranic, S. (2019). Molecular characterization of cancers with NTRK gene fusions. *Mod. Pathol.* 32, 147–153. doi: 10.1038/s41379-018-0118-3

George, J., Walter, V., Peifer, M., Alexandrov, L. B., Seidel, D., Leenders, F., et al. (2018). Integrative genomic profiling of large-cell neuroendocrine carcinomas reveals distinct subtypes of high-grade neuroendocrine lung tumors. *Nat. Commun.* 9:1048.

Hechtman, J. F., Benayed, R., Hyman, D. M., Drilon, A., Zehir, A., Frosina, D., et al. (2017). Pan-Trk Immunohistochemistry Is an Efficient and Reliable Screen for the Detection of NTRK Fusions. *Am. J. Surg. Pathol.* 41, 1547–1551. doi: 10.1097/pas.0000000000000911

Kheder, E. S., and Hong, D. S. (2018). Emerging Targeted Therapy for Tumors with NTRK Fusion Proteins. *Clin. Cancer Res.* 24, 5807–5814. doi: 10.1158/1078-0432.ccr-18-1156

Kirchner, M., Glade, J., Lehmann, U., Merkelbach-Bruse, S., Hummel, M., Lehmann, A., et al. (2020). NTRK testing: first results of the QuiP-EQA scheme and a comprehensive map of NTRK fusion variants and their diagnostic coverage by targeted RNA-based NGS assays. *Genes Chromosomes Cancer* 59, 445–453. doi: 10.1002/gcc.22853

Lee, S. G., Jung, S. P., Lee, H. Y., Kim, S., and Kim, H. Y. (2014). Secretory breast carcinoma: a report of three cases and a review of the literature. *Oncol. Lett.* 8, 683–686. doi: 10.3892/ol.2014.2213

Li, C. Y., Zhang, S., Zhang, X. B., Wang, P., Hou, G. F., and Zhang, J. (2013). Clinicopathological and prognostic characteristics of triple-negative breast cancer (TNBC) in Chinese patients: a retrospective study. *Asian Pac. J. Cancer Prev.* 14, 3779–3784. doi: 10.7314/apjcp.2013.14.6.3779

Marchio, C., Scaltriti, M., Ladanyi, M., Iafrate, A. J., Bibeau, F., Dietel, M., et al. (2019). ESMO recommendations on the standard methods to detect NTRK fusions in daily practice and clinical research. *Ann. Oncol.* 30, 1417–1427. doi: 10.1093/annonc/mdz204

Naito, Y., Mishima, S., Akagi, K., Igarashi, A., Ikeda, M., and Okano, S. (2020). Japan society of clinical oncology/Japanese society of medical oncology-led clinical recommendations on the diagnosis and use of tropomyosin receptor kinase inhibitors in adult and pediatric patients with neurotrophic receptor tyrosine kinase fusion-positive advanced solid tumors, cooperated by the Japanese society of pediatric hematology/oncology. *Int. J. Clin. Oncol.* 25, 403–417. doi: 10.1007/s10147-019-01610-y

Nakagawara, A. (2001). Trk receptor tyrosine kinases: a bridge between cancer and neural development. *Cancer Lett.* 169, 107–114. doi: 10.1016/s0304-3835(01)00530-4

Remoué, A., Conan-Charlet, V., Bourhis, A., Flahec, G. L., Lambros, L., Marcorelles, P., et al. (2019). Non-s ecretory breast carcinomas lack NTRK rearrangements and TRK protein expression. *Pathol. Int.* 69, 94–96. doi: 10.1111/pin.12766

Rosen, E. Y., Goldman, D. A., Hechtman, J. F., Benayed, R., and Fusions Are, T. R. K. (2020). Enriched in Cancers with Uncommon Histologies and the Absence of Canonical Driver Mutations. *Clin. Cancer Res.* 26, 1624–1632. doi: 10.1158/1078-0432.ccr-19-3165

Rudzinski, E. R., Lockwood, C. M., Stohr, B. A., Vargas, S. O., Sheridan, R., Black, J. O., et al. (2018). Pan-Trk Immunohistochemistry Identifies NTRK Rearrangements in Pediatric Mesenchymal Tumors. *Am. J. Surg. Pathol.* 42, 927–935. doi: 10.1097/pas.0000000000001062

Scott, L. J. (2019). Larotrectinib: First Global Approval. *Drugs* 79, 201–206. doi: 10.1007/s40265-018-1044-x

Solomon, J. P., Benayed, R., Hechtman, J. F., and Ladanyi, M. (2019). Identifying patients with NTRK fusion cancer. *Ann. Oncol.* 30, viii16–viii22. doi: 10.1093/annonc/mdz384

Solomon, J. P., and Hechtman, J. F. (2019). Detection of NTRK Fusions: merits and Limitations of Current Diagnostic Platforms. *Cancer Res* 79, 3163–3168. doi: 10.1158/0008-5472.can-19-0372

Stephen, D. S. (2008). The Biology of Neurotrophins, Signalling Pathways, and Functional Peptide Mimetics of Neurotrophins and their Receptors. *CNS Neurol. Disord. Drug Targets* 7, 46–62. doi: 10.2174/187152708783885174

Stransky, N., Cerami, E., Schalm, S., Kim, J. L., and Lengauer, C. (2014). The landscape of kinase fusions in cancer. *Nat. Commun.* 5:4846. doi: 10.1038/ncomms5846

Vasudev, P., and Onuma, K. (2011). Secretory breast carcinoma: unique, triple-negative carcinoma with a favorable prognosis and characteristic molecular expression. *Arch. Pathol. Lab. Med.* 135, 1606–1610. doi: 10.5858/arpa.2010-0351-rs

Vranic, S., Palazzo, J., Sanati, S., Florento, E., Contreras, E., Xiu, J., et al. (2019). Potential Novel Therapy Targets in Neuroendocrine Carcinomas of the Breast. *Clin. Breast Cancer* 19, 131–136. doi: 10.1016/j.clbc.2018.09.001

**Conflict of Interest:** The authors declare that the research was conducted in the absence of any commercial or financial relationships that could be construed as a potential conflict of interest.

**Publisher's Note:** All claims expressed in this article are solely those of the authors and do not necessarily represent those of their affiliated organizations, or those of the publisher, the editors and the reviewers. Any product that may be evaluated in this article, or claim that may be made by its manufacturer, is not guaranteed or endorsed by the publisher.

frontiers in Molecular Biosciences

ORIGINAL RESEARCH
published: 06 December 2021
doi: 10.3389/fmolb.2021.777921



OPEN ACCESS

**Edited by:**
Saber Imani,
Affiliated Hospital of Southwest Medical University, China

**Reviewed by:**
Yu-Chan Chang,
National Yang-Ming University, Taiwan
Ping Zheng,
The University of Melbourne, Australia
Jun Li,
Huazhong University of Science and Technology, China
Mazaher Maghsoudloo,
University of Tehran, Iran

***Correspondence:**
Jinsheng Hong
13799375732@163.com
Qiuyu Zhang
qiuyu.zhang@fjmu.edu.cn
Qiuyuan Yue
circlessoo@sina.cn
Fangqin Xue
xuefangqingsl@sina.com

†These authors have contributed equally to this work

**Specialty section:**
This article was submitted to Molecular Diagnostics and Therapeutics, a section of the journal Frontiers in Molecular Biosciences

**Received:** 16 September 2021
**Accepted:** 19 November 2021
**Published:** 06 December 2021

**Citation:**
Zhang M, Chen H, Liang B, Wang X, Gu N, Xue F, Yue Q, Zhang Q and Hong J (2021) Prognostic Value of mRNAsi/Corrected mRNAsi Calculated by the One-Class Logistic Regression Machine-Learning Algorithm in Glioblastoma Within Multiple Datasets. Front. Mol. Biosci. 8:777921. doi: 10.3389/fmolb.2021.777921

# Prognostic Value of mRNAsi/Corrected mRNAsi Calculated by the One-Class Logistic Regression Machine-Learning Algorithm in Glioblastoma Within Multiple Datasets

*Mingwei Zhang[1,2,3†], Hong Chen[4†], Bo Liang[5†], Xuezhen Wang[1†], Ning Gu[6], Fangqin Xue[4*], Qiuyuan Yue[7*], Qiuyu Zhang[2*] and Jinsheng Hong[1,3*]*

[1]Department of Radiotherapy, Cancer Center, The First Affiliated Hospital of Fujian Medical University, Fuzhou, China, [2]Institute of Immunotherapy, Fujian Medical University, Fuzhou, China, [3]Key Laboratory of Radiation Biology of Fujian Higher Education Institutions, The First Affiliated Hospital, Fujian Medical University, Fuzhou, China, [4]Department of Gastrointestinal Surgery, Fujian Provincial Hospital, Fuzhou, China, [5]Nanjing University of Chinese Medicine, Nanjing, China, [6]Nanjing Hospital of Chinese Medicine Affiliated to Nanjing University of Chinese Medicine, Nanjing, China, [7]Department of Radiology, Fujian Cancer Hospital & Fujian Medical University Cancer Hospital, Fuzhou, China

Glioblastoma (GBM) is the most common glial tumour and has extremely poor prognosis. GBM stem-like cells drive tumorigenesis and progression. However, a systematic assessment of stemness indices and their association with immunological properties in GBM is lacking. We collected 874 GBM samples from four GBM cohorts (TCGA, CGGA, GSE4412, and GSE13041) and calculated the mRNA expression-based stemness indices (mRNAsi) and corrected mRNAsi (c_mRNAsi, mRNAsi/tumour purity) with OCLR algorithm. Then, mRNAsi/c_mRNAsi were used to quantify the stemness traits that correlated significantly with prognosis. Additionally, confounding variables were identified. We used discrimination, calibration, and model improvement capability to evaluate the established models. Finally, the *CIBERSORTx* algorithm and ssGSEA were implemented for functional analysis. Patients with high mRNAsi/c_mRNAsi GBM showed better prognosis among the four GBM cohorts. After identifying the confounding variables, c_mRNAsi still maintained its prognostic value. Model evaluation showed that the c_mRNAsi-based model performed well. Patients with high c_mRNAsi exhibited significant immune suppression. Moreover, c_mRNAsi correlated negatively with infiltrating levels of immune-related cells. In addition, ssGSEA revealed that immune-related pathways were generally activated in patients with high c_mRNAsi. We comprehensively evaluated GBM stemness indices based on large cohorts and established a c_mRNAsi-based classifier for prognosis prediction.

**Keywords: glioblastoma, mRNAsi, OCLR, prognosis, stemness indices**

# 1 INTRODUCTION

Glioblastoma multiforme (GBM), is the most common and most malignant glial tumour (Young et al., 2015). There is no clear way to prevent GBM; the disease can be very difficult to treat, and a cure is often not possible. The typical treatment, which involves surgery, chemotherapy, and radiation therapy, (Gallego, 2015), may slow cancer progression and reduce signs and symptoms. However, cancer usually recurs despite treatment (Gallego, 2015). The most common length of survival following diagnosis is 12–15 months, with less than 3–5% of the patients surviving longer than 5 years (Gallego, 2015). Without treatment, the survival time is typically 3 months (McNeill, 2016). Therefore, developing and applying signatures or biomarkers that can effectively predict the prognosis of these patients is of vital importance. A good initial Karnofsky Performance Score (KPS), the methylation of the O6-methylguanine-DNA methyltransferase (*MGMT*) promoter, and mutations in isocitrate dehydrogenase 1 (*IDH1*) are associated with longer survival (Krex et al., 2007; Martinez et al., 2007; Burgenske et al., 2019; Chaddad et al., 2019). The above signatures or biomarkers can be used either alone or in combination to predict the prognosis of GBM (Molenaar et al., 2014). However, their predictive capacity is rather low and a new index is needed.

Stem-like cells, which are characterised by the self-renewal properties and therapeutic resistance, play crucial roles in various cancers, (Kaushal and Ramakrishna, 2020), especially in GBM (Wang et al., 2018). Although cancer stem-like cells are very important for prognosis in GBM, (Turaga et al., 2020), there are still some shortcomings and complications in quantifying these cells. The stemness features have been extensively studied using artificial intelligence and deep learning methods. (Pan et al., 2019). A good example is the calculation of the mRNA expression-based stemness index (mRNAsi) with the one-class logistic regression (OCLR) machine-learning algorithm (Sokolov et al., 2016; Malta et al., 2018). Tathiane M. Malta *et al.* used mRNAsi for the first time to reflect the degree of oncogenic dedifferentiation (Malta et al., 2018). They also found tumour heterogeneity at the single-cell level by measuring the mRNAsi and concluded that a lower mRNAsi correlated with better prognosis in various cancers. (Malta et al., 2018). The prognostic value of the mRNAsi differs among different cancers. Moreover, we have previously shown that the prediction performance of a single mRNAsi-based signature is not good in primary lower-grade glioma, (Zhang et al., 2020b), partly because the tissue biopsy samples are often mixed with non-tumour tissues (bulk tissues). This means that the expression data on which the mRNAsi is based may be contaminated with non-tumour information. Thus, tumour purity may solve this issue (Xia et al., 2020).

It remains unclear whether the mRNAsi is an independent prognostic indicator in GBM and whether the predictive capacity of mRNAsi is better than that of existing factors such as the mutational status of *IDH1* and the methylation status of *MGMT*. Previous studies have shown that the combination of clinical features with signatures or biomarkers can significantly improve prognosis prediction, (Zhang et al., 2020b; Zhang et al., 2020c), but this has not been verified with the mRNAsi, let alone the corrected mRNAsi (c_mRNAsi), which is acquired using 'Estimation of STromal and Immune cells in MAlignant Tumours using Expression data' (ESTIMATE) (Yoshihara et al., 2013) to calculate tumour purity. Whether c_mRNAsi can predict GBM better than mRNAsi is unknown. Furthermore, although Tathiane M. Malta *et al.*(Malta et al., 2018) analysed cancer stemness quite extensively, this was done in almost 12,000 samples of 33 tumour types from only The Cancer Genome Atlas (TCGA) (Hoadley et al., 2014). Thus, overfitting was inevitable and the generalisation ability of the mRNAsi was not evaluated. Therefore, the prognostic value of the mRNAsi in GBM needs to be validated in other independent databases, such as the Chinese Glioma Genome Atlas (CGGA) and Gene Expression Omnibus (GEO) (Barrett et al., 2013).

In this study, we used mRNA expression data and the OCLR machine-learning algorithm to simultaneously examine the independent prognostic value of mRNAsi/c_mRNAsi in TCGA, CGGA, and two GEO datasets. We compared mRNAsi/c_mRNAsi directly and evaluated the model improvement ability. Then, we applied the latest *CIBERSORTx* tool (Newman et al., 2019) to evaluate the relationship between mRNAsi/c_mRNAsi and immune cell infiltration and conducted single sample gene set enrichment analysis (ssGSEA) to comprehensively examine its prognostic value and relationship with the immune microenvironment.

# 2 MATERIALS AND METHODS

## 2.1 Data Acquisition

RNA-sequencing data (level 3) of 158 patients with GBM from TCGA and 279 patients with GBM from the CGGA were obtained. The data from TCGA were downloaded from the University of California Santa Cruz (UCSC) Xena website (https://xena.ucsc.edu/). Transcript abundances were measured in fragments per kilobase of transcript per million mapped reads (FPKM). We only included patients who had adequate clinical and pathological data. Then, to uncover the practicability and accuracy of independent prognostic factors for GBM, samples from the TCGA and CGGA cohorts were applied as training and validation cohorts, respectively. Moreover, we included two GEO datasets (GSE4412 (Freije et al., 2004) and GSE13041 (Lee et al., 2008)) with more than 100 samples and follow-up data as our external validation data. The characteristics of the patients from the databases are presented as means ± standard deviations (continuous variables that satisfied the normal distribution), median, minimum, maximum and quartile (continuous variables that did not satisfy the normal distribution), and percentage (categorical variables), as appropriate.

## 2.2 mRNAsi/c_mRNAsi Acquisition

The mRNAsi was calculated using the OCLR machine-learning algorithm (Malta et al., 2018). Tumour purity was evaluated with ESTIMATE (Yoshihara et al., 2013) and c_mRNAsi was obtained by dividing the mRNAsi by tumour purity (Zhang et al., 2020b). The gene expression-based mRNAsi/c_mRNAsi was represented using β values ranging from zero (no gene expression) to one (complete gene expression).

## 2.3 Analysis of Independent Prognostic Factors

### 2.3.1 The Relationship Between mRNAsi/c_mRNAsi and Overall Survival (OS)

To explore the effect of mRNAsi/c_mRNAsi on OS of patients with GBM, we used locally weighted scatterplot smoothing (Lowess) algorithm to flexibly evaluate the association of mRNAsi/c_mRNAsi with OS. The results were obtained as a fitting smooth curve. When the curve was linear, mRNAsi/c_mRNAsi was included as a continuous variable; otherwise, mRNAsi/c_mRNAsi was included as a dichotomous variable in the subsequent analysis.

### 2.3.2 Survival Analysis

When the variables were analysed as dichotomous variables, the optimal cut-off for each index with the associated hazard of OS was identified by log-rank statistics in a survfit model, using the *cutp* function of the *survMisc* package. Then, patients with GBM were included into either the high or the low group according to the optimal cut-off. Next, Kaplan-Meier analysis with log-rank test was conducted to estimate the survival curves of each group and to compare the prognosis between different groups, by using the *survival* package.

### 2.3.3 Identification of Confounding Variables

Residual confounding variables refer to incomplete adjustment for factors related to both exposure and outcome (Kernan et al., 2000). The confounding variables that may influence the OS of patients with GBM need to be identified. To estimate the magnitude of the effect of mRNAsi/c_mRNAsi on GBM, we used the Cox proportional hazards model. The regression coefficient changed more than 10% when the adjustment variables were included or not included or when those with $p < 0.1$ in the univariate analysis with OS were considered as confounding variables to be adjusted (adjusted I/II model) (Kernan et al., 2000). The common covariates in TCGA were age, gender, IDH, radiotherapy, chemotherapy, and subtype. In addition, 1p19q and MGMTp were common covariates in CGGA but without subtype. Afterward, an interaction test and a stratified analysis (Soria et al., 2015) of the association between mRNAsi/c_mRNAsi and OS were conducted in both the non-adjusted model and adjusted I model (identified confounders). A two-tailed $p < 0.05$ was considered statistically significant. Empower (www.empowerstats.com; X&Y solutions Inc., Boston, MA) and R (http://www.R-project.org) were used for the abovementioned statistical analyses.

## 2.4 Construction and Comparison of Prognostic Models

### 2.4.1 Model Establishment

After confirming the effect of mRNAsi/c_mRNAsi on OS, we further evaluated and compared the benefit of five different models, including the prognostic model constructed by well-established clinical factors (model 1), model 1 integrated with mRNAsi (model 2)/c_mRNAsi (model 3), and single mRNAsi (model 4)/c_mRNAsi (model 5).

### 2.4.2 Model Evaluation and Nomogram

We used discrimination, calibration, and model improvement capability to assess the performance of the different models. Discrimination was evaluated through the receiver operating characteristic (ROC) curve, (Zhou et al., 2019), concordance index (C-index) (Harrell et al., 1996) and the prediction error and decision curve analysis (DCA) curves (Kerr et al., 2016). Notably, the enhanced bootstrap method with 500 resamples was used for internal validation (Wang et al., 2019). Discrimination and calibration were evaluated by apparent and adjusted C-index and Brier Score. Finally, model improvement capability was evaluated by applying net reclassification improvement (NRI) and integrated discrimination improvement (IDI) using the *survIDINRI* package (Pencina et al., 2008). After the best model was identified, the *regplot* package was employed to construct the nomogram.

### 2.4.3 External Validation

We applied the data from CGGA and GEO as external validation. In CGGA, as described above, we performed mRNAsi/c_mRNAsi acquisition, independent prognostic factors analysis, and prognostic model construction and comparison. It should be noted that because the clinical information in TCGA and CGGA was not identical, common covariates were not the same. GSE4412 (Freije et al., 2004) and GSE13041, (Lee et al., 2008), which constitute GEO, were also applied for the external effect validation of mRNAsi/c_mRNAsi on OS. Similarly, patients were divided into the high or low group based on the optimal cut-off, which was previously calculated using the same package. Kaplan-Meier analysis was employed to assess the two groups with the log-rank test. Afterwards, ROC analysis of time-independent outcomes was also performed.

## 2.5 Function Analysis

### 2.5.1 Infiltrative Immune Cell Analysis

To characterise the abundance of 22 infiltrative immune cell types based on the expression matrix data of patients with GBM, the *CIBERSORTx* web tool (https://cibersortx.stanford.edu/) was applied (Newman et al., 2019). This tool uses batch correction to adjust the gene expression profile of the bulk of cells (mixture data) to eliminate possible cross-platform variations between the mixture data and the gene expression data of single cells (signature matrix) (Le et al., 2020). After enabling batch correction, performing the Bulk mode, and selecting the quantile normalisation algorithm, the absolute score for the proportion of 22 immune cell subsets in GBM samples was calculated. The samples with $p < 0.05$ were enrolled for further analysis because of the high reliability of the inferred results (Ali et al., 2016). Wilcoxon rank-sum test was used to compare the differences in the proportion of the 22 infiltrative immune cell subtypes between the high and low groups. The Spearman correlation test was used to further explore the correlation of the two indexes with immune cell types.

### 2.5.2 Single Sample Gene Set Enrichment Analysis (ssGSEA)

The ssGSEA method, (Barbie et al., 2009), which is a modification of GSEA, (Subramanian et al., 2005), was

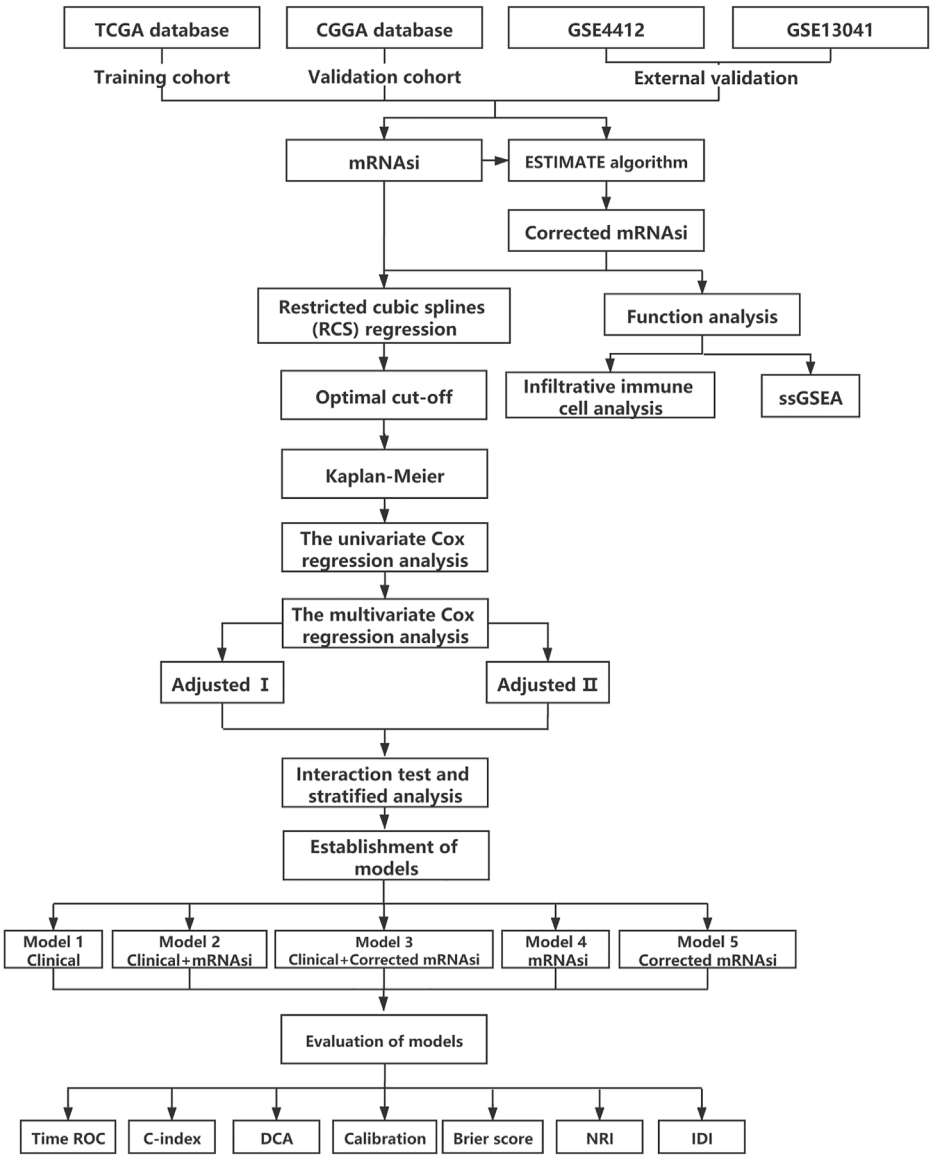


**FIGURE 1 |** Flow chart.

developed to obtain an enrichment score for a single sample instead of two groups of samples. Here, the ssGSEA was used to compare differentially enriched hallmarks of cancer gene sets (Barbie et al., 2009). To identify key pathways in different groups, we chose to focus on 50 hallmark gene sets, which were designed to highlight gene sets contained in the Molecular Signatures Database (MSigDB), (Liberzon et al., 2015), one of the most widely used and comprehensive databases of gene sets for performing gene set enrichment analysis. The hallmarks of the gene sets effectively summarise most of the relevant information of the original founder sets and, by reducing both variation and redundancy, provide more refined and concise inputs for gene set enrichment analysis (Liberzon et al., 2015). Gene symbol profiles for *Homo sapiens* were downloaded from the MSigDB. Then, the degree of association between each hallmark's ssGSEA profile was estimated using the *gsva* package. Next, differential analysis was performed with the *limma* package under the threshold of the absolute value of $t > 1$ and adjusted $p$ value <0.05.

# 3 RESULTS

## 3.1Patient Characteristics

An overview of the stemness indices-related signature development and validation workflow is presented in **Figure 1**. A total of 874 GBM samples (158 from TCGA as the training cohort, and 279 from CGGA and 437 from GEO as the validation

**TABLE 1 |** Patient characteristics.

| Character | Training cohort | External validation cohort | External validation GEO cohort | External validation GEO cohort |
|---|---|---|---|---|
| | TCGA (*n* = 158) | CGGA (*n* = 279) | GSE4412 (*n* = 170) | GSE13041 (*n* = 267) |
| Age | 59.6 (13.6) | 48.00 (39.5–57.0) | 42.0 (33.0–54.0) | 53.71 (13.8) |
| mRNAsi | 0.56 (0.22) | 0.50 (0.17) | 0.60 (0.23) | 0.42 (0.33–0.52) |
| c_mRNAsi | 0.74 (0.25) | 0.57 (0.16) | 0.71 (0.25) | 0.51 (0.15) |
| Male | 102 (64.56%) | 165 (59.14%) | 64 (37.65%) | 151 (63.18%) |
| IDH | | | | |
| Wild type | 148 (93.67%) | 211 (75.63%) | NA | NA |
| Mutation | 10 (6.33%) | 68 (24.37%) | NA | NA |
| Radiotherapy | | | | |
| No | 29 (18.35%) | 53 (19%) | NA | NA |
| Yes | 129 (81.65%) | 226 (81%) | NA | NA |
| Chemotherapy | | | | |
| No | 45 (28.48%) | 49 (17.56%) | NA | NA |
| Yes | 113 (71.52%) | 230 (82.44%) | NA | NA |

*Data are presented as median (interquartile range) or N (%). TCGA, the cancer genome atlas; CGGA, chinese glioma genome atlas; GEO, gene expression omnibus; IDH, isocitrate dehydrogenase; NA, not applicable.*

cohort) were obtained in our study. The patient characteristics are presented in **Table 1**.

## 3.2 mRNAsi/c_mRNAsi Acts as an Independent Prognostic Factor

### 3.2.1 Patients With High mRNAsi/c_mRNAsi GBM had a Better Prognosis

In the TCGA dataset, the relation between mRNAsi/c_mRNAsi and OS was nonlinear. Therefore, they were considered dichotomous variables in subsequent analysis (**Supplementary Figures S1A,B**). A total of 158 samples were clustered into the high- ($n$ = 111) or low- ($n$ = 47) mRNAsi group based on the optimal cut-off value identified by *survMisc* package (**Supplementary Figure S2A**). Patients in the high-mRNAsi group had better OS than those in the low-mRNAsi group ($p$ = 0.0003) (**Figure 2A**). Similarly, 158 patients were clustered into the high- ($n$ = 123) or low- ($n$ = 35) c_mRNAsi group based on the optimal cut-off value identified by the same package (**Supplementary Figure S2B**). Patients in the high-c_mRNAsi group had better OS than those in the low-c_mRNAsi group ($p$ = 0.0008) (**Figure 2B**). Moreover, we explored the relationship between mRNAsi/c_mRNAsi and disease-specific survival/progression-free interval in TCGA, and found that the trends for disease-specific survival ($p$ = 0.0028) (**Supplementary Figures S3A,B**) and progression-free interval ($p$ < 0.0001) (**Supplementary Figures S3C,D**) were similar to that for OS.

To determine whether the mRNAsi/c_mRNAsi-associated prognostic signature had a similar prognostic value in different populations, its prediction performance was validated externally in CGGA and GEO. Similarly, we considered mRNAsi/c_mRNAsi as a dichotomous variable in CGGA according to the Lowess result (**Supplementary Figures S1C,D**). All samples in CGGA and GEO were clustered into the high- or low-mRNAsi/c_mRNAsi group based on the optimal cut-off value identified by the same package (**Supplementary Figure S2C**). Consistent with the findings in TCGA, the Kalan-Meier curve in CGGA revealed that patients in the high-mRNAsi/c_mRNAsi group had better OS than those in the low-mRNAsi/c_mRNAsi group ($p$ = 0.0040 and 0.0011, respectively) (**Figures 2C,D**). GSE4412 has the transcriptional profiling of 170 GBM samples from 74 patients (Freije et al., 2004). A total of 170 GBM samples were divided into the high- ($n$ = 121) or low- ($n$ = 49) c_mRNAsi group based on the optimal cut-off value (**Supplementary Figure S2D**), and the high-c_mRNAsi group had better OS ($p$ = 0.0400) (**Figure 2E**). GSE13041 has 267 GBM samples from 239 patients, (Lee et al., 2008), which were divided into the high- ($n$ = 186) or low- ($n$ = 81) c_mRNAsi group based on the optimal cut-off value (**Supplementary Figure S2**). The high-c_mRNAsi group also had better OS ($p$ = 0.0040) (**Figure 2F**).

### 3.2.2 Identification of Confounding Variables

Given the possible interference of confounding variables, we carried out confounders identification and then adjusted for these potential confounding factors. In TCGA, we found that mRNAsi had to be adjusted for age through univariate analysis (**Figure 3A**). These covariates combined with common covariates (age, gender, IDH, radiotherapy, chemotherapy, and subtype) were enrolled into the adjusted II model. In the adjusted I model, after adjusting for confounders (age and IDH), mRNAsi was still associated with OS (hazard ratio (HR) = 0.561, 95% confidence interval (CI) 0.383–0.823, $p$ = 0.003) (**Figure 3B**). Furthermore, after adjusting for predominant clinical and prognostic factors (age, gender, IDH, radiotherapy, chemotherapy, and subtype) in the adjusted II model, mRNAsi independently predicted prognosis in TCGA (HR = 0.552, 95% CI 0.370–0.823, $p$ = 0.004) (**Figure 3C**). The interaction analysis revealed that gender played an interactive role in the association between mRNAsi and OS (**Supplementary Table S1**). Male patients had higher HRs between mRNAsi and OS (HR = 0.92; 95% CI, 0.11–7.59) than females (HR = 0.32; 95% CI, 0.17–0.61). In the same way, we found that only age should be adjusted on c_mRNAsi through univariate analysis (**Figure 3D**), and this covariate combined

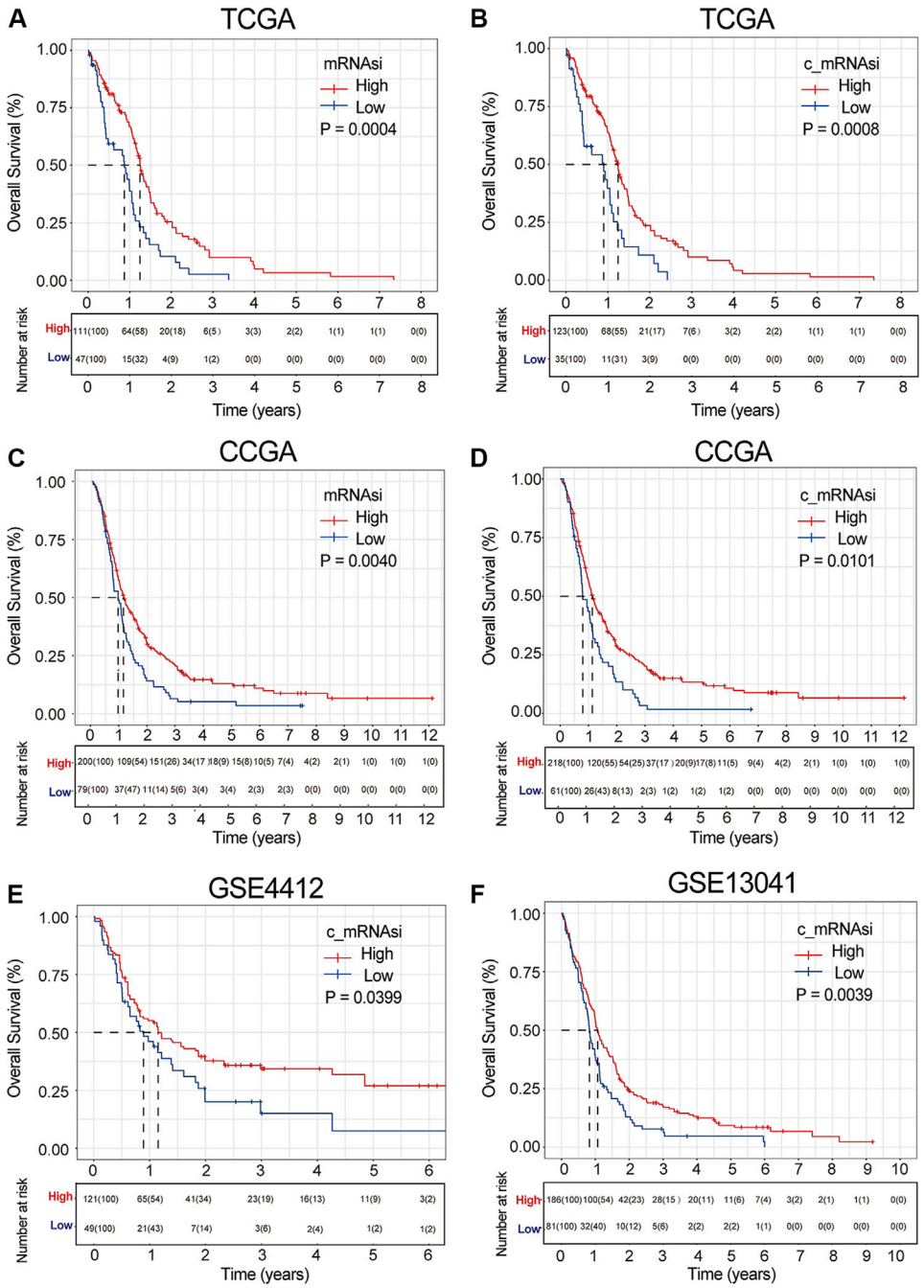


**FIGURE 2 |** Survival curve of mRNAsi/c_mRNAsi on prognosis. **(A)**. Overall survival curve of mRNAsi in TCGA. **(B)**. Overall survival curve of c_mRNAsi in TCGA. **(C)**. Overall survival curve of mRNAsi in CGGA. **(D)**. Overall survival curve of c_mRNAsi in CGGA. **(E)**. Overall survival curve of c_mRNAsi in GSE4412. **(F)**. Overall survival curve of c_mRNAsi in GSE13041.

with common covariates were enrolled in the adjusted II model. In the adjusted I model, after adjusting for the confounder (age), c_mRNAsi was still associated with OS (HR = 0.550, 95% CI 0.376–0.805, $p$ = 0.002) (**Figure 3E**). Furthermore, after adjusting for predominant clinical and prognostic factors in the adjusted II model, c_mRNAsi independently predicted prognosis in TCGA (HR = 0.552, 95% CI 0.356–0.856, $p$ = 0.008) (**Figure 3F**). The effect of mRNAsi/c_mRNAsi on OS was consistent across subgroups (**Supplementary Table S1**). Ultimately, mRNAsi/c_mRNAsi was an independent prognostic factor for OS in patients with GBM.

Moreover, in CGGA, we identified different confounders (IDH, chemotherapy, and 1p19q on mRNAsi, as well as IDH

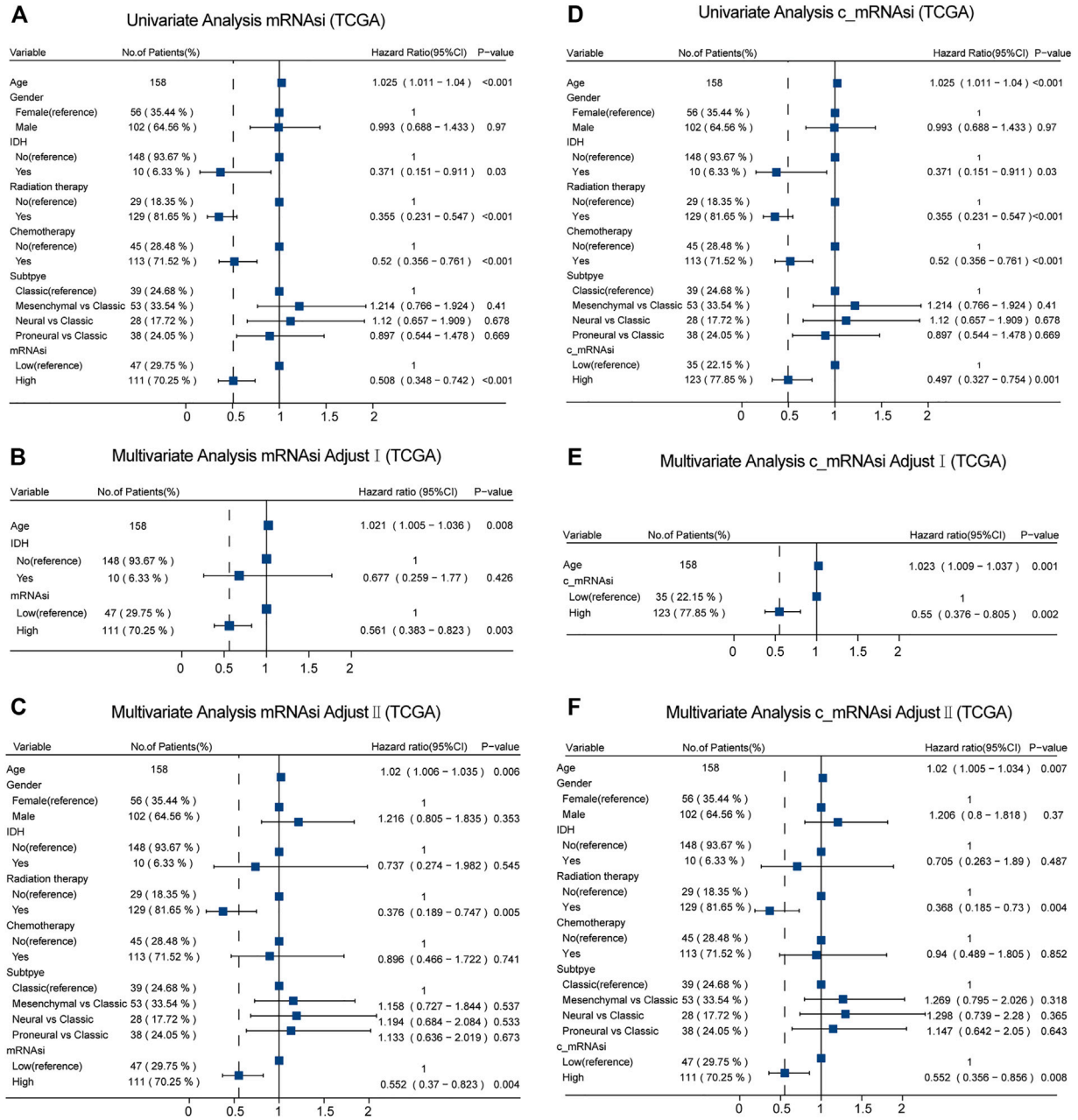


**FIGURE 3 |** Forest plots of univariate and multivariate Cox regression analysis in TCGA. **(A)**. Univariate Cox regression analysis of mRNAsi in TCGA. **(B)**. Multivariate Cox regression analysis of mRNAsi adjusted I model in TCGA. **(C)**. Multivariate Cox regression analysis of mRNAsi adjusted II model in TCGA. **(D)**. Univariate Cox regression analysis of c_mRNAsi in TCGA. **(E)**. Multivariate Cox regression analysis of c_mRNAsi adjusted I model in TCGA. **(F)**. Multivariate Cox regression analysis of c_mRNAsi adjusted II model in TCGA.

and 1p19q on c_mRNAsi) that had to be adjusted through univariate analysis (**Figures 4A,D**), and these confounders (adjusted I model, **Figures 4B,E**) combined with common covariates (age, gender, IDH, radiotherapy, chemotherapy, 1p19q, and MGMTp) were enrolled in the adjusted II model (**Figures 4C,F**). We found that only c_mRNAsi was an independent prognostic signature in patients with GBM in both the adjusted I and adjusted II models ($p$ = 0.008, 0.015, respectively) (**Figures 4E,F**) and across stratified analyses (**Supplementary Table S2**).

## 3.3 Construction and Evaluation of Prognostic Models

We used discrimination, calibration, and model improvement capability to evaluate five established models. Models 2 and 3 had

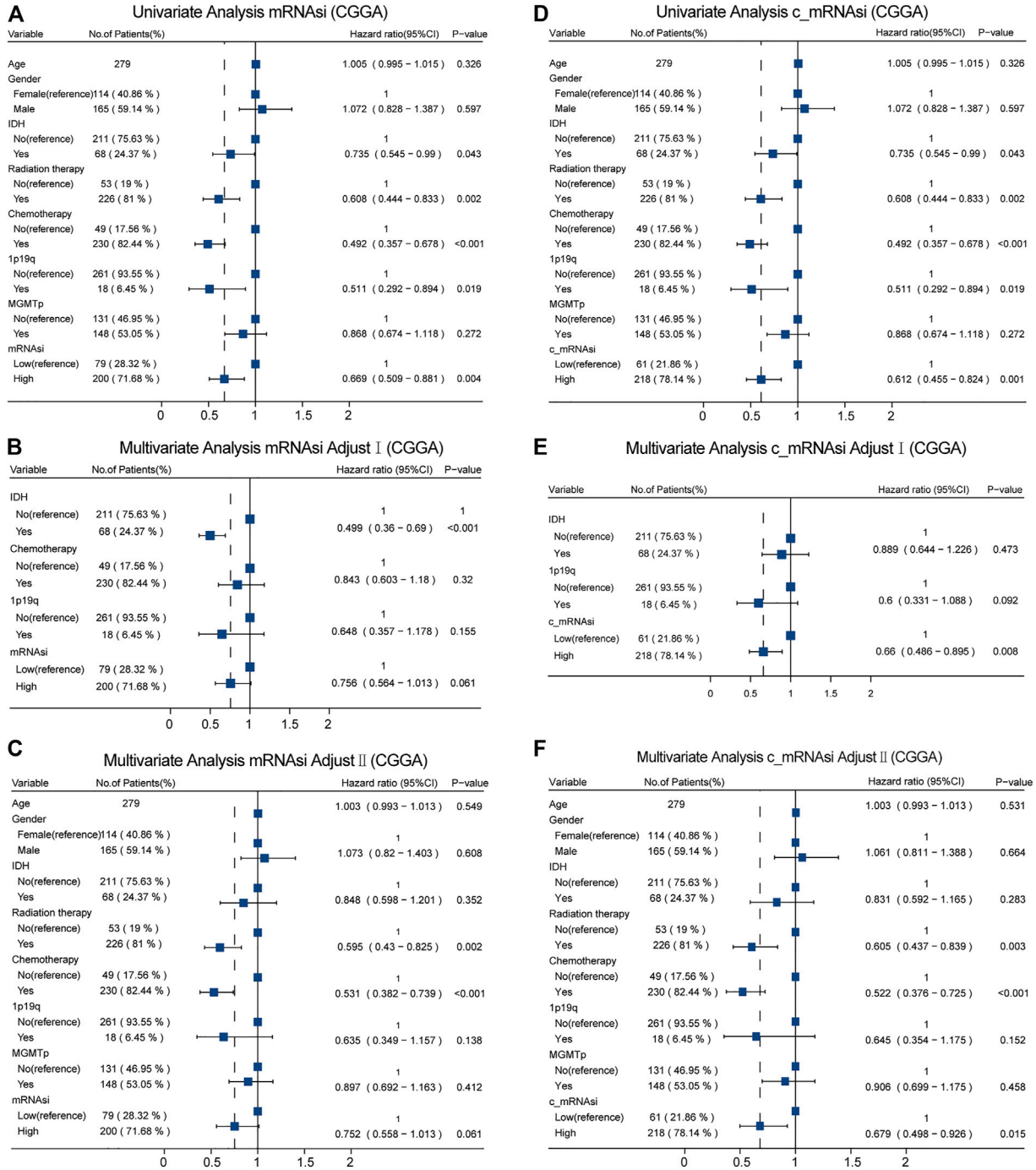


**FIGURE 4 |** Forest plots of univariate and multivariate Cox regression analysis in CGGA. **(A)**. Univariate Cox regression analysis of mRNAsi in CGGA. **(B)**. Multivariate Cox regression analysis of mRNAsi adjusted I model in CGGA. **(C)**. Multivariate Cox regression analysis of mRNAsi adjusted II model in CGGA. **(D)**. Univariate Cox regression analysis of c_mRNAsi in CGGA. **(E)**. Multivariate Cox regression analysis of c_mRNAsi adjusted I model in CGGA. **(F)**. Multivariate Cox regression analysis of c_mRNAsi adjusted II model in CGGA.

a higher area under the curve (AUC), better C-index, and lower prediction error than the other models (**Figures 5A–C**). The apparent and adjusted C-index as well as the Brier scores in years 0.5-, 1-, and 1.5-years indicated that models 2 and 3 were better than the others (**Supplementary Table S3**). DCA showed that the net benefit of models 2 and 3 in years 0.5 and 1 years was better than that of other models, but there was no significant difference in year 1.5 (**Figures 5D–F**). We found that the calibration of models 2 and 3 was better than that of other models in 0.5 and 1 years, while the calibration of the five models was poor in

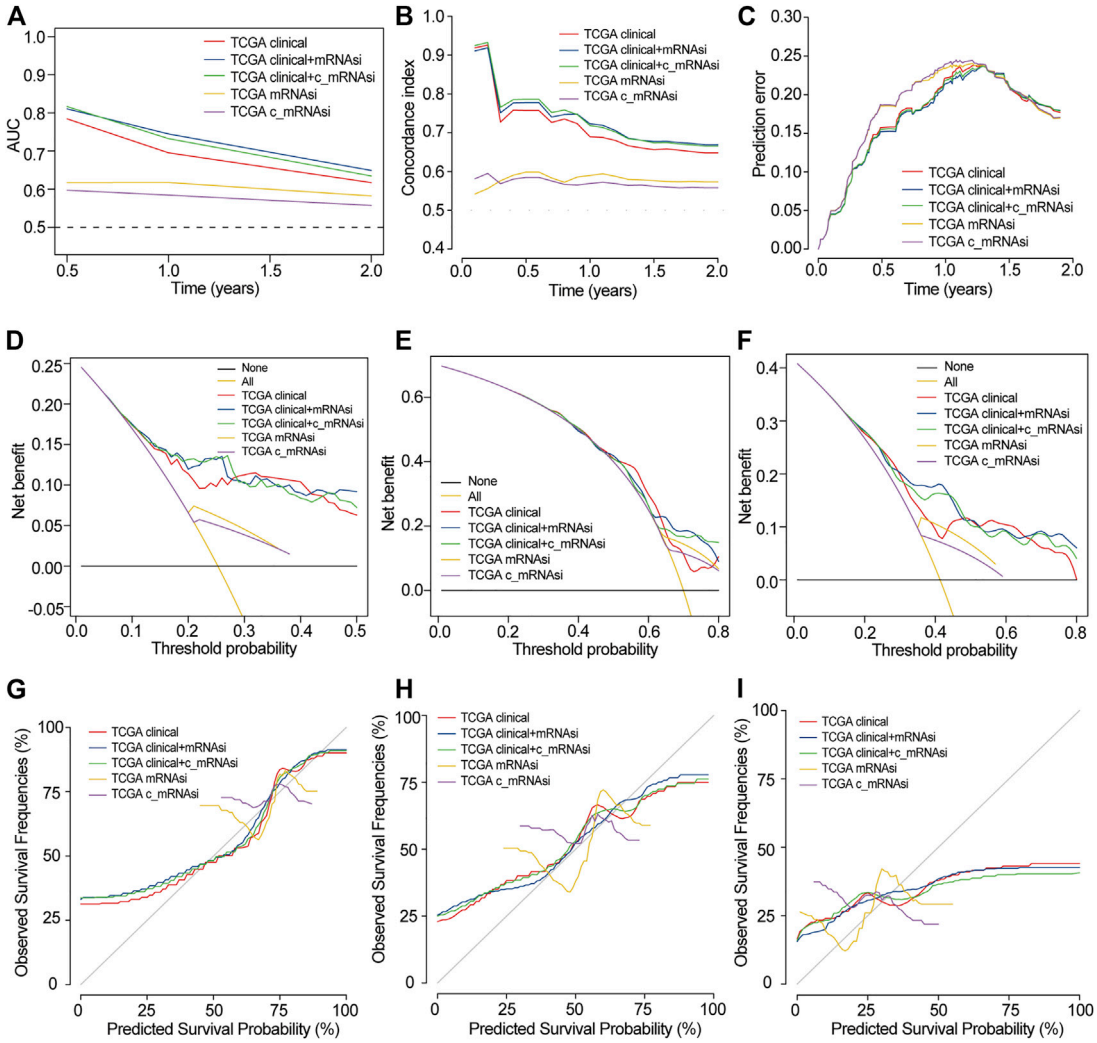


**FIGURE 5 |** Evaluation of prognostic models in TCGA. **(A)**. AUC in TCGA. **(B)**. C-index in TCGA. **(C)**. Prediction error in TCGA. **(D)**. 0.5-years DCA in TCGA. **(E)**. 1-year DCA in TCGA. **(F)**. 1.5-years DCA in TCGA. **(G)**. 0.5-years calibration in TCGA. **(H)**. 1-year calibration in TCGA. **(I)**. 1.5-years calibration in TCGA.

1.5 years (**Figures 5G–I**). As for model improvement capability, when model 1 was considered as the reference, the NRI and IDI of models 2 and 3 were both positive. In contrast, the NRI and IDI of models 4 and 5 were both negative, although there were no significant statistical differences (**Supplementary Table S4**). From the above results, we determined that models 2 and 3 had good discrimination and calibration in the OS prediction of patients with GBM.

In CGGA, we also built five models that were similar to those in TCGA. In TCGA, only 24 patients were followed up for more than 2 years, and the prognosis was very poor. Since the median follow-up time was only 12 months, the selected time points were 0.5, 1 and 1.5 years. In CGGA, since the 62 cases were followed up for more than 2 years, the time point was extended to 3 and 5 years. Here, models 2 and 3 also had a higher AUC and better C-index but had the same prediction error as the other models (**Supplementary Figures S4A–C**). DCA showed that the net benefit of model 2 in 0.5, 1, 1.5, and 3 years was higher than that of other models, but there was no significant difference in 5 years (**Supplementary Figures S4D–H**). The calibration of models 2 and 3 was better than that of other models in 0.5 and 1 years, while the calibration of the five models was poor in 1.5, 3, and 5 years (**Supplementary Figures S4I–M**). The Brier scores indicated that models 2 and 3 were better than the others (**Supplementary Table S5**). As for model improvement capability, when model 1 was considered as the reference, the NRI and IDI of models 2 and 3 were both positive. In contrast, the NRI and IDI of models 4 and 5 were both negative (**Supplementary Table S6**). Because of the limited clinical data of GEO, we only compared models 4 and 5. The AUCs were 0.536–0.618, 0.544–0.589 in GSE4412 and GSE13041, respectively (**Supplementary Figures S4N,O**).

Combined with the above results, we found that mRNAsi/c_mRNAsi is an independent prognostic factor in TCGA, but only c_mRNAsi is an independent prognostic factor in CGGA. In TCGA, the comparison of the five models revealed that models 2

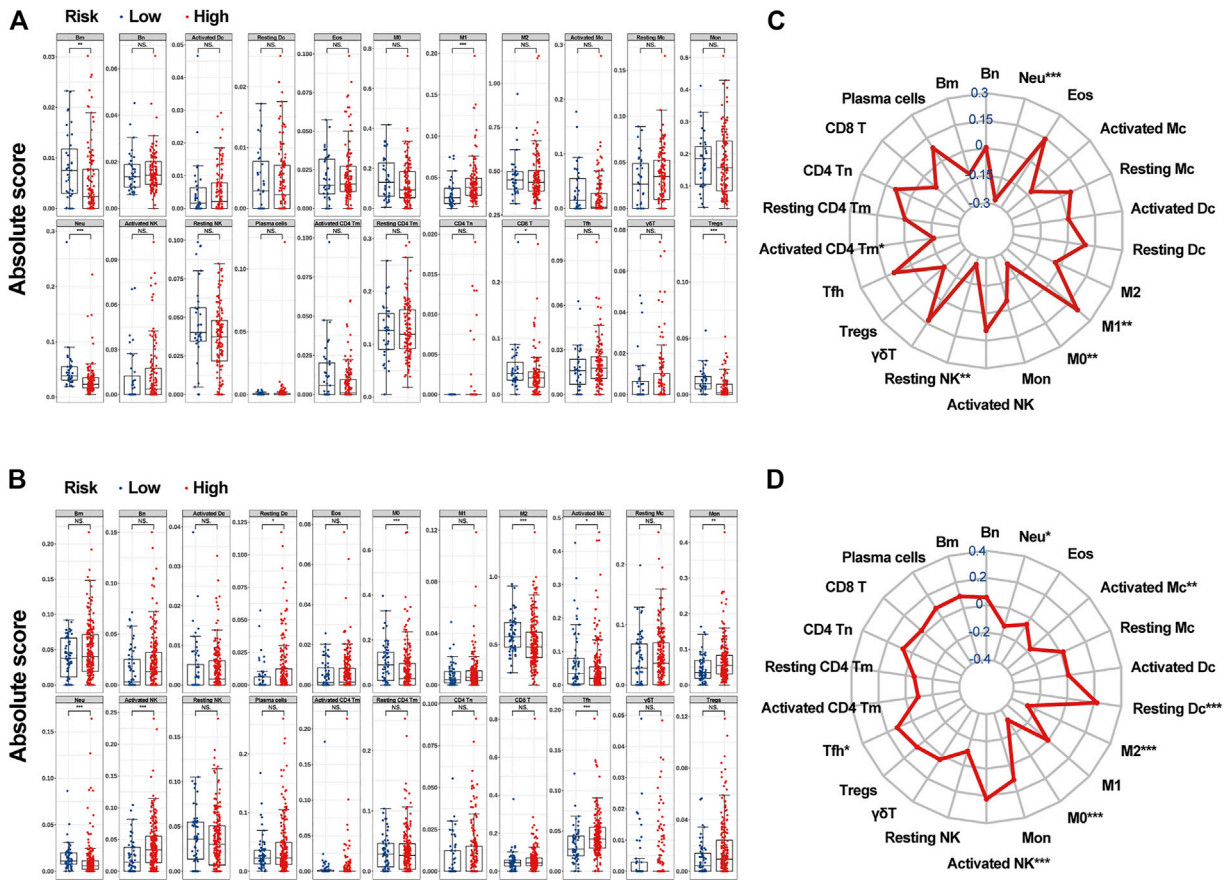


**FIGURE 6 |** The associations between c_mRNAsi and the abundance of infiltrative immune cells. **(A)**. Infiltrative immune cell analysis in TCGA. **(B)**. Infiltrative immune cell analysis in CGGA. **(C)**. Radar chart in TCGA. **(D)**. Radar chart in CGGA. Abbreviations: Bm, memory B cells; Bn, naive B cells; Dc, Dendritic cells; Eos, eosinophils; M0, macrophage M0; M1, macrophage M1; M2, macrophage M2; Mc, mast cells; Mon, monocytes; Neu, neutrophils; Tm, memory T cells; Tn, naïve T cells; Tfh, follicular helper T cells; γδT, gamma delta T cells; Treg, regulatory T cells.

and 3 were the best, and there was little difference between these two models. In CGGA, model 3 performed the best among the five models. In GEO, there was no significant difference between the single mRNAsi and c_mRNAsi models. Therefore, we finally decided to adopt model 3 (clinical factors integrated with the c_mRNAsi) to predict OS and construct a nomogram in TCGA (**Supplementary Figure S4**). According to the nomogram, a representative patient with the total point of 286, the 0.5-years, 1-year, and 1.5-years survival rates were 82.6, 68.9, and 40.4%, respectively (**Supplementary Figure S5**).

## 3.4 Functional Analysis

### 3.4.1 Differential Abundance of Infiltrative Immune Cells

By applying the *CIBERSORTx* algorithm, the relative proportions of 22 immune cell subsets in GBM were acquired. A total of 158 patients with GBM from TCGA and 279 patients with GBM from the CGGA were enrolled for further analysis. In the TCGA dataset, the infiltration level of M1 macrophages was significantly higher in the high-c_mRNAsi group, whereas the infiltration levels of memory B cells, neutrophils, $CD8^+$ T cells, and regulatory T cells were significantly higher in the low-c_mRNAsi group (**Figure 6A**). In CGGA, the infiltration levels of resting dendritic cells, monocytes, activated NK cells, and follicular T helper cells were significantly higher in the high-c_mRNAsi group, whereas macrophages (M0 and M2), activated mast cells, and neutrophils were significantly higher in the low-c_mRNAsi group (**Figure 6B**). Radar chart indicated that in the TCGA dataset, c_mRNAsi was positively correlated with M1 macrophages and negatively correlated with neutrophils, M0 macrophages, resting NK cells, and activated memory $CD4^+$ T cells in the training cohort (**Figure 6C**). In the CGGA dataset, c_mRNAsi was positively correlated with resting dendritic cells, activated NK cells, and follicular T helper cells, and negatively correlated with neutrophils, activated mast cells, and macrophages (M0 and M2) (**Figure 6D**).

### 3.4.2 Pathway Enrichment Analysis

The ssGSEA was used to estimate the degree of enrichment of the MSigDB hallmark gene set in individual samples from the high- and low-c_mRNAsi groups of both TCGA and CGGA. This allowed us to identify signalling pathways involved in GBM and

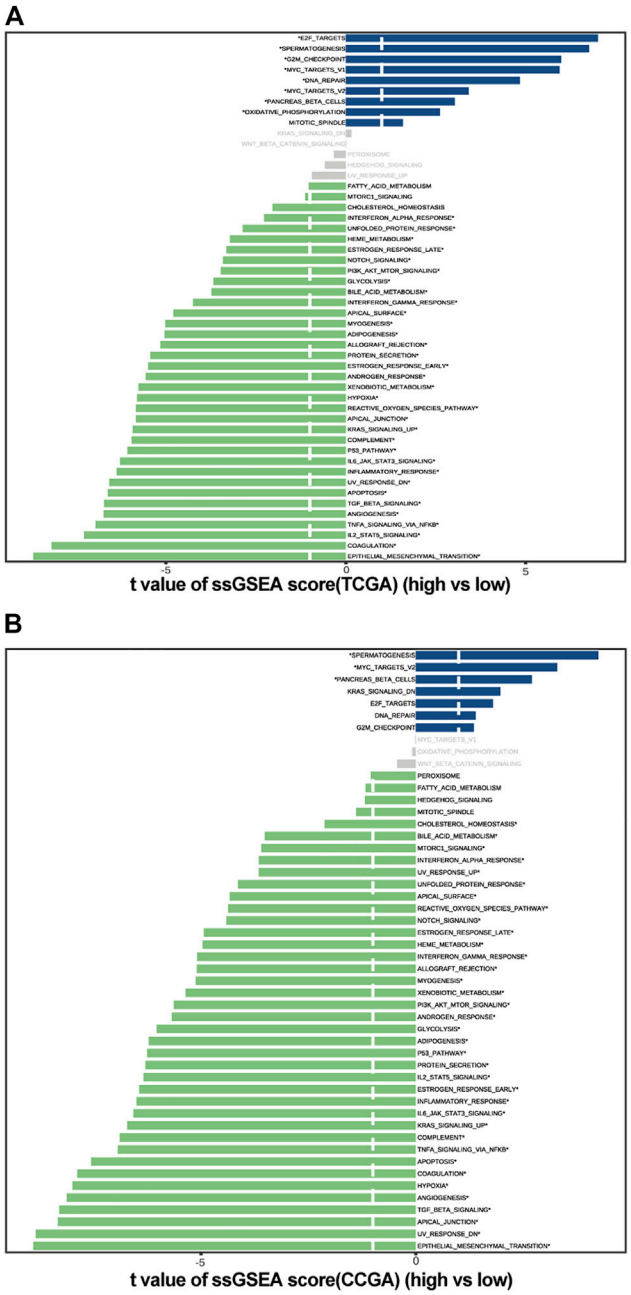


**FIGURE 7 |** Pathway enrichment analysis in high and low c_mRNAsi groups. **(A)**. Pathway enrichment analysis in TCGA. **(B)**. Pathway enrichment analysis in CGGA.

to estimate their degree of association with each group (high versus low). The results indicated that spermatogenesis, MYC targets v2, and pancreas beta cell pathways were involved significantly in the low-c_mRNAsi group of both TCGA and CGGA, whereas unfolded protein response, haem metabolism, early and late oestrogen response, NOTCH signalling, glycolysis, bile acid metabolism, interferon α/γ response, apical surface, myogenesis, adipogenesis, allograft rejection, androgen response, xenobiotic metabolism, hypoxia, reactive oxygen species pathway, apical junction, KRAS signalling, complement, P53, IL6/JAK/STAT3 signalling, inflammatory response, UV response DN, apoptosis, TGF-β signalling, angiogenesis, TNFα signalling via NF-κB, IL-2/STAT5 signalling, coagulation, and epithelial mesenchymal transition pathways were involved significantly in the high-c_mRNAsi group of both TCGA and CGGA (**Figures 7A,B**).

## 4 DISCUSSION

GBM is composed of non-homogeneous cell populations exhibiting varying degrees of genetic and functional heterogeneity. Cancer stem cells are capable of sustaining tumours by manipulating genetic and non-genetic factors to metastasise, resist treatment, and maintain the tumour microenvironment (Saygin et al., 2019). Understanding the key traits and mechanisms of stemness of cancer stem-like cells provides opportunities to improve patient outcomes via improved prognostic models and therapeutics. However, tumour cells are usually comprised of a heterogeneous mixture of subclones, each of which may have its own distinct characteristics. Therefore, accurately assessing the make-up of the different cell states within a tumour biopsy is very important. Here, we calculated an mRNAsi, which was also corrected by tumour purity (c_mRNAsi), based on the expression profile of 12,953 genes in 874 GBM samples from the TCGA, CGGA, and GEO public databases using the OCLR machine-learning algorithm. We found that, after confounding variable identification and interaction and stratified analyses, c_mRNAsi remained an independent prognostic factor in both TCGA and CGGA, whereas mRNAsi was affected by gender in TCGA and was no longer an independent prognostic factor after adjustment in CGGA. Model 2 (clinical factors integrated with mRNAsi) and model 3 (clinical factors integrated with c_mRNAsi) showed better calibration and discrimination than clinical factors alone in both TCGA and CGGA. Moreover, model 3 performed better than model 2, although there was no significant difference between the single mRNAsi and c_mRNAsi models in GEO. Therefore, we concluded that c_mRNAsi can be used as a new index for the construction of algorithms that predict the prognosis of patients with GBM. To explore the possible reasons for the difference in prognosis between the high- and low-c_mRNAsi groups, we applied the *CIBERSORTx* algorithm to infer the abundance of immune infiltrating cells in TCGA and CGGA and found differential infiltration patterns across 5 and 8 clusters in TCGA and CGGA, respectively. Importantly, we found that high mRNAsi correlated significantly with high infiltration of immune activated cells, especially M1 macrophages, dendritic cells, monocytes, activated NK cells, and follicular T helper cells. Lastly, we screened the potential signalling pathways of the c_mRNAsi-related signature and found that most of the pathways were immune-related.

In this study, we utilised the OCLR machine-learning algorithm to quantify mRNAsi and c_mRNAsi for each GBM sample. Using OCLR, we previously identified undiscovered biological mechanisms associated with the dedifferentiated oncogenic state (Lian et al., 2019). Moreover, OCLR exhibited comparable performance with a more flexible and convenient

formulation to that with traditional support vector machine-based one-class predictors (Sokolov et al., 2016). We drew support from OCLR machine-learning algorithm to derive two distinct molecular metrics of stemness indices and finally selected c_mRNAsi for subsequent validation analysis, owing to its observed prognostic significance in various data. Stemness indices had already been identified in several malignancies and had different prognostic values in ovarian cancer, (Kaipio et al., 2020), medulloblastoma, (Lian et al., 2019), colon cancer, (Tao et al., 2019), or acute myeloid leukaemia (Seneviratne et al., 2019). However, stemness indices are targeted at bulk tissues, a mixture of tumour tissue and normal tissue. Although some scholars developed new algorithms to adjust stemness indices, (Pan et al., 2019), the algorithms are complex. The ESTIMATE algorithm can adjust directly from transcriptome data, (Yoshihara et al., 2013), which is more convenient. In our multi-cohort screening, we examined the capacity of c_mRNAsi, which is obtained after correcting the index by the tumour purity calculated with ESTIMATE, (Yoshihara et al., 2013), to predict OS. Our findings demonstrate that c_mRNAsi can be implemented in clinical practice, something that has not been previously reported. Common clinical indicators of GBM include KPS, *MGMT*, *IDH1*, and epidermal growth factor receptor vIII (Burgenske et al., 2019; Chaddad et al., 2019). GBM-specific microRNAs, including miR-21 and miR-10b, have also been presented as biomarkers with promising prognostic values (Sasmita et al., 2018). Confounder identification and interaction tests could help us to better understand the relationship between the variables and disease. In our study, we first used the mRNAsi/c_mRNAsi calculated by the algorithm as a variable to carry out residual confounder identification and interaction test with common clinical indicators, so as to minimise the impact of confounding factors on GBM OS as much as possible. Furthermore, discrimination and calibration are the most commonly used indicators in the evaluation of clinical prediction models. However, a systematic review found that while 63% of the studies on prediction models reported discrimination data, only 36% included calibration data (Wessler et al., 2015). In the present study, we report both discrimination and calibration in the training and validation cohorts. In addition, we did not only use the enhanced bootstrap test for internal validation, but also directly compared multiple models in two data sets (TCGA and CGGA) to minimise model overfitting. This significantly differs from traditional studies of clinical models, and allowed us to select the optimal model for prognosis prediction in patients with GBM.

Previous studies have shown that the higher the stemness indices scores, the worse the overall survival outcomes, (Pei et al., 2020), which is the opposite from our results. Therefore, we wanted to further explore the reasons for the different prognosis among the groups. Using gene-expression-based metrics, a recent study reported the association of stemness with immune cell infiltration and genomic, transcriptomic, and clinical parameters across 21 solid cancers (Miranda et al., 2019). Pervasive negative associations between cancer stemness and anticancer immunity have also been found (Miranda et al., 2019). In line with the current pan-cancer findings, we also analysed infiltrative immune cells in distinct cohorts (TCGA and CGGA) using the *CIBERSORTx* algorithm and found that the high-c_mRNAsi group exhibited significant immune suppression. Based on the expression data in TCGA and CGGA, we observed that c_mRNAsi correlated negatively with infiltrating levels of immune cells. Promoting Treg overrepresentation and function induces systemic and intratumoural immunosuppression (Long et al., 2020). $CD8^+$ cytotoxic T lymphocyte cells, macrophages, Tregs, and other immune cells can respond to GBM treatment, including immunotherapy, to a certain extent (Choi et al., 2019). Meanwhile, high c_mRNAsi was associated with the up-regulation of M1 macrophages, resting dendritic cells, monocytes, activated NK cells, and follicular T helper cells. In addition, we also found that general immune-related pathways were activated in the high-c_mRNAsi group, which is consistent with previous findings (Zhang C. et al., 2020). Collectively, our results suggest that the better prognosis of patients with high c_mRNAsi may be owing to the presence of more tumour stem cells and more tumour neoantigens, which results in the higher infiltration of tumour immune cells. Based on our findings, we propose c_mRNAsi as a new marker for tumour immunotherapy in the future.

The stemness indices reflects the ability of self-renewal and unlimited proliferation. We found that significantly different enrichment pathways are mainly related to cell cycle, damage repair, proliferation, apoptosis, angiogenesis, glucose, lipid metabolism and energy metabolism through ssGSEA. The current view is that tumour stem cells are related to the inhibitory immune microenvironment (Alves et al., 2021). At present, it is found that the stemness indices is also related to IL6/JAK/STAT3, IL-2/STAT5, and TGF-β signalling pathways (Zhang et al., 2019; Liu et al., 2021; Mo et al., 2021; Zhou et al., 2021). Interleukins are closely related to the proliferation and function of T cells (Ceuppens et al., 1988; Popmihajlov et al., 2012; Raeber et al., 2018). Tregs are a key source of TGF-β ligands (Zhang Y. et al., 2020). Together, the pathways we enriched here are closely related to immune response.

There are several limitations in our study that need to be addressed in the future. First, we used four different datasets (TCGA, CGGA, GSE4412, and GSE13041) to test the prognostic value of mRNAsi/c_mRNAsi and found the power and robustness of c_mRNAsi. However, we could not definitively determine whether the c_mRNAsi obtained from the bulk tumour sequencing/array could be utilised for all types of GBM samples from diverse genetic backgrounds. Furthermore, the study was based on public data. We should use our own sequencing data to verify the c_mRNAsi and clinical model. Besides, the c_mRNAsi signature could distinguish differential subpopulations with distinct prognosis. Whether stemness indices mediate poor immunotherapy response requires further investigation. There is still a long way before we can accomplish individualised classifications for treatment because other clinical and genetic/epigenetic factors must be considered and incorporated into treatment decision-making (Mansouri et al., 2019). In addition, due to the limitation of GEO data sources, we could only verify the prognostic signature of c_mRNAsi, but could not identify confounding factors as in CGGA. Moreover, the c_mRNAsi-related signature should be further validated in large samples of patients with GBM from

multiple centres to identify the associations not only with survival outcomes but also conventional drug responses, especially immunotherapy. Lastly, although we performed functional analysis and identified numerous differences in infiltrative immune cell abundance and the regulation of related pathways, specific experimental validations need to be designed to assess the real effect. Despite the above shortcomings, our work has certain advantages that cannot be ignored. We calculated the mRNAsi/c_mRNAsi using a large number of samples and, for the first time, performed confounding variable identification and interaction and stratified analyses. Furthermore, we made a comprehensive comparison of several models, and proved the validity of our conclusions in multiple ways to verify the credibility of our results.

In conclusion, our study systematically assessed the GBM stemness indices based on multiple independent cohorts, providing a robust quantified mRNAsi/c_mRNAsi reflective of stemness indices, and the associations with immune infiltration and immune related pathways. The c_mRNAsi-based signature proved to be superior to other models in predicting OS prognosis, and may be a valuable classifier for uncovering distinct subgroups of stemness indices.

## DATA AVAILABILITY STATEMENT

The datasets presented in this study can be found in online repositories. The names of the repository/repositories and accession number(s) can be found in the article/ **Supplementary Material**.

## AUTHOR CONTRIBUTIONS

MZ and JH conceived and designed the study. HC analyzed the data. BL authored the paper. XW prepared figures and tables. NG supervised the study. FX and QY revised the manuscript. QZ audited the study.

## FUNDING

This study was supported by the National Natural Science Foundation of China (Nos. 82003386, 11601083, and U1805263), Fujian Provincial Committee of Natural Science and Technology (No. 2020J02039), National Collaboration Center in Immuno-Oncology (No. 2016sysbz02), Qihang Foundation of Fujian Medical University (No. 2018QH1088).

## SUPPLEMENTARY MATERIAL

The Supplementary Material for this article can be found online at: https://www.frontiersin.org/articles/10.3389/fmolb.2021.777921/full#supplementary-material

**Supplementary Figure 1 |** Lowess results. **(A)**. mRNAsi with OS in TCGA. **(B)**. c_mRNAsi with OS in TCGA. **(C)**. mRNAsi with OS in CGGA. **(D)**. c_mRNAsi with OS in CGGA.

**Supplementary Figure 2 |** Identification of optimal cut-off values. **(A)**. Optimal cut-off value of mRNAsi in TCGA. **(B)**. Optimal cut-off value of c_mRNAsi in TCGA. **(C)**. Optimal cut-off value of mRNAsi in CGGA. **(D)**. Optimal cut-off value of c_mRNAsi in CGGA.

**Supplementary Figure 3 |** Survival curve of mRNAsi/c_mRNAsi on prognosis. **(A)**. Disease-specific survival curve of mRNAsi in TCGA. **(B)**. Disease-specific survival curve of c_mRNAsi in TCGA. **(C)**. Progression-free interval curve of mRNAsi in TCGA. **(D)**. Progression-free interval curve of c_mRNAsi in TCGA.

**Supplementary Figure 4 |** External validation in CGGA and GEO. **(A)**. AUC in TCGA. **(B)**. C-index in CGGA. **(C)**. Prediction error in CGGA. **(D)**. 0.5-year DCA in CGGA. **(E)**. 1-year DCA in CGGA. **(F)**. 1.5-year DCA in CGGA. **(G)**. 3-year DCA in CGGA. **(H)**. 5-year DCA in CGGA. **(I)**. 0.5-year calibration in CGGA. (J). 1-year calibration in CGGA. **(K)**. 1.5-year calibration in CGGA. **(L)**. 3-year calibration in CGGA. **(M)**. 5-year calibration in CGGA. **(N)**. AUC in GSE4412. **(O)**. AUC in GSE13041.

**Supplementary Figure 5 |** Construction of prognostic nomogram.

## REFERENCES

Ali, H. R., Chlon, L., Pharoah, P. D. P., Markowetz, F., and Caldas, C. (2016). Patterns of Immune Infiltration in Breast Cancer and Their Clinical Implications: A Gene-Expression-Based Retrospective Study. *Plos Med.* 13 (12), e1002194. doi:10.1371/journal.pmed.1002194

Alves, A. L. V., Gomes, I. N. F., Carloni, A. C., Rosa, M. N., da Silva, L. S., Evangelista, A. F., et al. (2021). Role of Glioblastoma Stem Cells in Cancer Therapeutic Resistance: a Perspective on Antineoplastic Agents from Natural Sources and Chemical Derivatives. *Stem Cel Res Ther* 12 (1), 206. doi:10.1186/s13287-021-02231-x

Barbie, D. A., Tamayo, P., Boehm, J. S., Kim, S. Y., Moody, S. E., Dunn, I. F., et al. (2009). Systematic RNA Interference Reveals that Oncogenic KRAS-Driven Cancers Require TBK1. *Nature* 462 (7269), 108–112. doi:10.1038/nature08460

Barrett, T., Wilhite, S. E., Ledoux, P., Evangelista, C., Kim, I. F., Tomashevsky, M., et al. (2013). NCBI GEO: Archive for Functional Genomics Data Sets-Update. *Nucleic Acids Res.* 41 (Database issue), D991–D995. doi:10.1093/nar/gks1193

Burgenske, D. M., Yang, J., Decker, P. A., Kollmeyer, T. M., Kosel, M. L., Mladek, A. C., et al. (2019). Molecular Profiling of Long-Term IDH-Wildtype Glioblastoma Survivors. *Neuro-oncology* 21 (11), 1458–1469. doi:10.1093/neuonc/noz129

Ceuppens, J. L., Baroja, M. L., Lorre, K., Van Damme, J., and Billiau, A. (19881950). Human T Cell Activation with Phytohemagglutinin. The Function of IL-6 as an Accessory Signal. *J. Immunol.* 141 (11), 3868–3874.

Chaddad, A., Daniel, P., Sabri, S., Desrosiers, C., and Abdulkarim, B. (2019). Integration of Radiomic and Multi-Omic Analyses Predicts Survival of Newly Diagnosed IDH1 Wild-type Glioblastoma. *Cancers* 11 (8), 1148. doi:10.3390/cancers11081148

Choi, B. D., Maus, M. V., June, C. H., and Sampson, J. H. (2019). Immunotherapy for Glioblastoma: Adoptive T-Cell Strategies. *Clin. Cancer Res.* 25 (7), 2042–2048. doi:10.1158/1078-0432.CCR-18-1625

Freije, W. A., Castro-Vargas, F. E., Fang, Z., Horvath, S., Cloughesy, T., Liau, L. M., et al. (2004). Gene Expression Profiling of Gliomas Strongly Predicts Survival. *Cancer Res.* 64 (18), 6503–6510. doi:10.1158/0008-5472.can-04-0452

Gallego, O. (2015). Nonsurgical Treatment of Recurrent Glioblastoma. *Curr. Oncol.* 22 (4), 273–281. doi:10.3747/co.22.2436

Harrell, F. E., Jr., Lee, K. L., and Mark, D. B. (1996). Multivariable Prognostic Models: Issues in Developing Models, Evaluating Assumptions and Adequacy, and Measuring and Reducing Errors. *Statist. Med.* 15 (4), 361–387. doi:10.1002/(sici)1097-0258(19960229)15:4<361:aid-sim168>3.0.co;2-4

Hoadley, K. A., Yau, C., Wolf, D. M., Cherniack, A. D., Tamborero, D., Ng, S., et al. (2014). Multiplatform Analysis of 12 Cancer Types Reveals Molecular Classification within and across Tissues of Origin. *Cell* 158 (4), 929–944. doi:10.1016/j.cell.2014.06.049

Kaipio, K., Chen, P., Roering, P., Huhtinen, K., Mikkonen, P., Östling, P., et al. (2020). ALDH1A1-related Stemness in High-grade Serous Ovarian Cancer Is a Negative Prognostic Indicator but Potentially Targetable by EGFR/mTOR-PI3K/aurora Kinase Inhibitors. *J. Pathol.* 250 (2), 159–169. doi:10.1002/path.5356

Kaushal, K., and Ramakrishna, S. (2020). Deubiquitinating Enzyme-Mediated Signaling Networks in Cancer Stem Cells. *Cancers* 12 (11), 3253. doi:10.3390/cancers12113253

Kernan, W. N., Viscoli, C. M., Brass, L. M., Broderick, J. P., Brott, T., Feldmann, E., et al. (2000). Phenylpropanolamine and the Risk of Hemorrhagic Stroke. *N. Engl. J. Med.* 343 (25), 1826–1832. doi:10.1056/nejm200012213432501

Kerr, K. F., Brown, M. D., Zhu, K., and Janes, H. (2016). Assessing the Clinical Impact of Risk Prediction Models with Decision Curves: Guidance for Correct Interpretation and Appropriate Use. *Jco* 34 (21), 2534–2540. doi:10.1200/JCO.2015.65.5654

Krex, D., Klink, B., Hartmann, C., von Deimling, A., Pietsch, T., Simon, M., et al. (2007). Long-term Survival with Glioblastoma Multiforme. *Brain* 130 (Pt 10), 2596–2606. doi:10.1093/brain/awm204

Le, T., Aronow, R. A., Kirshtein, A., and Shahriyari, L. (2020). A Review of Digital Cytometry Methods: Estimating the Relative Abundance of Cell Types in a Bulk of Cells. *Brief. Bioinformatics* 22. doi:10.1093/bib/bbaa219

Lee, Y., Scheck, A. C., Cloughesy, T. F., Lai, A., Dong, J., Farooqi, H. K., et al. (2008). Gene Expression Analysis of Glioblastomas Identifies the Major Molecular Basis for the Prognostic Benefit of Younger Age. *BMC Med. Genomics* 1, 52. doi:10.1186/1755-8794-1-52

Li, H.-P., Wang, J., Guo, S., Cai, X., and Xu, J.-W. (2019). Establishment and Verification of a Surgical Prognostic Model for Cervical Spinal Cord Injury without Radiological Abnormality. *Neural Regen. Res.* 14 (4), 713–720. doi:10.4103/1673-5374.247480

Lian, H., Han, Y. P., Zhang, Y. C., Zhao, Y., Yan, S., Li, Q. F., et al. (2019). Integrative Analysis of Gene Expression and DNA Methylation through One-class Logistic Regression Machine Learning Identifies Stemness Features in Medulloblastoma. *Mol. Oncol.* 13 (10), 2227–2245. doi:10.1002/1878-0261.12557

Liberzon, A., Birger, C., Thorvaldsdóttir, H., Ghandi, M., Mesirov, J. P., and Tamayo, P. (2015). The Molecular Signatures Database Hallmark Gene Set Collection. *Cel Syst.* 1 (6), 417–425. doi:10.1016/j.cels.2015.12.004

Liu, S., Zhang, C., Wang, B., Zhang, H., Qin, G., Li, C., et al. (2021). Regulatory T Cells Promote Glioma Cell Stemness through TGF-β-NF-κB-IL6-STAT3 Signaling. *Cancer Immunol. Immunother.* 70 (9), 2601–2616. doi:10.1007/s00262-021-02872-0

Long, Y., Tao, H., Karachi, A., Grippin, A. J., Jin, L., Chang, Y., et al. (2020). Dysregulation of Glutamate Transport Enhances Treg Function that Promotes VEGF Blockade Resistance in Glioblastoma. *Cancer Res.* 80 (3), 499–509. doi:10.1158/0008-5472.CAN-19-1577

Malta, T. M., Sokolov, A., Gentles, A. J., Burzykowski, T., Poisson, L., Weinstein, J. N., et al. (2018). Machine Learning Identifies Stemness Features Associated with Oncogenic Dedifferentiation. *Cell* 173 (2), 338–e15. doi:10.1016/j.cell.2018.03.034

Mansouri, A., Hachem, L. D., Mansouri, S., Nassiri, F., Laperriere, N. J., Xia, D., et al. (2019). MGMT Promoter Methylation Status Testing to Guide Therapy for Glioblastoma: Refining the Approach Based on Emerging Evidence and Current Challenges. *Neuro-oncology* 21 (2), 167–178. doi:10.1093/neuonc/noy132

Martinez, R., Schackert, G., Yaya-Tur, R., Rojas-Marcos, I., Herman, J. G., and Esteller, M. (2007). Frequent Hypermethylation of the DNA Repair Gene MGMT in Long-Term Survivors of Glioblastoma Multiforme. *J. Neurooncol.* 83 (1), 91–93. doi:10.1007/s11060-006-9292-0

McNeill, K. A. (2016). Epidemiology of Brain Tumors. *Neurol. Clin.* 34 (4), 981–998. doi:10.1016/j.ncl.2016.06.014

Miranda, A., Hamilton, P. T., Zhang, A. W., Pattnaik, S., Becht, E., Mezheyeuski, A., et al. (2019). Cancer Stemness, Intratumoral Heterogeneity, and Immune Response across Cancers. *Proc. Natl. Acad. Sci. USA* 116 (18), 9020–9029. doi:10.1073/pnas.1818210116

Mo, F., Yu, Z., Li, P., Oh, J., Spolski, R., Zhao, L., et al. (2021). An Engineered IL-2 Partial Agonist Promotes CD8+ T Cell Stemness. *Nature* 597 (7877), 544–548. doi:10.1038/s41586-021-03861-0

Molenaar, R. J., Verbaan, D., Lamba, S., Zanon, C., Jeuken, J. W. M., Boots-Sprenger, S. H. E., et al. (2014). The Combination of IDH1 Mutations and MGMT Methylation Status Predicts Survival in Glioblastoma Better Than Either IDH1 or MGMT Alone. *Neuro-oncology* 16 (9), 1263–1273. doi:10.1093/neuonc/nou005

Newman, A. M., Steen, C. B., Liu, C. L., Gentles, A. J., Chaudhuri, A. A., Scherer, F., et al. (2019). Determining Cell Type Abundance and Expression from Bulk Tissues with Digital Cytometry. *Nat. Biotechnol.* 37 (7), 773–782. doi:10.1038/s41587-019-0114-2

Pan, S., Zhan, Y., Chen, X., Wu, B., and Liu, B. (2019). Identification of Biomarkers for Controlling Cancer Stem Cell Characteristics in Bladder Cancer by Network Analysis of Transcriptome Data Stemness Indices. *Front. Oncol.* 9, 613. doi:10.3389/fonc.2019.00613

Pei, J., Wang, Y., and Li, Y. (2020). Identification of Key Genes Controlling Breast Cancer Stem Cell Characteristics via Stemness Indices Analysis. *J. Transl Med.* 18 (1), 74. doi:10.1186/s12967-020-02260-9

Pencina, M. J., D' Agostino, R. B., D' Agostino., Vasan, R. S., Jr., and Vasan, R. S. (2008). Evaluating the Added Predictive Ability of a New Marker: from Area under the ROC Curve to Reclassification and beyond. *Statist. Med.* 27 (2), 157–172. doi:10.1002/sim.2929

Popmihajlov, Z., Xu, D., Morgan, H., Milligan, Z., and Smith, K. A. (2012). Conditional IL-2 Gene Deletion: Consequences for T Cell Proliferation. *Front. Immun.* 3, 102. doi:10.3389/fimmu.2012.00102

Raeber, M. E., Zurbuchen, Y., Impellizzieri, D., and Boyman, O. (2018). The Role of Cytokines in T-Cell Memory in Health and Disease. *Immunol. Rev.* 283 (1), 176–193. doi:10.1111/imr.12644

Sasmita, A. O., Wong, Y. P., and Ling, A. P. K. (2018). Biomarkers and Therapeutic Advances in Glioblastoma Multiforme. *Asia-pac J. Clin. Oncol.* 14 (1), 40–51. doi:10.1111/ajco.12756

Saygin, C., Matei, D., Majeti, R., Reizes, O., and Lathia, J. D. (2019). Targeting Cancer Stemness in the Clinic: From Hype to Hope. *Cell stem cell* 24 (1), 25–40. doi:10.1016/j.stem.2018.11.017

Seneviratne, A. K., Xu, M., Henao, J. J. A., Fajardo, V. A., Hao, Z., Voisin, V., et al. (2019). The Mitochondrial Transacylase, Tafazzin, Regulates AML Stemness by Modulating Intracellular Levels of Phospholipids. *Cell stem cell* 24 (4), 621–636. doi:10.1016/j.stem.2019.02.020

Sokolov, A., Paull, E. O., and Stuart, J. M. (2016). One-class Detection of Cell States in Tumor Subtypes. *Pac. Symp. Biocomput* 21, 405–416. doi:10.1142/9789814749411_0037

Soria, J.-C., Felip, E., Cobo, M., Lu, S., Syrigos, K., Lee, K. H., et al. (2015). Afatinib versus Erlotinib as Second-Line Treatment of Patients with Advanced Squamous Cell Carcinoma of the Lung (LUX-Lung 8): an Open-Label Randomised Controlled Phase 3 Trial. *Lancet Oncol.* 16 (8), 897–907. doi:10.1016/s1470-2045(15)00006-6

Subramanian, A., Tamayo, P., Mootha, V. K., Mukherjee, S., Ebert, B. L., Gillette, M. A., et al. (2005). Gene Set Enrichment Analysis: a Knowledge-Based Approach for Interpreting Genome-wide Expression Profiles. *Proc. Natl. Acad. Sci.* 102 (43), 15545–15550. doi:10.1073/pnas.0506580102

Tao, Y., Kang, B., Petkovich, D. A., Bhandari, Y. R., In, J., In, G., et al. (2019). Aging-like Spontaneous Epigenetic Silencing Facilitates Wnt Activation, Stemness, and BrafV600E-Induced Tumorigenesis. *Cancer cell* 35 (2), 315–328. doi:10.1016/j.ccell.2019.01.005

Turaga, S. M., Silver, D. J., Bayik, D., Paouri, E., Peng, S., Lauko, A., et al. (2020). JAM-A Functions as a Female Microglial Tumor Suppressor in Glioblastoma. *Neuro-oncology* 22, 1591–1601. doi:10.1093/neuonc/noaa148

Wang, X., Prager, B. C., Wu, Q., Kim, L. J. Y., Gimple, R. C., Shi, Y., et al. (2018). Reciprocal Signaling between Glioblastoma Stem Cells and Differentiated Tumor Cells Promotes Malignant Progression. *Cell Stem Cell* 22 (4), 514–528. doi:10.1016/j.stem.2018.03.011

Wessler, B. S., Lai Yh, L., Kramer, W., Cangelosi, M., Raman, G., Lutz, J. S., et al. (2015). Clinical Prediction Models for Cardiovascular Disease. *Circ. Cardiovasc. Qual. Outcomes* 8 (4), 368–375. doi:10.1161/circoutcomes.115.001693

Xia, P., Li, Q., Wu, G., and Huang, Y. (2020). Identification of Glioma Cancer Stem Cell Characteristics Based on Weighted Gene Prognosis Module Co-expression Network Analysis of Transcriptome Data Stemness Indices. *J. Mol. Neurosci.* 70, 1512–1520. doi:10.1007/s12031-020-01590-z

Yoshihara, K., Shahmoradgoli, M., Martínez, E., Vegesna, R., Kim, H., Torres-Garcia, W., et al. (2013). Inferring Tumour Purity and Stromal and Immune Cell Admixture from Expression Data. *Nat. Commun.* 4, 2612. doi:10.1038/ncomms3612

Young, R. M., Jamshidi, A., Davis, G., and Sherman, J. H. (2015). Current Trends in the Surgical Management and Treatment of Adult Glioblastoma. *Ann. Transl Med.* 3 (9), 121. doi:10.3978/j.issn.2305-5839.2015.05.10

Zhang, B., Ye, H., Ren, X., Zheng, S., Zhou, Q., Chen, C., et al. (2019). Macrophage-expressed CD51 Promotes Cancer Stem Cell Properties via the TGF-B1/smad2/3 axis in Pancreatic Cancer. *Cancer Lett.* 459, 204–215. doi:10.1016/j.canlet.2019.06.005

Zhang, C., Chen, T., Li, Z., Liu, A., Xu, Y., Gao, Y., et al. (2020a). Depiction of Tumor Stemlike Features and Underlying Relationships with hazard Immune Infiltrations Based on Large Prostate Cancer Cohorts. *Brief. Bioinformatics* 22, bbaa211. doi:10.1093/bib/bbaa211

Zhang, M., Wang, X., Chen, X., Guo, F., and Hong, J. (2020b). Prognostic Value of a Stemness Index-Associated Signature in Primary Lower-Grade Glioma. *Front. Genet.* 11, 441. doi:10.3389/fgene.2020.00441

Zhang, M., Wang, X., Chen, X., Zhang, Q., and Hong, J. (2020c). Novel Immune-Related Gene Signature for Risk Stratification and Prognosis of Survival in Lower-Grade Glioma. *Front. Genet.* 11, 363. doi:10.3389/fgene.2020.00363

Zhang, Y., Lazarus, J., Steele, N. G., Yan, W., Lee, H.-J., Nwosu, Z. C., et al. (2020d). Regulatory T-Cell Depletion Alters the Tumor Microenvironment and Accelerates Pancreatic Carcinogenesis. *Cancer Discov.* 10 (3), 422–439. doi:10.1158/2159-8290.CD-19-0958

Zhou, J.-G., Liang, B., Jin, S.-H., Liao, H.-L., Du, G.-B., Cheng, L., et al. (2019). Development and Validation of an RNA-Seq-Based Prognostic Signature in Neuroblastoma. *Front. Oncol.* 9, 1361. doi:10.3389/fonc.2019.01361

Zhou, M., Venkata, P. P., Viswanadhapalli, S., Palacios, B., Alejo, S., Chen, Y., et al. (2021). KDM1A Inhibition Is Effective in Reducing Stemness and Treating Triple Negative Breast Cancer. *Breast Cancer Res. Treat.* 185 (2), 343–357. doi:10.1007/s10549-020-05963-1

**Conflict of Interest:** The authors declare that the research was conducted in the absence of any commercial or financial relationships that could be construed as a potential conflict of interest.

**Publisher's Note:** All claims expressed in this article are solely those of the authors and do not necessarily represent those of their affiliated organizations, or those of the publisher, the editors and the reviewers. Any product that may be evaluated in this article, or claim that may be made by its manufacturer, is not guaranteed or endorsed by the publisher.

frontiers in Molecular Biosciences

ORIGINAL RESEARCH
published: 07 December 2021
doi: 10.3389/fmolb.2021.777370

# PD-1H Expression Associated With CD68 Macrophage Marker Confers an Immune-Activated Microenvironment and Favorable Overall Survival in Human Esophageal Squamous Cell Carcinoma

*Yuangui Chen[1,2†], Rui Feng[3,4†], Bailin He[5], Jun Wang[5], Na Xian[3], Gangxiong Huang[3]* and Qiuyu Zhang[1,3]**

[1]Department of Immunology, School of Basic Medical Sciences, Fujian Medical University, Fuzhou, China, [2]Department of Radiation Oncology, Fujian Medical University Union Hospital, Fuzhou, China, [3]Institute of Immunotherapy, Fujian Medical University, Fuzhou, China, [4]Department of Oncology, Fujian Medical University Union Hospital, Fuzhou, China, [5]Zhongshan School of Medicine, Sun Yat-Sen University, Guangzhou, China

Esophageal squamous cell carcinoma (ESCC) is the most common type of esophageal carcinoma (EC) in China. Although the PD-1 inhibitor pembrolizumab has been approved to treat patients with EC, its therapeutic efficacy is limited. Thus, additional immunotherapeutic targets for EC treatment are needed. Programmed Death-1 Homolog (PD-1H) is a negative checkpoint regulator that inhibits antitumor immune responses. Here, PD-1H expression in 114 patients with ESCC was evaluated by immunohistochemistry. Next, 12 randomly selected tumor tissue sections were used to assess the colocalization of PD-1H protein and multiple immune markers by multiplex immunohistochemistry. Our results demonstrated that PD-1H was expressed at high frequency in ESCC tumor tissues (85.1%). PD-1H protein was predominantly expressed in $CD68^+$ tumor-associated macrophages and expressed at low levels in $CD4^+$ T cells and $CD8^+$ T cells in ESCC tumor tissues. Furthermore, based on ESCC data in The Cancer Genome Atlas (TCGA), the gene expression levels of PD-1H were positively associated with the infiltration levels of immune-activated cells especially $CD8^+$ cytotoxic T cells. In contrast, the gene expression levels of PD-1H were negatively correlated with myeloid-derived suppressor cells (MDSCs). Importantly, PD-1H expression in tumor sites was significantly correlated with favorable overall survival in patients with ESCC. Collectively, our findings first provided direct information on the PD-1H expression pattern and distribution in ESCC, and positive correlation of PD-1H expression with overall survival suggested PD-1H expression levels could be a significant prognostic indicator for patients with ESCC. Future studies need to explore the immunoregulatory of PD-1H in the tumor microenvironment of ESCC.

**Keywords: esophageal squamous cell carcinoma, tumor microenvironment, CD68 + myeloid cells, programmed death-1 homolog, prognosis**

OPEN ACCESS

***Edited by:***
*Saber Imani,*
*Affiliated Hospital of Southwest Medical University, China*

***Reviewed by:***
*Jun Wang,*
*New York University, United States*
*Junjiang Fu,*
*Southwest Medical University, China*
*Ju Qiu,*
*Shanghai Institute of Nutrition and Health (CAS), China*

****Correspondence:***
*Gangxiong Huang*
*gangxiong.huang@fjmu.edu.cn*
*Qiuyu Zhang*
*qiuyu.zhang@fjmu.edu.cn*

*†These authors have contributed equally to this work and share first authorship*

***Specialty section:***
*This article was submitted to Molecular Diagnostics and Therapeutics, a section of the journal Frontiers in Molecular Biosciences*

***Received:*** *15 September 2021*
***Accepted:*** *04 November 2021*
***Published:*** *07 December 2021*

***Citation:***
*Chen Y, Feng R, He B, Wang J, Xian N, Huang G and Zhang Q (2021) PD-1H Expression Associated With CD68 Macrophage Marker Confers an Immune-Activated Microenvironment and Favorable Overall Survival in Human Esophageal Squamous Cell Carcinoma. Front. Mol. Biosci. 8:777370. doi: 10.3389/fmolb.2021.777370*

# INTRODUCTION

Esophageal carcinoma (EC) is one of the most fatal diseases worldwide and is the fourth most common cause of cancer-related death in China (Chen et al., 2016; Feng et al., 2019). Unlike North America and Europe, esophageal squamous cell carcinoma (ESCC) is the predominant subtype of esophageal carcinoma (EC) in China, accounting for approximately 90% of all patients with EC (Zeng et al., 2016). Targeting immune checkpoints has been demonstrated as a promising strategy in EC. Pembrolizumab, a PD-1-blocking checkpoint immunotherapy, was approved for advanced, PD-L1-positive ECs by the United States Food and Drug Administration (FDA) in 2017; however, only a small proportion of patients achieved therapeutic response (Kojima et al., 2020). Further exploration of novel immunotherapeutic targets for ESCC is needed. Programmed Death-1 Homolog (PD-1H), also known as V-domain Immunoglobulin Suppressor of T-cell activation (VISTA), DD1α, c10orf54, Dies1, or Gi24, is a novel T-cell cosignaling molecule. Previous studies demonstrated that the immuneregulatory pathways for PD-1 and PD-1H are functionally nonredundant by using PD-1H and programmed death-1 (PD-1) knockout mice (Liu et al., 2015). PD-1H can function as both a receptor in T lymphocytes and a ligand on antigen-presenting cells (Bharaj et al., 2014; Flies et al., 2014; Le Mercier et al., 2014; Lines et al., 2014a). Moreover, PD-1H was highly expressed on $CD11b^+$ myeloid cells and macrophages and was expressed at low levels on T cells, including $CD4^+$ T cells, $CD8^+$ effector T cells, and $Foxp3^+$ Tregs (Bharaj et al., 2014; Le Mercier et al., 2014). PD-1H showed constitutive expression characteristics (Lines et al., 2014b). Considering different expression patterns of PD-1H and its nonredundant activities compared to other immune checkpoint regulators, PD-1H has become a promising target of cancer immunotherapy [11].

Recently, PD-1H was reported to be highly expressed in various human cancers, including prostate cancer (Gao et al., 2017), non-small cell lung cancer (Villarroel-Espindola et al., 2018), colorectal carcinoma (Xie et al., 2018), ovarian and endometrial cancer (Mulati et al., 2019), esophageal adenocarcinoma (Loeser et al., 2019), and epithelioid malignant pleural mesothelioma (Muller et al., 2020); however, limited data about PD-H expression in ESCC have been reported. Here, we analyzed the PD-1H expression pattern in tumor microenvironment of 114 patients with ESCC and its correlation with the infiltrating number of T cells and myeloid cells. Next, the relationships between *PD-1H* mRNA levels and the infiltration of various immune cells were assessed in ESCC based on The Cancer Genome Atlas (TCGA) database. We further investigated the correlation of PD-1H expression with the survival outcomes of ESCC patients.

# MATERIALS AND METHODS

## Patients and Sample Preparation

Tumor tissues were obtained from 114 patients with ESCC who underwent surgery at Fujian Medical University Union Hospital from 2015 to 2016. None of these patients received preoperative radiotherapy or chemotherapy before surgery. A retrospective review of the medical records of these patients was performed between January 1, 2015 and June 30, 2020. Relevant clinical data were collected by retrospective review of the files of the patients, and follow-up data were available for all patients. Peripheral blood mononuclear cells (PBMCs) were isolated from six patients with ESCC using Ficoll-Paque PLUS (#171140, GE Healthcare, United States) according to the manufacturer's instructions. All procedures followed the national and institutional ethical standards, and all samples were obtained in accordance with the institutional policies. All protocols were reviewed and approved by the Research Ethics Committee of Fujian Medical University Union Hospital (No. 2020ky085).

## Immunohistochemistry

Tumor tissues were fixed in formaldehyde and paraffin-embedded following standard procedures. Tissue sections were incubated with PD-1H antibodies (1:200, #64953, Cell Signaling Technology) and then immunostained using the MaxVision™ HRP-Polymer anti-Rabbit IHC Kit (KIT-5005, Maixin Biol, Fuzhou, China) following the manufacturer's instructions. Immunostaining of PD-1H was microscopically evaluated (Olympus BX53, Japan). During evaluation of immunostained sections, the investigators were blinded to the clinical status of the patients. After screening the whole section, 10 randomly selected microscopic fields were examined at × 200 magnification (×20 objective lens and ×10 ocular lens; 0.74 $mm^2$ per field). Expression levels for PD-1H were scored semiquantitatively based on staining intensity and percentage of stained cells using the immunoreactive score (IRS) as described (Kakavand et al., 2015). The percentage of positively stained cells (PP) was assigned as a numerical score: 0, negative; 1, <25%; 2, 26–50%; 3, 51–75%; and 4, >75% positive cells. The intensity (SI) of the immunostained areas was defined as follows: 0, negative; 1, weak (+); 2, moderate (++); and 3, strong (+++). An immunoreactive score (IRS) ranging from 0 to 12 was calculated using the following formula: IRS = PP × SI. The expression of PD-1H was defined as follows: 0–1, negative; >1–4, mild; >4–8, moderate; >8–12, strong. Based on this formula, the average expression score for each patient was calculated, and the score with the maximum split in survival was chosen as the cutoff using the cutpoint function of Evaluate Cutpoints software (R survMisc package) as described (Ogluszka et al., 2019). Then, the patients were classified into high- or low-expression score groups by a 7.2 score.

## Multiplex Immunohistochemistry

Multiplex immunohistochemistry (mIHC) was performed by staining 4-μm-thick formalin-fixed, paraffin-embedded whole-tissue sections with multiple primary antibodies and a TSA 5-color fluorescent IHC kit (Yuanxi Bio, China) as described in a previous study (Stack et al., 2014). The concentration and order of the four antibodies were

optimized, and the spectral library was built based on the single-stained slides. Four primary antibody/fluorophore pairs were applied in order: anti-CD4 antibody (#YX32005, Yuanxi Bio)/NEON-TSA 520, anti-CD8 (#YX63005, Yuanxi Bio)/NEON-TSA 620, anti-CD68 (#GM087602, Gene Tech)/NEON-TSA 670, and anti-PD-1H (#64953, Cell Signaling Technology)/NEON-TSA 570. Twelve randomly selected tumor tissue sections were used for mIHC. The slides were deparaffined with a graded series of xylene, and dehydrated in a gradient of alcohols, and then antigen retrieval was performed by microwave. After incubation with 3% $H_2O_2$ for 10 min, the tissues were blocked in blocking buffer for another 10 min at room temperature. Then, the tissues were incubated with primary antibodies, followed by secondary-HRP and TSA working solutions, respectively, according to the manufacturer's instructions. Finally, the slides were mounted with ProLong Gold Antifade Reagent with DAPI (#P36931, Invitrogen). All slides were scanned using an Aperio Versa 8 tissue imaging system (Leica, Germany). Images were analyzed using HALO image analysis software (Indica Lab, United States).

## Acquisition of PD-1H Expression Profiles From TCGA Datasets

RNA sequencing (RNA-Seq) data and clinical information for 182 esophageal carcinoma patients (TCGA ESCC) were collected and downloaded through the TCGA data portal (https://portal.gdc.cancer.gov/). The transcript expression levels were estimated using the fragments per kilobase per million fragments mapped (FPKM) method in HTSeq. Kaplan–Meier survival curve analysis was used to analyze survival between the PD-1H $^{high}$ and PD-1H $^{low}$ groups as previously described (Rich et al., 2010). Immune cell infiltration was evaluated using Cell-type Identification By Estimating Relative Subsets Of RNA Transcripts (CIBERSORT) algorithm (Newman et al., 2015) based on Tumor Immune Estimation Resource (TIMER) (Li et al., 2020) as described. The gene expression data with standard annotation were uploaded to the CIBERSORT web portal (http://cibersort.stanford.edu/). The algorithm was run by 1,000 permutations and the LM22 signature. Samples with CIBERSORT $p < 0.05$ were considered eligible for subsequent analysis. The correlation between PD-1H expression and immune infiltration patterns was estimated using linear regression analysis.

## Flow Cytometry

Human peripheral blood mononuclear cells (PBMCs) were isolated from the whole blood of six patients with ESCC, and then T cells and monocytes were enriched by Rosettesep™ Human T Cell Enrichment Cocktail and Human Monocyte Enrichment Cocktail (#15028_c, Stemcell Technologies, United States), respectively. T cells and monocytes were stained with antibodies against human CD3e (#560352, BD Biosciences), CD4 (#300532, BioLegend), CD8a (#300922, BD Biolegend), CD14 (#301807, BioLegend), PD-1H (#566672, BD Biosciences), and matched isotype controls (#555749, BD Biosciences) at different time points after blood collection (6, 24, and 48 h). PBMCs, purified T cells, and purified monocytes were stimulated with PMA (50 ng/ml, #P1585, Sigma-Aldrich), LPS (200 ng/ml, #L4391, Sigma-Aldrich), and polyI:C (2 μg/ml, #P0913, Sigma-Aldrich), and anti-CD3/anti-CD28 Dynabeads (#11132D, Gibco) for 24 h. T cells were treated with different concentrations of polyhydroxyalkanoate (PHA) (#PZ0135, Sigma-Aldrich) for 5 h. Samples were run on a BD FACSVerse™ (BD Biosciences, United States) and analyzed using FlowJo software version 10 (BD Biosciences, United States).

## Quantitative Real-Time PCR

Human T cells were stimulated with different concentrations of PHA for 5 h. Total RNA of T cells was extracted using TRIzol (#15596-026, Invitrogen) and was reverse-transcribed into cDNA using a One Step TB Green® PrimeScript PLUS RT-PCR Kit (#RR096A, Takara Bio, United States) according to the manufacturer's instructions. Quantitative real-time polymerase chain reaction (qRT-PCR) was performed with SYBR™ Green PCR Master Mix (#4309155, Invitrogen). PD-1H primer sequences were as follows: forward (5′-ACGCCGTATTCC CTGTATGTC-3′) and reverse (5′-TTGTAGAAGGTCACA TCGTGC-3′). The expression levels of *PD-1H* were normalized to the expression of GAPDH. The relative expression levels of *PD-1H* mRNA in treated cells were calculated using their expression in control cells as a reference transcript.

## Statistical Analysis

All statistical analyses were performed using GraphPad Prism 8.0 (GraphPad, Canada). All data are shown as the mean ± SD unless otherwise stated. The chi-squared and Fisher's exact tests were used for interdependence between staining and clinical data. Univariate and multivariate analyses were performed for prognostic factors of overall survival with the Cox regression model, and the Kaplan–Meier method and the log-rank test were used for survival curves with a plot. $p < 0.05$ was considered statistically significant. The results represent at least two experiments unless otherwise stated.

# RESULTS

## PD-1H Protein Was Highly Expressed in ESCC Tumor Tissues

The clinical pathological features of 114 patients with ESCC are listed in **Table 1**. A total of 85.1% tumor tissues (97/114 cases of ESCC) were positive for PD-1H expression by IHC staining. According to the IRS-classification scoring systems, predominant expression evaluation was moderate positive staining (46.5%, 53/114) followed by mild positive staining (23.7%, 27/114), strong positive staining (14.9%, 17/114) and negative staining (14.9%, 17/114), and the representative images of four categories of classification are shown in **Figures 1A–D**. **Figures 1E,F** indicated that PD-1H protein was predominantly located in the membrane and cytoplasm of positive staining cells. Next,

**TABLE 1 |** The correlation of PD-1H expression and clinicopathologic parameters in 114 patients with ESCC.

| | | *N* | % | PD-1H expression | | | | |
|---|---|---|---|---|---|---|---|---|
| | | | | Low | % | High | % | *p*-value |
| Sex | Female | 32 | 28.1 | 23 | 71.8 | 9 | 28.1 | 0.811 |
| | Male | 82 | 71.9 | 62 | 75.6 | 20 | 24.3 | |
| Age group | <65 years | 85 | 74.5 | 63 | 74.1 | 22 | 25.8 | 1.000 |
| | ≥65 years | 29 | 25.5 | 22 | 75.8 | 7 | 24.1 | |
| Tumor stage | T1 | 25 | 21.9 | 15 | 60 | 10 | 40 | 0.287 |
| | T2 | 21 | 18.4 | 16 | 76.2 | 5 | 23.8 | |
| | T3 | 66 | 57.8 | 52 | 78.8 | 14 | 21.2 | |
| | T4 | 2 | 1.7 | 2 | 100 | 0 | 0 | |
| Lymph node metastasis | N0 | 51 | 44.7 | 31 | 60.8 | 20 | 39.2 | 0.020 |
| | N1 | 35 | 30.7 | 30 | 85.7 | 5 | 24.3 | |
| | N2 | 23 | 20.1 | 19 | 82.7 | 4 | 17.3 | |
| | N3 | 5 | 4.3 | 5 | 100 | 0 | 0 | |
| Grades of differentiation | G1 | 38 | 33.3 | 25 | 65.8 | 13 | 34.2 | 0.276 |
| | G2 | 55 | 48.2 | 43 | 78.2 | 12 | 21.8 | |
| | G3 | 9 | 7.8 | 8 | 88.8 | 1 | 11.2 | |
| UICC stage | I | 27 | 23.7 | 17 | 63 | 10 | 37 | 0.009 |
| | II | 37 | 32.4 | 23 | 62.2 | 14 | 37.8 | |
| | III | 44 | 38.6 | 39 | 88.6 | 5 | 11.4 | |
| | IV | 6 | 5.3 | 6 | 100 | 0 | 0 | |

*UICC, union for international cancer control; PD-1H, Programmed death-1 homolog; ESCC, esophageal squamous cell carcinoma.*

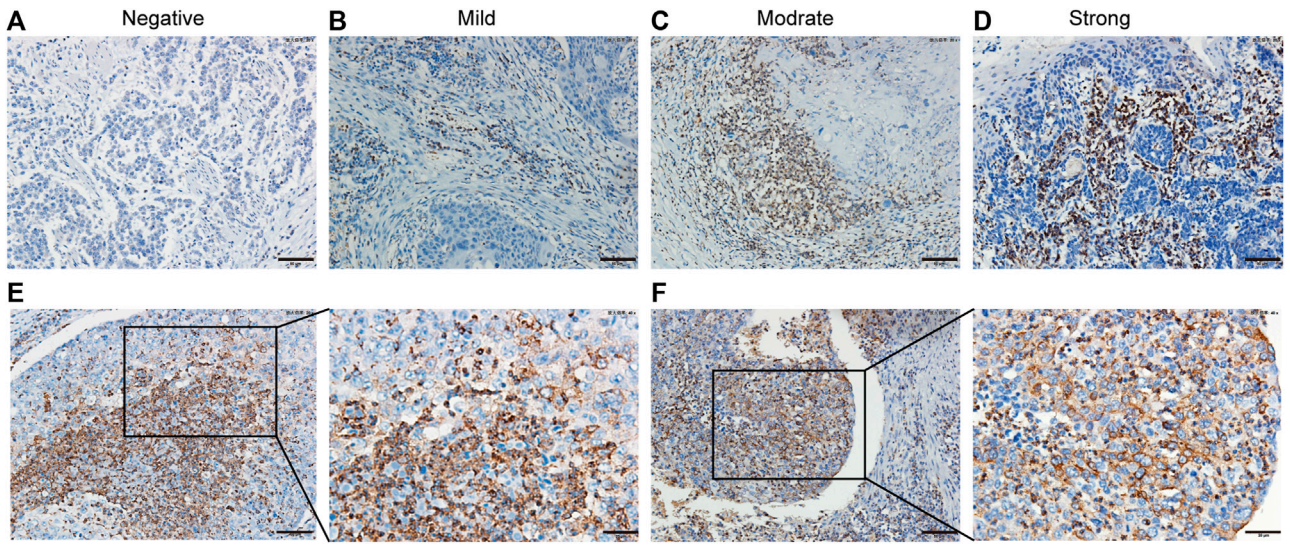


**FIGURE 1 |** PD-1H expression in ESCC analyzed by immunohistochemistry. **(A–D)** Immunohistochemistry staining of PD-1H in ESCC tumor tissues was performed and calculated using immunoreactive score (IRS), which was categorized as 0–1 (negative), >1–4 (mild), >4–8 (moderate), or >8–12 (strong). Representative images of four categories of classification of PD-1H expression in ESCC tumor tissues are shown. **(E–F)** Two representative cases with strong positive PD-1H staining demonstrated that PD-1H protein was predominantly located in the membrane and cytoplasm of tumor cells and immune cells. Scale bars: 50 μm, original magnification × 200; 25 μm, original magnification ×400. PD-1H: Programmed Ddeath-1 Homolog; ESCC: esophageal squamous cell carcinoma. Scale bar: 25 μm, original magnification × 400.

the optimal cutoff for "low" and "high" expression was determined by the inbuilt algorithm in the survMisc R package. A score of 7.2 was used as an optimal cutoff point and all patients were divided into a high-expression group (74.5%, 85/114) and a low-expression group (25.5%, 29/114). Then, the relationships of PD-1H expression level and clinical characteristics of ESCC were investigated. Our results showed that PD-1H expression level was negatively associated with lymph node metastasis ($p$ = 0.020) and Union for International Cancer Control (UICC) stages ($p$ = 0.009)

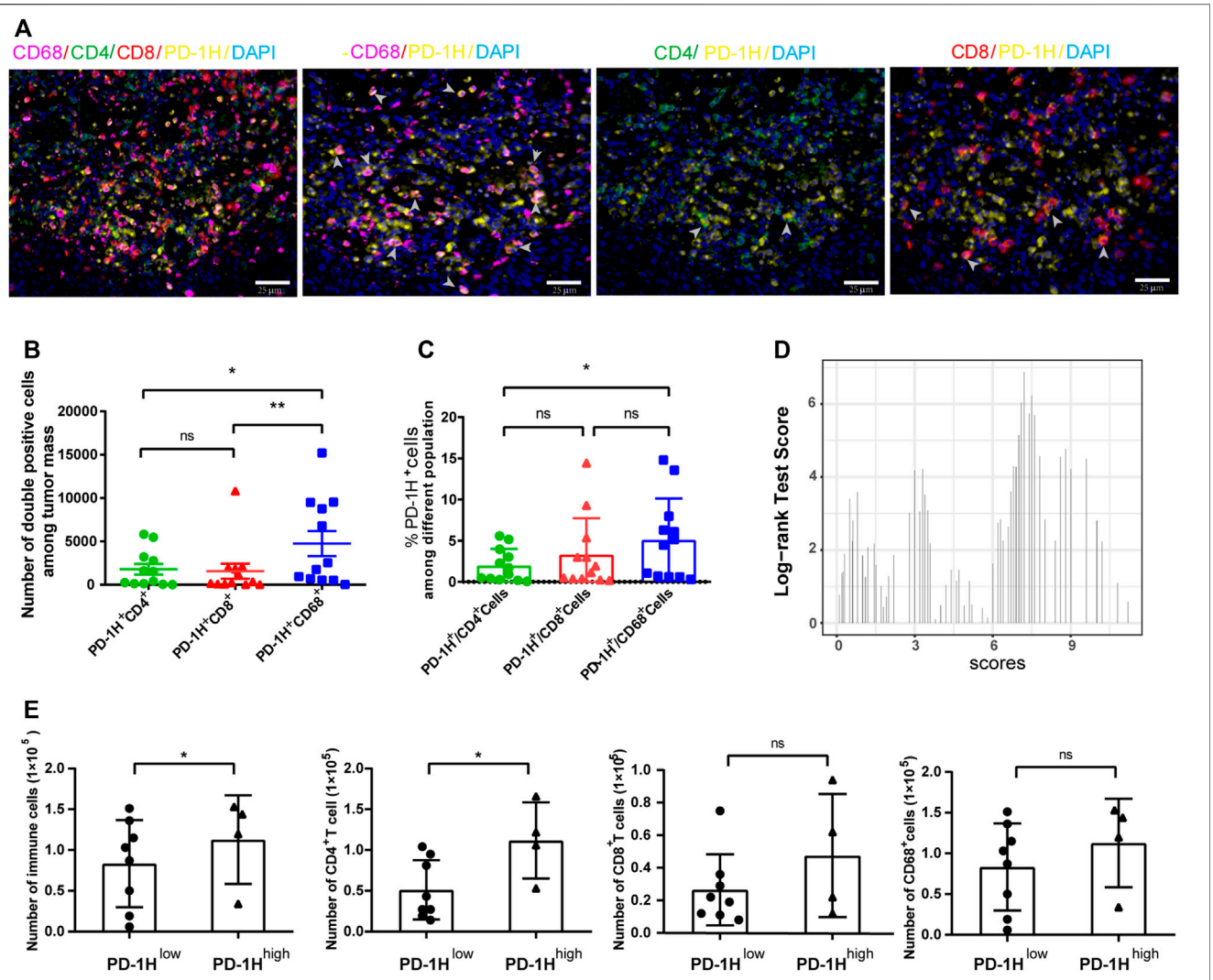


**FIGURE 2 |** PD-1H expression in tumor-infiltrating immune cells assessed by multiplex immunohistochemistry (mIHC). **(A)** Representative images of mIHC staining of PD-1H, CD4, CD8, CD68, and DAPI in ESCC tumor tissues. Scale bar: 25 μm, original magnification × 400. **(B)** The cell numbers of PD-1H$^+$CD68$^+$ myeloid cells were significantly higher than cell numbers of PD-1H$^+$CD4$^+$ and PD-1H$^+$CD8$^+$ cells. **(C)** The percentage of PD-1H positive cells among CD4$^+$ T cells, CD8$^+$ T cells, and CD68$^+$ cells was estimated. **(D)** The expression score of PD-1H was calculated and classified into high-expression (PD-1H $^{high}$) or low-expression (PD-1H $^{low}$) groups by using the R package of "survMisc". **(E)** The absolute counts of immune cells and CD4$^+$ T cells in tumor sites were significantly higher in patients with high PD-1H expression than in patients with low PD-1H expression. ns = non-significant, *$p < 0.05$, **$p < 0.01$.

(**Table 1**). However, the expression of PD-1H exhibited no correlation with sex, age, tumor stage, or tumor grades of differentiation.

## PD-1H Was Predominantly Expressed in CD68$^+$ Myeloid Cells of the Tumor Immune Microenvironment

To further investigate cell types with PD-1H expression in the tumor immune microenvironment, we randomly selected 12 tumor sections from 114 ESCC patients for multiplexed immunohistochemistry. Colocalization staining of PD-1H and multiple immunohistochemical markers was measured in tumor tissues. Our results documented that the majority of the PD-1H protein were colocalized with the CD68 macrophage marker. In contrast, CD4 and CD8 colocalized with PD-1H to significantly lower levels, although some areas of colocalization could be found (**Figure 2A**). The Halo image analysis platform was used to quantify the density and colocalization of positively stained cells. The results showed that the amount of PD-1H colocalized with CD68 was significantly higher than that colocalized with the amount of PD-1H colocalized CD4 ($p = 0.0069$) or CD8 cells ($p = 0.0115$) (**Figure 2B**). Likewise, among PD-1H-positive cells, the percentage of CD68$^+$ cells were significantly higher than the percentage of CD4$^+$ cells ($p = 0.0142$) (**Figure 2C**). Consistent with this result, the absolute number of CD4$^+$ T cells and total immune cells was higher in the high PD-1H

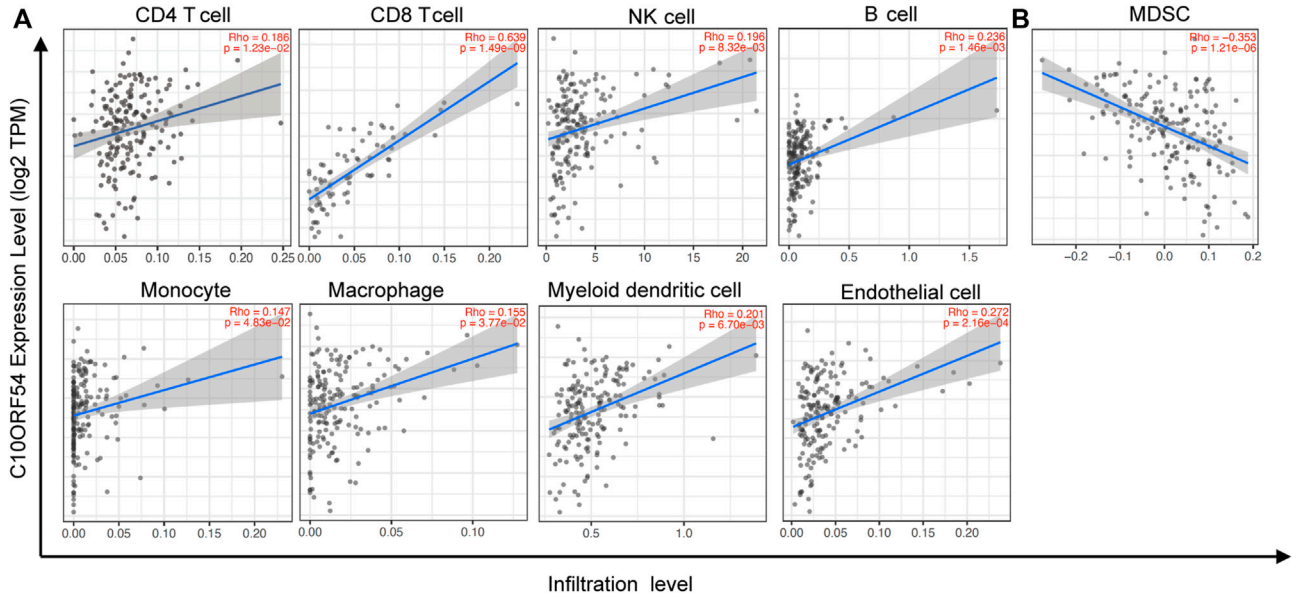


**FIGURE 3 |** The relationships of PD-1H expression with immune cell infiltration were assessed in ESCC based on TCGA database. The CIBERSORT algorithm was used to identify the immune cell infiltration signatures. **(A)** Positive correlations of PD-1H with $CD4^+$ T cells (Rho = 0.186, $p = 0.012$), $CD8^+$ T cells (Rho = 0.639, $p < 0.001$), $CD68^+$ macrophages (Rho = 0.155, $p = 0.038$), $CD1c^+$ myeloid dendritic cells (Rho = 0.201, $p = 0.007$), $CD14^+$ monocytes (Rho = 0.147, $p = 0.048$), $CD56^+$ NK cells (Rho = 0.196, $p = 0.008$), $CD20^+$ B cells (Rho = 0.236, $p = 0.001$), and $CD31^+$ endothelial cells (Rho = 0.272, $p < 0.001$). **(B)** The negative correlation of PD-1H with $CD11b^+CD33^+HLA\text{-}DR^-$MDSCs (Rho = −0.353, $p < 0.001$). CIBERSORT: Cell type Identification By Estimating Relative Subsets Of RNA Transcripts.

**TABLE 2 |** Univariate Kaplan–Meier analyses of prognostic parameters in 114 patients with ESCC.

| | — | *N* | 95% CI | | |
|---|---|---|---|---|---|
| | | | Lower | Upper | *p*-value |
| Sex | Female | 32 | 44.344 | 59.210 | 0.048 |
| | Male | 82 | 37.524 | 47.943 | |
| Age group | <65 years | 85 | 41.353 | 51.432 | 0.357 |
| | ≥65 years | 29 | 33.415 | 50.281 | |
| Tumor stage | T1 or T2 | 46 | 50.219 | 60.281 | 0.001 |
| | T3 or T4 | 68 | 32.621 | 44.444 | |
| Lymph node metastasis | N0 | 51 | 47.522 | 58.686 | 0.002 |
| | Nx | 63 | 33.024 | 44.976 | |
| Grades of differentiation | G1 or G2 | 93 | 39.684 | 49.429 | 0.979 |
| | G3 | 9 | 26.669 | 56.183 | |
| UICC stage | I or II | 64 | 47.030 | 56.931 | 0.001 |
| | III or IV | 50 | 29.825 | 43.627 | |
| PD-1H expression | Low | 85 | 37.550 | 47.429 | 0.029 |
| | High | 29 | 45.389 | 60.823 | |

*CI, confidence interval; HR, hazard ratio; UICC, union for international cancer control; PD-1H, programmed death-1 homolog; ESCC, esophageal squamous cell carcinoma.*

**TABLE 3 |** Multivariate analyses for the prediction of overall survival in patients with ESCC.

| | HR | 95% CI | | |
|---|---|---|---|---|
| | | Lower | Upper | *p*-value |
| Sex (female vs. male) | 0.679 | 0.342 | 1.351 | 0.270 |
| Age group (<65 vs. ≥ 65 years) | 1.997 | 0.901 | 4.426 | 0.089 |
| Tumor stage (T1/2 vs. T3/4) | 2.589 | 1.100 | 6.096 | 0.029 |
| Lymph node metastasis (N0 vs. Nx) | 1.97 | 0.766 | 5.068 | 0.16 |
| Grades of differentiation (G1/2 vs. G3) | 1.290 | 0.439 | 3.789 | 0.642 |
| UICC stage (I/II vs. III/IV) | 0.749 | 0.265 | 2.119 | 0.586 |
| PD-1H expression (low vs. high) | 0.637 | 0.260 | 1.402 | 0.240 |

*CI, confidence interval; HR, hazard ratio; UICC, union for international cancer control; PD-1H, Programmed death-1 homolog; ESCC, esophageal squamous cell carcinoma.*

expression group than in the low PD-1H expression group (**Figures 2D,E**).

## PD-1H mRNA Levels Were Correlated with Immune Cell Infiltration in ESCC

As our results indicated that PD-1H was highly expressed in $CD68^+$ myeloid cells of human ESCC tumors, we next assessed possible relationships of *PD-1H* mRNA expression level and the infiltration of nine types of immune cells by searching ESCC datasets from TCGA. The data showed that *PD-1H* mRNA (C10orf54) expression levels were significantly positively correlated with cell infiltration of $CD4^+$ T cells (Rho = 0.186, $p = 0.012$), $CD8^+$ T cells (Rho = 0.639, $p < 0.001$), $CD68^+$ macrophages (Rho = 0.155, $p = 0.038$), $CD1c^+$ myeloid dendritic cells (Rho = 0.201, $p = 0.007$), $CD14^+$ monocytes (Rho = 0.147, $p = 0.048$), $CD56^+$ NK cells (Rho = 0.196, $p = 0.008$), $CD19^+$ B cells (Rho = 0.236, $p = 0.001$), and $CD31^+$ endothelial cells (Rho = 0.272, $p < 0.001$) (**Figure 3A**). In contrast, the *PD-1H* mRNA expression level was negatively correlated with $CD11b^+CD33^+HLA\text{-}DR^-$ myeloid-derived suppressor cells (MDSCs) (Rho = −0.353 $p < 0.001$) (**Figure 3B**).

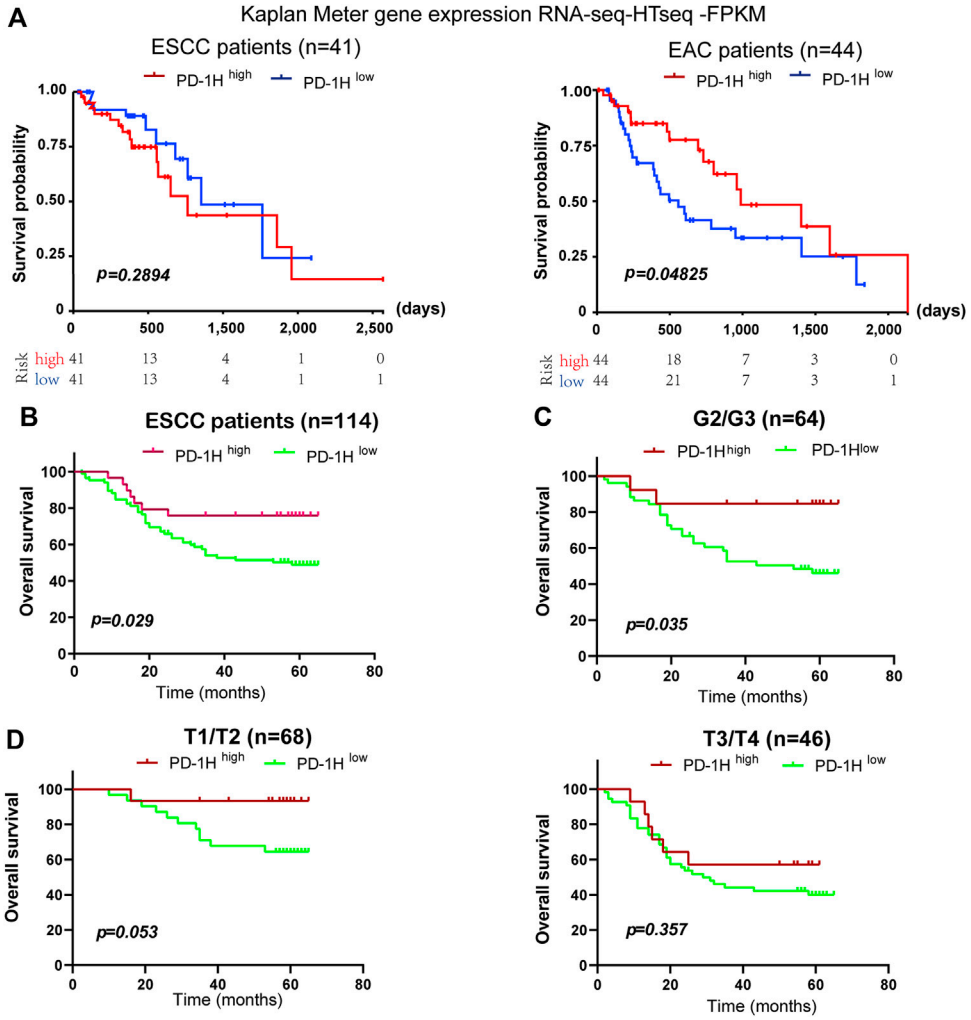


**FIGURE 4 |** The association between PD-1H expression levels and overall survival in ESCC. **(A)** The association of *PD-1H* mRNA expression and overall survival of patients was assessed in 41 ESCC patients and 44 EAC patients from the TCGA database. **(B–D)** With the applied scoring system, a score of 7.2 as the optimal cutoff point was identified by the "survMisc" package in R. The correlation between PD-1H protein expression and prolonged overall survival in 114 ESCC patients **(B)**, in the G1 and G2/3 subgroups **(C)** and in the T1/T2 and T3/T4 tumor stage subgroups **(D)** was analyzed by using log-rank (Mantel-Cox) test in GraphPad 8.0. ESCC, esophageal squamous cell carcinoma; EAC, esophageal adenocarcinoma; G (G2/G3), Grades of differentiation; T (T1/T2, T3/T4), Tumor stage.

## PD-1H Protein Expression Level Was Correlated with Overall Survival of Patients with Human ESCC

Recent studies demonstrate that high PD-1H expression correlates with a favorable prognosis in patients with colorectal cancer, high-grade serous ovarian cancer, triple-negative breast cancer, hepatocellular carcinoma, and esophageal adenocarcinoma (Zhang et al., 2018; Loeser et al., 2019; Cao et al., 2020; Zong et al., 2020; Zong et al., 2021). Here, 114 patients who were followed for 65 months were subjected to survival analysis, and the correlation of PD-1H expression with clinicopathologic parameters was analyzed by Kaplan–Meier survival and Cox regression models (**Tables 2**, **3**). In the validation cohort, univariate Kaplan–Meier analyses showed that tumor stage ($p$ = 0.001), lymph node metastasis ($p$ = 0.0 02), UICC stage ($p$ = 0.001), and PD-1H expression ($p$ = 0.029) were associated with the overall survival of patients with human ESCC. However, only tumor stage remained significant on multivariate Cox regression analysis. Although no statistically significant association was found between *PD-1H* mRNA expression and overall survival in ESCC from TCGA (**Figure 4A**), Kaplan–Meier analyses showed that ESCC patients with high PD-1H protein expression had significantly improved overall survival (HR = 0.60; 95% CI, 0.27–0.93; $p$ = 0.029; **Figure 4B**) in the exploratory cohort, especially among the G2/3 subgroup (**Figures 4C,D**). These results indicated that the PD-1H expression level is positively associated with a favorable prognosis in patients with ESCC.

## PD-1H Expression Was Detected in Activated T Cells and Peripheral Monocytes

Given that high PD-1H expression was found in the tumor microenvironment of ESCC, we further examined PD-1H

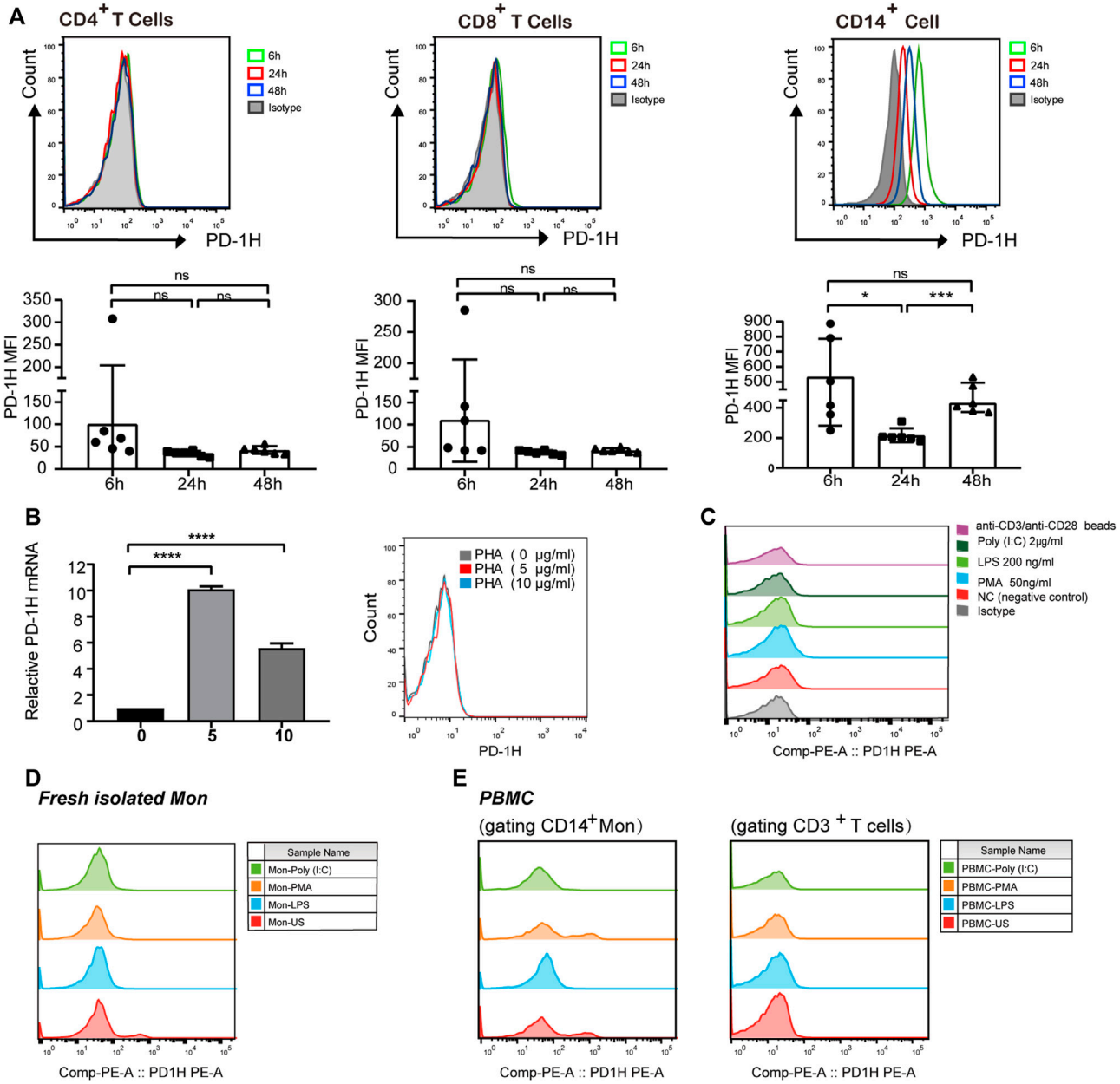


**FIGURE 5 |** PD-1H expression in peripheral T cells and monocytes. **(A)** PD-1H expression on the surface of $CD4^+$ T cells, $CD8^+$ T cells, and $CD14^+$ monocytes was analyzed by FCM at 6, 24, and 48 h after blood collection. The expression levels of PD-1H cells are shown in a representative FCM histogram (upper graph), and the mean fluorescence intensity (MFI) of PD-1H positive staining was pooled from two independent experiments (lower graph). **(B)** T cells were treated with different concentrations of PHA (0, 5, and 10 μg/ml), and then *PD-1H* mRNA and PD-1H cell surface expression was analyzed by qRT-PCR (left graph) and FCM (right graph), respectively. **(C)** Membrane PD-1H expression was analyzed 24 h after T cells were treated with PMA (50 ng/ml), LPS (200 ng/ml), poly I:C (2 μg/ml), or anti-CD3/anti-CD28 beads. **(D,E)** Membrane PD-1H expression was analyzed on the cell surface of purified monocytes and PBMCs after the cells were stimulated with PMA, LPS, and poly (I:C) for 24 h. The data are representative of at least two independent experiments. ns = non-significant, $^*p < 0.05$, $^{***}p < 0.001$, $^{****}p < 0.0001$. FCM, flow cytometry; qRT-PCR, real-time quantitative reverse transcription PCR; PBMC, peripheral blood mononuclear cells; Mon, monocytes; NC, negative control; PHA, polyhydroxyalkanoates; LPS, lipopolysaccharide; poly (I:C), polyinosinic:polycytidylic acid; PMA, Phorbol 12-myristate 13-acetate.

expression in peripheral T cells and monocytes derived from six ESCC patients by FCM and qRT-PCR. No positive staining was detected on the surface of $CD4^+$ and $CD8^+$ T cells PD-1H expression at 6, 24, and 48 h of blood collection. In contrast, PD-1H expression was found in $CD14^+$ monocytes, and the mean fluorescence intensity (MFI) of PD-1H positive staining on monocytes at 24 and 48 h of blood collection was lower than MFI of PD-1H positive staining on monocytes at 6 h (**Figure 5A**). Although the expression levels of *PD-1H* mRNA in $CD3^+$ T cells were upregulated by the stimulation with PHA for 24 h

(**Figure 5B**), PD-1H protein on the surface of T cells was not detectable (**Figure 5C**). Moreover, no significant PD-1H expression was detected on the T cell surface after T cells were stimulated with different stimulators, including PMA, LPS, poly (I:C), and TCR signaling (anti-CD3/anti-CD28 Dynabeads). PD-1H expression on $CD14^+$ cells was transiently downregulated 24 h after isolation, and membrane PD-1H on $CD14^+$ monocytes was decreased by the treatment with PMA, LPS, or poly (I:C) (**Figure 5D**). Intriguingly, PD-1H expression was maintained on CD14-positive cell surface after monocytes were mixed with T cells and treated with the PMA for 24 h**.** However, no detectable PD-1H membrane expression was found in activated T cells (**Figure 5E**).

## DISCUSSION

Following the initial identification of the immune checkpoint receptors CTLA-4 and PD-1, other Ig superfamily T-cell inhibitory ligands/receptors, such as LAG-3, TIM-3, TIGIT, BTLA, B7-H3, and B7-H4 have been indicated as important regulators of antitumor immunity (Gavrieli et al., 2006; Yi and Chen, 2009; Anderson et al., 2016; Andrews et al., 2017; Janakiram et al., 2017). PD-1H belongs to the CD28 superfamily, sharing 24 and 32% sequence similarity with PD-L1 and PD-1 molecules, respectively (Flies et al., 2011; Wang et al., 2011). Unlike other immune checkpoint receptors that are induced on activated T lymphocytes, PD-1H was reported to be constitutively expressed on myeloid cells and naïve T cells, exerting both ligand and receptor functions (Lines et al., 2014a; Gao et al., 2017; ElTanbouly et al., 2020). Increasing evidence indicates that PD-1H has a different expression pattern in the tumor microenvironment of different tumor subtypes. Mulati et al. reported that PD-1H was highly expressed in tumor cells of human ovarian and endometrial cancers using tissue microarray analysis and immunohistochemical staining (Mulati et al., 2019). Several lines of evidence support that PD-1H was expressed predominantly in myeloid cells of multiple myeloma, melanoma, and colorectal carcinoma, which were assessed mainly by multiplex immunofluorescence (Choi et al., 2020; Mutsaers et al., 2021; Zong et al., 2021). PD-1H has also been reported to be constitutively expressed in naïve T cells by single-cell RNA and ATAC sequencing technologies (ElTanbouly et al., 2020). The discrepancy between these studies might be due to the different PD-1H antibodies and variable tumor samples used in the experiments. Recently, PD-1H was reported to be expressed with CD68 and CD4 in most cases of esophageal adenocarcinoma (EAC) and to have no reliable coexpression with CD8 (Loeser et al., 2019). To date, little is known about PD-1H expression in human squamous cell carcinoma (ESCC). In this study, our data demonstrated that PD-1H was expressed at a high frequency in tumor tissues of ESCC (85.1%, 97/114), as analyzed by immunohistochemical staining. Multiplex immunohistochemistry showed that PD-1H was detected in CD4 T cells, CD8 T cells, and CD68 macrophages of ESCC tumor tissues. PD-1H protein was diffusely distributed within the plasma membrane of tumor infiltrating immune cells, and PD-1H expression levels were significantly higher in CD68-positive macrophages than T cells. Next, the optimal cutoff for PD-1H expression levels was determined using the method implemented in the survMisc R package. Our data showed that the number of immune cells, especially $CD4^+$ T cells, was significantly higher in ESCC cases with high levels of PD-1H expression than in ESCC cases with low levels of PD-1H. Altogether, our findings firstly provide direct information on PD-1H expression pattern and distribution in ESCC tumor tissues. ESCC and EAC have almost completely distinct geographic patterns, time trends, and primary risk factors (Abnet et al., 2018; Salem et al., 2018). In EAC, PD-1H was found to be coexpressed with CD68 and CD4; however, no reliable coexpression with CD8 was detectable. The different expression patterns of PD-1H between ESCC and EAC suggested the potentially different immune regulation mechanism of PD-1H in ESCC.

To explore the potential role of PD-1H in ESCC, we examined the association between the levels of *PD-1H* mRNA expression and the transcripts of various immune genes in ESCC datasets of 182 patients from TCGA. Intriguingly, high levels of *PD-1H* mRNA expression were significantly associated with stronger $CD8^+$ cytotoxic T-cell tumor infiltration. A weaker positive association was found in $CD4^+$ helper T cells, $CD56^+$ NK cells, $CD20^+$ B lymphocytes, $CD14^+$ monocytes, $CD68^+$ macrophages, $CD1c^+$ myeloid dendritic cells, and $CD31^+$ endothelial cells. Conversely, the *PD-1H* mRNA expression level was negatively correlated with myeloid-derived suppressor cells (MDSCs). Monocytes, macrophages, and MDSCs represent different stages of myeloid differentiation. MDSCs represent a phenotypically heterogeneous population of immature myeloid cells and can be divided into granulocytic (G-MDSCs) and monocytic (M-MDSCs) subpopulations. Macrophages are the most abundant tumor-infiltrating immune cells and display noticeable plasticity, which allows them to perform several functions within the tumor microenvironment (Kwak et al., 2020). PD-1H expression was observed in a range of tumor-infiltrating immune cells with inconsistent expression profiles in different types of cancers. Most previous studies supported that PD-1H is a negative immune regulator. PD-1H/VISTA is highly expressed on MDSCs derived from patients with AML, and *PD-1H* gene knockdown by siRNA potently reduces the MDSC-mediated inhibition of CD8 T-cell activity (Wang et al., 2018). In a B16 melanoma model, PD-1H blockade with antibodies decreased the infiltration of M-MDSCs in the tumor microenvironment through impairment of M-MDSC migration into tumor sites (Le Mercier et al., 2014). Broughton et al. found that PD-1H deficiency reduced the migration of *PD-1H* KO macrophages and MDSCs into the tumor microenvironment by altering chemokine receptor recycling (Broughton et al., 2019). Recently, Rogers et al. reported that agonistic PD-1H antibodies promoted human monocytes to express HLA, CD80, and CD40 in an Fc effector functional manner, indicating that PD-1H can serve as an activating receptor on human monocytes (Rogers et al., 2021). Our findings showed that the *PD-1H* mRNA expression level was positively correlated with the infiltration of $CD8^+$ T cells, $CD4^+$

T cells, and $CD68^+$ macrophages, whereas the *PD-1H* mRNA expression level was negatively correlated with HLA-$DR^-CD33^+$ MDSC infiltration. Based on our findings, it is tempting to speculate that high levels of PD-1H expression associated with an immune-activated microenvironment contribute favorable clinical outcomes in human esophageal squamous cell carcinoma.

Increasing evidence suggests a correlation between PD-1H expression and tumor patient prognosis. Boger et al. reported that PD-1H expression did not correlate with prognosis in patients with gastric cancer (Boger et al., 2017). Nonetheless, a higher level expression of PD-1H combined with low CD8 expression in tumor microenvironment is associated with poor prognosis and lymph node metastases in patients with oral squamous cell cancer (Wu et al., 2017). In contrast, higher expression of PD-1H in the tumor compartment predicted longer overall survival in patients with nonsmall cell lung cancer (Villarroel-Espindola et al., 2018), high-grade serous ovarian cancer (Zong et al., 2020), colorectal carcinoma (Zong et al., 2021), hepatocellular carcinoma (Zhang et al., 2018), triple-negative breast cancer (Cao et al., 2020), hepatocellular carcinoma, and epithelioid malignant pleural mesothelioma (Muller et al., 2020). Loeser et al. also demonstrated an improved median overall survival in EAC patients with PD-1H expression compared to those without PD-1H expression, especially in the pT1/2 subgroup in EAC (Loeser et al., 2019). Consistent with most previous reports, our results showed that PD-1H expression was positively correlated with favorable overall survival of ESCC patients, especially in the G2/G3 subgroup. Nevertheless, there was no significant association between *PD-1H* mRNA expression and overall survival of patients with esophageal cell carcinoma from TCGA database. These paradoxical results might be due to the different tumor samples used in the experiments. Given that "mRNA expression" is always inconsistent with "protein expression" for multiple immune regulators, we further analyzed *PD-1H* mRNA and surface protein expression in peripheral T cells and monocytes. PD-1H membrane-bound expression was positive in $CD14^+$ monocytes derived from ESCC patients, whereas no detectable surface expression was found in $CD4^+$ and $CD8^+$ T cells. Intriguingly, the PD-1H MFI on the cell surface was decreased after monocyte isolation, indicating that PD-1H expression was potentially dependent on cell–cell interactions *in vivo*. PD-1H was reported to be constitutively expressed on cell surface of naïve $CD4^+$ and $CD8^+$ T cells, and could be further upregulated by PMA plus ionomycin (a non-specific activator of T cells) (Flies et al., 2011). Our findings demonstrated that membrane PD-1H expression was still detected when monocytes were cocultured with PMA-activated T cells. Nevertheless, membrane PD-1H expression was undetectable on T cells by the stimulation of PHA, LPS, poly (I:C), or TCR signaling *in vitro*. These results indicated that PD-1H expression on the cell surface of monocytes was dependent on T-cell activation. The modulatory mechanism of the PD-1H protein in tumor microenvironment of ESCC remains unclear and worthwhile for further investigation.

In conclusion, our study demonstrated that PD-1H, which was predominantly expressed in $CD68^+$ myeloid cells in ESCC tumor tissues, was positively associated with the infiltration levels of immune-activated cells. Importantly, high levels of PD-1H expression were correlated with favorable overall survival in patients with ESCC, suggesting that PD-1H protein could be a prognostic indicator for patients with ESCC. Moreover, T-cell activation by nonspecific agents was beneficial to maintain PD-1H expression on the cell surface of monocytes. Additional studies are warranted to understand the role and regulatory mechanism of PD-1H in the tumor microenvironment of ESCC.

## DATA AVAILABILITY STATEMENT

The raw data supporting the conclusion of this article will be made available by the authors, without undue reservation.

## ETHICS STATEMENT

The studies involving human participants were reviewed and approved by the Research Ethics Committee of Fujian Medical University Union Hospital. The patients/participants provided their written informed consent to participate in this study. Written informed consent was obtained from the individual(s) for the publication of any potentially identifiable images or data included in this article.

## AUTHOR CONTRIBUTIONS

YC and GH conceived and designed the study; YC, RF, and BH acquired patient samples and gathered clinical data; JW and NX analyzed and interpreted the data; YC and RF drafted the article; YC and QZ supervised the study and reviewed the article. All authors read and approved the final article.

## FUNDING

This work was supported by grants from the National Key Research and Development Program (2019YFC1316102), the National Natural Science Foundation of China (No. 82073350), and the Natural Science Foundation of Fujian Province (Nos. 2021J01740, 2020J02039 and 2020J01657).

## REFERENCES

Abnet, C. C., Arnold, M., and Wei, W. Q. (2018). Epidemiology of Esophageal Squamous Cell Carcinoma. *Gastroenterology* 154, 360–373. doi:10.1053/j.gastro.2017.08.023

Anderson, A. C., Joller, N., and Kuchroo, V. K. (2016). Lag-3, Tim-3, and TIGIT: Co-Inhibitory Receptors with Specialized Functions in Immune Regulation. *Immunity* 44, 989–1004. doi:10.1016/j.immuni.2016.05.001

Andrews, L. P., Marciscano, A. E., Drake, C. G., and Vignali, D. A. A. (2017). LAG3 (CD223) as a Cancer Immunotherapy Target. *Immunol. Rev.* 276, 80–96. doi:10.1111/imr.12519

Bharaj, P., Chahar, H. S., Alozie, O. K., Rodarte, L., Bansal, A., Goepfert, P. A., et al. (2014). Characterization of Programmed Death-1 Homologue-1 (PD-1H) Expression and Function in Normal and HIV Infected Individuals. *Plos One* 9, e109103, 2014 . ARTN e109103. doi:10.1371/journal.pone.0109103

Böger, C., Behrens, H.-M., Krüger, S., and Röcken, C. (2017). The Novel Negative Checkpoint Regulator VISTA Is Expressed in Gastric Carcinoma and Associated with PD-L1/PD-1: A Future Perspective for a Combined Gastric Cancer Therapy? *Oncoimmunology* 6, e1293215. doi:10.1080/2162402X.2017.1293215

Broughton, T. W. K., ElTanbouly, M. A., Schaafsma, E., Deng, J., Sarde, A., Croteau, W., et al. (2019). Defining the Signature of VISTA on Myeloid Cell Chemokine Responsiveness. *Front. Immunol.* 10, 2641. doi:10.3389/fimmu.2019.02641

Cao, X., Ren, X., Zhou, Y., Mao, F., Lin, Y., Wu, H., et al. (2020). VISTA Expression on Immune Cells Correlates with Favorable Prognosis in Patients with Triple-Negative Breast Cancer. *Front. Oncol.* 10, 583966. doi:10.3389/fonc.2020.583966

Chen, W., Zheng, R., Baade, P. D., Zhang, S., Zeng, H., Bray, F., et al. (2016). Cancer Statistics in China, 2015. *CA: A Cancer J. Clin.* 66, 115–132. doi:10.3322/caac.21338

Choi, J. W., Kim, Y. J., Yun, K. A., Won, C. H., Lee, M. W., Choi, J. H., et al. (2020). The Prognostic Significance of VISTA and CD33-Positive Myeloid Cells in Cutaneous Melanoma and Their Relationship with PD-1 Expression. *Sci. Rep.* 10, 14372. doi:10.1038/s41598-020-71216-2

ElTanbouly, M. A., Zhao, Y., Nowak, E., Li, J., Schaafsma, E., Le Mercier, I., et al. (2020). VISTA Is a Checkpoint Regulator for Naïve T Cell Quiescence and Peripheral Tolerance. *Science* 367, 1–14. doi:10.1126/science.aay0524

Feng, R.-M., Zong, Y.-N., Cao, S.-M., and Xu, R.-H. (2019). Current Cancer Situation in China: Good or Bad News from the 2018 Global Cancer Statistics? *Cancer Commun.* 39, 22. doi:10.1186/s40880-019-0368-6

Flies, D. B., Wang, S., Xu, H., and Chen, L. (2011). Cutting Edge: A Monoclonal Antibody Specific for the Programmed Death-1 Homolog Prevents Graft-Versus-Host Disease in Mouse Models. *J.Immunol.* 187, 1537–1541. doi:10.4049/jimmunol.1100660

Flies, D. B., Han, X., Higuchi, T., Zheng, L., Sun, J., Ye, J. J., et al. (2014). Coinhibitory Receptor PD-1H Preferentially Suppresses CD4(+) T Cell-Mediated Immunity. *J. Clin. Invest.* 124, 1966–1975. doi:10.1172/Jci74589

Gao, J., Ward, J. F., Pettaway, C. A., Shi, L. Z., Subudhi, S. K., Vence, L. M., et al. (2017). VISTA Is an Inhibitory Immune Checkpoint that Is Increased after Ipilimumab Therapy in Patients with Prostate Cancer. *Nat. Med.* 23, 551–555. doi:10.1038/nm.4308

Gavrieli, M., Sedy, J., Nelson, C. A., and Murphy, K. M. (2006). BTLA and HVEM Cross Talk Regulates Inhibition and Costimulation. *Adv. Immunol.* 92, 157–185. doi:10.1016/S0065-2776(06)92004-5

Janakiram, M., Shah, U. A., Liu, W., Zhao, A., Schoenberg, M. P., and Zang, X. (2017). The Third Group of the B7- CD 28 Immune Checkpoint Family: HHLA 2, TMIGD 2, B7x, and B7-H3. *Immunol. Rev.* 276, 26–39. doi:10.1111/imr.12521

Kakavand, H., Wilmott, J. S., Menzies, A. M., Vilain, R., Haydu, L. E., Yearley, J. H., et al. (2015). PD-L1 Expression and Tumor-Infiltrating Lymphocytes Define Different Subsets of MAPK Inhibitor-Treated Melanoma Patients. *Clin. Cancer Res.* 21, 3140–3148. doi:10.1158/1078-0432.CCR-14-2023

Kojima, T., Shah, M. A., Muro, K., Francois, E., Adenis, A., Hsu, C.-H., et al. (2020). Randomized Phase III KEYNOTE-181 Study of Pembrolizumab versus Chemotherapy in Advanced Esophageal Cancer. *J. Clin. Oncol.* 38, 4138–4148. doi:10.1200/JCO.20.01888

Kwak, T., Wang, F., Deng, H., Condamine, T., Kumar, V., Perego, M., et al. (2020). Distinct Populations of Immune-Suppressive Macrophages Differentiate from Monocytic Myeloid-Derived Suppressor Cells in Cancer. *Cel Rep.* 33, 108571. doi:10.1016/j.celrep.2020.108571

Le Mercier, I., Chen, W., Lines, J. L., Day, M., Li, J., Sergent, P., et al. (2014). VISTA Regulates the Development of Protective Antitumor Immunity. *Cancer Res.* 74, 1933–1944. doi:10.1158/0008-5472.CAN-13-1506

Li, T., Fu, J., Zeng, Z., Cohen, D., Li, J., Chen, Q., et al. (2020). TIMER2.0 for Analysis of Tumor-Infiltrating Immune Cells. *Nucleic Acids Res.* 48, W509–W514. doi:10.1093/nar/gkaa407

Lines, J. L., Pantazi, E., Mak, J., Sempere, L. F., Wang, L., and O'Connell, S. (2014a). Correction: VISTA Is an Immune Checkpoint Molecule for Human T Cells. *Cancer Res.* 74, 3195. doi:10.1158/0008-5472.Can-14-1185

Lines, J. L., Sempere, L. F., Broughton, T., Wang, L., and Noelle, R. (2014b). VISTA Is a Novel Broad-Spectrum Negative Checkpoint Regulator for Cancer Immunotherapy. *Cancer Immunol. Res.* 2, 510–517. doi:10.1158/2326-6066.Cir-14-0072

Liu, J., Yuan, Y., Chen, W., Putra, J., Suriawinata, A. A., Schenk, A. D., et al. (2015). Immune-checkpoint Proteins VISTA and PD-1 Nonredundantly Regulate Murine T-Cell Responses. *Proc. Natl. Acad. Sci. USA* 112, 6682–6687. doi:10.1073/pnas.1420370112

Loeser, H., Kraemer, M., Gebauer, F., Bruns, C., Schröder, W., Zander, T., et al. (2019). The Expression of the Immune Checkpoint Regulator VISTA Correlates with Improved Overall Survival in pT1/2 Tumor Stages in Esophageal Adenocarcinoma. *Oncoimmunology* 8, e1581546. doi:10.1080/2162402X.2019.1581546

Mulati, K., Hamanishi, J., Matsumura, N., Chamoto, K., Mise, N., Abiko, K., et al. (2019). VISTA Expressed in Tumour Cells Regulates T Cell Function. *Br. J. Cancer* 120, 115–127. doi:10.1038/s41416-018-0313-5

Muller, S., Victoria Lai, W., Adusumilli, P. S., Desmeules, P., Frosina, D., Jungbluth, A., et al. (2020). V-domain Ig-Containing Suppressor of T-Cell Activation (VISTA), a Potentially Targetable Immune Checkpoint Molecule, Is Highly Expressed in Epithelioid Malignant Pleural Mesothelioma. *Mod. Pathol.* 33, 303–311. doi:10.1038/s41379-019-0364-z

Mutsaers, P., Balcioglu, H. E., Kuiper, R., Hammerl, D., Wijers, R., van Duin, M., et al. (2021). V-Domain Ig Suppressor of T Cell Activation (VISTA) Expression Is an Independent Prognostic Factor in Multiple Myeloma. *Cancers* 13, 2219. doi:10.3390/cancers13092219

Newman, A. M., Liu, C. L., Green, M. R., Gentles, A. J., Feng, W., Xu, Y., et al. (2015). Robust Enumeration of Cell Subsets from Tissue Expression Profiles. *Nat. Methods* 12, 453–457. doi:10.1038/Nmeth.3337

Ogłuszka, M., Orzechowska, M., Jędroszka, D., Witas, P., and Bednarek, A. K. (2019). Evaluate Cutpoints: Adaptable Continuous Data Distribution System for Determining Survival in Kaplan-Meier Estimator. *Comput. Methods Programs Biomed.* 177, 133–139. doi:10.1016/j.cmpb.2019.05.023

Rich, J. T., Neely, J. G., Paniello, R. C., Voelker, C. C. J., Nussenbaum, B., and Wang, E. W. (2010). A Practical Guide to Understanding Kaplan-Meier Curves. *Otolaryngol. Head Neck Surg.* 143, 331–336. doi:10.1016/j.otohns.2010.05.007

Rogers, B. M., Smith, L., Dezso, Z., Shi, X., DiGiammarino, E., Nguyen, D., et al. (2021). VISTA Is an Activating Receptor in Human Monocytes. *J. Exp. Med.* 218, e20201601. doi:10.1084/jem.20201601

Salem, M. E., Puccini, A., Xiu, J., Raghavan, D., Lenz, H. J., Korn, W. M., et al. (2018). Comparative Molecular Analyses of Esophageal Squamous Cell Carcinoma, Esophageal Adenocarcinoma, and Gastric Adenocarcinoma. *Oncol.* 23, 1319–1327. doi:10.1634/theoncologist.2018-0143

Stack, E. C., Wang, C., Roman, K. A., and Hoyt, C. C. (2014). Multiplexed Immunohistochemistry, Imaging, and Quantitation: a Review, with an Assessment of Tyramide Signal Amplification, Multispectral Imaging and Multiplex Analysis. *Methods* 70, 46–58. doi:10.1016/j.ymeth.2014.08.016

Villarroel-Espindola, F., Yu, X., Datar, I., Mani, N., Sanmamed, M., Velcheti, V., et al. (2018). Spatially Resolved and Quantitative Analysis of VISTA/PD-1H as a Novel Immunotherapy Target in Human Non-Small Cell Lung Cancer. *Clin. Cancer Res.* 24, 1562–1573. doi:10.1158/1078-0432.CCR-17-2542

Wang, L., Rubinstein, R., Lines, J. L., Wasiuk, A., Ahonen, C., Guo, Y., et al. (2011). VISTA, a Novel Mouse Ig Superfamily Ligand that Negatively Regulates T Cell Responses. *J. Exp. Med.* 208, 577–592. doi:10.1084/jem.20100619

Wang, L., Jia, B., Claxton, D. F., Ehmann, W. C., Rybka, W. B., Mineishi, S., et al. (2018). VISTA Is Highly Expressed on MDSCs and Mediates an Inhibition of T Cell Response in Patients with AML. *Oncoimmunology* 7, e1469594. doi:10.1080/2162402X.2018.1469594

Wu, L., Deng, W.-W., Huang, C.-F., Bu, L.-L., Yu, G.-T., Mao, L., et al. (2017). Expression of VISTA Correlated with Immunosuppression and Synergized with CD8 to Predict Survival in Human Oral Squamous Cell Carcinoma. *Cancer Immunol. Immunother.* 66, 627–636. doi:10.1007/s00262-017-1968-0

Xie, S., Huang, J., Qiao, Q., Zang, W., Hong, S., Tan, H., et al. (2018). Expression of the Inhibitory B7 Family Molecule VISTA in Human Colorectal Carcinoma Tumors. *Cancer Immunol. Immunother.* 67, 1685–1694. doi:10.1007/s00262-018-2227-8

Yi, K. H., and Chen, L. (2009). Fine Tuning the Immune Response through B7-H3 and B7-H4. *Immunol. Rev.* 229, 145–151. doi:10.1111/j.1600-065X.2009.00768.x

Zeng, H., Zheng, R., Zhang, S., Zuo, T., Xia, C., Zou, X., et al. (2016). Esophageal Cancer Statistics in C Hina, 2011: Estimates Based on 177 Cancer Registries. *Thorac. Cancer* 7, 232–237. doi:10.1111/1759-7714.12322

Zhang, M., Pang, H.-J., Zhao, W., Li, Y.-F., Yan, L.-X., Dong, Z.-Y., et al. (2018). VISTA Expression Associated with CD8 Confers a Favorable Immune Microenvironment and Better Overall Survival in Hepatocellular Carcinoma. *BMC Cancer* 18, 511–518. doi:10.1186/s12885-018-4435-1

Zong, L., Zhou, Y., Zhang, M., Chen, J., and Xiang, Y. (2020). VISTA Expression Is Associated with a Favorable Prognosis in Patients with High-Grade Serous Ovarian Cancer. *Cancer Immunol. Immunother.* 69, 33–42. doi:10.1007/s00262-019-02434-5

Zong, L., Yu, S., Mo, S., Zhou, Y., Xiang, Y., Lu, Z., et al. (2021). High VISTA Expression Correlates with a Favorable Prognosis in Patients with Colorectal Cancer. *J. Immunother.* 44, 22–28. doi:10.1097/CJI.0000000000000343

**Conflict of Interest:** The authors declare that the research was conducted in the absence of any commercial or financial relationships that could be construed as a potential conflict of interest.

**Publisher's Note:** All claims expressed in this article are solely those of the authors and do not necessarily represent those of their affiliated organizations, or those of the publisher, the editors, and the reviewers. Any product that may be evaluated in this article, or claim that may be made by its manufacturer, is not guaranteed or endorsed by the publisher.

frontiers in Molecular Biosciences

ORIGINAL RESEARCH
published: 13 December 2021
doi: 10.3389/fmolb.2021.764900

# ELK1 Enhances Pancreatic Cancer Progression Via LGMN and Correlates with Poor Prognosis

*Qiang Yan[1]*†, Chenming Ni[2†], Yingying Lin[3], Xu Sun[1], Zhenhua Shen[1], Minjie Zhang[1], Shuwen Han[1], Jiemin Shi[1], Jing Mao[1], Zhe Yang[4] and Weilin Wang[5]**

[1]Department of General Surgery, Huzhou Central Hospital, Huzhou, China, [2]Department of Pancreatic Hepatobiliary Surgery, Changhai Hospital, Shanghai, China, [3]Department of Neurosurgery, RenJi Hospital, Shanghai JiaoTong University School of Medicine, Shanghai, China, [4]Department of Hepatobiliary and Pancreatic Surgery, Department of Liver Transplantation, Shulan (Hangzhou) Hospital, Zhejiang Shuren University School of Medicine, Hangzhou, China, [5]Department of Hepatobiliary and Pancreatic Surgery, The Second Affiliated Hospital of Zhejiang University, School of Medicine, Hangzhou, China

OPEN ACCESS

**Edited by:**
Saber Imani,
Affiliated Hospital of Southwest Medical University, China

**Reviewed by:**
Weimiao Yu,
Bioinformatics Institute (A*STAR), Singapore
Xuan Ye,
Novartis Institutes for BioMedical Research, United States
Qiuyu Zhang,
Fujian Medical University, China

***Correspondence:**
Qiang Yan
yianq@hzhospital.com
Weilin Wang
wam@zju.edu.cn

†These authors have contributed equally to this work and share first authorship

**Specialty section:**
This article was submitted to Molecular Diagnostics and Therapeutics, a section of the journal Frontiers in Molecular Biosciences

**Received:** 26 August 2021
**Accepted:** 22 November 2021
**Published:** 13 December 2021

**Citation:**
Yan Q, Ni C, Lin Y, Sun X, Shen Z, Zhang M, Han S, Shi J, Mao J, Yang Z and Wang W (2021) ELK1 Enhances Pancreatic Cancer Progression Via LGMN and Correlates with Poor Prognosis. Front. Mol. Biosci. 8:764900. doi: 10.3389/fmolb.2021.764900

Pancreatic cancer is one of the most lethal cancers and its prognosis is extremely poor. Clarification of molecular mechanisms and identification of prognostic biomarkers are urgently needed. Though we previously found that LGMN was involved in pancreatic carcinoma progression, the upstream regulation of LGMN remains unknown. We used reliable software to search for the potential transcription factors that may be related with LGMN transcription, we found that ELK1 could be a new regulator of LGMN transcription that binded directly to the LGMN promoter. Moreover, knocking down of ELK1 reduced pancreatic cancer cells proliferation, invasion and survival, while LGMN restored the malignancy of pancreatic cancer *in vitro* and *in vivo*. Overexpression of ELK1 further increased cancer cells proliferation, invasion and survival. Clinically, ELK1 and LGMN were positively correlated with clinical stage, degree of differentiation and Lymph node infiltration. ELK1 and LGMN were identified as independent prognostic factors for overall survival. The patients with low expression of ELK1/LGMN survived an average of 29.65 months, whereas those with high expression of ELK1/LGMN survived an average of 16.67 months. In conclusive, our results revealed a new mechanism by which ELK1 promoted the progression of pancreatic cancer *via* LGMN and conferred poor prognosis.

**Keywords: pancreatic carcinoma, LGMN, Elk1, proliferation, invasion, apoptosis**

## INTRODUCTION

Pancreatic adenocarcinoma is one of the most common malignancies (Bray et al., 2018). Due to the symptoms of pancreatic adenocarcinoma are usually non-specific, the early diagnosis rate is extremely low, which results in the late detection of pancreatic adenocarcinoma, with extensive metastasis and poor prognosis ((Wood, 2014), (Liu et al., 2015)). The median survival time of patients with locally advanced pancreatic cancer was merely 8–12 months. The medium survival time of metastatic cancer patients was only 3–6 months (Colbert et al., 2014). The 5-year survival rate

**Abbreviations:** AEP, asparaginyl endopeptidase; CI, confidence interval; DMEM, Dulbecco's Modified Eagle Medium; ECL, enhanced chemiluminescence; FACS, fluorescence-activated cell sorting; FBS, fetal bovine serum; FCM, Flow cytometry; GBM, glioblastoma; LGMN, legumain; PDAC, pancreatic ductal adenocarcinoma; qRT-PCR, quantitative real-time PCR; SDS, sodium dodecyl sulfate; UUTUC, upper urinary tract urothelial carcinoma.

for patients with metastatic pancreatic ductal adenocarcinoma (PDAC) is only 8% (the lowest survival rate of all types of cancer), and pancreatic adenocarcinoma is the fourth leading cause of cancer-related death ((Jagadeeshan et al., 2015), (Ibrahim and Wang, 2016)). Despite the introduction of new therapies, the survival rates of PDAC patients has not increased significantly in recent years (Al Haddad and Adrian, 2014). Thus, there is an urgent need to identify potential mechanisms for pancreatic cancer metastasis.

Legumain (LGMN), also calls asparaginyl endopeptidase (AEP), belongs to the C13 family of cysteine proteases. LGMN specifically cleaves peptide bonds in asparaginyl residue in the mammalian genome (Haugen et al., 2013). Normally, LGMN exists in acidic endosomes/lysosomes and participates in intracellular protein degradation under physiological conditions (Herskowitz et al., 2012). LGMN functions in kidney physiology (Miller et al., 2011), immunity (van Endert, 2009) and osteoclast formation (Choi et al., 1999). LGMN has been determined to be highly expressed in many solid tumors, including colorectal cancer, breast cancer and glioblastoma (GBM), and high expression of LGMN correlated with a more metastatic phenotype, which is partially mediated by the activation of cathepsins and pro-MMP2 (Zhen et al., 2015; D'Costa et al., 2014; Sevenich and Joyce, 2014; Edgington-Mitchell et al., 2015). Recently, LGMN has been shown to exhibit a vesicular staining pattern, and high expression of LGMN was significantly related to an advanced tumor stage, a high Gleason score, perineural invasion, and large pancreatic adenocarcinoma tumors (Zhu et al., 2016). Although we previously found that high LGMN expression was involved in the progression of pancreatic carcinoma in an exosome-dependent manner and LGMN could independently indicate poor prognosis, the upstream regulation of LGMN remains unknown (Yan et al., 2018).

In this study, we investigated the transcriptional regulation of LGMN in pancreatic cancer cells and analyzed the functional interaction between the transcription factors and LGMN *in vitro* and *in vivo*. Their correlation was also analyzed in clinical samples.

# MATERIALS AND METHODS

## Patients and Tissue Samples

Our study was approved by the Ethics Committee of Huzhou Central Hospital (Approval number 20141103-01, Date of approval: November 27, 2014). Written consent was obtained from patients enrolled in this study. A total of 176 patients (males: 108, females: 68) with histologically confirmed PDAC at Shanghai Changhai Hospital were recruited for this study. The mean patient age was 60.6 years (range 32–75). Patient diagnoses were independently reviewed by two pathologists and classified by WHO criteria. Follow-up data were completed on May 1, 2019.

## Cell Lines

The human pancreatic cancer cell lines PANC-1, BxPC3, SW1990 and ASPC-1 were purchased from the Cell Bank of the Chinese Academy of Sciences. BxPC3 and ASPC-1 were cultured in RPMI1640 medium. SW1990 was cultured in Leibovitz's L-15 Medium. PANC-1was maintained in Dulbecco's Modified Eagle Medium (DMEM). All the medium were supplemented with 10%

**TABLE 1 |** Association of LGMN expression with clinicopathological variables in pancreatic ductal adenocarcinoma.

| Clinicopathological characteristic | *n* (%) | LGMN staining (*n*; %) | | *p*-value |
|---|---|---|---|---|
| | | Low | High | |
| Age (year) | | | | 0.137 |
| <60 | 86 (48.86) | 42 (48.84) | 44 (51.16) | |
| ≥60 | 90 (51.14) | 54 (60.00) | 36 (40.00) | |
| Sex | | | | 0.224 |
| Male | 108 (61.36) | 55 (50.93) | 53 (49.07) | |
| Female | 68 (38.64) | 41 (60.29) | 27 (39.71) | |
| Clinical stages | | | | *0.004 |
| I/II | 138 (78.41) | 83 (60.14) | 55 (39.86) | |
| III/IV | 38 (21.59) | 13 (34.21) | 25 (65.79) | |
| Tumor location | | | | 0.198 |
| Head | 112 (63.64) | 57 (50.89) | 55 (49.11) | |
| Body/tail | 64 (36.36) | 39 (60.93) | 25 (39.07) | |
| Tumor size | | | | 0.160 |
| ≤4 cm | 58 (32.95) | 36 (62.07) | 22 (37.93) | |
| >4 cm | 118 (67.05) | 60 (50.85) | 58 (49.15) | |
| Differentiation | | | | *0.012 |
| Weak to moderately | 110 (62.50) | 68 (61.82) | 42 (38.18) | |
| Poorly | 66 (37.50) | 28 (42.42) | 38 (57.58) | |
| N infiltration | | | | 0.060 |
| Positive | 165 (93.75) | 87 (52.73) | 78 (47.27) | |
| Negative | 11 (6.25) | 9 (81.82) | 2 (18.18) | |
| Lymphnode infiltration | | | | *0.020 |
| Positive | 128 (72.73) | 63 (49.22) | 65 (50.78) | |
| Negative | 48 (27.27) | 33 (68.75) | 15 (31.25) | |

heat-inactivated fetal bovine serum (FBS; Invitrogen, Carlsbad, CA, United States), penicillin (100 U/ml), and streptomycin (100 μg/ml) at 37°C in a humidified atmosphere of 5% $CO_2$. All the cells were free of mycoplasma contamination.

## Plasmids and Reagents

Lentivirus vectors for ELK1 and LGMN knockdown or overexpression were constructed by Hanyin Biotech (Hanyin Biotech, Shanghai, China). The lentivirus was packaged using psPAX2 and pMD2G (Hanyin Biotech, Shanghai, China). To obtain stable cells with ELK1 or LGMN knockdown or overexpression, lentivirus supernatant was added to cells, followed by selection with 1 μg/ml puromycin for 2 weeks. siRNA sequences for transcription factors are listed in **Supplementary Table S1**.

Anti-human LGMN antibody (AF2199, MAB2199; R&D), anti-human ELK1 antibody (ab27708; Abcam), anti-actin antibody (ab8227; Abcam), anti-goat IgG (ab6741; Abcam) and anti-rabbit IgG (#7074; Cell Signaling Technology) were used in this study.

## Western Blot Analysis

Lysates (50 μg per lane) collected from pancreatic cancer cells or exosomes were separated by sodium dodecyl sulfate (SDS)-polyacrylamide gel electrophoresis and transferred to nitrocellulose

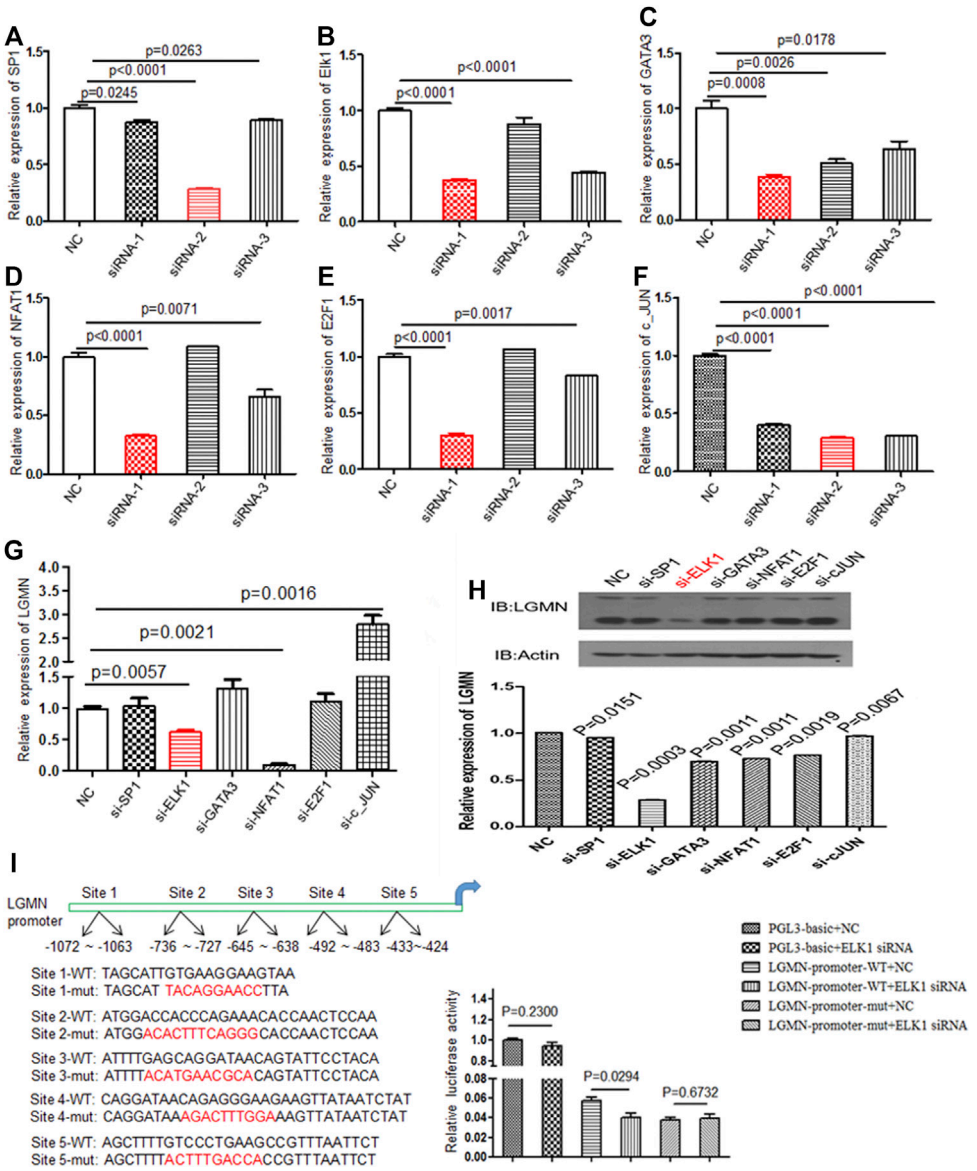


**FIGURE 1 |** Knockdown of ELK1 reduced LGMN expression in pancreatic cancer cells. **(A–F)** RT-PCR analysis of SP1, ELK1, GATA3, NFAT1, E2F1 and c-JUN levels after transfection of respective siRNAs in PANC-1 cells. Three types of siRNA were used. **(G)** RT-PCR analysis of LGMN mRNA expression after transfection of effective siRNAs in PANC-1 cells, the mRNA level was normalized to GAPDH. $p = 0.0057$ between ELK1-KD and control group, $p = 0.0021$ between NFAT1 and control group. **(H)** Western blot analysis of LGMN levels after transfection of effective siRNAs in PANC-1 cells. **(I)** Luciferase assay of LGMN transcriptional activity after transfection of ELK1 siRNAs or control in PANC-1 cells. $p = 0.029$ between LGMN-promoter-WT+siELK1 and control group.

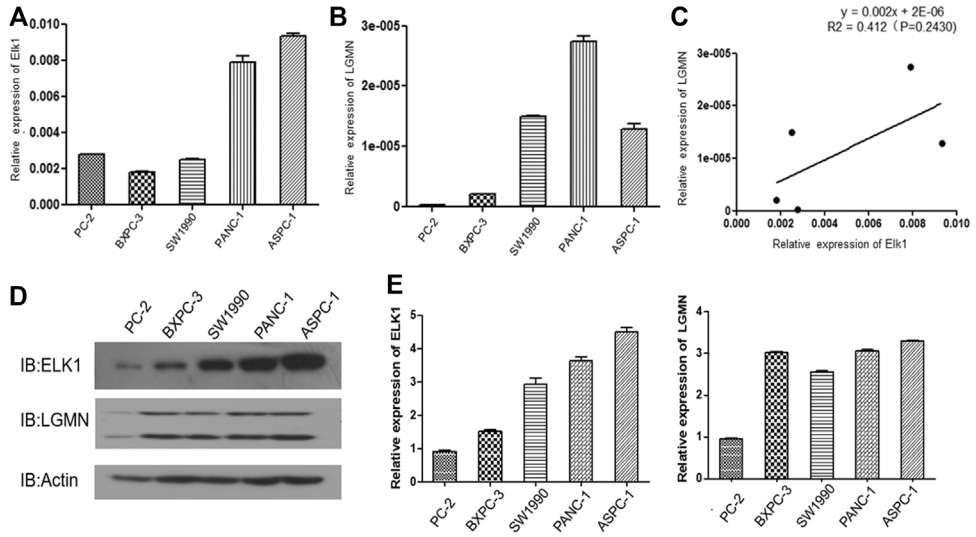


**FIGURE 2 |** ELK1 positively correlated with LGMN expression in pancreatic cancer cells. **(A,B)** ELK1 and LGMN expression in four pancreatic cancer cell lines were detected by RT-PCR. **(C)** Correlation between ELK1and LGMN in pancreatic cancer cells were analyzed. **(D,E)** ELK1, LGMN expression and beta-catenin in four pancreatic cancer cell lines determined by Western blot.

membranes. After incubation with 5% nonfat milk for 30 min at 25°C, the membranes were further incubated with primary antibodies (1:500 dilution) overnight at 4°C. Horseradish peroxidase-conjugated secondary antibodies (1:3,000 dilution) were added and incubated for 60 min at 25°C. Immune-reactive proteins were captured by enhanced chemiluminescence (ECL).

## Total RNA Isolation and Quantitative Real-Time PCR (qRT-PCR) Analysis

Total RNA was extracted from pancreatic adenocarcinoma cancer cells using TRIzol reagent according to the manufacturer's instructions (Invitrogen). cDNA was transcribed from 1 μg of total RNA. qRT-PCR was performed with SYBR Premix Ex Taq (TaKaRa, Dalian, China). PCR primers are listed in **Supplementary Table S2** (Shenggong Biotech, Shanghai, China).

The cycling conditions were as follows: initial denaturation at 95°C for 5 min, followed by 36 cycles of denaturation at 95°C for 10 s and annealing at 60°C for 30 s. The relative mRNA expression levels were calculated using the comparative Ct (ΔΔCt) method. Actin was used as an internal control.

## CCK8 Assay

We examined cell proliferation using CCK8 assays (Dojindo, Japan).

## Cell Invasion Assay

Cells were seeded onto the upper chamber of Matrigel-coated transwell inserts with a pore size of 8 μm in serum-free medium. FBS (10%) was added to the lower chamber as a chemoattractant. After 24 h, the upper surface of the insert was gently scratched with a cotton swab. Cells invading the lower chamber were fixed with 4% paraformaldehyde and stained with crystal violet. The numbers of invading cells were counted under a microscope. Five random microscopic fields were analyzed for each insert.

## Flow Cytometry (FCM) Analysis

Cell apoptosis was analyzed by annexin V staining. Briefly, cells were seeded for 24 h and then transfected with the appropriate lentivirus for another 48 h. The cells were then harvested, washed twice with PBS, stained with annexin V and DAPI in binding buffer, and detected by FCM after a 15-min incubation at room temperature in the dark. Early apoptotic cells (annexin V+/DAPI−) and late apoptotic cells (annexin V+/DAPI+) were quantified.

## Nude Mouse Model

Mouse experiments of our study was approved by the Animal Ethics Committee of Huzhou Institute of Food and Drug Inspection (Approval number HSYJ2017001, Date of approval: December 14, 2017). Male BALB/c athymic nude mice, 4–6 weeks old and weighing 20–22 g, were purchased from the SLAC (Shanghai, China). The following ASPC-1 cells ($5 \times 10^6$) were subcutaneously injected into mice: (Bray et al., 2018) ASPC-1-NC (negative control), (Wood, 2014) ASPC-1 ELK1-KD (knockdown), and (Liu et al., 2015) ASPC-1 ELK1-KD/LGMN-OE (overexpressing). Tumor volumes were monitored every week. After 6 weeks, all the mice were euthanized, and the tumors were collected.

## Histological and Immunohistochemical Analyses

Histological and immunohistochemical analyses were performed as previously described (Liu et al., 2003). Rabbit anti-ELK1

antibody (ab32106, lot#: GR259320-21; Abcam) and rabbit anti-LGMN antibody (ab232870, lot#: GR97368-48; Abcam), diluted 1:50 in blocking buffer, were used as primary antibodies. Normal rabbit immunoglobulin G (Abcam) was included as a negative control. Three pathologists from Shanghai Changhai Hospital individually scored samples in a blinded manner before drawing conclusions.

## Quantification of IHC Parameters

ELK1 and LGMN were selected as markers respectively. The expression of these immunosuppressive proteins in tissues were evaluated *via* immunohistochemical analysis. Two pathologists to score the intensity and the percentage of positive cells in the tumor tissue independently. Staining intensity: 0 (No staining); 1 (Light yellow); 2 (Light brown); 3 (Brown). The percentage of positive cells: 0 (<5%); 1 (5–25%); 3 (>25–50%); 4 (≥50–75%); 4 (>75%), these two grades were multiplied and specimens were assigned to four groups according to the achieved score: 0–3, negative; 4–6, weak positive (+); 7–9, moderate positive (++); 10–12, strong positive (+++). Negative control staining was carried out with cold PBS in place of primary antibody. Known positive tissues were used as positive controls. Five fields were randomly taken from each sheet and photographed (magnification ×200–×400)

## Statistical Analysis

Survival was calculated starting from the date of surgery to the date of death or the last follow-up. Survival curves for LGMN were plotted using the Kaplan–Meier method and compared using the log-rank test. The median time and hazard ratio are shown with the 95% confidence interval (CI). Data are presented as the mean ± SD or as the number and percentage. The differences between groups and categorical variables were compared by the chi-square test. For normally distributed data, continuous variables were compared *via* an independent samples *t* test. Statistical analysis was performed with SPSS 15.0 (Chicago, IL, United States). Significance was defined as a $p$ value <0.05.

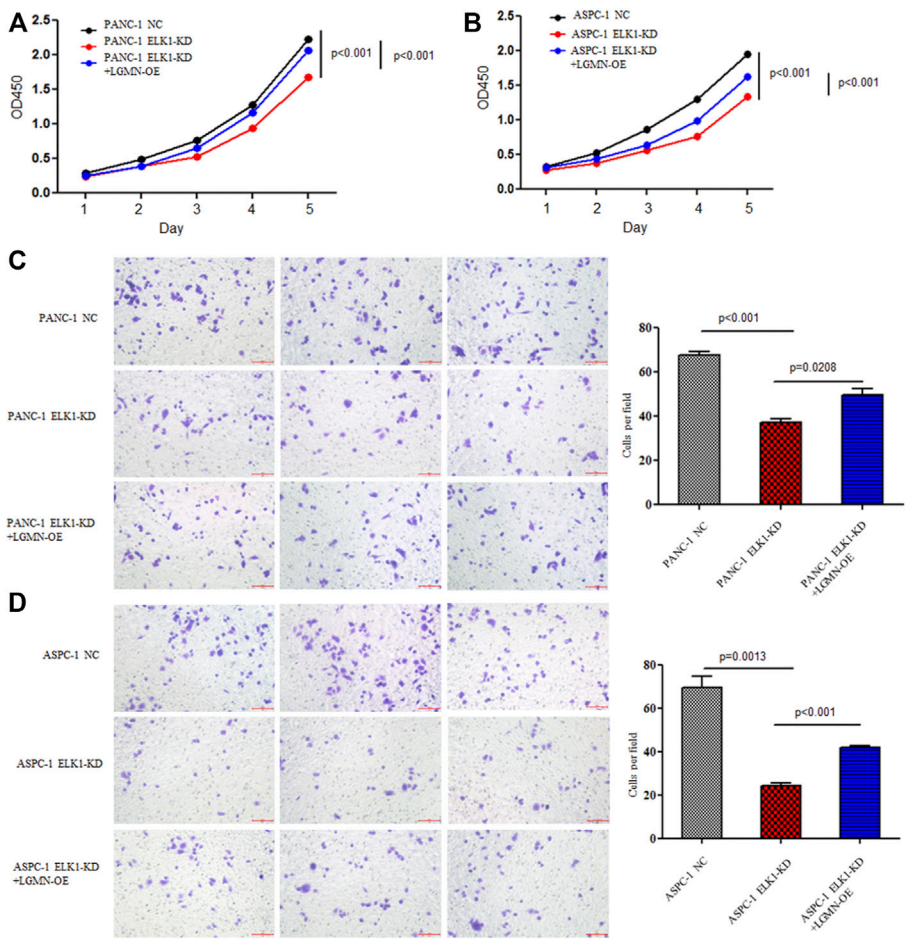


**FIGURE 3 |** ELK1 promoted pancreatic cancer cell proliferation and invasion *via* LGMN. **(A,B)** CCK8 analysis of PANC-1 and ASPC-1 cells with ELK1 knocked down as well as LGMN rescued. *$p$ < 0.001, **$p$ < 0.001, between ELK1-KD group and control group, ELK1-KD group and ELK1-KD+LGMN-OE group in PANC-1 cells **(A)**. *$p$ < 0.001, **$p$ < 0.001, between ELK1-KD group and ELK1-KD+LGMN-OE group in ASPC-1 cells **(B)**. **(C,D)** Matrigel-Transwell analysis of PANC-1 and ASPC-1 cells with ELK1 knocked down as well as LGMN rescued. Five random microscopic fields were analyzed for each insert (shown at ×200 magnification).

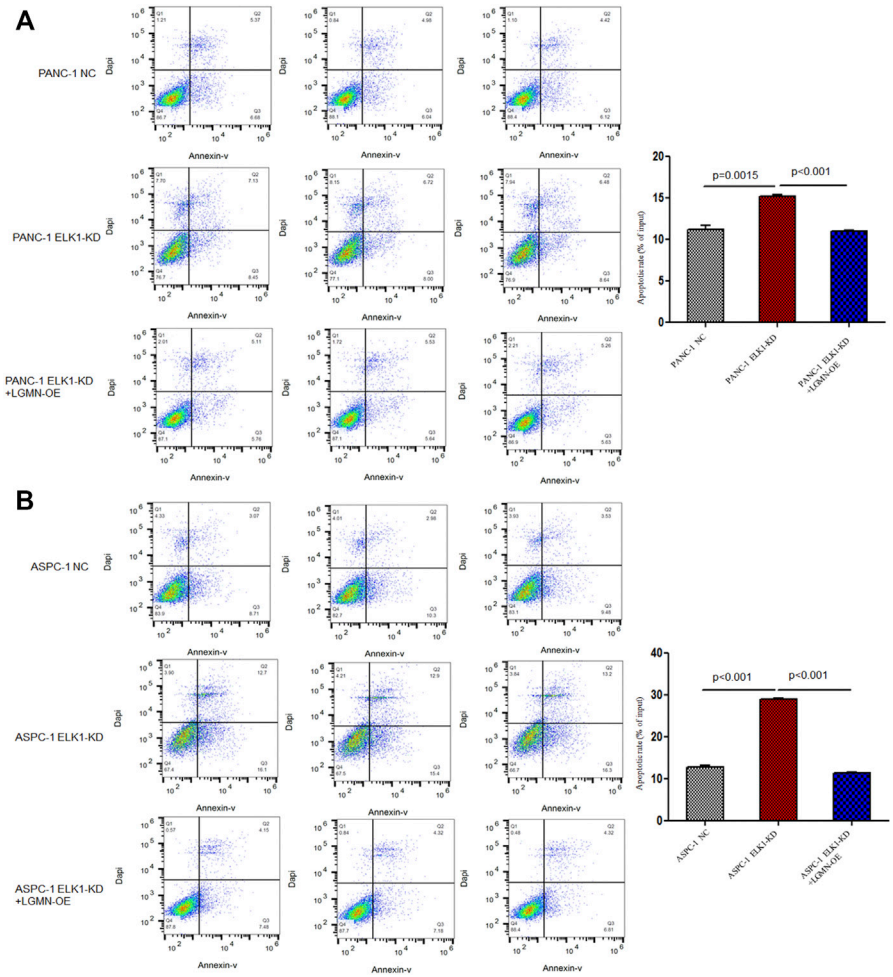


**FIGURE 4 |** ELK1 promoted pancreatic cancer cells survival *via* LGMN. **(A,B)** FACS apoptotic analysis of PANC-1 and ASPC-1 cells with ELK1 knocked down as well as LGMN rescued. *$p$ = 0.0015, **$p$ < 0.001 between ELK1-KD group and control group, ELK1-KD group and ELK1-KD+LGMN-OE group in PANC-1 cells. *$p$ < 0.001, **$p$ < 0.001, between ELK1-KD group and control group, ELK1-KD group and ELK1-KD+LGMN-OE group in ASPC-1 cells.

# RESULTS

## ELK1 Promoted LGMN Expression in Pancreatic Cancer Cells

Although we previously found that high expression of LGMN is involved in the progression of PDAC, the upstream regulation of LGMN remains unknown (18). In order to study the upstream regulation of LGMN in PDAC, we used JASPR and PROMP to search for potential transcription factors in LGMN promoter. SP1, ELK1, GATA3, NFAT1, E2F1 and c-JUN scored high in both software programs. Therefore, we knocked down each of these factors by siRNAs (**Table 1**) and determined their effect on LGMN expression in PANC-1 cells (**Figures 1A–F**). As shown in the figure, the mRNA level of LGMN decreased significantly after knockdown of ELK1 and NFAT1 (*$p$ = 0.0057, **$p$ = 0.0021, **Figure 1G**), LGMN protein also decreased after the inhibition of ELK1 (*$p$ = 0.0003, **Figure 1H** and **Supplementary Figure S5**). Therefore, we constructed the LGMN promoter, and luciferase detection showed that knockdown of ELK1 significantly reduced the transcriptional activity of LGMN mRNA (*$p$ = 0.029, **Figure 1I**).

We then analyzed the expression of ELK1 and LGMN in four different pancreatic cancer cell lines. RT-PCR results showed that ELK1 was relatively high in PANC-1 and ASPC-1 cells compared with BXPC3 and SW1990 cells (**Figure 2A**), LGMN was relatively high in PANC-1, ASPC-1 and SW1990 cells compared with BXPC3 cells (**Figure 2B**). A positive correlation between ELK1 and LGMN was observed in the mRNA level of pancreatic cancer cells ($R^2$ = 0.412, $p$ = 0.2430, **Figure 3C**).As shown in results, ELK1 protein expression was relatively high in PANC-1 and ASPC-1 cells compared with BXPC3 and SW1990 cells (**Figure 2D**), LGMN protein expression was higher than that in control (**Figure 2D**). We chose to overexpress ELK1 in BXPC3 and SW1990 cells and found the protein level of ELK1 increased

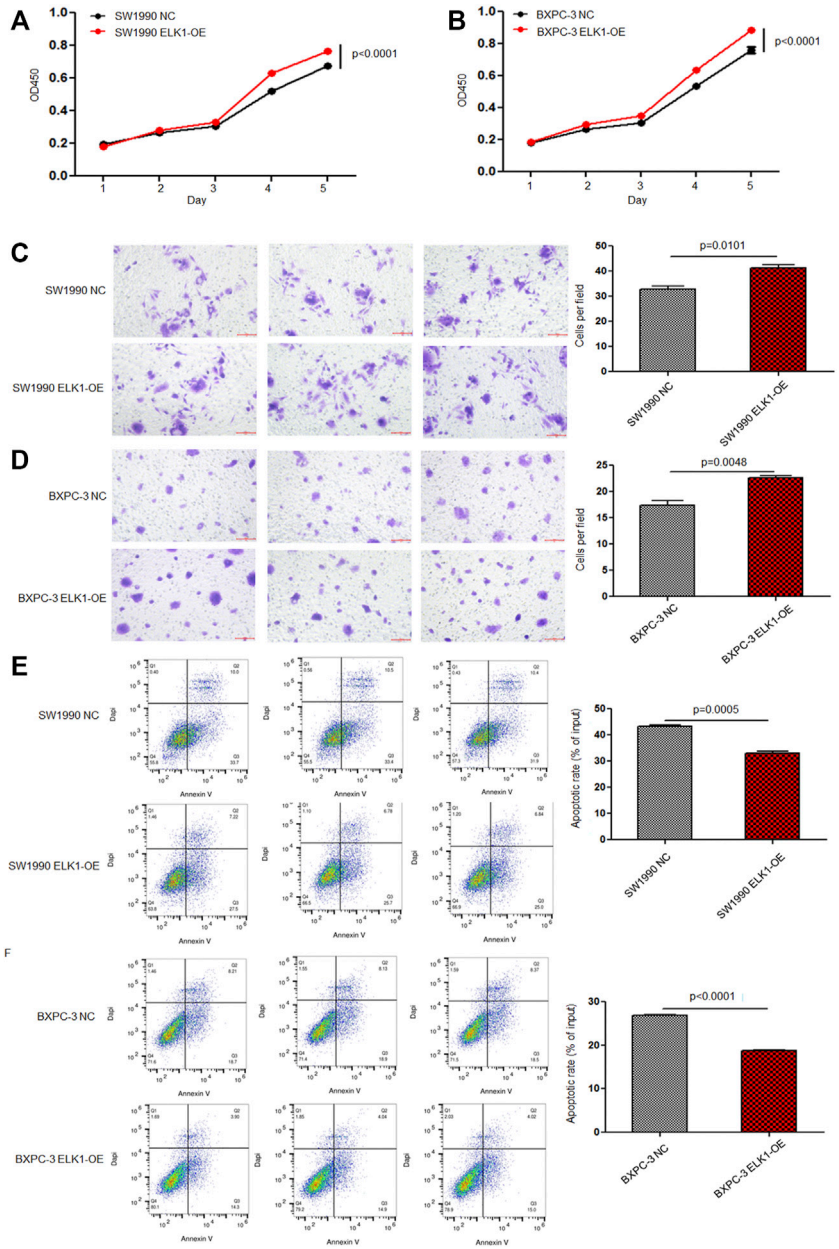


**FIGURE 5 |** ELK1 overexpression promoted pancreatic cancer cells proliferation, invasion and survival. **(A,B)** CCK8 analysis of SW1990 and BxPC3 cells with or without ELK1 overexpression. *$p < 0.001$, **$p < 0.001$, between ELK1-OE group and control group in SW1990 and BxPC3 cells. **(C,D)** Matrigel-Transwell analysis of SW1990 and BxPC3 cells with or without ELK1 overexpression. *$p = 0.0101$, **$p = 0.0048$, between ELK1-OE group and control group in SW1990 and BxPC3 cells. **(E,F)** FACS apoptotic analysis of SW1990 and BxPC3 cells with or without ELK1 overexpression. *$p = 0.0005$, **$p < 0.001$, between ELK1-OE group and control group in SW1990 and BxPC3 cells.

(**Supplementary Figure S2A**). We also knocked down ELK1 in PANC-1 and ASPC-1 cells and found the protein level of ELK1 and LGMN decreased, while the expression of LGMN was saved in cells supplemented with over-expressed LGMN (**Supplementary Figure S2B**). Taken together, these results indicated that transcription factor ELK1 promoted the expression of LGMN in pancreatic cancer cells.

## ELK1 Promoted Pancreatic Cancer Cells Proliferation, Invasion and Survival *via* LGMN

To elucidate the role of ELK1 in PDAC, we examined the proliferation, invasion and survival of pancreatic cancer cells. CCK8 experiment showed that knockdown of ELK1 gene significantly inhibited the proliferation of PANC-1 and

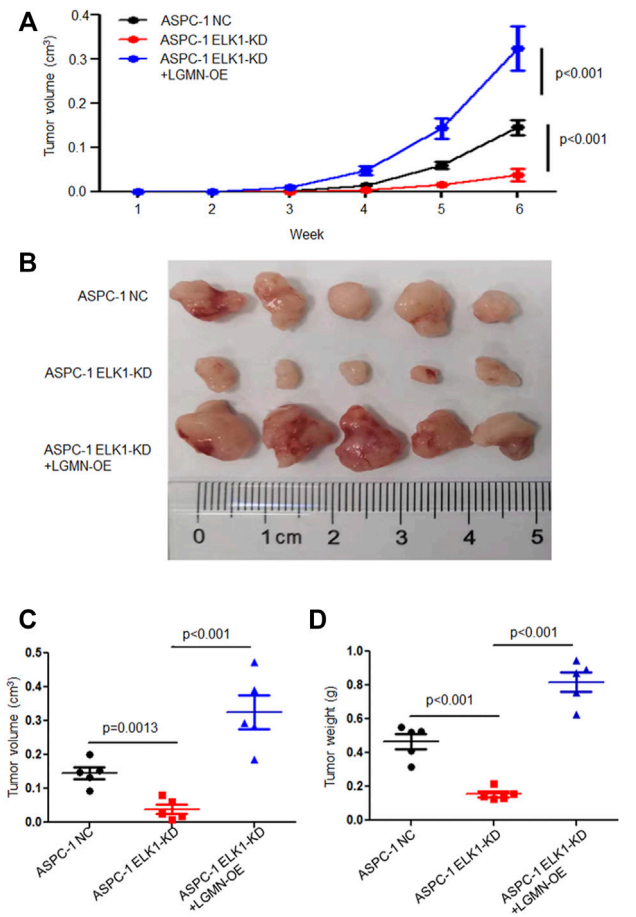


**FIGURE 6 |** ELK1 promoted pancreatic cancer cells progression *via* LGMN *in vivo*. **(A–C)** Tumor volume of ASPC-1 cells with ELK1 knocked down as well as LGMN rescue were monitored. $*p < 0.001$, $**p < 0.001$, between ELK1-KD group and control group, ELK1-KD+LGMN-OE group and control group in ASPC-1 cells **(A)**. $*p = 0.0013$, $**p < 0.001$, between ELK1-KD group and control group, ELK1-KD group and ELK1-KD+LGMN-OE group in ASPC-1 cells **(C)**. **(D)** Tumor weight of ASPC-1 cells with ELK1 knocked down as well as LGMN rescued were analyzed. $*p < 0.001$, $**p < 0.001$, between ELK1-KD group and control group, ELK1-KD group and ELK1-KD+LGMN-OE group in ASPC-1 cells.

ASPC-1 cells ($*p < 0.001$, $**p < 0.001$, **Figures 3A,B**). In addition, Matrigel Transwell invasion experiment indicated that inhibition of ELK1 weakened the invasive capacity of PANC-1 and ASPC-1 cells ($*p < 0.001$, $**p = 0.0013$, **Figures 3C,D**). Fluorescence-activated cell sorting (FACS) showed that the percentage of apoptotic cells increased after knocking down of ELK1 in PANC-1 and ASPC-1 cells ($*p = 0.0015$, $**p < 0.001$, **Figures 4A,B**), and yet LGMN rescued ELK1-KD cells and restored the proliferation, invasion and survival of PANC-1 and ASPC-1 cells (**Figures 3**, **4**). Furthermore, overexpression of ELK1 promoted proliferation, invasion and survival of SW1990 and BXPC3 cells (**Figure 5**). The CCK8 assay showed that overexpression of ELK1 gene significantly promoted the proliferation of SW1990 and BXPC3 cells ($*p < 0.001$, $**p < 0.001$, **Figures 5A,B**). Matrigel Transwell invasion experiment indicated that overexpression of ELK1 enhanced the invasive capacity of SW1990 and BXPC3 cells ($*p = 0.0101$, $**p = 0.0048$, **Figures 5C,D**). Fluorescence-activated cell sorting (FACS) showed that the percentage of apoptotic cells decreased after SW1990 and BXPC3 cells overexpressed ELK1 ($*p = 0.0005$, $**p < 0.001$, **Figures 5E,F**). In conclusion, our study revealed that ELK1 promoted the proliferation, invasion and survival of pancreatic cancer cells by LGMN.

To further confirm the effects of ELK1 on PDAC development *in vivo*, we constructed Xenograft models by subcutaneous injection ASPC-1 NC cells, ASPC-1 ELK-KD cells and ASPC-1 ELK1-KD/LGMN-OE cells. Tumor volume analysis showed that tumors grew slower in ELK1-KD group than that in ELK1-KD/LGMN-OE group ($*p < 0.001$, $**p < 0.001$, **Figures 6A–C**). Consistent with the above results, tumors were lighter in ELK1-KD group than that in ELK1 -KD/LGMN-OE group ($p < 0.001$, $p < 0.001$, **Figure 6D**). Collectively, these *in vivo* experiment confirmed our *in vitro* data and identified ELK1 promoted pancreatic cancer cell proliferation, invasion and survival through LGMN.

## Relationship Between ELK1 and LGMN and Prognosis in Pancreatic Adenocarcinoma Patients

To evaluate the potential clinical significance of ELK1 and LGMN in the prognosis and diagnosis of PDAC, we used immunostaining to detect their expression in 176 PDAC patients. According to pathological findings, PDAC patients were divided into three groups, stage T1, T2, T3. We found that the expressions of LGMN and ELK1 were reduced in ELK1-KD group, while LGMN was saved in ELK1-KD/LGMN-OE group (**Figures 7A,B**). Representative expression patterns in pancreatic adenocarcinoma samples are shown in **Figure 8A**.

Besides, according to the expression of ELK1 and LGMN in pancreatic adenocarcinoma samples, all patients were distributed into two groups: the low expression group and the high expression group (**Tables 1**, **2**). The immunohistochemical staining results revealed that ELK1 and LGMN levels were significantly associated with clinical stage, degree of differentiation and lymph node infiltration (**Tables 1**, **2**).

To assess the relationship of ELK1 expression with patient prognosis, the log-rank test and Kaplan–Meier analysis were used to evaluate the effect of ELK1 expression on patient survival. Patients with high levels of ELK1 and LGMN expression in tumor tissues experienced significantly shorter OS than patients with low ELK1 expression ($n = 173$, $p < 0.0001$, **Figures 8B–D**). The mean survival time of patients with low ELK1 expression was 27.93 months ($n = 96$, 95% CI: 25.61–30.24), whereas the survival time of patients with high ELK1 expression was 18.65 months ($n = 77$, 95% CI: 16.92–20.38). The log-rank test (univariate analysis) demonstrated that patients with low LGMN expression had a longer overall survival (OS) time than patients with high LGMN expression ($\chi^2 = 36.644$, $p < 0.0001$). Moreover, the mean survival time of patients with low LGMN expression was 26.23 months ($n = 119$, 95% CI: 24.14–28.41), whereas the mean survival time of patients with high LGMN expression

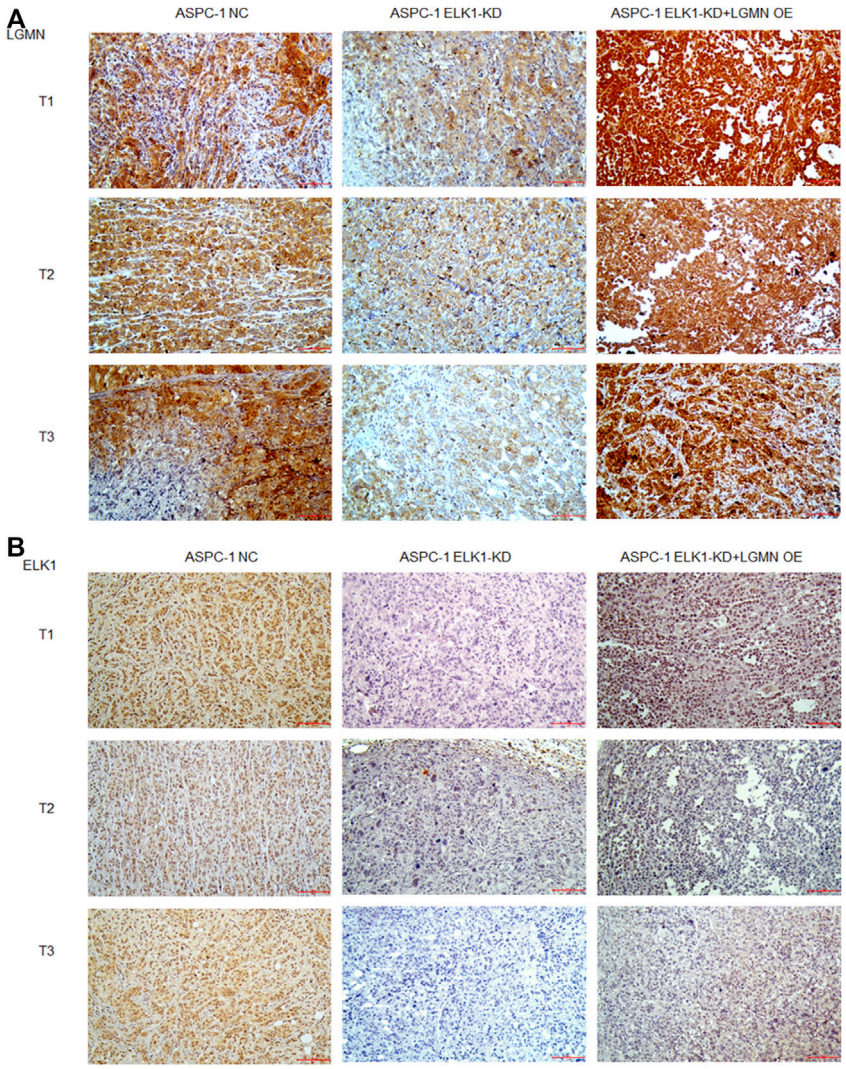


**FIGURE 7 |** ELK1 positively correlated with LGMN expression *in vivo*. **(A,B)** Immunohistochemical analysis of LGMN **(A)** and ELK1 **(B)** expression of ASPC-1 cells. Figures shown that ELK1 and LGMN were expressed in ASPC-1 cells. ELK1 was not expressed in ELK1-KD group and ELK1-KD+LGMN-OE group. LGMN was rarely expressed in ELK1-KD group and rescued its expression in ELK1-KD+LGMN-OE group.

was 18.33 months ($n$ = 54, 95% CI: 16.73–19.94). The log-rank test (univariate analysis) demonstrated that the patients with low LGMN expression had a longer OS time than patients with high LGMN expression ($\chi^2$ = 28.434, $p < 0.0001$). Multivariate Cox regression analysis was also performed to explore whether ELK1 is an independent prognostic factor for survival. As presented in **Figures 8B,C**, ELK1 expression and LGMN expression were identified as independent prognostic factors (ELK1: HR = 2.45, 95% CI: 1.79–3.37, $p < 0.0001$; LGMN: HR = 2.40, 95% CI: 1.69–3.40, $p < 0.0001$).

## DISCUSSION

Pancreatic cancer is one of the most deadly cancers and and its prognosis is extremely poor, mainly due to its low early detection rate and high metastatic rate (Kamisawa et al., 2016). Though LGMN is highly expressed in the majority of human solid tumors and is associated with a more invasive and metastatic phenotype, the underlying mechanisms of its tumor-promoting effects have yet to be fully elucidated (Mai et al., 2017). We previously found that high expression of LGMN is involved in the progression of pancreatic carcinoma in an exosome-dependent manner and that LGMN independently indicated poor prognosis; however, the upstream regulation of LGMN remains unknown (Yan et al., 2018). The regulation of gene expression by transcription factors is a common cellular event. It has been reported that an inflammation-regulated transcription factor known as CCAAT-enhancer-binding protein (C/EBPβ) can modulate LGMN expression in the pathogenesis of Alzheimer's disease (Wang et al., 2018). As a well-known tumor suppressor, the transcription factor p53 binds to intron 1 of the human LGMN

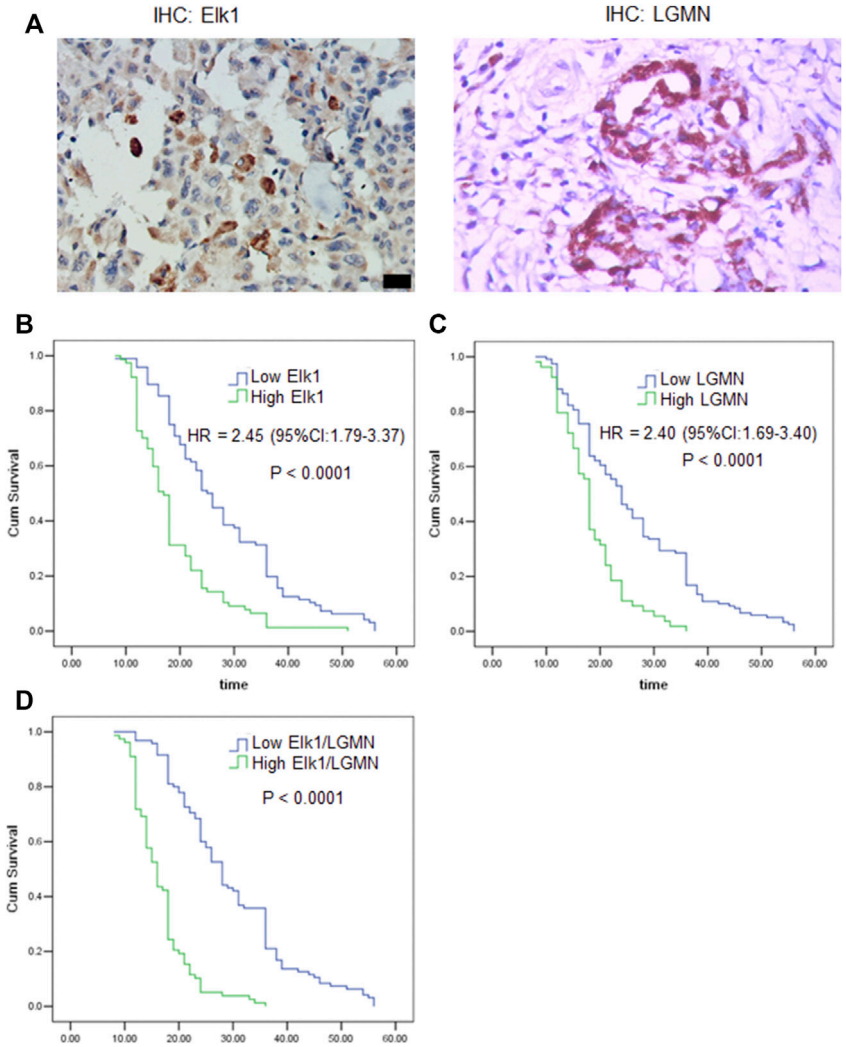


**FIGURE 8 |** ELK1 and LGMN negatively associated with prognosis in pancreatic adenocarcinoma patients. **(A)** Expression of ELK1 and LGMN in pancreatic cancer tissues. **(B–D)** Kaplan-Meier survival analysis in PDAC patients ($n$ = 173) according to the ELK1 and LGMN expression. High ELK1 **(B)**, LGMN **(C)** and both **(D)** expression patients showed significantly shorter 5-year OS than patients with low ELK1 **(B)**, LGMN **(C)** and both **(D)** expression in their tumors by long-rank test ($p$ < 0.0001).

gene and regulates LGMN expression at the transcriptional level (Yamane et al., 2013). In this study, we discovered that the transcription factor ELK1 functions in PDAC by regulating LGMN. Knocking down of ELK1 inhibited pancreatic cancer cells proliferation, invasion and survival, while LGMN could restore their malignancy. Overexpression of ELK1 further promoted pancreatic cancer cells proliferation, invasion and survival. An animal model showed that tumors grew slower in the ELK1-KD group and faster in the ELK1-KD/LGMN-OE group. Clinically, ELK1 and LGMN expression were positively correlated with clinical stage, degree of differentiation and lymph node infiltration. ELK1 and LGMN were determined to be independent prognostic factors for OS.

ELK1, as a transcriptional activator involved in the MAPK/ERK pathway, induces the proliferation and/or migration/invasion of bladder and prostate cancer cells as well as resistance to the cytotoxic effects of the chemotherapeutic agent cisplatin in bladder cancer cells ((Kawahara et al., 2015), (Kawahara et al., 2016)). ELK1 is a regulator of c-Fos. c-Fos has been shown to form a heterodimer with Jun, leading to the formation of the AP-1 complex and the regulation of target gene expression and is thereby involved in tumorigenesis (Angel and Karin, 1991). The direct regulation of BRCA1, variations in which are linked to increased risks of breast and ovarian cancers, by ELK1/c-Fos/Jun has also been documented (Zhong et al., 2004). Knocking down of ELK1 in MCA-exposed SVHUC-AR cells resulted in a significant decrease in the expression of several oncogenes, including c-Fos, Jun, and Myc, and a significant increase in several tumor suppressors, such as p53, PTEN, and UGT1A (Inoue et al., 2018a). Nonetheless, further search is needed to accurately determine how ELK1 signal regulates PDAC progress. In this study, we have

**TABLE 2 |** Association of ELK1 expression with clinicopathological variables in pancreatic ductal adenocarcinoma.

| Clinicopathological characteristic | *n* (%) | Elk1 staining (*n*; %) | | *p*-value |
|---|---|---|---|---|
| | | Low | High | |
| Age (year) | | | | 0.137 |
| <60 | 86 (48.86) | 44 (51.16) | 42 (48.84) | |
| ≥60 | 90 (51.14) | 56 (62.22) | 34 (37.78) | |
| Sex | | | | 0.173 |
| Male | 108 (61.36) | 57 (52.78) | 51 (47.22) | |
| Female | 68 (38.64) | 43 (63.23) | 25 (36.76) | |
| Clinical stages | | | | *0.005 |
| I/II | 138 (78.41) | 86 (62.32) | 52 (39.86) | |
| III/IV | 38 (21.59) | 14 (36.84) | 24 (63.16) | |
| Tumor location | | | | 0.142 |
| Head | 112 (63.64) | 59 (50.89) | 53 (49.11) | |
| Body/tail | 64 (36.36) | 41 (60.93) | 23 (39.07) | |
| Tumor size | | | | 0.102 |
| ≤4 cm | 58 (32.95) | 38 (62.07) | 20 (37.93) | |
| >4 cm | 118 (67.05) | 62 (50.85) | 56 (49.15) | |
| Differentiation | | | | *0.041 |
| Weak to moderately | 110 (62.50) | 69 (62.73) | 41 (37.27) | |
| Poorly | 66 (37.50) | 31 (46.97) | 35 (53.03) | |
| N infiltration | | | | 0.271 |
| Positive | 165 (93.75) | 92 (55.76) | 73 (44.24) | |
| Negative | 11 (6.25) | 8 (72.73) | 3 (27.27) | |
| Lymphnode infiltration | | | | *0.050 |
| Positive | 128 (72.73) | 67 (52.34) | 61 (47.66) | |
| Negative | 48 (27.27) | 33 (68.75) | 15 (31.25) | |

revealed a new mechanism by which ELK1 promotes the progression of pancreatic cancer through LGMN.

Considering the unique role of ELK1 in activating gene transcription associated with cancer progression, its value as a prognostic marker deserves in-depth evaluation. Researchers have confirmed ELK1 is a strong independent predictor of prostate cancer recurrence (Pardy et al., 2020). Overexpression of phospho-ELK1, the activated form of ELK1, has also been discovered to be a predictor of poor prognosis in patients with upper urinary tract urothelial carcinoma (UUTUC) (Inoue et al., 2018b). In our study, high levels of ELK1 and LGMN were associated with advanced clinical stage and short OS, consistent with previous studies. Therefore, ELK1 can be used as a reliable indicator for predicting the prognosis of PDAC.

In conclusion, our results suggest that ELK1 promotes pancreatic cancer progression *via* LGMN and correlates with poor prognosis.

## DATA AVAILABILITY STATEMENT

The raw data supporting the conclusions of this article will be made available by the authors, without undue reservation.

## ETHICS STATEMENT

The studies involving human participants were reviewed and approved by Ethics Committee of Huzhou Central Hospital. The patients/participants provided their written informed consent to participate in this study. The animal study was reviewed and approved by Animal Ethics Committee of Huzhou Institute of Food and Drug Inspection.

## AUTHOR CONTRIBUTIONS

QY and CN: Conceptualization, Methodology, Writing–Original draft preparation. YL and ZS: Visualization, Investigation. XS, MZ, and SH: Data curation, Writing–Original draft preparation. JS and JM: Supervision. WW: Conceptualization, Software, Validation. ZY: Editing. All authors contributed to the article and approved the submitted version.

## FUNDING

This study was supported by the Huzhou public welfare research project (Class A) (No. 2018GY14), Provincial medical and health appropriate technology cultivation and promotion project (No. 2021ZH043) and Cancer research project (Zhengda qingchunbao special project) (No. 2016ZYC-A66).

## SUPPLEMENTARY MATERIAL

The Supplementary Material for this article can be found online at: https://www.frontiersin.org/articles/10.3389/fmolb.2021.764900/full#supplementary-material

## REFERENCES


Al Haddad, A. H., and Adrian, T. E. (2014). Challenges and Future Directions in Therapeutics for Pancreatic Ductal Adenocarcinoma. *Expert Opin. Investig. Drugs* 23 (11), 1499–1515. doi:10.1517/13543784.2014.933206

Angel, P., and Karin, M. (1991). The Role of Jun, Fos and the AP-1 Complex in Cell-Proliferation and Transformation. *Biochim. Biophys. Acta* 1072 (2-3), 129–157. doi:10.1016/0304-419x(91)90011-9

Bray, F., Ferlay, J., Soerjomataram, I., Siegel, R. L., Torre, L. A., and Jemal, A. (2018). Global Cancer Statistics 2018: GLOBOCAN Estimates of Incidence and Mortality Worldwide for 36 Cancers in 185 Countries. *CA: a Cancer J. clinicians* 68 (6), 394–424. doi:10.3322/caac.21492

Choi, S. J., Reddy, S. V., Devlin, R. D., Menaa, C., Chung, H., Boyce, B. F., et al. (1999). Identification of Human Asparaginyl Endopeptidase (Legumain) as an Inhibitor of Osteoclast Formation and Bone Resorption. *J. Biol. Chem.* 274 (39), 27747–27753. doi:10.1074/jbc.274.39.27747

Colbert, L. E., Hall, W. A., Nickleach, D., Switchenko, J., Kooby, D. A., Liu, Y., et al. (2014). Chemoradiation Therapy Sequencing for Resected Pancreatic Adenocarcinoma in the National Cancer Data Base. *Cancer* 120 (4), 499–506. doi:10.1002/cncr.28530

D'Costa, Z. C., Higgins, C., Ong, C. W., Irwin, G. W., Boyle, D., McArt, D. G., et al. (2014). TBX2 Represses CST6 Resulting in Uncontrolled Legumain Activity to Sustain Breast Cancer Proliferation: A Novel Cancer-Selective Target Pathway with Therapeutic Opportunities. *Oncotarget* 5 (6), 1609–1620. doi:10.18632/oncotarget.1707

Edgington-Mitchell, L. E., Rautela, J., Duivenvoorden, H. M., Jayatilleke, K. M., van der Linden, W. A., Verdoes, M., et al. (2015). Cysteine Cathepsin Activity Suppresses Osteoclastogenesis of Myeloid-Derived Suppressor Cells in Breast Cancer. *Oncotarget* 6 (29), 27008–27022. doi:10.18632/oncotarget.4714

Haugen, M. H., Johansen, H. T., Pettersen, S. J., Solberg, R., Brix, K., Flatmark, K., et al. (2013). Nuclear Legumain Activity in Colorectal Cancer. *PLoS One* 8 (1), e52980. doi:10.1371/journal.pone.0052980

Herskowitz, J. H., Gozal, Y. M., Duong, D. M., Dammer, E. B., Gearing, M., Ye, K., et al. (2012). Asparaginyl Endopeptidase Cleaves TDP-43 in Brain. *Proteomics* 12 (15-16), 2455–2463. doi:10.1002/pmic.201200006

Ibrahim, A. M., and Wang, Y. H. (2016). Viro-immune Therapy: A New Strategy for Treatment of Pancreatic Cancer. *Wjg* 22 (2), 748–763. doi:10.3748/wjg.v22.i2.748

Inoue, S., Ide, H., Mizushima, T., Jiang, G., Kawahara, T., and Miyamoto, H. (2018). ELK1 Promotes Urothelial Tumorigenesis in the Presence of an Activated Androgen Receptor. *Am. J. Cancer Res.* 8 (11), 2325–2336.

Inoue, S., Ide, H., Fujita, K., Mizushima, T., Jiang, G., Kawahara, T., et al. (2018). Expression of Phospho-ELK1 and its Prognostic Significance in Urothelial Carcinoma of the Upper Urinary Tract. *Ijms* 19 (3), 777. doi:10.3390/ijms19030777

Jagadeeshan, S., Krishnamoorthy, Y. R., Singhal, M., Subramanian, A., Mavuluri, J., Lakshmi, A., et al. (2015). Transcriptional Regulation of Fibronectin by P21-Activated Kinase-1 Modulates Pancreatic Tumorigenesis. *Oncogene* 34 (4), 455–464. doi:10.1038/onc.2013.576

Kamisawa, T., Wood, L. D., Itoi, T., and Takaori, K. (2016). Pancreatic Cancer. *The Lancet* 388 (10039), 73–85. doi:10.1016/s0140-6736(16)00141-0

Kawahara, T., Ide, H., Kashiwagi, E., Patterson, J. D., Inoue, S., Shareef, H. K., et al. (2015). Silodosin Inhibits the Growth of Bladder Cancer Cells and Enhances the Cytotoxic Activity of Cisplatin via ELK1 Inactivation. *Am. J. Cancer Res.* 5 (10), 2959–2968.

Kawahara, T., Aljarah, A. K., Shareef, H. K., Inoue, S., Ide, H., Patterson, J. D., et al. (2016). Silodosin Inhibits Prostate Cancer Cell Growth via ELK1 Inactivation and Enhances the Cytotoxic Activity of Gemcitabine. *Prostate* 76 (8), 744–756. doi:10.1002/pros.23164

Liu, C., Sun, C., Huang, H., Janda, K., and Edgington, T. (2003). Overexpression of Legumain in Tumors Is Significant for Invasion/metastasis and a Candidate Enzymatic Target for Prodrug Therapy. *Cancer Res.* 63 (11), 2957–2964.

Liu, P., Zhu, Y., and Liu, L. (2015). Elevated Pretreatment Plasma D-Dimer Levels And Platelet Counts Predict Poor Prognosis In Pancreatic Adenocarcinoma. *Ott* 8, 1335–1340. doi:10.2147/ott.S82329

Mai, C.-W., Chung, F. F.-L., and Leong, C.-O. (2017). Targeting Legumain as a Novel Therapeutic Strategy in Cancers. *Cdt* 18 (11), 1259–1268. doi:10.2174/1389450117666161216125344

Miller, G., Matthews, S. P., Reinheckel, T., Fleming, S., and Watts, C. (2011). Asparagine Endopeptidase Is Required for Normal Kidney Physiology and Homeostasis. *FASEB j.* 25 (5), 1606–1617. doi:10.1096/fj.10-172312

Pardy, L., Rosati, R., Soave, C., Huang, Y., Kim, S., and Ratnam, M. (2020). The Ternary Complex Factor Protein ELK1 Is an Independent Prognosticator of Disease Recurrence in Prostate Cancer. *The Prostate* 80 (2), 198–208. doi:10.1002/pros.23932

Sevenich, L., and Joyce, J. A. (2014). Pericellular Proteolysis in Cancer. *Genes Dev.* 28 (21), 2331–2347. doi:10.1101/gad.250647.114

van Endert, P. (2009). Toll-like Receptor 9: AEP Takes Control. *Immunity* 31 (5), 696–698. doi:10.1016/j.immuni.2009.10.004

Wang, Z.-H., Gong, K., Liu, X., Zhang, Z., Sun, X., Wei, Z. Z., et al. (2018). C/EBPβ Regulates Delta-secretase Expression and Mediates Pathogenesis in Mouse Models of Alzheimer's Disease. *Nat. Commun.* 9 (1), 1784. doi:10.1038/s41467-018-04120-z

Wood, N. J. (2014). Pancreatic Tumour Formation and Recurrence after Radiotherapy Are Blocked by Targeting CD44. *Nat. Rev. Gastroenterol. Hepatol.* 11 (2), 73. doi:10.1038/nrgastro.2014.1

Yamane, T., Murao, S., Kato-Ose, I., Kashima, L., Yuguchi, M., Kozuka, M., et al. (2013). Transcriptional Regulation of the Legumain Gene by P53 in HCT116 Cells. *Biochem. Biophysical Res. Commun.* 438 (4), 613–618. doi:10.1016/j.bbrc.2013.08.007

Yan, Q., Yuan, W.-B., Sun, X., Zhang, M.-J., Cen, F., Zhou, S.-Y., et al. (2018). Asparaginyl Endopeptidase Enhances Pancreatic Ductal Adenocarcinoma Cell Invasion in an Exosome-dependent Manner and Correlates with Poor Prognosis. *Int. J. Oncol.* 52 (5), 1651–1660. doi:10.3892/ijo.2018.4318

Zhen, Y., Chunlei, G., Wenzhi, S., Shuangtao, Z., Na, L., Rongrong, W., et al. (2015). Clinicopathologic Significance of Legumain Overexpression in Cancer: A Systematic Review and Meta-Analysis. *Sci. Rep.* 5, 16599. doi:10.1038/srep16599

Zhong, H., Zhu, J., Zhang, H., Ding, L., Sun, Y., Huang, C., et al. (2004). COBRA1 Inhibits AP-1 Transcriptional Activity in Transfected Cells. *Biochem. Biophysical Res. Commun.* 325 (2), 568–573. doi:10.1016/j.bbrc.2004.10.079

Zhu, W., Shao, Y., Yang, M., Jia, M., and Peng, Y. (2016). Asparaginyl Endopeptidase Promotes Proliferation and Invasiveness of Prostate Cancer Cells via PI3K/AKT Signaling Pathway. *Gene* 594 (2), 176–182. doi:10.1016/j.gene.2016.08.049


**Conflict of Interest:** The authors declare that the research was conducted in the absence of any commercial or financial relationships that could be construed as a potential conflict of interest.

# Advantages of publishing in Frontiers

**OPEN ACCESS**
Articles are free to read for greatest visibility and readership

**FAST PUBLICATION**
Around 90 days from submission to decision

**HIGH QUALITY PEER-REVIEW**
Rigorous, collaborative, and constructive peer-review

**TRANSPARENT PEER-REVIEW**
Editors and reviewers acknowledged by name on published articles

**Frontiers**
Avenue du Tribunal-Fédéral 34
1005 Lausanne | Switzerland

**Visit us:** www.frontiersin.org
**Contact us:** frontiersin.org/about/contact

**REPRODUCIBILITY OF RESEARCH**
Support open data and methods to enhance research reproducibility

**DIGITAL PUBLISHING**
Articles designed for optimal readership across devices

**FOLLOW US**
@frontiersin

**IMPACT METRICS**
Advanced article metrics track visibility across digital media

**EXTENSIVE PROMOTION**
Marketing and promotion of impactful research

**LOOP RESEARCH NETWORK**
Our network increases your article's readership